

PULMONARY DELIVERY OF RESVERATROL-LOADED
NANOCOMPOSITE MICROPARTICLES TO TREAT LUNG
CANCER

ASHLEY GEORGE MULLER

A thesis submitted in partial fulfilment of the requirements of Liverpool John
Moore's University for the degree of Doctor of Philosophy

November 2019

Acknowledgements

Firstly, I would like to thank my supervisors, **Prof. Gillian Hutcheon**, **Dr Amos Fatokun**, and **Prof. Satyajit Sarker**, for all their support and guidance throughout this PhD process, without which I would not have been able to get this far. To the sponsors of my PhD, **AESOP+**, I extend my deepest gratitude for allowing me the opportunity to further my studies. To **Dr Francesca Giuntini**, even though I was not under your supervision, you never failed to provide assistance and I thank you for that.

Special mentions go to Dr Nicola Dempster, Mr Robert Allen, Mr Phil Salmon, and all the other technicians that helped me along the way.

Secondly, I would like to thank my parents and my grandparents for raising me and making me the person I am today.

Thirdly, to my wife, Silvia Borrelli, who has supported me in all aspects of the word during my PhD. I will eternally be grateful to you for putting up with me during this stressful period.

To my guys, both in the UK and in SA, Adam, Adrien, Dane, Kan, Kieran, Shadley, and Shane, your conversations and company has not gone unnoticed.

Finally, to all the friends and colleagues I have met in room 2.01, your assistance will not be forgotten as each and every one has played a role in my PhD journey.

I leave all of you with a well-known African proverb:

I am, because you are!

Table of Contents

LIST OF FIGURES.....	X
LIST OF TABLES	XIV
LIST OF ABBREVIATIONS	XVI
ABSTRACT.....	XXV
1 CHAPTER 1: GENERAL INTRODUCTION.....	1
1.1. Introduction	2
1.1.1 Lung cancer	2
1.1.1.1 A brief history of lung cancer.....	2
1.1.1.2 Causes of lung cancer	3
1.1.1.3 Lung cancer statistics	4
1.1.1.4 Economics of lung cancer	5
1.1.2 Side-effects of current cancer chemotherapy treatment	8
1.1.3 Resveratrol as an alternative treatment for lung cancer treatment.....	10
1.1.3.1 Phenolic compounds	10
1.1.3.1.1 Resveratrol.....	10
1.1.3.1.1.1 <i>In vitro</i> evidence of efficacy against lung cancer	11
1.1.3.1.1.2 <i>In vivo</i> evidence of efficacy against lung cancer	16
1.1.3.1.2 Bioavailability.....	18
1.1.4 Nanoparticulate delivery systems	20
1.1.4.1 Polymeric nanoparticulate drug delivery system	20
1.1.4.2 Preparation of nanoparticles	33
1.1.4.2.1 Emulsion solvent evaporation	33
1.1.5 Pulmonary delivery.....	35

1.1.5.1.	Anatomy of the lungs.....	35
1.1.5.2.	Drug delivery to the lungs.....	36
1.1.5.3.	Pulmonary delivery of nanocomposite microparticles	38
1.1.5.3.1.	Preparation of nanocomposite microparticles	38
1.1.5.3.1.1.	Spray drying	38
1.1.5.3.2.	Delivery of nanocomposite microparticles	39
1.1.5.3.2.1.	Dry powder inhaler (DPI)	40
1.1.5.3.3.	Delivery described in literature	42
1.2.	Thesis hypothesis	48
1.3.	Thesis aim and objectives.....	48
2	CHAPTER 2: THE FORMULATION AND EVALUATION OF RESVERATROL NANOPARTICLES	50
2.1.	Introduction	51
2.2.	Aim and Objectives	54
2.3.	Materials and Methods.....	55
2.3.1.	Materials	55
2.3.2.	Methods	56
2.3.2.1.	Polymer synthesis	56
2.3.2.1.1.	PGA-co-PDL synthesis	56
2.3.2.1.2.	PGA-co-PDL-PEG ₂₀₀₀	58
2.3.2.1.3.	Poly(<i>D,L</i> -lactide-co-glycolide) (PLGA)	58
2.3.2.1.4.	PEG methyl ether-block-poly(lactide-co-glycolide) (mPEG-PLGA).....	59
2.3.2.2.	Polymer analysis	59
2.3.2.2.1.	Molecular weight analysis - Gel Permeation Chromatography (GPC)	59

2.3.2.2.2.	Chemical structure analysis – Fourier Transform Infra-Red (FT-IR) Spectroscopy and Nuclear Magnetic Resonance (NMR) Spectroscopy.....	61
2.3.2.2.2.1.	Fourier Transform Infra-Red (FT-IR) Spectroscopy	61
2.3.2.2.2.2.	Nuclear Magnetic Resonance (NMR).....	61
2.3.2.2.3.	Thermal analysis – Differential Scanning Calorimetry (DSC)	61
2.3.2.3.	Polymeric nanoparticle synthesis	62
2.3.2.4.	Polymeric nanoparticle analysis	63
2.3.2.4.1.	Particle size and zeta potential.....	63
2.3.2.4.2.	Drug loading and encapsulation efficiency (EE%).....	63
2.3.2.4.3.	Release study.....	65
2.3.2.4.3.1.	Sacrificial method	65
2.3.2.4.3.2.	Replacement method	65
2.3.2.5.	Cell culture	66
2.3.2.6.	Cell viability studies	66
2.3.2.6.1.	Alamar Blue (resazurin sodium salt).....	66
2.3.2.6.2.	Lactate Dehydrogenase (LDH) assay.....	68
2.3.2.7.	Statistical analyses and IC ₅₀ calculations	70
2.3.3.	Results	70
2.3.3.1.	Monomer analysis	70
2.3.3.1.1.	FT-IR and NMR.....	70
2.3.3.1.1.1.	ω -Pentadecalactone (PDL).....	70
2.3.3.1.1.2.	Divinyl adipate (DVA)	71
2.3.3.1.1.3.	Glycerol	71
2.3.3.1.1.4.	Poly(ethylene glycol) methyl ether (mPEG ₂₀₀₀).....	72
2.3.3.2.	Polymer analysis	72
2.3.3.2.1.	Molecular weight – GPC	72
2.3.3.2.1.1.	PGA-co-PDL	73
2.3.3.2.1.2.	PGA-co-PDL-PEG ₂₀₀₀	73
2.3.3.2.1.3.	PLGA.....	73

2.3.3.2.1.4.	mPEG-PLGA.....	73
2.3.3.2.2.	Chemical structure – FT-IR and NMR.....	73
2.3.3.2.2.1.	PGA-co-PDL.....	73
2.3.3.2.2.2.	PGA-co-PDL-PEG ₂₀₀₀	76
2.3.3.2.2.3.	PLGA.....	78
2.3.3.2.2.4.	mPEG-PLGA.....	80
2.3.3.2.3.	Thermal analysis – DSC.....	82
2.3.3.2.3.1.	PGA-co-PDL.....	82
2.3.3.2.3.2.	PGA-co-PDL-PEG ₂₀₀₀	83
2.3.3.2.3.3.	PLGA.....	84
2.3.3.2.3.4.	mPEG-PLGA.....	85
2.3.3.3.	Nanoparticle analysis.....	85
2.3.3.3.1.	Particle size, polydispersity index (PDI), and zeta potential.....	85
2.3.3.3.2.	Drug loading and encapsulation efficiency (EE%).....	87
2.3.3.3.2.1.	Drug loading and encapsulation efficiency.....	87
2.3.3.3.3.	PGA-co-PDL NPs stability.....	89
2.3.3.3.3.1.	Size and zeta potential at 4°C.....	89
2.3.3.3.3.2.	Size when NPs are stored at 37 °C.....	91
2.3.3.3.4.	Release study of PGA-co-PDL.....	94
2.3.3.3.5.	Cell viability studies of PGA-co-PDL.....	94
2.3.3.3.5.1.	Alamar Blue (resazurin sodium salt).....	94
2.3.3.3.5.1.1.	Determining the IC ₅₀ of free-resveratrol.....	94
2.3.3.3.5.1.2.	Determining IC ₅₀ of resveratrol loaded into PGA-co-PDL NPs.....	96
2.3.3.3.5.1.2.1.	5% Resveratrol-loaded NPs.....	96
2.3.3.3.5.1.2.2.	10% Resveratrol-loaded NPs.....	98
2.3.3.3.5.1.2.3.	Percentage changes in IC ₅₀	100
2.3.3.3.5.1.3.	Effect of resveratrol-loaded NPs vs blank NPs on Calu 3 cells.....	100
2.3.3.3.5.2.	LDH assay.....	102
2.3.3.3.5.2.1.	48-hour treatment.....	102

2.3.3.3.5.2.2.	72-hour treatment	104
2.3.4.	Discussion	106
2.3.4.1.	Polymer synthesis and analysis.....	106
2.3.4.2.	Polymeric nanoparticle synthesis and analysis.....	109
2.3.4.2.1.	Size and charge	109
2.3.4.2.2.	Drug loading and encapsulation efficiency (EE%).....	110
2.3.4.2.3.	Stability studies.....	113
2.3.4.2.4.	Release studies	113
2.3.4.3.	Cell viability studies	115
2.3.5.	Conclusion	122

3 CHAPTER 3: FORMULATION OF RESVERATROL LOADED PGA-CO-PDL NANOPARTICLES INTO AEROSOLISABLE MICROCARRIERS..... 123

3.1.	Introduction	124
3.2.	Aims and Objectives.....	126
3.3.	Materials and Methods.....	127
3.3.1.	Materials	127
3.3.2.	Methods	127
3.3.2.1.	Polymeric nanoparticle synthesis and analysis.....	127
3.3.2.2.	Polymeric nanoparticle formulation.....	127
3.3.2.3.	Nanocomposite microparticle formulation	127
3.3.2.3.1.	Spray drying	127
3.3.2.4.	Nanocomposite microparticle analysis.....	128
3.3.2.4.1.	Yield	128
3.3.2.4.2.	Particle size and zeta potential.....	129
3.3.2.4.3.	Morphology	129
3.3.2.4.4.	Moisture content.....	129

3.3.2.4.5.	Drug loading and encapsulation efficiency (EE).....	129
3.3.2.4.6.	Release study.....	131
3.3.2.4.7.	<i>In vitro</i> aerosolisation studies.....	131
3.3.2.5.	Cell culture	133
3.3.2.5.1.	Cell toxicity studies	133
3.3.2.6.	Statistical analyses	134
3.3.3.	Results	134
3.3.3.1.	Nanocomposite microparticle analysis.....	134
3.3.3.1.1.	Yield	134
3.3.3.1.2.	Particle size and zeta potential.....	134
3.3.3.1.3.	Morphology	136
3.3.3.1.4.	Moisture content.....	137
3.3.3.1.5.	Drug loading and encapsulation efficiency (EE%).....	138
3.3.3.1.6.	Release study.....	140
3.3.3.1.7.	<i>In vitro</i> aerosolisation studies.....	141
3.3.3.1.8.	Cell viability studies	143
3.3.3.1.8.1.	LDH assay	143
3.3.4.	Discussion.....	145
3.3.5.	Conclusion	154

4 CHAPTER 4: THE FUNCTIONALISATION OF PGA-CO-PDL USING A MODIFIED GLYCEROL..... 155

4.1.	Introduction	156
4.2.	Aims and Objectives.....	161
4.3.	Materials and Methods.....	162
4.3.1.	Materials	162
4.3.2.	Methods	163

4.3.2.1.	Synthesis of glycerol (2-(prop-2-yn-1-yloxy)propane-1,3-diol).....	163
4.3.2.1.1.	Stage 1: synthesis of 2-phenyl-[1,3]-dioxan-5-ol	163
4.3.2.1.2.	Stage 2: synthesis of 2-phenyl-5-(prop-2-yn-1-yloxy)-1,3-dioxane	164
4.3.2.1.3.	Stage 3: synthesis of 2-(prop-2-yn-1-yloxy)propane-1,3-diol	165
4.3.2.2.	Synthesis of NBD azide	166
4.3.2.3.	Polymer synthesis	167
4.3.2.3.1.	PGA-co-PDL.....	168
4.3.2.3.2.	Alkyne-PGA-co-PDL.....	168
4.3.2.3.3.	50 % alkyne-PGA-co-PDL	169
4.3.2.3.4.	10 % alkyne-PGA-co-PDL	169
4.3.2.4.	Metal catalysed azide-alkyne 'click' reaction.....	170
4.3.2.4.1.	NBD azide reacted with 10 % alkyne-PGA-co-PDL.....	170
4.3.2.4.2.	NBD azide reacted with 2-phenyl-5-(prop-2-yn-1-yloxy)-1,3-dioxane	171
4.3.3.	Results	173
4.3.3.1.	Synthesis of modified glycerol	173
4.3.3.1.1.	Stage 1: synthesis of 2-phenyl-[1,3]-dioxan-5-ol	173
4.3.3.1.2.	Stage 2: synthesis of 2-phenyl-5-(prop-2-yn-1-yloxy)-1,3-dioxane	174
4.3.3.1.3.	Stage 3: synthesis of 2-(prop-2-yn-1-yloxy)propane-1,3-diol	175
4.3.3.2.	Synthesis of NBD azide	176
4.3.3.3.	Polymer synthesis	176
4.3.3.3.1.	PGA-co-PDL.....	176
4.3.3.3.2.	alkyne-PGA-co-PDL	177
4.3.3.3.3.	50 % alkyne-PGA-co-PDL	177
4.3.3.3.4.	10 % alkyne-PGA-co-PDL	178
4.3.4.	Discussion.....	178
4.3.5.	Conclusion	185

5 CHAPTER 5: GENERAL DISCUSSION AND FUTURE WORK 186

5.1. Overview	187
5.1.1. Formulation of polymeric nanoparticles	188
5.1.2. Cytotoxicity studies	191
5.1.3. Spray drying of resveratrol-loaded nanoparticles into NCMPs	193
5.1.4. Polymer modification through click chemistry.....	194
5.2. Future work	196
5.2.1. Optimisation and validation of cytotoxicity studies.....	197
5.2.2. Increase scale of click chemistry	198
5.3. Conclusion	199
6 REFERENCES	200
7 APPENDIX	263

List of Figures

Figure 1-1 Chemical structure of resveratrol	11
Figure 1-2 Schematic diagram of emulsion solvent evaporation technique (modified from (Kunda et al., 2013))	34
Figure 2-1 Enzymatic synthesis of PGA-co-PDL via ring opening polymerisation and polycondensation	57
Figure 2-2 Enzymatic synthesis of PGA-co-PDL-PEG ₂₀₀₀ via ring opening polymerisation and polycondensation	58
Figure 2-3 PLGA structure	59
Figure 2-4 mPEG-PLGA structure	59
Figure 2-5 Plate layout for LDH assay	69
Figure 2-6 Structure of ω -pentadecalactone	70
Figure 2-7 Structure of divinyl adipate	71
Figure 2-8 Structure of glycerol	71
Figure 2-9 Structure of mPEG ₂₀₀₀	72
Figure 2-10 Polymer standard curve using GPC ($R^2=0.992$) $n=3$	72
Figure 2-11 FT-IR spectrum of PGA-co-PDL	75
Figure 2-12 ¹ H-NMR spectrum (A) and structure of PGA-co-PDL (B) with protons labelled	75
Figure 2-13 FT-IR spectrum of PGA-co-PDL-PEG ₂₀₀₀	77
Figure 2-14 ¹ H-NMR spectrum (A) and structure of PGA-co-PDL-PEG ₂₀₀₀ (B) with protons labelled	77
Figure 2-15 FT-IR spectrum of PLGA	79
Figure 2-16 ¹ H-NMR spectrum of PLGA	80
Figure 2-17 FT-IR spectrum of PEG-PLGA	81

Figure 2-18 ¹ H-NMR spectrum of mPEG-PLGA	82
Figure 2-19 DSC of PGA-co-PDL	83
Figure 2-20 DSC of PGA-co-PDL-PEG ₂₀₀₀	84
Figure 2-21 DSC of PLGA	85
Figure 2-22 Resveratrol standard curve ($R^2=0.9981$) with SD as error bars (n=3)	88
Figure 2-23 Effect of storage time on size of PGA-co-PDL NPs in water stored at 4°C ± SD (n=3)	90
Figure 2-24 Effect of storage time on zeta potential of PGA-co-PDL NPs in water stored at 4°C ± SD (n=3)	91
Figure 2-25 Effect of storage time on size of PGA-co-PDL NPs stored at 37°C in water ± SD (n=3)	92
Figure 2-26 Effect of storage time on size of PGA-co-PDL NPs stored at 37°C in media ± SD (n=3)	93
Figure 2-27 Representative Log concentration-viability response curve showing effects of free-resveratrol using Alamar blue assay ± SE	95
Figure 2-28 Representative Log concentration-viability response curve showing effects of 5% resveratrol-loaded NPs using Alamar blue assay ± SE	97
Figure 2-29 Representative Log concentration-viability response curve showing effects of 10% resveratrol-loaded NPs using Alamar blue assay ± SE	99
Figure 2-30 Calu 3 cell viability as determined by Alamar blue assay after 24-hour exposure to blank nanoparticles (BNP), 5% resveratrol-loaded PGA-co-PDL nanoparticles (5% RNP), and 10% resveratrol-loaded PGA-co-PDL nanoparticles (10% RNP). Data represent mean ± standard error of mean for n=3 independent experiments.	101

Figure 2-31 The effects of blank PGA-co-PDL nanoparticles (BNP), 5% resveratrol-loaded PGA-co-PDL nanoparticles (5% RNP), 10% resveratrol-loaded PGA-co-PDL nanoparticles (10% RNP), and free-resveratrol on LDH release in Calu 3 cells after 48 hours. Data represent mean \pm standard error of mean for n=3 independent experiments. 103

Figure 2-32 The effects of blank PGA-co-PDL nanoparticles (BNP), 5% resveratrol-loaded PGA-co-PDL nanoparticles (5% RNP), 10% resveratrol-loaded PGA-co-PDL nanoparticles (10% RNP), and free-resveratrol on LDH release in Calu 3 cells after 72 hours. Data represent mean \pm standard error of mean of n=3 independent experiments 105

Figure 3-1 Illustration of nanocomposite microparticle containing resveratrol-loaded nanoparticles 125

Figure 3-2 Size of PGA-co-PDL nanoparticles vs PGA-co-PDL nanoparticles reconstituted from nanocomposite microparticles in distilled water, n=3. Unpaired t-test was used to compare each pair of means as shown. 135

Figure 3-3 Charge of PGA-co-PDL nanoparticles vs reconstituted PGA-co-PDL nanoparticles from nanocomposite microparticles in distilled water, n=3. Unpaired t-test was used to compare each pair of means as shown. 136

Figure 3-4 SEM images of NCMP-BNPs. Pictures were taken at 3000x and 5000x magnifications 137

Figure 3-5 Thermogram of (a) NCMP-BNP, (B) NCMP-5% RNP, and (c) NCMP-10% RNP 138

Figure 3-6 Resveratrol standard curve using HPLC ($R^2=0.9995$) n=3 139

Figure 3-7 *In vitro* release profile of NCMPs-5% RNP and NCMPs-10% RNP in PBS (pH 7.4) at 37 °C 140

Figure 3-8 Percentage of NCMPs deposited at each stage of the NGI n=4142	
Figure 3-9 The effect of NCMP-5% RNP and NCMP-10% RNP on LDH release in Calu 3 cells after 48 hours	144
Figure 4-1 Structure of 2-phenyl-[1,3]-dioxan-5-ol with protons labelled for NMR	173
Figure 4-2 Structure of 2-phenyl-5-(prop-2-yn-1-yloxy)-1,3-dioxane with protons labelled for NMR	174
Figure 4-3 Structure of 2-(prop-2-yn-1-yloxy)propane-1,3-diol with protons labelled for NMR	175
Figure 4-4 Structure of 1.25 mmol PGA-co-PDL with protons labelled for NMR	176
Figure 4-5 Structure of 1.25 mmol alkyne-PGA-co-PDL with protons labelled for NMR	177
Figure 4-6 FT-IR spectrum of (a) 1.25 mmol PGA-co-PDL and (b) 125 mmol PGA-co-PDL and ¹ H-NMR of (c) 1.25 mmol PGA-co-PDL and (d) 125 mmol PGA-co-PDL	181
Figure 4-7 FT-IR of (a) alkyne-PGA-co-PDL, (b) 50 % alkyne-PGA-co-PDL and (c) 10 % alkyne-PGA-co-PDL showing the gradual re-emergence of the hydroxyl trough and (d) ¹ H-NMR of 10 % alkyne-PGA-co-PDL	182
Figure 4-8 (a) FT-IR and (b) ¹ H-NMR of NDB azide	183
Figure 4-9 (a) FT-IR and (b) ¹ H-NMR spectra of the CuAAC reaction between NBD azide and 10 % alkyne-PGA-co-PDL	184
Figure 4-10 ¹ H-NMR of (a) 2-phenyl-5-(prop-2-yn-1-yloxy)-1,3-dioxane and (b) CuAAC reaction between 2-phenyl-5-(prop-2-yn-1-yloxy)-1,3-dioxane and NBD azide	185

List of Tables

Table 1-1 List of resveratrol <i>in vitro</i> studies against lung cancer cells	14
Table 1-2 List of resveratrol <i>in vivo</i> studies against lung cancer animal models	17
Table 1-3 Resveratrol loaded into polymeric NPs	29
Table 1-4 Delivery of nanocomposite microparticles	46
Table 2-1 Particle size, PDI, and zeta potential of NPs before and after centrifugation	86
Table 2-2 Drug loading and encapsulation efficiency of 5% resveratrol-loaded NPs (RNP) and 10% RNP of various polymeric NPs	89
Table 2-3 Percentage changes in IC ₅₀ for resveratrol-encapsulated NPs compared to free resveratrol	100
Table 3-1 Drug loading and encapsulation efficiency of NCMP-5% RNP and NCMP-10% RNP	139
Table 3-2 Emitted Dose, Respirable Fraction, and Fine Particle Fraction of NCMP-BNP, NCMP-5% RNP, and NCMP-10% RNP	142
Table 4-1 Ratios of glycerol or 2-(prop-2-yn-1-yloxy)propane-1,3-diol integrated into various polymers	168

List of Schemes

Scheme 4-1 Synthesis of (A) 2-phenyl-[1,3]-dioxan-5-ol and (B) 2-phenyl-5-(prop-2-yn-1-yloxy)-1,3-dioxane.....	164
Scheme 4-2 Synthesis of 2-(prop-2-yn-1-yloxy)propane-1,3-diol.....	166
Scheme 4-3 Synthesis of 4-Azido-7-nitro-2,1,3-benzoxadiazole (NBD-azide)	167
Scheme 4-4 Synthesis of alkyne-PGA-co-PDL.....	169
Scheme 4-5 CuAAC reaction of NBD azide with 10 % alkyne-PGA-co-PDL	171
Scheme 4-6 CuAAC reaction of NBD azide with 2-phenyl-5-(prop-2-yn-1-yloxy)-1,3-dioxane.....	172

List of Abbreviations

¹H NMR: Proton Nuclear Magnetic Resonance

2-ME: 2-Methoxyestradiol

AcOH: Acetic Acid

ANOVA: Analysis Of Variance

API: Active Pharmaceutical Ingredient

ATCC: American Type Culture Collection

AUC: Area Under Curve

Avi: Avidin

AviBioCS: Avidin and Biotin Modified Chitosan

Bcl-2: B-Cell Lymphoma 2

Bio: Biotin

BNP: Blank Nanoparticles

BUPA: British United Provident Association

CDCl₃: Deuterated Chloroform

CDK inhibitors: Cyclin-Dependent Kinase Inhibitors

CDK4: Cyclin-Dependent Kinase 4

CDK6: Cyclin-Dependent Kinase 6

CIA: Chemotherapy-Induced Alopecia

CIPN: Chemotherapy-Induced Peripheral Neuropathy

C_{max}: Maximum Concentration

CMCS: Carboxymethyl Chitosan

CRR: Cumulative Resveratrol Release

CS: Modified Chitosan

CuAAC: Copper-Catalysed Azide–Alkyne Cycloaddition

DCM: Dichloromethane

dH₂O: Deionised Water

DIPEA: N,N-Diisopropylethylamine

DL: Drug Loading

DNA: Deoxyribonucleic Acid

DPI: Dry Powder Inhaler

DSC: Differential Scanning Calorimetry

DTX: Docetaxel

DVA: Divinyl Adipate

ED: Emitted Dose

EDC: 1-Ethyl-3-(3-Dimethylaminopropyl)-Carbodiimide

EE%: encapsulation efficiency

EF1A: Elongation Factor 1-Alpha

EGF: Epidermal Growth Factor

EMT: Epithelial–Mesenchymal Transition

EPR: Enhanced permeability and retention effect

ESI: Electrospray Ionisation

fBNPs: Fluorescently-Labelled Bovine Serum Albumin

FBS: Foetal Bovine Serum

FDA: Food and Drug Administration

FOXC2: Forkhead Box Protein C2

FPF: Fine Particle Fraction

FT-IR: Fourier Transform Infra-Red

fWNPs: Fluorescently-Labelled WGA

GPC: Gel Permeation Chromatography

GSD: Geometric Standard Deviation

hbPG: Hyperbranched Polyglycerol

hexyn-pDLLA: Alkyne-Functionalised Homopolymer Of *D,L*-Lactide

HPLC: High Performance Liquid Chromatography

IC₅₀: 50% Inhibitory Concentration

IC₉₀: 90% Inhibitory Concentration

Ikk1: IκB Kinase 1

LDH: Lactate Dehydrogenase

LLC: Lewis Lung Cancer

LNCaP: Prostate Cancer Cell Line

lncRNAs: long Noncoding RNAs

LOD: Limit Of Detection

LOQ: Limit Of Quantification

LPNs: Conjugated Lipid-Polymer Hybrid NPs

MEM: Minimum Essential Medium Eagle

MMAD: Mass Median Aerodynamic Diameter

MMP: Mitochondrial Membrane Potential

mPEG: Poly(Ethylene Glycol) Methyl Ether

mPEG-PLGA: Poly(Ethylene Glycol) Methyl Ether-Block-Poly(Lactide-Co-Glycolide)

MPs: Microparticles

MRT: Mean Residence Time

mTOR: Mammalian Target Of Rapamycin

MTT: 3-(4,5-Dimethylthiazol-2-yl)-2,5-Diphenyltetrazolium Bromide

MWt: Molecular Weight

NAD⁺: Oxidised Nicotinamide Adenine Dinucleotide

NADH: Reduced Nicotinamide Adenine Dinucleotide

NaH: Sodium Hydride

NAPDH: Nicotinamide Adenine Dinucleotide Phosphate Hydrogen

NBD: Nitrobenzoxadiazole

NCMPs: Nanocomposite Microparticles

NF- κ B: Nuclear Factor Kappa-Light-Chain-Enhancer Of Activated B Cells

NGI: Next Generation Impactor

NHS: National Health Service

NMR: Nuclear Magnetic Resonance

Nox5: NADPH Oxidase-5

NP: Nanoparticle

NPs: Nanoparticles

o/w: Oil-in-Water

PADDOCC: Pharmaceutical Aerosol Deposition Device On Cell Cultures

PAHs: Polycyclic Aromatic Hydrocarbons

PBCA: Polybutylcyanoacrylate

PBS: Phosphate Buffered Saline

PCL: Poly(ϵ -Caprolactone)

PDI: Polydispersity Index

PDL: Pentadecalactone

Pdots: Polymer Dots

PEG: Poly(Ethylene Glycol)

PFBT: Poly[(9,9-Dioctylfluorenyl-2,7-Diyl)-co-(1,4-Benzo-{2,1',3}-Thiadiazole)]

PGA-co-PDL: Poly(Glycerol Adipate-Co- ω -Pentadecalactone)

PI3K: Phosphatidylinositol-3-Kinase

PLA: Poly(*D,L*-Lactic Acid)

PLGA: Poly(*D,L*-Lactic-Co-Glycolic Acid)

PLGA–PEO: PLGA-Polyethylene Oxide

pMDI: Pressurized Metered Dose Inhaler

P-OA-CTS: Paclitaxel- Oleic Acid-Conjugated Chitosan NPs

PP2A/C: Protein Phosphatase 2

PQ-CTS-MPs: Co-Loaded P-OA-CTS and Q-OA-CTS Microparticles

PSL: pH Sensitive Liposomes

PSMA: Poly(Styrene-Co-Maleic Anhydride)

PTSA: p-Toluenesulfonic Acid Monohydrate

PVA: Polyvinyl Alcohol

Q-OA-CTS: Quercetin-Oleic Acid-Conjugated Chitosan NPs

Res-AviBioCS: Resveratrol-Loaded Avidin and Biotin Modified Chitosan

Res-CMCSNPs: Resveratrol-Loaded Carboxymethyl Chitosan NPs

Res-Gel: Resveratrol-Loaded Gelatin

Res-GNPs: Resveratrol-Loaded Galactosylated NPs

Res-NPs: Resveratrol NPs Made With PEG

Res-PCL: Resveratrol-Loaded PCL

Res-PEG-PLGA: Resveratrol-Loaded PEG-PLGA

Res-PLGA: Resveratrol Loaded PLGA

Res-PLGA-BNPs: Resveratrol-Loaded PLGA- α -Tocopheryl PEG 1000 Succinate Blend NPs

RF: Respirable Fraction

RNA: Ribonucleic Acid

RNP: Resveratrol-Loaded NPs

ROS: Reactive Oxygen Species

RR: Resveratrol Released

RSV: Resveratrol

SACT: Systemic Anticancer Therapy

SAFC: Sigma-Aldrich Fine Chemicals

SA- β -gal: Senescence-Associated β -Galactosidase

SC: Sildenafil Citrate

SC-PLGA NPs: Sildenafil Citrate-loaded PLGA NPs

SD: Standard Deviation

SE: Standard Error Of Mean

SEM: Scanning Electron Microscopy

SFS: Spray-Dried Free Sildenafil Citrate

SIRT1: Sirtuin 1

SSN: Spray-Dried Sildenafil Nanocomposite

TAMs: Tumour Associated Macrophages

TAS-103: 6-[2-(dimethylamino)ethylamino]-3-hydroxyindeno[2,1-c]quinolin-7-one

TDL: Theoretical Drug Loading

TGA: Thermo Gravimetric Analysis

TGF- β 1: Transforming Growth Factor Beta 1

THF: Tetrahydrofuran

TLC: Thin-Layer Chromatography

T_m: Melting Point

t_{max}: Maximum Time

T-NCMPs: TSA-103-Loaded Nanocomposite Microparticles

ToF: Time Of Flight

TPGS: α -Tocopheryl PEG 1000 Succinate

TPP: Tripolyphosphate

TRAIL: Tumour Necrosis Factor-Related Apoptosis-Inducing Ligand

t-Res: Trans-Resveratrol

USA or US: United States of America

USP: United States Pharmacopeia

w1/o/w2: Water-In-Oil/In-Water

w1/o: Primary Emulsion

w1: First Water Phase

WGA: Wheat Germ Agglutinin

wrt: With Respect To

Abstract

Lung cancer was a rare disease in the latter part of the 19th century, but grew into a full-scale epidemic in the 20th century, becoming the most common cause of cancer-related death worldwide. Current cancer chemotherapy, involves the administration of cytotoxic drugs that kill all cells exhibiting a high rate of proliferation and regeneration, which is a characteristic of cancer cells, but also non-cancerous cells, such as hair follicles, bone marrow and gastrointestinal tract cells. Therefore, the systemic delivery of chemotherapy leads to adverse effects, such as chemotherapy-induced alopecia (CIA) and chemotherapy-induced peripheral neuropathy (CIPN), which can range from life-altering to life-threatening. Moreover, the economic impact of current cancer chemotherapy is unsustainable and, thus, an alternative therapy for lung cancer need to be investigated. Towards this goal, resveratrol-loaded polymeric nanoparticles (NPs) formulated into nanocomposite microparticles (NCMPs) using L-leucine and chitosan were developed for the pulmonary delivery via dry powder inhalation.

Resveratrol was loaded into NPs of poly(glycerol adipate-co- ω -pentadecalactone) (PGA-co-PDL) with sizes ranging between 220-230 nm, which are ideal for uptake into cells. The 5%- and 10% resveratrol-loaded NPs (5% RNP and 10% RNP) had a high encapsulation efficiency of 39 ± 0.12 and $70 \pm 0.89\%$ and a drug loading of 78 ± 0.24 μg and 70 ± 0.89 μg (w/w), respectively. The PGA-co-PDL blank NPs (BNP) at 1 mg/mL showed good cytocompatibility in Calu 3 cells with a cell viability of $87.5 \pm 4.7\%$ after 24-hour exposure. Meanwhile, the 5% RNP and 10% RNP decreased the IC₅₀ of resveratrol in Calu 3 cells after 24 hours from 213 ± 63 μM to 47 ± 30 μM and 48 ± 12 μM , respectively. This is a reduction in IC₅₀ of up to 78%. The PGA-co-PDL NPs were spray-dried in NCMPs with mass median aerodynamic

diameters (MMADs) between 3.1-4 μm , which is within the ideal range of 1-5 μm for particles to be able to deposit in the deep regions of the lung. Furthermore, the NCMPs showed a slow release profile, with only 25% of resveratrol being released over 24 hours. Lastly, a novel polymer was synthesised which possessed an alkyne that can allow for the attachment of various ligands, including a fluorescent probe to visualise uptake of the NPs. Overall, the obtained results demonstrate that these NPs/NCMPs show promise as pulmonary drug delivery systems for lung cancer.

1 CHAPTER 1: General introduction

1.1. Introduction

1.1.1 Lung cancer

1.1.1.1 A brief history of lung cancer

The documented history of lung cancer began in Germany at the Institute of Pathology at the University of Dresden, where in 1878 malignant lung tumours represented just 1% of all cancers discovered during autopsies (Witschi, 2001; Semenova, Nagel and Berns, 2015).

It took 40 years for that number to increase to almost 10% and another decade to reach more than 14% (Witschi, 2001). Dr Isaac Adler, in his 1912 book entitled *Primary Malignant Growths of the Lungs and Bronchi*, could only verify 374 cases of lung cancer reported in the published literature worldwide (Spiro and Silvestri, 2005; Ong and Ost, 2017). In 1910, lung cancer was still such a rarity that Dr Alton Ochsner, one of the early leaders in lung cancer surgery, recalled, while a student at Washington University, being asked to attend the autopsy of a patient with lung cancer since he may never see another case again (Ochsner, 1973). It took 17 years for Dr Ochsner to see another case of lung cancer while working at Charity Hospital in New Orleans (Ochsner, 1973; Spiro and Silvestri, 2005). In less than 6 months, Dr Ochsner witnessed 8 more cases of lung cancer at the hospital and noted all were men, they all smoked heavily and had begun smoking in World War 1; thus began what he called an epidemic (Ochsner, 1973; Spiro and Silvestri, 2005).

What began as a rarity in the latter part of the 19th century grew into a full-scale epidemic in the 20th century and it seems that this trend will continue into the 21st century.

1.1.1.2. *Causes of lung cancer*

It is now understood that smoking is one of the leading causes of lung cancer, but this was not always the case. For many years smoking was considered healthy and even promoted by physicians (Spiro and Silvestri, 2005; Ong and Ost, 2017). About 150 years ago lung cancer was a rarity, but during the turn of the 20th century the disease became more prevalent and this coincided with the increase in tobacco smoking. At first, cigarettes were hand-rolled which made them expensive. However, towards the end of the 20th century a tobacco rolling machine was patented which increased the production of cigarettes. This lowered their price and with World War 1 popularising the smoking of cigarettes amongst soldiers to lower the stress experienced in the trenches, smoking became a popular habit (Witschi, 2001; Ong and Ost, 2017). In the United Kingdom (UK), smoking is linked to 80% of lung cancer cases (Parkin, Boyd and Walker, 2011; Gemine *et al.*, 2019). Research shows that with tobacco control interventions comes a reduction in lung cancer mortality (Hunt *et al.*, 2018; Luo *et al.*, 2019). That said, nearly 10-15% of lung cancer cases develop in patients who were never active smokers (Samet *et al.*, 2009; Dias *et al.*, 2017). As to what can be the cause of lung cancer in never smokers, several epidemiological studies suggest various aetiologies, including second-hand smoking, other inhalable air pollutants such as asbestos, radon, coal, polycyclic aromatic hydrocarbons (PAHs), and nitric oxide, amongst others (Witschi, 2001; Anand *et al.*, 2008; Samet *et al.*, 2009; Raaschou-Nielsen *et al.*, 2011, 2013; Peddireddy, 2016). Some studies point towards an increase in the proportion of lung cancer attributable to never smokers (Toh *et al.*, 2018).

1.1.1.3. Lung cancer statistics

In 1912, only 374 cases of lung cancer were reported (Spiro and Silvestri, 2005; Ong and Ost, 2017). However, in 2018 there were over 2 million new cases of lung cancer reported worldwide (International Agency for Research on Cancer, 2018).

In the UK alone there were 46 388 new cases of lung cancer in 2015 corresponding to 35 620 deaths from lung cancer in 2016 (Cancer Research UK, 2019). Lung cancer is the 3rd most common cancer in the UK (13% of all new cases in 2015) but is by far the most common cause of cancer death (21% of all cancer deaths in males and females combined in 2016) (Cancer Research UK, 2019). It is estimated that in the UK, 1 in 13 (8%) of males and 1 in 15 (7%) females will develop lung cancer in their lifetime (Cancer Research UK, 2019).

Roughly 60% of all newly diagnosed malignant tumours and 70% of all cancer mortality occurs amongst people aged 65 years or older, adding weight to the fact that age is the most significant risk factor for developing cancer (Smith *et al.*, 2009; Al-Mansour, Pang and Bathini, 2019). Demographic data from around the world shows that the median age of the population is increasing with a subsequent increase in cancer incidence (Torre *et al.*, 2016; Bray *et al.*, 2018; Pilleron *et al.*, 2018; Al-Mansour, Pang and Bathini, 2019). This trend leads to the inevitable conclusion that cancer incidence and mortality will increase, leading to concerns about the economic impact.

1.1.1.4. *Economics of lung cancer*

Statistics on the economics of cancer is hard to come by for 2019. However, the annual cost of all cancers to the UK economy was £15.8 billion for 2012 (University of Oxford, 2012). The cost of lung cancer is the highest among all cancers at £2.4 billion per annum with the average lung cancer patient costing the National Health Service (NHS) £9 071 annually in treatments (Taylor, 2012; University of Oxford, 2012). The main drivers of the high cost of lung cancer is the potential wage loss due to premature deaths from people in employment, which accounts for roughly 60% of the total economic costs, and the high health care costs (University of Oxford, 2012). That said, there are both direct and indirect costs of cancer.

The direct costs of cancer include the cost of medication and administration of the treatment on the NHS. Innovation in cancer therapeutics is making the drugs more and more expensive, driving up the cost of cancer treatment. There is a growing body of evidence that suggests modern oncology drugs are unaffordable and that it is becoming unsustainable for healthcare providers, such as the NHS, to make these drugs available (Sullivan *et al.*, 2011; Kantarjian and Patel, 2017). Studies have shown that the anticancer drugs and the administration of these drugs make up almost 50% of the cost of treating cancer (Storme *et al.*, 2016). There has been an overall increase of 88.6% in new systemic anticancer therapy (SACT) courses for lung cancer over a 5 year period from 2013-2018 (Bhimani *et al.*, 2019). The number of treatment-related attendances for either intravenous or oral therapies for lung cancer saw an increase of 109% (Bhimani *et al.*, 2019). There is also concern that this increase in patient numbers and patient treatment visits, along with

the complexity and lengthy treatment times, would lead to a scarcity of cancer specialists as the demand outstrips the supply (Yang *et al.*, 2014; Cancer Research UK, 2017; Bhimani *et al.*, 2019). This concern has already been realised as NHS England reported that their ability to meet their own target of 96% of patients with cancer starting treatment within 31 days of diagnosis, is slowly decreasing since they lack the diagnostic capacity to cope with the increasing number of patients (Burki, 2019). Evidence suggests that this will only worsen with time (Appleby, 2019). The concern is that as these trends are projected to increase, it would hinder the ability of the NHS to treat cancer, leading to a decrease in the rate of cancer survival (Bupa, 2011; NHS, 2011).

Although the direct costs of cancer are important for the providers of care, indirect costs can also impact the receiver of the care (the patient). When diagnosed with cancer, the patient is faced with a myriad of burdens; emotional, financial, and physical. The emotional and physical burdens come from the effect of the cancer on the patient's body and mind, as well as their families/caregivers. Direct financial costs, such as anticancer medication, are handled by the NHS, but the indirect financial costs, for example, transportation to and from the health care facility for treatment, child care, and lost wages are some of the burdens that the patients and their families have to bear (Kim, 2007; CLIC Sargent, 2019). These indirect costs can lead to financial distress on top of the angst that comes with the cancer diagnosis itself. Evidence shows that financial distress could impact the successful completion of the treatment and, in turn, could impact survival rates (Gordon *et al.*, 2009; Zafar *et al.*, 2013; Bestvina *et al.*, 2014; Peppercorn, 2014; Callahan and Brintzenhofeszoc, 2015; Yousuf Zafar, 2016; Altice *et al.*, 2017).

It is quite evident that both the direct as well as the indirect costs of cancer put tremendous strain on the resources of all stakeholders, patients and the NHS. This strain could lead to a decrease in the positive outcomes of the treatment. A report compiled by BUPA gave a few suggestions on how to use resources more efficiently, including finding new ways to address the cost of tests and treatments for cancer, making it easier for people to navigate their cancer treatment pathway, and most importantly, changing how and where cancer patients and survivors are treated (Bupa, 2011). It was suggested that the option to receive chemotherapy at home should be a standard choice for patients (Bupa, 2011). The studies proposing homebased chemotherapy cite several benefits, such as a reduction in the amount of time spent in the hospital (which lowers the cost to the NHS), reduction in anxiety levels, not having to worry about getting to a hospital on time, reduced travel costs to patients and decreased exposure to others who may be seriously ill (Nursing Times, 2002; O'Neill and Wallis, 2009; Tralongo *et al.*, 2011; Crisp *et al.*, 2014; Evans *et al.*, 2016).

This project will aim to propose a way to reduce costs by advocating chemotherapy at home by administering resveratrol loaded into nanocomposite microparticles (NCMPs) via pulmonary delivery.

1.1.2. Side-effects of current cancer chemotherapy treatment

About of 70% lung cancers are diagnosed during the advanced stages of the disease where surgery or radiation alone may no longer be viable options (Travis, Brambilla and Riely, 2013).

Chemotherapy is considered the first line therapy for advanced stages of lung cancer. Cancer chemotherapy, involves the administration of cytotoxic drugs that kill all cells exhibiting a high rate of proliferation and regeneration (Feitelson *et al.*, 2015). Targeting of cells with high proliferation and regeneration rates means that the cytotoxic drugs not only affects cancer cells, but also rapidly dividing non-cancerous cells such as skin cells, hair matrix cells, hematopoietic cells of the bone marrow, and epithelium cells of the mouth and gastrointestinal tract. This leads to the common side effects of loss of hair (alopecia), impaired bone marrow function, nausea and vomiting (Trüeb, 2009; Wagland *et al.*, 2016). This process of normal cells and tissues being affected is known as chemotherapy toxicity (Maguire *et al.*, 2018). Chemotherapy toxicity may result in symptoms that range from distressing (e.g. breathlessness, nausea, vomiting) to dangerous (e.g. neutropenia) and have been associated with a decreased quality of life, poor treatment adherence, and ultimately increased mortality, which in turn drives up the cost of cancer for health care systems (McKenzie *et al.*, 2011; Maguire *et al.*, 2018). Chemotherapy-induced alopecia (CIA) is the most neglected side effect of chemotherapy and, while not life-threatening, has a lot of stigma attached to it and reports suggest that it would lead 8% of people rejecting chemotherapy treatment (Hesketh *et al.*, 2004; van den Hurk *et al.*, 2015; Rubio-Gonzalez *et al.*, 2018). CIA affects about 65% of those receiving chemotherapy, depending

on the type of medication and treatment regimen (Suchonwanit and McMichael, 2018). Although in most cases CIA is temporary, there are cases where it results in permanent hair loss (Kang *et al.*, 2019). CIA has a severe effect on quality of life for patients undergoing chemotherapy (Hesketh *et al.*, 2004; Freitas-Martinez *et al.*, 2019). Another chemotherapy-induced side effect that leads to a reduction in quality of life, is peripheral neuropathy. Chemotherapy-induced peripheral neuropathy (CIPN) occurs in up to 80% of patients receiving oxaliplatin and paclitaxel, which are commonly used in the treatment of lung cancer (De luliis *et al.*, 2015). If use of the treatment persists it often leads to increased severity and permanent damage to the patient causing impaired function (Ezendam *et al.*, 2014).

Although CIA may not be life-threatening, the consequences for the patients experiencing it may be as life-altering and devastating as CIPN and other chemotherapy side effects and should be considered when evaluating treatment options. After all, the primary goal of the therapy is not only the prolonging of life, but also the preservation of the quality of life (Mols *et al.*, 2014).

It is with that in mind, that the aim of this project is to establish the viability of using NCMPs to deliver resveratrol to the lungs via pulmonary delivery to cut down on the possible side effects.

1.1.3. Resveratrol as an alternative treatment for lung cancer treatment

1.1.3.1. Phenolic compounds

Phenolic compounds are diverse in structure, but are characterised as having at least one aromatic ring possessing one or more hydroxyl groups (Harborne, 1999; Yang *et al.*, 2018). Several classes of phenolic compounds exist, namely, flavonoids, phenolic acids, phenolic alcohols, stilbenes and lignans (Harborne, 1991; Sarker and Nahar, 2019). They are produced as secondary metabolites by the plants as a defence to various stressors, including oxidative stress (Heleno *et al.*, 2015). Several phenolic compounds have been shown to have anti-lung cancer properties, both *in vitro* and *in vivo* (Fantini *et al.*, 2015; Hashemzaei *et al.*, 2017; Duan *et al.*, 2019; Lakshmi *et al.*, 2019; Muller *et al.*, 2019; Santos *et al.*, 2019). Resveratrol is one of the phenolic compounds that has shown potential (Feng, Zhou and Jiang, 2016; Sun *et al.*, 2017; Elshaer *et al.*, 2018; Monteillier *et al.*, 2018; Rauf *et al.*, 2018; Saha *et al.*, 2018).

1.1.3.1.1. Resveratrol

Resveratrol (*trans*-3,5,4'-trihydroxystilbene) is the most common natural stilbene found abundantly in a large number of fruits and vegetables, most notably grapes (**Figure 1-1**) (Francioso *et al.*, 2014). It has anti-inflammatory, anti-oxidative, proapoptotic and cell cycle arrest properties (Albuquerque *et al.*, 2015; Yu *et al.*, 2016).

A systematic review reported that resveratrol inferred a relative risk reduction of 0.64 (p=0.002) for tumour incidence compared to a control group (Feng, Zhou and Jiang, 2016).

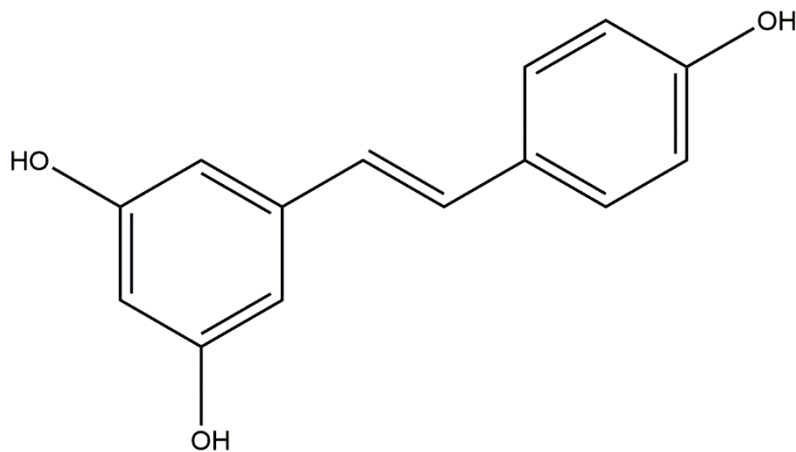


Figure 1-1 Chemical structure of resveratrol

1.1.3.1.1.1. *In vitro* evidence of efficacy against lung cancer

There are numerous studies that have looked at the effect of resveratrol as a single therapeutic agent in various lung cancer cells, but only the evidence accumulated over the last 10 years will be summarised here (**Table 1-1**). Resveratrol (20, 50 & 100 μM) inhibited the phosphatidylinositol-3-kinase (PI3K) pathway and decreased mammalian target of rapamycin (mTOR) phosphorylation in A549, A427 and NCI-H23 cells (Ebi *et al.*, 2009). SPC-A-1 cells treated with resveratrol (20, 50 & 100 μM) showed decreased proliferation, increased apoptosis and cell cycle arrest caused by activation of caspase-3 and reduced survivin levels (Zhao *et al.*, 2010). It was found that resveratrol (12.5, 25, & 50 μM) administered to 16HBE-T and H460 cells caused upregulation of miR-622 expression (a downstream target of K-ras) resulting in a reduction in cell viability and proliferation and initiation of G0 cell cycle arrest (Han *et al.*, 2012). Resveratrol (50 μM) induced autophagic degradation of P62 activating caspase-8-mediated Beclin-1 cleaving, which resulted in apoptosis in A549 cells (Zhang *et al.*, 2015). In A549 and H460

cells, resveratrol (10, 20, & 50 μM) was shown to increase senescence-associated β -galactosidase (SA- β -gal), NADPH oxidase-5 (Nox5), p53 and p21 expression, while decreasing elongation factor 1-alpha (EF1A) expression and causing reactive oxygen species (ROS)-mediated deoxyribonucleic acid (DNA) damage leading to inhibition of cell growth. Resveratrol (10 μM) inhibited cell viability and induced G2/M cell cycle arrest and apoptosis by increasing p53, p21, and tumour necrosis factor-related apoptosis-inducing ligand (TRAIL) receptor 1 and 2 expression, while downregulating B-cell lymphoma 2 (Bcl-2), cyclin D, nuclear factor kappa-light-chain-enhancer of activated B cells (NF- κ B) and I κ B kinase 1 (I κ k1) expression in A549 cells pre-treated with Benzo(a)pyrene (20 μM), a carcinogenic polycyclic aromatic hydrocarbon (Ulasli *et al.*, 2013). Resveratrol (2, 4, 8, 16, 32, & 64 μM) caused a dose-dependent inhibition of A549 cells via caspase 3 activation (Yin *et al.*, 2013). Another study showed the effect of resveratrol (5.5-175.2 μM) on activation of caspase 3 and subsequent cell inhibition and viability (Lucas and Kolodziej, 2015). Resveratrol (25 μM) was also shown to downregulate AK001796, long noncoding RNAs (lncRNAs), that acts as an oncogene in lung cancer carcinogenesis (Yang *et al.*, 2015). This downregulation results in reduced cell viability and increased cell cycle arrest, which results in a reduction in cell proliferation (Yang *et al.*, 2015). Yang *et al.* administered resveratrol (25-150 μM) to A549 cells which caused decreased cell proliferation and G0/G1 cell cycle arrest in a p53-independent manner. Resveratrol (20 μM) showed the ability to inhibit CL1-5, A549, H322 and H1435 tumour cell migration by upregulating miR-520h-mediated protein phosphatase 2 (PP2A/C) expression leading to inactivation of NF- κ B and

further inhibition of the expression of forkhead box protein C2 (FOXC2), an important factor in epithelial–mesenchymal transition (EMT), which correlate with tumour metastasis (Yu *et al.*, 2013). In another study, resveratrol (10-40 μ M) was shown to inhibit the invasion and migration of A549 cells by preventing transforming growth factor beta 1 (TGF- β 1) induced EMT (Wang *et al.*, 2013).

Table 1-1 List of resveratrol *in vitro* studies against lung cancer cells

Cancer Cell Line	Dose/Duration	Findings	Mechanism	Reference
A549, A427 and NCI-H23	20, 50, 100 μ M for 2, 4 or 8 h	<ul style="list-style-type: none"> ↓ PI3K pathway ↓ tumour formation 	<ul style="list-style-type: none"> ↓ mTOR phosphorylation 	Ebi <i>et al.</i> , 2009
SPC-A-1	20, 50, 100 μ M for up to 96 h	<ul style="list-style-type: none"> ↓ cell proliferation ↑ apoptosis ↑ cell cycle arrest 	<ul style="list-style-type: none"> ↑ caspase-3 ↓ survivin levels 	Zhao <i>et al.</i> , 2010
16HBE-T and H460	12.5, 25, 50 μ M for 48 h	<ul style="list-style-type: none"> ↓ cell proliferation ↓ cell viability ↑ cell cycle arrest 	<ul style="list-style-type: none"> ↑ G0 cell cycle arrest ↑ miR-622 expression K-ras is downstream target of miR-622 	Han <i>et al.</i> , 2012
A549	50 μ M for up to 96 h	<ul style="list-style-type: none"> ↑ apoptosis ↑ autophagy 	<ul style="list-style-type: none"> Degradation of P62 Activation of caspase-8 	Zhang <i>et al.</i> , 2015
A549 and H460	10, 20, 50 μ M 24 h to 10-12 days	<ul style="list-style-type: none"> ↓ cell growth 	<ul style="list-style-type: none"> ↑ SA-B-gal ↑ p53 and p21 expression ↓ EF1A expression ↑ DNA damage ↑ ROS ↑ Nox5 expression 	Luo <i>et al.</i> , 2013

Cancer Cell Line	Dose/Duration	Findings	Mechanism	Reference
A549	20 μ M Benzo(a)pyrene for 48 h pre-treatment + 10 μ M resveratrol for 24 h	<ul style="list-style-type: none"> ↑ G2/M cell cycle arrest ↑ apoptosis ↓ cell viability 	<ul style="list-style-type: none"> ↑ p21 and p53 ↑ TRAIL receptor 1 and 2 ↓ Bcl-2 and cyclin D ↓ NF-κB and IKK1 	Ulasli <i>et al.</i> , 2013
A549	2, 4, 8, 16, 32, 64 μ M for 48 h	<ul style="list-style-type: none"> ↑ cell inhibition 	<ul style="list-style-type: none"> ↑ caspase-3 	Yin <i>et al.</i> , 2013
A549	5.5-175.2 μ M for 24h	<ul style="list-style-type: none"> ↓ cell viability 	<ul style="list-style-type: none"> ↑ caspase-3 	Lucas and Kolodziej, 2015
A549	25 μ M for 48 h	<ul style="list-style-type: none"> ↓ cell proliferation ↓ cell viability ↑ cell cycle arrest 	Downregulation of AK001796	Yang <i>et al.</i> , 2015
A549	25, 50, 100, 150 μ M for 24, 48, 72 h	<ul style="list-style-type: none"> ↓ cell proliferation G0/G1 cell cycle arrest 	<ul style="list-style-type: none"> ↑ p53 nuclear expression ↓ cyclin D1, CDK4, CDK6 expression ↑ CDK inhibitors (p21 & p27) 	Yuan <i>et al.</i> , 2015
CL1-5, A549, H322 and H1435	20 μ M for 48 h	<ul style="list-style-type: none"> ↑ tumour suppression ↓ cell migration 	<ul style="list-style-type: none"> ↑ miR-520h-mediated PP2A/C expression ↓ FOXC2 expression 	Yu <i>et al.</i> , 2013
A549	10-40 μ M for 48 h	<ul style="list-style-type: none"> ↓ cell migration ↓ cell invasion 	Preventing TGF- β 1-induced EMT	Wang <i>et al.</i> , 2013

1.1.3.1.1.2. *In vivo* evidence of efficacy against lung cancer

In contrast to *in vitro* studies, *in vivo* studies for resveratrol as a single therapeutic agent against lung cancer are a little harder to come by (**Table 1-2**). Resveratrol (1 or 3 g/kg/day) consumed in the diet for 28 days inhibited tumour growth in BALB/c mice injected subcutaneously with SPC-A-1 cells into their flanks (Zhao *et al.*, 2010). Sun *et al.* showed that resveratrol (20 mg/kg) for 25 days led to an inhibition of metastasis and sirtuin 1 (SIRT1), the class III deacetylase, activation leading to a suppression of EMT in Nude mice inoculated with A549 cells (Sun *et al.*, 2013). Similarly, nude mice inoculated with A549 cells and then treated with resveratrol (15, 30 or 60 mg/kg) injections for 15 days showed a dose-dependent inhibition of lung cancer cell growth (Yin *et al.*, 2013). C57BL/6 mice were subcutaneously injected with Lewis lung cancer (LLC) tumour cells. After 10 days, the mice were treated with resveratrol (100 mg/kg) for 4 weeks and then sacrificed. It was found that resveratrol reduced expression of F4/80 positive cells, a type of antigen found on mouse macrophage cells and M2 polarisation in tumours leading to inhibition of lung cancer cell growth (Sun *et al.*, 2017). Tumour associated macrophages (TAMs) have an important role in cancer progression and evasion of the immune system and inhibition of M2 polarisation of TAMs is an effective therapy for cancer (Ostuni *et al.*, 2015).

Table 1-2 List of resveratrol *in vivo* studies against lung cancer animal models

Animal Model	Dose/Duration	Findings	Mechanism	Reference
18 female BALB/c mice injected with SPC-A-1 cells	Diet supplemented with 1 or 3 g/kg/day resveratrol for 28 days	↓ tumour growth	No mechanism identified	Zhao <i>et al.</i> , 2010
4-6 weeks old nude mice inoculated with A549 cells	20 mg/kg resveratrol every other day for 25 days	↓ metastasis	Activation of SIRT1	Sun <i>et al.</i> , 2013
old nude mice inoculated with A549 cells	15, 30 or 60 mg/kg resveratrol injections for 15 days	↓ lung cancer growth	No mechanism identified	Yin <i>et al.</i> , 2013
C57BL/6 mice injected with LLC tumour cells	100 mg/kg resveratrol 10 days after injection for 4 weeks	↓ lung cancer growth	↓ F4/80+ macrophages expression ↓ M2 polarisation	Sun <i>et al.</i> , 2017

1.1.3.1.2. Bioavailability

Both the *in vitro* and *in vivo* studies on the effects of resveratrol against lung cancer shows that there is great promise for its therapeutic application to treat cancer, but one major hindrance to this use is the low bioavailability resveratrol exhibits. Bioavailability refers to the fraction of the drug, i.e. resveratrol, that reaches the bloodstream unaltered (Peng *et al.*, 2018).

According to the Biopharmaceutical Classification System (BCS), resveratrol, due to its poor water solubility and high membrane permeability, is classified as a class II compound (Santos *et al.*, 2019). Resveratrol has relatively high oral absorption (at least 70% absorbed), but has a low oral bioavailability (Walle *et al.*, 2004; Chimento *et al.*, 2019). It is postulated that the low oral bioavailability could be due to the rapid sulphate conjugation of resveratrol by the liver/intestine (Walle *et al.*, 2004; Chimento *et al.*, 2019). Resveratrol is rapidly metabolised into several forms including, resveratrol 3-O-glucuronide, resveratrol 4-O-glucuronide, and resveratrol trisulphate, that retain some biological effects (Gambini *et al.*, 2015; Wang and Sang, 2018).

Several studies in humans concluded that after oral administration of approximately 25 mg resveratrol, the blood plasma concentration of the free form of resveratrol was between 1 and 5 ng/mL (Soleas, Yan and Goldberg, 2001a, 2001b; Almeida *et al.*, 2009; Loira-Pastoriza, Todoroff and Vanbever, 2014). Higher doses of resveratrol (up to 5 g) yielded blood plasma levels of 539 ng/mL for free resveratrol (Boocock *et al.*, 2007). Repeated doses, 13 in total, of resveratrol (150 mg each) in 2 days did not yield better results, with a maximum plasma level of 64 ng/mL (Almeida *et al.*, 2009; Wang and Sang, 2018).

Resveratrol has shown to be effective *in vivo*, despite having a low oral bioavailability. This could be due to target organs such as the liver converting the resveratrol metabolites back into its original form, enterohepatic recirculation of the metabolites, followed by deconjugation and reabsorption, or it could all just be due to the metabolites and their own activity (Gambini *et al.*, 2015).

In vitro studies of the effects of resveratrol on lung cancer are quite promising, but concerns arise when trying to replicate the effects *in vivo*. In mammalian models, resveratrol, despite being lipophilic, shows poor oral bioavailability due to its extensive metabolism and rapid elimination (Wang and Sang, 2018). The *in vitro* studies indicate what resveratrol can do once accumulated at the site of action and in sufficient concentration. However, in reality when orally ingesting resveratrol from your diet, it has to navigate many obstacles to get to the bloodstream and ultimately the site of action. Phenolic compounds, such as resveratrol, degrade in the high acidity environment of the stomach which can cause uncontrolled release which, in turn, can cause decreased absorption from the intestines (Esfanjani, Assadpour and Jafari, 2018). Therefore, it is not possible to obtain, via the oral route, the concentration of resveratrol necessary to have the effects described in the *in vitro* studies.

Resveratrol seems to be well tolerated with minimal side effects, even, at very high concentrations (Patel *et al.*, 2011). There is tremendous potential for resveratrol, as evident by the preclinical testing, but it is yet to fully be realised in human trials (Tomé-Carneiro *et al.*, 2013; Borriello *et al.*, 2014; Singh, Ndiaye and Ahmad, 2015). The crux of the matter is the low oral bioavailability of resveratrol and, therefore, the focus should be on improving the

pharmacokinetic profile of resveratrol (Chimento *et al.*, 2019). Towards this endeavour nanoparticulate drug delivery systems could efficiently transport the resveratrol to the site of action.

1.1.4. Nanoparticulate delivery systems

Nanoparticles (NPs) and liposomes are useful strategies to overcome the poor absorption, rapid metabolism, and elimination inherent in most natural products; helping to increase their bioavailability and target specific sites, such as the lung tumour cells. Several different nanoparticle (NP) systems exist that have been used to improve the bioavailability and efficacy of nutraceuticals, such as resveratrol (Arora and Jaglan, 2016). These NP systems include, liposomes, micelles, and polymeric NPs.

1.1.4.1. *Polymeric nanoparticulate drug delivery system*

Polymeric NPs refer to colloidal systems with a spherical or irregular shape that either encapsulates or entraps a biologically active substance (Vittorio *et al.*, 2017). The advantages of polymeric NPs include; controllable physico-chemical properties, high stability, homogenous size distribution, high drug encapsulation, and controllable drug release (Hu, Aryal and Zhang, 2010; Farooq *et al.*, 2019). The therapeutic agents (i.e. resveratrol) can be delivered through adsorption, encapsulation, or conjugation either internally or on the surface of the polymeric NPs (Ahmadi, Mohammadinejad and Ashrafizadeh, 2019). Numerous biodegradable polymers, both synthetic and natural, can be utilised to create polymeric NPs, including poly(*D,L*-lactic-co-glycolic acid) (PLGA), poly(*D,L*-lactic acid) (PLA), poly(ϵ -caprolactone) (PCL), chitosan and gelatin (Kumari, Yadav and Yadav, 2010).

The United States of America (USA) Food and Drug Administration (FDA) have approved PLA and PLGA for human applications. PLA and PLGA are broken down in an organism into their biodegradable biocompatible monomeric building blocks, lactic and glycolic acid, which can enter cell metabolic pathways (Kumari, Yadav and Yadav, 2010; Chereddy, Payen and Pr  at, 2018). When PLA and PLGA are administered intravenously, they are normally quickly cleared by the immune system of the host (Siddiqui *et al.*, 2009; Sharma *et al.*, 2016). To combat this, and increase the circulation time, NPs are often coated with poly(ethylene glycol) (PEG), a polymer that can aid in evading clearance by the immune system (Sanchez, Yi and Yu, 2016). Chitosan is a natural polycationic linear polysaccharide, that has been shown to be mucoadhesive, non-immunogenic and non-toxic (Cheung *et al.*, 2015). Gelatin is a protein-based biopolymer that is highly biocompatible and biodegradable with low toxicity and low antigenicity (Karthikeyan, Hoti and Prasad, 2015).

Polymeric NPs have been extensively studied for their drug delivery capacity (**Table 1-3**). PLGA is, due to FDA approval, the most popular polymer used for NP delivery. It is safe and highly stable in colloidal suspensions and particles have been shown to have controlled release properties (Jensen *et al.*, 2012; Sharma *et al.*, 2016). PLGA NPs with or without chitosan coating have cytocompatibility with A549 cells at concentrations as high as 5 mg/mL (Tahara *et al.*, 2009).

Resveratrol-loaded PLGA (Res-PLGA) NPs were prepared via nanoprecipitation and compared with free-resveratrol against a prostate cancer cell line (LNCaP) (Nassir *et al.*, 2018). Encapsulation of resveratrol in

the Res-PLGA NPs decreased the IC₅₀ and IC₉₀ by nearly half as compared to the free-resveratrol, 15.6 µM and 41.1 µM and 9.7 µM and 77.2 µM, respectively (Nassir *et al.*, 2018). It was shown that Res-PLGA induced apoptosis in LNCaP cells through cell cycle arrest, DNA damage, externalisation of phosphatidylserine, generation of reactive ROS, and loss of mitochondrial membrane potential (MMP) (Nassir *et al.*, 2018). The Res-PLGA showed cytocompatibility with murine macrophages even at 200 µM (Nassir *et al.*, 2018). A solvent diffusion technique, using PLGA, N-oleoyl-d-galactosamine and Tween 80, was employed to synthesise resveratrol-loaded galactosylated NPs (Res-GNPs) and compared with both resveratrol NPs made with PEG (Res-NPs) and free-resveratrol (Siu *et al.*, 2018). The Res-GNPs presented with a high encapsulation efficiency (EE%) (97.22% ± 2.31%) and a slow release profile (Siu *et al.*, 2018). To assess oral bioavailability, Sprague-Dawley rats were given either, resveratrol suspensions (dispersed in 0.3% carboxymethylcellulose sodium solution) (intra-gastric), Res-NPs (intra-gastric), Res-GNPs (intra-gastric) or resveratrol solution (intravenous) (Siu *et al.*, 2018). Intra-gastric and intravenous preparations were administered 40 mg/kg and 8 mg/kg, respectively. Compared with resveratrol suspensions (intra-gastric), the administration of Res-NPs (intra-gastric) and Res-GNPs (intra-gastric) resulted in a 165.7% and 335.7% increase in the relative bioavailability (AUC), respectively (Siu *et al.*, 2018). Res-GNPs administration to mouse macrophage RAW 264.7 cells caused a significant decrease in proinflammatory cytokines (Interleukin 6 (IL)-6, nitrous oxide (NO), and tumour necrosis factor (TNF)-α) as compared with Res-NPs and free-resveratrol (Siu *et al.*, 2018). A single-emulsion solvent evaporation technique was utilised to

synthesise resveratrol-loaded PLGA- α -tocopheryl PEG 1000 succinate (TPGS) blend NPs (Res-PLGA-BNPs) (Vijayakumar *et al.*, 2016). The Res-PLGA-BNPs had an EE% of 31.79–61.81%, depending on the ratio of PLGA:TPGS, with a sustained release profile (Vijayakumar *et al.*, 2016). The MTT assay was used to evaluate the *in vitro* cytotoxicity of resveratrol, RSV-PLGA-BNPs and blank PLGA-BNPs on C6 glioma cells. The RSV-PLGA-BNPs showed the highest cytotoxicity and subsequent tests using coumarin 6 attached to the PLGA-BNPs showed good cellular uptake in the C6 glioma cells (Vijayakumar *et al.*, 2016). Charles Foster rats were used in the pharmacokinetic and tissue distribution studies. The rats were intravenously injected with either resveratrol solubilised using β -cyclodextrin (0.3 M) or RSV-PLGA-BNPs (equivalent to 2 mg/kg of resveratrol). The RSV-PLGA-BNPs had an increased systemic circulation of time (up to 36 h) and a 18-fold higher plasma half-life compared to free-resveratrol (Vijayakumar *et al.*, 2016). More recently, trans-resveratrol (t-Res) nanocrystals were prepared via probe sonication using TPGS as a stabiliser and lecithin and pluronic F127 as co-stabilisers (Singh *et al.*, 2017). Sprague Dawley rats were orally administered, either, the t-Res nanocrystals or a resveratrol suspension, both equivalent to 20 mg/kg. Results showed that t-Res nanocrystals increased the C_{max} (2.2-fold), area under curve (AUC), (3.5-fold) and mean residence time (MRT) (1.2-fold) as compared to free-resveratrol (Singh *et al.*, 2017). All this evidence points to an overall increase in bioavailability produced by the t-Res nanocrystals. The reasons given for the increase included, enhanced nanocrystal dissolution in the gastrointestinal fluid, increased bio-adhesion and/or direct uptake of nanocrystals across the intestinal barrier (Singh *et al.*, 2017). The

nanoprecipitation method was used to produce resveratrol-loaded PLGA (Res-PLGA) NPs (Singh and Pai, 2014). The Res-PLGA NPs had an EE% of between 42-72% with a long, sustained release profile over 12 days (Singh and Pai, 2014). *In vivo* pharmacokinetic studies and biodistribution assays were performed via oral administration of the Res-PLGA NPs to male Wistar rats. The Res-PLGA increased bioavailability (10.6-fold increase in AUC values, 28-fold increase in t_{max} and 1.2-fold increase in C_{max} values compared with free-resveratrol) (Singh and Pai, 2014). Resveratrol-loaded PEG-PLGA NPs (Res-PEG-PLGA) were prepared using double emulsion solvent evaporation (Li *et al.*, 2016). The Res-PEG-PLGA NPs had an EE% of 68.2% and showed sustained release for more than 13 days (Li *et al.*, 2016). The *in vitro* cytotoxicity studies performed on HepG2 liver cancer cells showed a time- and dosage-dependent inhibition of cell growth caused by the Res-PEG-PLGA NPs (Li *et al.*, 2016).

Resveratrol-loaded PEG-PLA NPs showed dose-dependent inhibitory effects on CT26 colon cancer cell viability and proliferation (Jung *et al.*, 2015). BALB/c nude mice injected with CT26 colon cancer cells to form a tumour were used as an animal model for the *in vivo* studies. When the tumour mass grew to a visible size, the mice were injected with either empty PEG-PLA NPs or RSV-PEG-PLA NPs twice per week for 21 days (Jung *et al.*, 2015). Subsequent analysis showed a significant decrease in tumour growth with an increase in survival of the mice that received the RSV-PEG-PLA NPs as compared with the empty PEG-PLA NPs (Jung *et al.*, 2015).

Resveratrol-loaded PCL nanocapsules (Res-PCL) were prepared using interfacial deposition followed by solvent displacement (Carletto *et al.*, 2016).

The Res-PCL had a very high EE% (97%) and reduced cell viability of B16F10 murine melanoma cells (Carletto *et al.*, 2016). C57BL/6J mice were subcutaneously injected with B16F10 cells (5×10^4) into their posterior flank. About 10 days after the injection, the mice developed a visible and palpable tumour. Then, the mice were either given no treatment, blank PCL nanocapsules, Res-PCL nanocapsules (5 mg/kg/day), or free-resveratrol (5 mg/kg/day). The mice treated with Res-PCL nanocapsules showed a statistically significant decrease in tumour volume as compared with the other groups (Carletto *et al.*, 2016).

An ionic cross-linking method was used to prepare resveratrol-loaded chitosan-sodium tripolyphosphate (TPP) NPs (J. Wu *et al.*, 2017). Particle size analysis showed that the chitosan-TPP NPs were between 172–217 nm (J. Wu *et al.*, 2017). The highest EE% obtained was 11.1%, which is quite low, and the NPs had a biphasic release with an initial burst for 2 hours followed by a slow and sustained release. The resveratrol-loaded chitosan-TPP NPs elicited a 10-30% increase in antioxidant activity as compared with the free-resveratrol (J. Wu *et al.*, 2017). Fluorescence microscopy and the MTT assay were used to show cellular uptake and cytotoxicity, respectively, in both human hepatocellular carcinoma cells SMMC7721 and human normal hepatocyte cells LO2 (J. Wu *et al.*, 2017). The resveratrol-loaded chitosan-TPP NPs had a higher uptake and increased cytotoxicity as compared with free-resveratrol against the cancerous cell line, but had a lower cytotoxic effect than free-resveratrol on the normal cell line (J. Wu *et al.*, 2017). Emulsion cross-linking was used to prepare resveratrol-loaded carboxymethyl chitosan NPs (Res-CMCSNPs) (Zu *et al.*, 2016). The Res-CMCSNPs had an EE% of 44.5% and

the *in vitro* drug release in simulated GI tract gave a delayed release profile as compared to free-resveratrol (Zu *et al.*, 2016). Six healthy male Sprague-Dawley rats were separated into two groups and orally administered, either, free-resveratrol or Res-CMCSNPs (both 50 mg/kg dosage equivalent resveratrol). The resveratrol absorption and bioavailability in rats was enhanced, 3.5 times higher, when encapsulated as compared to non-encapsulated resveratrol (Zu *et al.*, 2016). Bu *et al.*, prepared resveratrol-loaded avidin (Avi) and biotin (Bio) modified chitosan (CS) (Res-AviBioCS). The Res-AviBioCS NPs had a good EE% (66.4%) with a sustained release profile (Bu *et al.*, 2013). Kunming mice (4 groups of 28) were injected (0.25 mg/kg) with, either, free-resveratrol, resveratrol-loaded CS NPs, Bio-CS NPs, and Res-AviBioCS NPs. Compared with free-resveratrol, the Res-AviBioCS NPs showed an AUC that was 2.6-fold higher, t_{max} that was 25-fold higher, and an MRT which was 4.5-fold greater (Bu *et al.*, 2013).

Resveratrol-loaded gelatin (Res-Gel) NPs were synthesised through a coacervation-phase separation technique (Karthikeyan *et al.*, 2013). The Res-Gel NPs had a very high EE% (93.6%) and a sustained release profile over 2 days (Karthikeyan *et al.*, 2013). NCI-H460 non-small cell lung cancer cells were used to assess the *in vitro* uptake and cytotoxicity of Res-Gel NPs. Compared to free-resveratrol, the Res-Gel NPs had a very rapid and enhanced cellular uptake, higher generation of ROS, DNA damage, apoptotic incidence and reduced the IC₅₀ by half from 10 µg/mL for free-resveratrol to 5 µg/mL for Res-Gel NPs (Karthikeyan *et al.*, 2013). Swiss albino mice (2 groups of 6) were intravenously administered (10 mg/kg) free-resveratrol or Res-Gel

NPs. The resveratrol serum concentration of the mice treated with Res-Gel NPs were twice as high as the mice treated with free-resveratrol.

Epidermal growth factor (EGF) conjugated lipid-polymer hybrid NPs (LPNs) were synthesised to co-deliver docetaxel (DTX) and resveratrol for lung cancer therapy (Song *et al.*, 2018). The EGF-LPNs had an encapsulation efficiency (EE%) of 90% with a sustained release profile (Song *et al.*, 2018). Flow cytometry showed significantly higher uptake of blank and DTX/resveratrol loaded EGF-LPNs as compared with normal LPNs and the free drugs in HCC827 human adenocarcinoma cells (Song *et al.*, 2018). The *in vitro* studies showed a significant decrease in tumour cell (HCC827 and NCIH2135) viability as compared to DTX or resveratrol LPNs (Song *et al.*, 2018). The *in vivo* studies showed that mice injected with DTX/resveratrol EGF-LPNs presented with inhibition of tumour growth with a reduction in the size of the tumour (Song *et al.*, 2018). The method developed by Chou and Talalay to assess the effects of multiple drugs to determine their summation, synergism and antagonism, was used to evaluate the interaction of resveratrol and DTX (Chou and Talalay, 1984). The equation showed that resveratrol and DTX had a synergistic effect (Song *et al.*, 2018).

The wide range of studies reported in the literature demonstrate that polymeric NPs can enhance the bioavailability of resveratrol and many other studies also show that encapsulated resveratrol not only retain the anticancer effects mentioned in sections 1.1.3.1.1.1 and 1.1.3.1.1.2, but the polymeric NPs also help enhance these effects (Karthikeyan, Hoti and Prasad, 2015; Summerlin *et al.*, 2015; Singh, Lillard and Singh, 2018; Suktham *et al.*, 2018). However,

to maximise efficacy, delivery of the drug directly to the required site of action is crucial. In the case of lung cancer, local delivery to the lungs is beneficial.

Table 1-3 Resveratrol loaded into polymeric NPs

Polymeric Nanoparticle	Cell Line/ Animal Model	Finding(s)	Reference
PLGA	LNCaP	Halved IC ₅₀ and IC ₉₀ as compared to free-resveratrol. Induced apoptosis via: cell cycle arrest DNA damage Externalisation of phosphatidylserine ROS generation Loss of MMP. Well tolerated by murine macrophages even at 200 µM.	Nassir <i>et al.</i> , 2018
Galactosylated PLGA	RAW 264.7 cells Sprague-Dawley rats	Increased bioavailability of resveratrol. Suppression of proinflammatory cytokines.	Siu <i>et al.</i> , 2018
PLGA-BNPs	C6 glioma cells Charles Foster rats	Increased cytotoxicity and cellular uptake. Enhanced systemic circulation and half-life vs free-resveratrol (increased bioavailability).	Vijayakumar <i>et al.</i> , 2016
TPGS	Sprague-Dawley rats	Increased bioavailability Compared to free-resveratrol: increased C _{max} (2.2-fold),	Singh <i>et al.</i> , 2017

Polymeric Nanoparticle	Cell Line/ Animal Model	Finding(s)	Reference
		AUC (3.5-fold) MRT (1.2-fold)	
PLGA	Male Wistar rats	Good EE% and prolonged release profile. Compared to free-resveratrol: 10.6-fold increase in AUC values 28-fold increase in t_{max} 1.2-fold increase in C_{max} values	Singh and Pai, 2014
PEG-PLGA	HepG2	Good EE% and prolonged release profile. Dose and time dependant growth inhibitory effects.	Li <i>et al.</i> , 2016
PEG-PLA	CT26 colon cancer cells BALB/c nude mice injected with CT26 cells	Dose dependant inhibitory effect. Increased survival time of mice and decreased tumour growth.	Jung <i>et al.</i> , 2015
PCL	B16F10 C57BL/6J mice injected with B16F10	High EE% and reduction of cell viability. Statistically significant decrease in tumour volume vs free-resveratrol	Carletto <i>et al.</i> , 2016
Chitosan-TPP	SMMC7721 and LO2	Increased cellular uptake. Increased cytotoxicity against cancer cells vs resveratrol.	Wu <i>et al.</i> , 2017

Polymeric Nanoparticle	Cell Line/ Animal Model	Finding(s)	Reference
		Less cytotoxic to normal cells vs free-resveratrol.	
CMCS	Sprague-Dawley	Good EE% and prolonged release profile. Increased bioavailability compared with free-resveratrol: AUC 3.5-fold increase C _{max} 1.2-fold increase t _{max} 2.1-fold increase	Zu et al., 2016
AviBioCS	Kunming mice	Good EE% and prolonged release profile. Increased bioavailability vs free-resveratrol: AUC 2.6-fold higher t _{max} 25-fold higher MRT 4.5-fold greater	Bu <i>et al.</i> , 2013
Gelatin	NCI-H460 Swiss albino mice	Very high EE% and a sustained release profile over 2 days Increased bioavailability 2-fold increase in serum levels	Karthikeyan <i>et al.</i> , 2013
EGF conjugated LPNs	HCC827 and NCIH2135	High EE% and sustained <i>in vitro</i> release. Decreased tumour cell viability in cell lines.	Song <i>et al.</i> , 2018

Polymeric Nanoparticle	Cell Line/ Animal Model	Finding(s)	Reference
	BALB/c nude mice (6–8 weeks old) injected with HCC827 cells	Inhibition of tumour growth and decreased size <i>in vivo</i> .	

1.1.4.2. Preparation of nanoparticles

Methods for the preparation of polymeric NPs are usually broken down into two main groups, viz. 1. diffusion of preformed polymer; and 2. polymerisation of monomers (Soppimath *et al.*, 2001; Amoabediny *et al.*, 2018).

There are several methods for manufacturing polymeric NPs from preformed polymers, namely; dialysis, emulsification/solvent diffusion, emulsion solvent evaporation, high-pressure homogenisation, nanoprecipitation, salting out, spray drying, and supercritical fluid technology (Amoabediny *et al.*, 2018). The intended use of the polymeric NPs and the chemistry of the drug determines the method to be used. For the purposes of this project, the emulsion solvent evaporation method will be employed.

1.1.4.2.1. Emulsion solvent evaporation

Emulsion solvent evaporation was the first technique developed to manufacture polymeric NPs (Masood, 2016).

In this method, an emulsion is created by dissolving the polymer in an organic volatile solvent, such as dichloromethane and chloroform (Amoabediny *et al.*, 2018) (**Figure 1-2**). The organic phase consists of the polymer (synthetic, semi-synthetic or natural) dissolved in the organic solvent and the aqueous phase consists of the water along with stabiliser/surfactant (Masood, 2016). Single (oil-in-water, o/w) and double emulsification (water-in-oil/in-water, w1/o/w2) methods are employed for the creation of the emulsion (Masood, 2016). Secondly, the exposure of the emulsion to a high energy source, such as a homogeniser or ultrasonicator, converts it into a nanoparticle suspension (Amoabediny *et al.*, 2018). Lastly, the volatile solvent is removed by

evaporation through increasing the temperature under pressure or by continuous stirring (Reis *et al.*, 2006; Iqbal *et al.*, 2015). The polymeric NPs are then usually collected via lyophilisation or centrifugation (Nagavarma *et al.*, 2012).

Several factors influence and control NP characteristics, including homogeniser type, polymer concentration, and stirring speed (Amoabediny *et al.*, 2018).

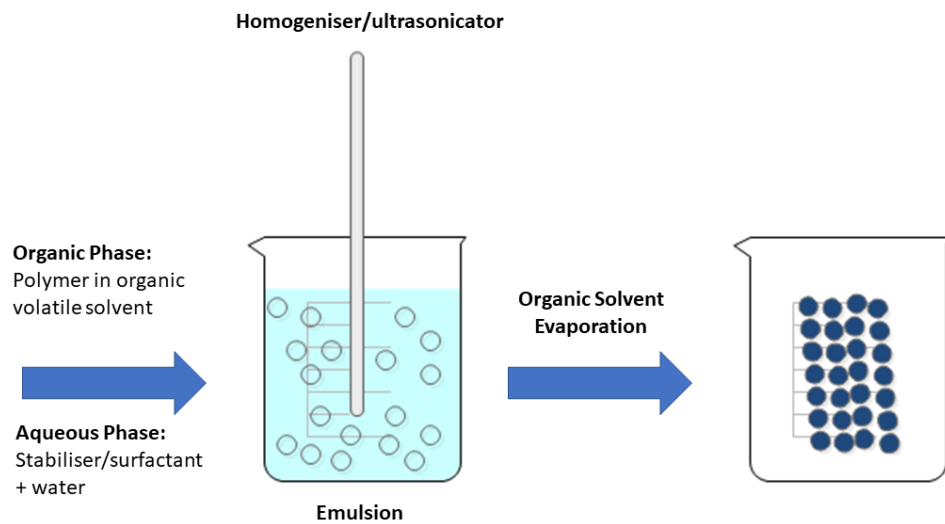


Figure 1-2 Schematic diagram of emulsion solvent evaporation technique (modified from (Kunda *et al.*, 2013))

1.1.5. Pulmonary delivery

1.1.5.1. *Anatomy of the lungs*

The lungs consist of the right lung, separated into three lobes (upper, middle, lower) by the oblique and horizontal fissures, and the left lung, separated into two lobes (upper and lower) by a single oblique fissure (Kradin, 2017). The visceral and parietal pleura, which are lubricated with pleural fluid, separates the lungs from the thoracic cage (Barrow and Pandit, 2014). Upon inhalation, air travels via the oral (mouth) and nasal (nose) cavity, from the larynx to the trachea. In the trachea, the air splits at the carina into the left and right mainstem bronchi, then it branches into lobar bronchi (one for each of the lobes (two on the left and three on the right), followed by segmental bronchi which divides further for approximately 15 to 20 times down to the level of the terminal bronchioles (Weinberger, Cockrill and Mandel, 2019). These conductive airways are the smallest units that do not play a part in gas exchange (Weinberger, Cockrill and Mandel, 2019). The entire airway as far as the respiratory bronchioles are lined with ciliated columnar epithelium containing mucus-secreting goblet cells, which acts as a physical defence barrier via the mucociliary escalator (Barrow and Pandit, 2014). The mucus covering the airways is moved towards the mouth via the coordinated movement of the cilia. This process is known as the mucociliary escalator. It serves as a line of defence and removes any foreign material that lands on the bronchial surfaces (Kradin, 2017).

After the terminal bronchioles, further divisions give rise to the respiratory bronchioles, alveolar ducts, and alveoli which form the part of the lung responsible for gas exchange.(Weinberger, Cockrill and Mandel, 2019). These

alveolar ducts and sacs are lined with squamous epithelium (Barrow and Pandit, 2014). The average human lung is said to comprise of 300 million alveoli with the surface area approximately the size of a tennis court (Weinberger, Cockrill and Mandel, 2019).

Any particles, including that of a drug delivery system, encounter several obstacles before getting to the lung cells.

1.1.5.2. Drug delivery to the lungs

Pulmonary drug delivery allows for the non-invasive administration of a drug/bioactive compound via inhalation (Zhang *et al.*, 2018). There are many advantages to delivering drugs via the lungs for both local and systemic treatment, including high bioavailability since the first pass metabolism is bypassed, rapid onset of action due to direct targeting at the site of action (lung cancer cells), self-administration (similar to how asthmatics use their inhalation devices) and non-invasiveness (which increases patient compliance) (Sung, Pulliam and Edwards, 2007; Mahmud and Discher, 2011; Thorley and Tetley, 2013; Lee *et al.*, 2015).

One of the biggest challenges for cancer chemotherapy is the non-specific targeting/ distribution of the anticancer agent and the severe side effects this produces (Alexiou *et al.*, 2000; Ray, 2019). NP-mediated pulmonary delivery will aid in overcoming this obstacle through targeted delivery; by reducing the dosage required to treat the cancer and reducing the amount of drug the healthy cells are exposed to.

However, there are several obstacles to overcome in order for pulmonary delivery to be effective. The pulmonary drug delivery system will have to evade

the natural defences of the lung, including phagocytosis by alveolar macrophages and the mucociliary escalator (Chishti *et al.*, 2019). Furthermore, the delivery system has to be carefully designed to ensure the highest delivery of the formulation to the middle or deep regions of the lungs where NPs have effectiveness (Kaminskas *et al.*, 2014). The reduced clearance of macromolecules from tumours leads to more inhalable particles depositing in tumour tissue than in healthy cells, thus increasing the circulation time of the drug-loaded NPs in the interstitial tissue of the tumours (Maeda, 2001; Godugu *et al.*, 2013; d'Angelo *et al.*, 2015)

The nano-sized ($< 1 \mu\text{m}$) nanoparticulate system inherently has the ability to overcome mucociliary clearance and macrophages phagocytosis (Kanehira *et al.*, 2016). That said, that same size advantage makes spray-dried NPs incapable of depositing directly into the lungs since they get exhaled without settling in the alveoli (Pilcer and Amighi, 2010; Rezazadeh *et al.*, 2018). Aerodynamic particle size has an important role in determining the deposition and retention of the inhaled particles. The ideal range for particles to be able to deposit in the deep regions of the lung is between 1 and 5 μm aerodynamic diameter (El-Sherbiny and Smyth, 2012; Elsayed and AbouGhaly, 2016; Rezazadeh *et al.*, 2018).

If the inhaled particles are $< 1 \mu\text{m}$, they may be exhaled rather than deposited in the lung, due the effect of Brownian movement (Florence, 2012). However, if the inhaled particles are $> 5 \mu\text{m}$, they would collide with the lining of the mucosal membranes, particularly at bifurcations, due to inertial impaction caused by gravity (Islam *et al.*, 2017).

1.1.5.3. Pulmonary delivery of nanocomposite microparticles

NPs can be placed into nanocomposite microparticles (NCMPs) using a carrier system such as lactose or mannitol microparticles (MPs). This carrier system should improve the size of the particles and allow for a suitable fine particle fraction (FPF) for delivery to the deep regions of the lungs. FPF refers to the fraction of the dose \leq to the effective cut-off aerodynamic diameter of 5.5 μm at a specific flow rate (i.e. 60 L/min) (Rezazadeh *et al.*, 2018).

1.1.5.3.1. Preparation of nanocomposite microparticles

1.1.5.3.1.1. Spray drying

Spray drying is an established technique for the production of particles which involves the transformation of a fluid material into dried particles, by means of a gaseous hot drying medium (Cal and Sollohub, 2010; Deshmukh, Wagh and Naik, 2016). The spray drying process can be divided into three major phases, namely, atomisation, droplet-to-particle conversion (solvent evaporation), and particle collection (Sosnik and Seremeta, 2015).

Firstly, a solution (emulsion or suspension) is pumped to an atomiser which breaks up the liquid feed into a spray of fine droplets (Santos *et al.*, 2017). Secondly, the fine droplets are expelled into a drying gas chamber which causes solvent evaporation, leading to the formation of dry particles (Santos *et al.*, 2017). Lastly, the dried particles are separated from the drying medium, using an appropriate device such as a cyclone, and can then be collected in a tank (Santos *et al.*, 2017).

Several parameters influence the characteristics of the final dry particles, including atomisation pressure, feed flow rate, feed viscosity, feed surface

tension, inlet temperature, drying gas flow rate, outlet temperature, residence time inside drying chamber, and glass transition temperature (Santos *et al.*, 2017).

Spray drying is advantageous for pulmonary delivery since it can produce inhalable powder that is in the respirable size range for pulmonary delivery (Santos *et al.*, 2017). Spray drying allows for the control of the particle size, shape, density and moisture content by altering the parameters mentioned before (Muralidharan *et al.*, 2015). This combined with the possibility of continuous manufacturing, ease of scalability, good uniformity of molecular dispersion and cost-effectiveness in large scale production with high recoveries, make spray drying an attractive method to use (Patel, Patel and Chakraborty, 2014). Recently, spray drying has been used to produce NCMPs loaded with levofloxacin and bovine serum albumin (Merchant *et al.*, 2014; Kunda, Alfagih, Dennison, Tawfeek, *et al.*, 2015).

1.1.5.3.2. Delivery of nanocomposite microparticles

Delivery of inhalable particles can be achieved by different inhalation devices, namely, the nebuliser, the pressurized metered dose inhaler (pMDI), Respimat® Soft Mist™ inhaler, and the dry powder inhaler (DPI). The nebuliser was the first inhalation therapy device developed and uses an air jet or ultrasound to generate aerosol droplets from a drug solution or suspension which are then inhaled by the patient over a couple of minutes (Steckel and Eskandar, 2003; Hertel, Winter and Friess, 2015). The main disadvantages of the nebuliser is that it is non-portable, requires lengthy administration, needs constant cleaning and maintenance, and they suffer from poor reproducibility in delivering an accurate dose and are only commonly used in hospitals

(Malcolmson and Embleton, 1998; Peng *et al.*, 2016). The pMDI is a portable and convenient multidose device which generates a metered dose of an aerosol through an atomisation nozzle using a propellant under pressure (Dolovich and Dhand, 2011; Ivey, Vehring and Finlay, 2015). However, pMDI require successful coordination between the actuation of the device and inhalation by the patient (Dolovich *et al.*, 2019). Some other concerns include issues with the environmental impacts of the propellant, solubility and compatibility between the drug and propellant, as well as physicochemical stability concerns (Muralidharan *et al.*, 2015). On top of that, DPIs often give a better stability profile for the loaded bioactive compound than aerosols or nebulisers (Ungaro *et al.*, 2012). It is with this in mind that the DPI has emerged as a better candidate.

1.1.5.3.2.1. Dry powder inhaler (DPI)

The DPI is a device that contains an active pharmaceutical ingredient (API) that is in a suitable aerodynamic size (usually 1–5 μm) for inhalation, which upon inhalation, causes sufficient deagglomeration of particles resulting in the delivery of a therapeutic dose to the lungs (Peng *et al.*, 2016). There are several advantages of the DPI, including propellant-free, non-invasive, portable, user-friendly, low-cost, and the powder is more stable than liquid dosage forms (Lee *et al.*, 2015).

The DPI was developed in response to the poor actuation–inhalation coordination inherent with other inhalers of the time (Hoppentocht *et al.*, 2014). The biggest hurdle with micron-sized particles as used in the DPI is that they have high cohesive forces (making them stick together) and adhesive forces (making them stick to any surface they encounter) (Young *et al.*, 2008; Peng

et al., 2016). This results in poor flowability and performance with the formulation being prone to get stuck within the inhaler (Young *et al.*, 2008). Many of the APIs also require a lower dose for pulmonary delivery than systemic delivery, which necessitate their reduction in order to give accurate metering of doses. These limitations has led to the development of carriers or excipients which have several functions including, enhancing the flowability of drug particles to ease filling of the DPI, enhancing dispersion of drug particles during emission, and decreasing concentration of the drug to facilitate accurate delivery of dose (Peng *et al.*, 2016).

A formulation for DPI either consists of a respirable API or an API blended with non-respirable excipients such as lactose, which, until now, is the sole FDA-approved non-respirable carrier in the US (Lee *et al.*, 2015). Outside the USA, several other non-respirable excipients have been used including glucose, maltitol, mannitol, raffinose, sorbitol, sucrose, and xylitol (Lee *et al.*, 2015).

One of the first DPIs, Spinhaler®, started being commercially available in 1971 (Sanders, 2011; Hoppentocht *et al.*, 2014). Since then, many others have followed.

1.1.5.3.3. Delivery described in literature

Polymeric NPs have been used for the pulmonary delivery of small molecules, genes and proteins/peptides (Yamamoto *et al.*, 2005; Azarmi, Roa and Löbenberg, 2008; Mansour, Rhee and Wu, 2009; Menon *et al.*, 2014; Gaul *et al.*, 2018; Nieto-Orellana *et al.*, 2018; Rodrigues *et al.*, 2018).

However, studies using polymeric NP-mediated microparticles for pulmonary delivery of phenolic compounds are a little less ubiquitous in the literature (**Table 1-4**).

NPs in MPs, that is NCMPs, were synthesised for deep lung delivery. PLGA NPs loaded with TAS-103, an anti-cancer drug, was synthesised with an average size of 200 nm (Tomoda *et al.*, 2009). The TAS-103-loaded PLGA NPs were then spray-dried with trehalose as an excipient (Tomoda *et al.*, 2009). The TSA-103-loaded nanocomposite microparticles (T-NCMPs) had an enhanced *in vitro* cytotoxicity effect against A549 cells when compared to free TAS-103 (Tomoda *et al.*, 2009). It is thought that the NCMPs are completely disintegrated into NPs in the presence of cell media and, therefore, this might lead to better internalisation of NPs through endocytosis or passive diffusion (Tomoda *et al.*, 2009). Male Sprague-Dawley rats were divided into two groups and administered the TAS-103-loaded NCMPs using an animal DPI or free TAS-103 in saline (equivalent to the drug concentration administered via DPI) using intravenous administration as a control. Administration via DPI resulted in significantly higher drug concentration in the lungs (300-fold) than in the plasma (Tomoda *et al.*, 2009). Moreover, the drug concentration in the lungs via inhalation was 13 times higher than with intravenous administration (Tomoda *et al.*, 2009).

2-Methoxyestradiol (2-ME) PLGA NPs were prepared using a single emulsion (o/w) method and coated with chitosan (Guo *et al.*, 2014). The 2-ME PLGA-chitosan NPs were incorporated into NCMPs using lactose, leucine, and Poloxamer 188, as excipients. The 2-ME PLGA-chitosan NPs had an average size of 221 nm before spray drying and 225 nm after reconstitution from the NCMPs (Guo *et al.*, 2014). Two cell lines, SPC-A1 and A549, were exposed to free 2-ME in solution or encapsulated in the various particles (PLGA NPs, PLGA-chitosan NPs and the 2-ME-loaded PLGA-chitosan NCMPs (2-ME-PLGA-chitosan MPs)). The 2-ME-PLGA-chitosan MPs resulted in an 9-fold and 4-fold decrease of IC₅₀ in SPC-A1 and A549, respectively (Guo *et al.*, 2014). The 2-ME was replaced with 6-cumarin to prepare 6-cumarin-PLGA-chitosan MPs and it was intratracheally administered to rats. Results showed uptake of 6-cumarin-PLGA-chitosan MPs in alveolar and bronchial wall, showing that the 2-ME PLGA-chitosan NPs could reach deep lung tissue through nanocomposite microparticle delivery (Guo *et al.*, 2014). The strong fluorescence on the bronchial wall indicates chitosan NPs easily sticks to the mucus layer of the cilia surface (Guo *et al.*, 2014).

More recently, sildenafil citrate (SC)-loaded PLGA NPs (SC-PLGA NPs) with an average size of 210 nm were formulated (Ghasemian *et al.*, 2016). The SC-PLGA NPs were then incorporated into microparticles using spray drying with lactose (1:1 w/w) as an excipient. Free SC was also spray dried using lactose (1:50 w/w). The average size and fine particle fraction of the spray-dried sildenafil nanocomposite (SSN) and spray-dried free SC (SFS) was 7 µm and 4.5 µm, and 60.2% and 68.2%, respectively (Ghasemian *et al.*, 2016). Male Sprague-Dawley rats were randomly divided into four experimental groups

and either received 1 mL intravenous injection (100 µg/mL SC solution), 1 mL oral administration (100 µg/mL SC solution), SSN or SFS (both equal to 100 µg SC). The SSN and SFS was delivered to the rats via insufflation. Results showed that SSN is detected in the lung twice as long as the next best formulation (SFS), 12 hours vs 6 hours, and unlike SFS, it has a sustained release profile in the lung (Ghasemian *et al.*, 2016).

Liu *et al.* prepared paclitaxel- oleic acid-conjugated chitosan NPs (P-OA-CTS) and quercetin-oleic acid-conjugated chitosan NPs (Q-OA-CTS) and then co-loaded both NPs into microparticles by spray drying the NPs with hydroxypropyl-β-cyclodextrin, lactose, and mannitol as excipients (Liu *et al.*, 2017). The microparticles (PQ-CTS-MPs) obtained was shown to be in the ideal range of between 1 and 5 µm with a slow release profile (Liu *et al.*, 2017). Wistar rats were separated into four groups. The four groups received equivalent doses of either, PQ-CTS-MPs (intratracheally), paclitaxel, quercetin, or paclitaxel and quercetin (all intravenously). The study ascertained that intravenous delivery of the microspheres caused more accumulation of the encapsulated drug in the liver and kidney than in the lung, while pulmonary administration lead to a significant majority of the drug depositing in the lungs with minimal amounts accumulating in the other organs (Liu *et al.*, 2017). Furthermore, 6 hours after pulmonary administration, paclitaxel and quercetin concentration in the lung remained high (206.27 µg/g) with comparatively low distribution in the liver (8.82 µg/g), spleen (6.94 µg/g), kidney (5.01 µg/g) and heart (2.61 µg/g) at the same time. Whereas, 6 hours after intravenous delivery the concentration of paclitaxel and quercetin in all organs were ≤ 5 µg/g. It was reported that quercetin helped increase the

circulatory time of paclitaxel (Liu *et al.*, 2017). Combined, this shows that pulmonary delivery of microparticles not only improved the retention time of the drugs, but also allowed for the accumulation of the drug in the lung with only minimal amount of drug accumulating in other organs. This should lead to lower side-effects.

Table 1-4 Delivery of nanocomposite microparticles

Dry Powder Formulation			Cell Line/ Animal Model	Finding(s)	Reference
NPs	Drug	Excipient			
PLGA	TAS-103	Trehalose	A549 Sprague-Dawley rats	T-NCMPs more cytotoxic, <i>in vitro</i> , than free-TAS-103. 13-fold increase in drug concentration in lungs from DPI administration of T-NCMPs vs free-TAS-103. 300-fold increase in drug concentration in lungs vs plasma when administering T-NCMPs using DPI.	Tomoda <i>et al.</i> , 2009
PLGA- chitosan	2- methoxyestradiol (2-ME)	lactose, leucine, and Poloxamer 188	SPC-A1 and A549 Rats	2-ME-loaded NCMPs vs free-drug 9-fold and 4-fold decrease of IC ₅₀ in SPC-A1 and A549, respectively. Strong uptake of NCMPs in the lungs.	Guo <i>et al.</i> , 2014

Dry Powder Formulation			Cell Line/ Animal Model	Finding(s)	Reference
NPs	Drug	Excipient			
PLGA	sildenafil citrate	Lactose	Sprague-Dawley rats	NCMPs has enhanced pharmacokinetics vs spray-dried free drug following pulmonary delivery.	Ghasemian <i>et al.</i> , 2016
Chitosan and oleic acid	Paclitaxel Quercetin	Hydroxypropyl- β -cyclodextrin, lactose, and mannitol	Wistar rats	Pulmonary delivery: Improved the retention time of the drugs. Allowed for the accumulation of the drug in the lung with only minimal amount of drug accumulating in other organs.	Liu <i>et al.</i> , 2017

1.2. Thesis hypothesis

Resveratrol-loaded aerosolisable NCMPs can be used for the treatment of lung cancer.

1.3. Thesis aim and objectives

To develop, design, formulate and characterise resveratrol-loaded aerosolisable NCMPs as a potential treatment for lung cancer by dry powder delivery directly to the lungs.

In order to achieve the aim of the thesis a systematic study was designed considering the following objectives:

- 1) Development of a resveratrol-loaded nanoparticle delivery system
 - a. To optimise formulation of resveratrol into various polymeric NPs and assess their characteristics.
 - b. To design protocols to evaluate the effect of free-resveratrol and nanoparticle-loaded resveratrol on lung cancer cells.
- 2) Incorporation of optimum resveratrol-loaded NPs into NCMPs via spray drying with L-leucine and chitosan as microcarrier.
 - a. Optimisation of NCMPs formulations in term of morphology and yield%.
 - b. A study of the *in vitro* aerosolisation behaviour, *in vitro* release and cell toxicity.
- 3) To design and synthesise a modified polymer to allow for attachment of fluorescent ligands to enable detection of the particles within cells

- a. Designing chemical experiments in order to evaluate the feasibility for using click chemistry.
- b. Modification of glycerol to attach alkyne group.
- c. Polymerisation of modified polymer.
- d. Development of a fluorescent azide to attach to alkyne group.

2 CHAPTER 2: The Formulation and Evaluation of Resveratrol Nanoparticles

2.1. Introduction

Resveratrol has shown very good anticancer activity both *in vitro* and *in vivo*, but, like many phenolic compounds, it suffers from poor oral bioavailability (Walle *et al.*, 2004; Yuan *et al.*, 2015; Zhang *et al.*, 2015; Sun *et al.*, 2017). Therefore, this chapter focusses on our aim to enhance bioavailability by encapsulating resveratrol into polymeric nanoparticles (NPs) which protects it from metabolic degradation.

Polymeric NPs possess many advantages including controllable physico-chemical properties, high stability, homogenous size distribution, high drug encapsulation, and controllable drug release (Hu, Aryal and Zhang, 2010; Farooq *et al.*, 2019). Several biodegradable polymers, both synthetic and natural, can be utilised to create polymeric NPs, including poly (lactic-co-glycolic acid) (PLGA), polylactic acid (PLA), polycaprolactone (PCL), poly(glycerol adipate-co- ω -pentadecalactone) (PGA-co-PDL), chitosan and gelatin (Kumari, Yadav and Yadav, 2010; Kunda, Alfagih, Dennison, Tawfeek, *et al.*, 2015). The resveratrol can be incorporated into the NPs through either adsorption, encapsulation, or by conjugation, either to the polymer or externally to the nanoparticle (NP) surface (Ahmadi, Mohammadinejad and Ashrafizadeh, 2019).

There are various methods for manufacturing polymeric NPs from preformed polymers, namely, dialysis, emulsification/solvent diffusion, emulsion solvent evaporation, high-pressure homogenisation, nanoprecipitation, salting out, spray drying, and supercritical fluid technology (Amoabediny *et al.*, 2018). The solvent evaporation method was used in this study.

In this method, an emulsion is created by dissolving the polymer in a volatile organic solvent, such as dichloromethane and chloroform, which is known as the organic phase (Masood, 2016; Amoabediny *et al.*, 2018). The aqueous phase consists of the water along with stabiliser/surfactant (Masood, 2016). Single (oil-in-water, o/w) and double emulsification (water-in-oil/in-water, w1/o/w2) methods are employed for the creation of the emulsion (Masood, 2016). Secondly, the exposure of the emulsion to a high energy source, such as a homogeniser or ultrasonicator, converts it into a NP suspension (Amoabediny *et al.*, 2018). Lastly, the volatile solvent is removed by evaporation through increasing the temperature under pressure or by continuous stirring (Reis *et al.*, 2006).

Several factors influence and control NP characteristics, including homogenizer type, polymer concentration, ratio of organic and aqueous phases and stirring speed (Kunda, Alfagih, Dennison, Tawfeek, *et al.*, 2015; Amoabediny *et al.*, 2018). Polymeric NPs of between 100-200 nm were desirable since studies suggests these particles are ideal for uptake and evasion of the alveolar macrophages and they show rapid penetration of the respiratory mucus (Dandekar *et al.*, 2010; Schuster *et al.*, 2013; Youngren-Ortiz *et al.*, 2017; Dabbagh *et al.*, 2018).

Cell culture is an intrinsic and versatile methodological platform in cellular and molecular biology, facilitating the study of the normal biochemistry and physiology of cells and how drugs and toxic compounds affect cells, carcinogenesis and mutagenesis (Shwetha *et al.*, 2019). The bronchial Calu 3 epithelial cell line, originating from a human lung adenocarcinoma, can be used for cytotoxicity studies as a relevant *in vitro* pulmonary model for

polymeric NP delivery (Dekali *et al.*, 2014; Kreft *et al.*, 2015). The Calu 3 cell line expresses many characteristics of the bronchial epithelium including the formation of tight polarised monolayers with tight junctions and appreciable transepithelial resistance values, expression of microvilli, along with mucin granules, and the lung surfactant-specific protein prosurfactant protein-C (Fiegel *et al.*, 2003; Grainger *et al.*, 2006; Kreft *et al.*, 2015). Lastly, Calu-3 cells show rapid and reliable growth over a wide passage range (Foster *et al.*, 2000; Kreft *et al.*, 2015).

Cell proliferation assessment is a good indicator of cell health maintenance or cell death induction in response to drugs or chemical agents and is thus used to determine cell viability (Adan, Kiraz and Baran, 2016). Cell viability is the amount of healthy, living cells in a given population (Adan, Kiraz and Baran, 2016). There are various methods for measuring cytotoxicity that are based on biochemical or morphological aberrations induced in healthy cells, including with respect to ATP production, cell adherence, cell membrane permeability, co-enzyme production, DNA synthesis, dye uptake, enzyme release, metabolic activities and nucleotide uptake activity (Weyermann, Lochmann and Zimmer, 2005; Aslantürk, 2018). This study made use of two assays, one of which is a metabolic cell proliferation assay (Alamar Blue Assay, assessed cell viability) and the other a cell membrane integrity and cell metabolism assay (Lactate Dehydrogenase Assay - assessed cell death).

The Alamar Blue (resazurin sodium salt) assay involves the reduction of resazurin (blue and nonfluorescent) by healthy cells to resorufin, which is pink and highly fluorescent (Brien *et al.*, 2000). The reduction is due to the enzymatic actions of mitochondrial, cytosolic, and microsomal enzymes

(Vega-Avila and Pugsley, 2011; Rampersad, 2012; Munshi, Twining and Dahl, 2014). Alamar Blue is extremely stable, exhibits no toxicity to the cells, and allows for continuous monitoring of cultures over time (Al-Nasiry *et al.*, 2007).

The lactate dehydrogenase (LDH) assay was first developed to measure cytotoxicity in immune cells (Adan, Kiraz and Baran, 2016). It works on the principle that the cytosolic enzyme, LDH, is present in many cells and that upon plasma membrane damage, in cases of necrotic or late apoptotic cells, it gets released into the cell culture medium. Extracellular LDH then catalyses the conversion of lactate to pyruvate via the reduction of NAD⁺ to NADH (Decker and Lohmann-Matthes, 1988; Fotakis and Timbrell, 2006; Han *et al.*, 2011). Diaphorase, NADH dehydrogenase, utilises NADH to reduce a tetrazolium salt (INT) to a red formazan product which can be measured to determine the amount of LDH released into the cell culture medium (Nachlas *et al.*, 1960; Decker and Lohmann-Matthes, 1988).

2.2. Aim and Objectives

The aim of this study was to synthesise and analyse optimised polymeric NPs containing resveratrol and to evaluate the efficacy of the formulation compared to free-resveratrol.

The main objectives were:

To optimise the formulation of resveratrol-encapsulated PLGA, mPEG-PLGA, PGA-co-PDL, and PGA-co-PDL-PEG₂₀₀₀ NPs.

To evaluate the nanoparticles in terms of; particle size, polydispersibility index (PDI), zeta potential, resveratrol encapsulation efficiency, and NP stability;

To study the *in vitro* cytotoxicity of the optimised formulation on Calu 3 cells.

2.3. Materials and Methods

2.3.1. Materials

Polymer synthesis: Divinyl adipate (DVA) was purchased from TCI, USA. ω -pentadecalactone (PDL) was obtained from Sigma-Aldrich Fine Chemicals (SAFC, UK). Glycerol, Novozyme® 435 (discontinued and replaced by lipase acrylic resin), polyvinyl alcohol (PVA) 89000-98000 molecular weight (MWt), PLGA, mPEG-PLGA, PEG-2000, and the various polystyrene standards (2430 Da, 3680 Da, 13 700 Da, 18 700 Da, and 29 300 Da) were purchased from Sigma-Aldrich, UK. Tetrahydrofuran (THF), dichloromethane (DCM), and methanol (HPLC grade) were purchased from Fisher Scientific, UK.

Cell culture: Minimum Essential Medium Eagle (MEM), L-glutamine, Penicillin-Streptomycin, foetal bovine serum (FBS), resazurin sodium salt, and sodium pyruvate solution were obtained from Sigma-Aldrich, UK. TrypLE™ 1X was purchased from Thermofisher, US. Phosphate buffered saline (PBS) was purchased from Fisher Scientific, UK. Human lung adenocarcinoma cell line, Calu-3, was purchased from American Type Culture Collection (ATCC). The Alamar Blue and LDH assay kit were purchased from Fisher Scientific, UK.

2.3.2. Methods

2.3.2.1. *Polymer synthesis*

2.3.2.1.1. PGA-co-PDL synthesis

PGA-co-PDL was synthesised via enzyme catalysed ring opening polymerisation and polycondensation as described in various papers (Namekawa, Uyama and Kobayashi, 2000; Thompson *et al.*, 2006) (**Figure 2-1**). The various monomers were added in an equimolar ratio (1:1:1) - PDL (0.125 mol), DVA (0.125 mol), and glycerol (0.125 mol) - to a dry 250 mL three-necked round-bottomed flask. THF (20 mL) was then added to prevent the reaction from becoming too viscous. The filled flask was then placed in a water bath (50 °C) to the level of the solution. The central neck of the round-bottomed flask was equipped with a mechanical stirring rod fitted with a Teflon paddle (105 mm) and kept in place with an adaptor. One of the other necks was fitted with an open top condenser to act as an outlet for the acetaldehyde produced by the reaction. The third neck which was used to add the monomers was closed with a stopper. The solution in the round-bottomed flask was stirred for 20 minutes to allow the monomers to dissolve and the temperatures to equilibrate. The enzyme, Novozyme® 435 (1 g), was weighed into a glass dispenser and then added to the free open neck of the round-bottomed flask. THF (5 mL) was used to wash any of the remaining enzyme into the flask. The open neck was then closed again using the stopper and the reaction was permitted to proceed for 6.5 hours.

After 6.5 hours, the resultant viscous polymer was dissolved using DCM (200 mL) while still being stirred. The enzyme complex was removed via Buchner filtration using 1 layer of filter paper (Whatman GF/A). Warm DCM (300 mL)

was used to expedite the filtration. The filtrate was then transferred to a round-bottomed flask and the DCM was then removed via rotary evaporation at 80 °C (Laborota 4000, Heidolph Instruments attached to a Divac pump) until approximately 20 mL DCM remained.

This solution was then charged with methanol (100 mL) and the round-bottomed flask was agitated to precipitate the co-polymer. The co-polymer was then filtered using Buchner filtration with 1 layer of filter paper (Whatman GF/A). Methanol was used to expedite the filtration. The solid co-polymer trapped on the filter paper was left to air dry overnight.

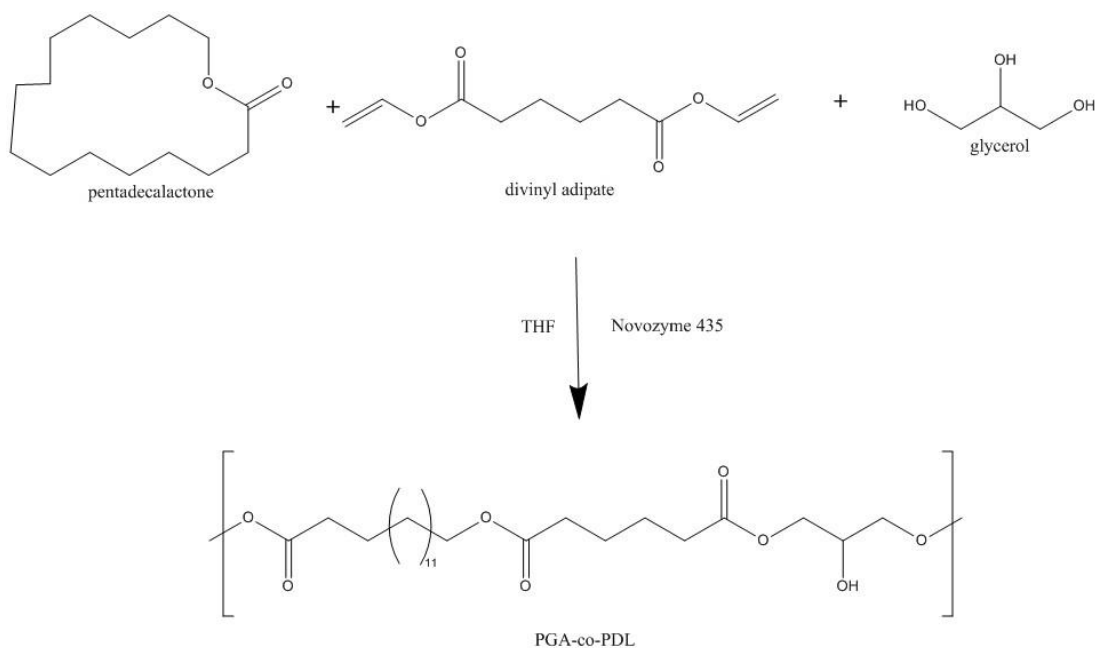


Figure 2-1 Enzymatic synthesis of PGA-co-PDL via ring opening polymerisation and polycondensation

2.3.2.1.2. PGA-co-PDL-PEG₂₀₀₀

Synthesis of Poly(ethylene glycol methyl ether)-PGA-co-PDL (PGA-co-PDL-PEG₂₀₀₀) followed the same procedure as in 2.3.2.1.1, except that Poly(ethylene glycol) methyl ether (mPEG₂₀₀₀) monomer was added at a molar ratio of 0.01 (PDL:DVA:Glycerol:mPEG₂₀₀₀, 1:1:1:0.01) (**Figure 2-2**).

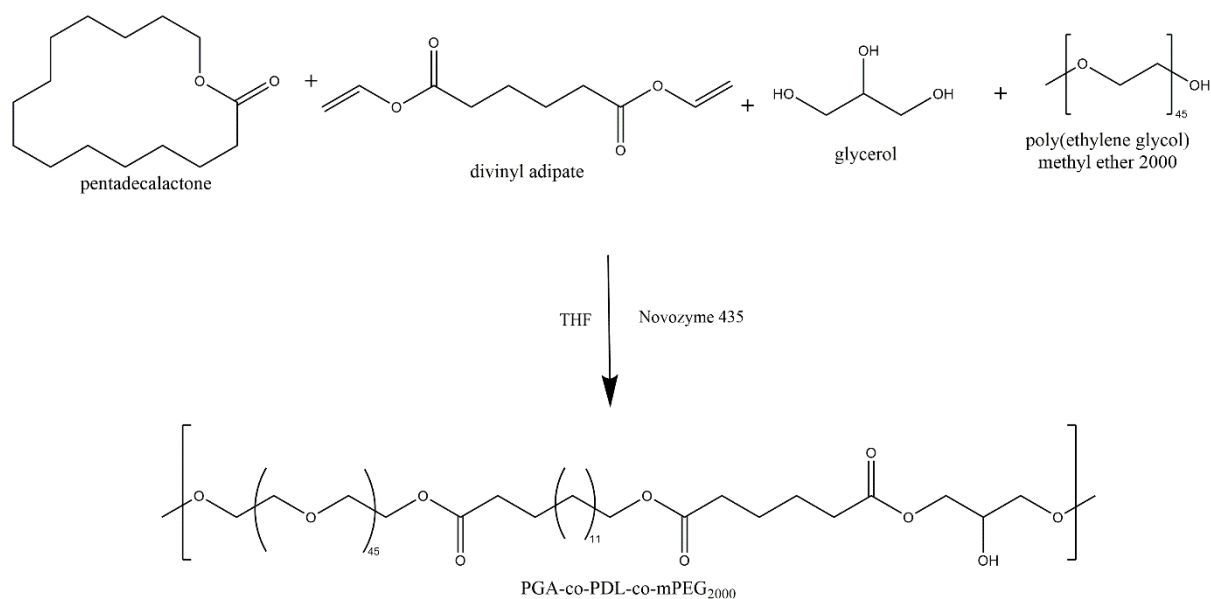


Figure 2-2 Enzymatic synthesis of PGA-co-PDL-PEG₂₀₀₀ via ring opening polymerisation and polycondensation

2.3.2.1.3. Poly(*D,L*-lactide-co-glycolide) (PLGA)

Resomer® RG 502 H, Poly(*D,L*-lactide-co-glycolide) (**Figure 2-3**) was purchased from Aldrich chemistry.

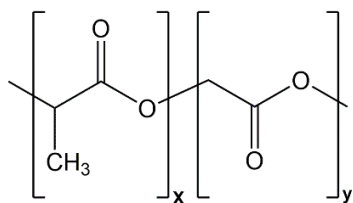


Figure 2-3 PLGA structure

2.3.2.1.4. PEG methyl ether-block-poly(lactide-co-glycolide) (mPEG-PLGA)

Poly(ethylene glycol) methyl ether-block-poly(lactide-co-glycolide) (**Figure 2-4**) was purchased from Aldrich chemistry.

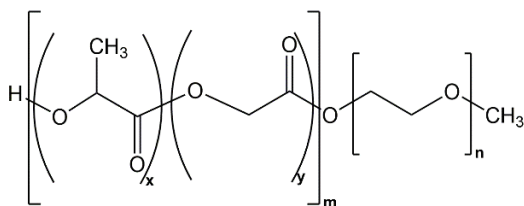


Figure 2-4 mPEG-PLGA structure

2.3.2.2. *Polymer analysis*

2.3.2.2.1. Molecular weight analysis - Gel Permeation Chromatography (GPC)

GPC was used to obtain the molecular weight (MWt) of the polymers. The GPC instrument (Malvern Viscotek TDA Model 300) connected to a GPC max integrated solvent and sample module (degasser, pump, and auto sampler) was used with OmniSEC 5.1 software to determine molecular weight and molecular weight distribution. The GPC system was equipped with two ViscoGEL GMHHR-N columns, stored in the detector oven at 40 °C. The

eluent used was THF, at a flow rate of 1 mL/min. Prior to analysis, the GPC system was purged for 5 minutes, every 30 minutes, until stability of the RI detector baseline was achieved.

The GPC was calibrated using polystyrene standards (2430 Da, 3680 Da, 13 700 Da, 18 700 Da, and 29 300 Da). Preparation of the polystyrene standard samples (5 mg/mL) involved dissolving each polystyrene standard (10 mg) in THF (2 mL) and mixing it using a benchtop vortex mixer (Velp Scientifica Vortex) at 3000 rpm for 20 seconds. The standard solutions were filtered into clean GPC vials using a glass syringe coupled with a filter system fitted with 1 layer of PTFE syringe filter (0.2 μm , Whatman). The filter was wetted with THF (1 mL) before use. A new filter was used for each polystyrene standard. Polytetrafluoroethylene (PTFE) septa (Sigma) were used in vial lids to prevent evaporation and clogging up of the injection needle. A GPC vial containing THF (used as a blank) was also prepared and all vials were placed in the instrument. The GPC system was set up to take 3 injections (100 μL) from each vial beginning with the THF blank and then the polystyrene standards from the lowest to the highest MWt. A calibration curve of log MWt versus retention volume was obtained by analysing the retention volume at the peak maxima of each polystyrene standard.

Preparation of polymer samples (5 mg/mL) involved dissolving the co-polymer (10 mg) in THF (2 mL) and mixing it using a benchtop vortex mixer (Velp Scientifica Vortex) at 3000 rpm for 20 seconds. The co-polymer sample was filtered using the method described earlier. The retention volume of the peak maxima was used to determine the MWt by using the calibration curve obtained previously.

2.3.2.2.2. Chemical structure analysis – Fourier Transform Infra-Red (FT-IR) Spectroscopy and Nuclear Magnetic Resonance (NMR) Spectroscopy

2.3.2.2.2.1. Fourier Transform Infra-Red (FT-IR) Spectroscopy

The chemical structures of the co-polymers were obtained using Agilent Technologies MicroLab FT-IR software running on an Agilent Technologies Cary 630 FT-IR Spectrometer (Agilent, USA). The spectra were collected from 650-4000 cm^{-1} at a resolution of 4 cm^{-1} .

2.3.2.2.2.2. Nuclear Magnetic Resonance (NMR)

Proton nuclear magnetic resonance (^1H NMR) spectra for the polymers were obtained using a Bruker Avance III 300 MHz spectrometer operated with Topspin v3.2. The NMR spectra were expressed in parts per million (δ) with trimethylsilane as an internal standard.

A sample of each polymer (10 mg) was measured and dissolved into deuterated chloroform (CDCl_3) (0.7 mL). This solution was then filtered and transferred into an NMR tube (Wilmad 5 mm NMR tube, Goss Scientific Instruments Ltd.) and capped. The obtained spectra were analysed using MestReNova software.

2.3.2.2.3. Thermal analysis – Differential Scanning Calorimetry (DSC)

The thermal stability of each polymer was determined using a Perkin Elmer DSC 8000 with Pyris software. An indium reference standard was used to calibrate the system. A small sample of the polymer (4-15 mg) was hermetically sealed in standard aluminium pans (Perkin Elmer, USA) and placed in the sample chamber. The samples were heated from 25 $^{\circ}\text{C}$ to 70 $^{\circ}\text{C}$ at a rate of 20 $^{\circ}\text{C}/\text{min}$ and then cooled from 70 $^{\circ}\text{C}$ to 25 $^{\circ}\text{C}$ at a rate of

20 °C/min. The samples were then reheated from 25 °C to 70 °C at a rate of 20 °C/min.

2.3.2.3. Polymeric nanoparticle synthesis

Blank polymeric NPs were synthesised via a modified water-in-oil-in water ($w_1/o/w_2$) double emulsion evaporation method. The co-polymer (50 mg) was weighed into a clean vial and dissolved using DCM (2 mL). This co-polymer solution (organic phase) was subsequently mixed using an ultrasonic water bath (Ultrawave) for 2 minutes. The organic phase was then probe sonicated for 2 minutes at 65% amplitude (QSonica sonicator, USA) while adding dropwise 10% w/v PVA (0.5 mL) (1st aqueous solution) to form an emulsion. This process was performed in ice. This primary emulsion was then probe sonicated for 2 minutes at 65% amplitude (QSonica sonicator, USA) while adding dropwise 1% w/v PVA (20 mL) (2nd aqueous solution) to form a second emulsion. This process was also performed in ice. This final emulsion was immediately added to a beaker on a Jeio Tech MS-53M magnetic stirrer (Jeiotech, South Korea) stirring at a speed of 500 rpm. The mixture was left stirring at room temperature for 3 hours to facilitate the evaporation of DCM. After 3 hours, the nanoparticle suspensions were collected via ultracentrifugation (Beckman Coulter Optima XPN-80) using a 70.1 Ti rotor at 35 000 rpm for 40 minutes at 4 °C. The resulting NPs were washed and then fresh deionised water (dH₂O) (5mL) was added before another ultracentrifugation step at the same parameters was performed.

A series of 5% (2.5 mg) w/w- and 10 % (5 mg) w/w resveratrol-encapsulated polymeric NPs (5% RNP and 10% RNP) were synthesised using the procedure described for the blank nanoparticles (BNP). The resveratrol was

added to the polymer (50 mg) before the addition of DCM (2 mL) to produce the organic phase. The procedure was then followed exactly as with the BNP.

2.3.2.4. Polymeric nanoparticle analysis

2.3.2.4.1. Particle size and zeta potential

Dynamic light scattering with a particle size analyser (Zetasizer Nano ZS, Malvern Instruments Ltd, UK) was employed to measure the particle size, zeta potential, and polydispersity index (PDI). An aliquot (100 μ L) of the nanoparticle suspension (before ultracentrifugation) was diluted in dH₂O (5 mL), then it was transferred into a cuvette and measured at 25 °C (n=3). Measurements were also taken from the NPs obtained after ultracentrifugation. The NPs (10 mg) were suspended in dH₂O (5 mL) and dispersed using an ultrasonic water bath (Ultrawave, UK) for 1 minute. An aliquot (500 μ L) of the resulting suspension was diluted in dH₂O (5 mL), then it was transferred into a cuvette and measured at 25 °C (n=3).

2.3.2.4.2. Drug loading and encapsulation efficiency (EE%)

Centrifugation of the polymeric NPs (BNP, 5% RNP, 10% RNP) resulted in the formation of a pellet of NPs. The NPs were dispersed in dH₂O (5 mL). This solution was then transferred to 5mL screw top vials (Agilent Technologies, USA) and frozen using liquid nitrogen. These solid samples were then loaded into a beaker and attached to a Telstar Lyoquest Freeze-drier coupled with a Telstar bomba Torricelli vacuum pump (Azbil Telstar, UK). The samples were allowed to dry overnight. The dry samples were collected and weighed.

High performance liquid chromatography (HPLC) (1200 series; Agilent Technologies, USA) using a YMC-Triart C18 150 x 4.6 mm I.D. S-5 μ m, 12 nm

column (YMC Co. LTD., Japan) was used to determine the amount of resveratrol encapsulated in the polymeric NPs. A sample (10 mg) of the previously freeze dried polymeric NPs (BNP, 5% RNP, and 10% RNP) were dispersed in the mobile phase methanol:water (51:49; v/v) (2.5 mL). These solutions (4mg/mL) were filtered into clean 2mL crimp vials (Agilent Technologies, USA) using a plastic syringe fitted with a Captiva Econofilter PTFE 13 mm 0.45 μm filter (Agilent Technologies, USA). The samples (10 μL) were injected into the system with a flow rate of 0.54 mL/min. The variable wavelength detector (VWD; Agilent Technologies, USA) was set at 306 nm. The BNP was used as a control.

Previously, resveratrol standards (0.3 μg –625 μg) were run on the HPLC using the same parameters as above. The results of the area under the curve were plotted against the various concentrations to obtain a calibration curve. This calibration curve was used to determine the amount of resveratrol encapsulated in the polymeric NPs.

Theoretical drug loading (TDL) was calculated using the following equation:

$$TDL = \frac{\text{Weight of resveratrol (mg) added}}{\text{weight of polymer (mg)}} \quad \text{Equation 2-1}$$

$$5\% \text{ RNP (TDL)} = \frac{2.5 \text{ mg}}{50 \text{ mg}} = 0.05 \text{ mg} = 50 \mu\text{g/mg (w/w)}$$

$$10\% \text{ RNP (TDL)} = \frac{5 \text{ mg}}{50 \text{ mg}} = 0.1 \text{ mg} = 100 \mu\text{g/mg (w/w)}$$

EE% was calculated using the following equation:

$$EE\% = \frac{\text{Drug loading calculated from standard curve } (\mu\text{g})}{TDL (\mu\text{g})} \times 100 \quad \text{Equation 2-2}$$

2.3.2.4.3. Release study

PGA-co-PDL NPs (BNP, 5% RNP, and 10% RNP; 10mg) were obtained after centrifugation (Beckman Coulter Optima XPN-80) using a 70.1 Ti rotor at 35 000 rpm for 40 minutes at 4 °C. Percentage resveratrol released (RR) was calculated as follows:

$$RR \% = \frac{\text{resveratrol released at time point } (\mu\text{g})}{\text{resveratrol loaded } (\mu\text{g})} \times 100 \% \quad \text{Equation 2-3}$$

Two methods were attempted:

2.3.2.4.3.1. Sacrificial method

A weighted amount (10 mg) of the NPs (BNP, 5% RNP, and 10 %RNP) were placed in separate sealed Falcon tubes containing PBS (10 mL; pH 7.4). An aliquot (2 mL) was transferred to a fresh Eppendorf tube (1 mg/mL). The Eppendorf tubes (3x5) were placed on a Grant-Bio PTR-35 multi-function rotator (Grant Instruments, UK) stirring at 30 rpm in a Stuart S160 incubator (Stuart Equipment, UK) at 37 °C. At pre-determined intervals, one Eppendorf tube per formulation was removed from stirring and centrifuged using an Eppendorf 5415 D centrifuge (Eppendorf, Germany) at 12000 rpm for 10 minutes. The supernatant was analysed via HPLC for resveratrol content using the method described in 2.3.2.4.2.

2.3.2.4.3.2. Replacement method

This method was performed in the same way as in 2.3.2.4.3.1. However, there was only 1 Eppendorf tube per formulation. At pre-determined intervals, the Eppendorf tubes, one for each formulation, were removed from stirring and centrifuged using an Eppendorf 5415 D centrifuge (Eppendorf, Germany) at

12000 rpm for 10 minutes. Afterwards, an aliquot (1 mL) of the supernatant was removed and replaced with a fresh aliquot of PBS (1 mL). The supernatant was analysed via HPLC for resveratrol content using the method described in 2.3.2.4.2.

2.3.2.5. Cell culture

Human lung adenocarcinoma cells (Calu-3) were grown in Minimum Essential Medium Eagle (MEM) media supplemented with 10% foetal bovine serum (FBS), 1% L-glutamine, 1% penicillin-streptomycin, 1% MEM Non-essential amino acids and 1% sodium pyruvate in a 75 cm² tissue culture flask in a humidified incubator at 37 °C with 5% CO₂.

2.3.2.6. Cell viability studies

2.3.2.6.1. Alamar Blue (resazurin sodium salt)

Resazurin sodium salt (7-Hydroxy-3H-phenoxazin-3-one-10-oxide sodium salt), also known as Alamar Blue, was used to assess the *in vitro* cytotoxicity of the PGA-co-PDL BNP and resveratrol-encapsulated NPs. Resazurin, which is blue and nonfluorescent, is reduced by healthy cells, to resorufin, which is pink and highly fluorescent (O'Brien *et al.*, 2000).

The cells were cultured as described in 2.3.2.5.

For the assay, cells in the T75 flask were counted using a C-Chip Neubauer improved haemocytometer (LabTech, UK) and diluted with fresh cell culture media to give a density of 10⁴ cells/mL in a final volume of 10 mL. An aliquot (100 µL) of this suspension of cells was seeded into each well (10³ cells/well) of a Corning 96-well, opaque, clear flat-bottom plate (Sigma-Aldrich, UK). The plate was then placed in the incubator at 37 °C for 48 hours with 5% CO₂. After

48 hours, the spent media was removed and replaced with fresh cell culture medium (100 μ L/well). Then, an aliquot (100 μ L) each of BNP, 5% RNP, and 10% RNP, freshly prepared in complete cell culture medium to an appropriate range of working concentrations (0-1 mg/mL) (n=3), was added to the wells, with 10% dimethyl sulfoxide (DMSO) used as a positive control. After 24 hours of incubation at 37 °C with 5% CO₂, all the spent media was removed and the wells were rinsed with PBS (100 μ L). Then, resazurin sodium salt (50 mg) was added to PBS (10 mL) to form a 10x solution of resazurin sodium salt. Afterwards, an aliquot (1 mL) of the 10x resazurin sodium salt solution was added to PBS (9 mL) to make up a 1x solution. An aliquot (10 μ L) of this 1x solution was then added to each well, which already contained fresh cell culture media (100 μ L), giving a final concentration of 50 μ g/mL that the cells were exposed to, and the plate was again incubated at 37 °C with 5% CO₂. After 3 hours, the fluorescence intensity of the solution, which directly correlates with the number of viable cells, was measured (excitation: 540 nm; emission: 590 nm) using a CLARIOstar plate reader (BMG Labtech, Germany). The percentage of viable cells in each well was determined by taking the fluorescence intensity of the negative (untreated) control as 100% viability and normalising the fluorescence intensity of each treatment to it.

2.3.2.6.2. Lactate Dehydrogenase (LDH) assay

The cells were cultured and plated as described in 2.3.2.6.1, except the cells were treated with different concentrations: BNP, 10% RNP, Free-resveratrol (18.8-300 μ M) and 5% RNP (9.375-150 μ M) (n=3). After 48 hours or 72 hours of incubation at 37 °C with 5% CO₂, the protocol supplied with the kit was followed (catalogue #: 88954, ThermoFisher). Briefly, lysis buffer (10 μ L), supplied with the kit, and ultrapure water (10 μ L), as a control for the lysis buffer, were added to separate wells (triplicates). The plate was then incubated at 37 °C with 5% CO₂ for 45 minutes. After 45 minutes, an aliquot (25 μ L) of each well containing cells was taken and transferred to a fresh Falcon 96-well flat bottom plate (Corning, USA) (**Figure 2-5**). Reaction mixture (25 μ L) was added to each sample well and mixed by gentle tapping. The plate was incubated at room temperature for 30 minutes protected from light. After 30 minutes, stop solution (25 μ L) was added to each sample well and mix by gentle tapping. The absorbance at 490nm and 680nm was measured using a CLARIOstar plate reader (BMG Labtech, Germany). For the analysis, the absorbance value at 680 nm (background signal from instrument) was subtracted from the absorbance value at 490 nm.

						300	150	75	37.5	18.8	9.375		
		1	2	3	4	5	6	7	8	9	10	11	12
A		X	X	X	X	X	X	X	X	X	X	X	X
B		X	LB	LBC	VC	VCR	BNP	5% RNP	X				
C		X	LB	LBC	VC	VCR	BNP	5% RNP	X				
D		X	LB	LBC	VC	VCR	BNP	5% RNP	X				
E		X	10% RNP	FR	FR	FR	FR	FR	X				
F		X	10% RNP	FR	FR	FR	FR	FR	X				
G		X	10% RNP	FR	FR	FR	FR	FR	X				
H		X	X	X	X	X	X	X	X	X	X	X	X
			300	150	75	37.5	18.8	300	150	75	37.5	18.8	

X	Empty wells containing only media
LB	Cells treated with lysis buffer
LBC	Cells treated with lysis buffer control (ultrapure water)
VC	Cells treated with vehicle control for particles (complete media)
VCR	Cells treated with vehicle control for resveratrol (complete media with ethanol)
BNP	Cells treated with blank NP
5% RNP	Cells treated with 5% Resveratrol-loaded NP
10% RNP	Cells treated with 10% Resveratrol-loaded NP
FR	Cells treated with free resveratrol

Figure 2-5 Plate layout for LDH assay

2.3.2.7. Statistical analyses and IC₅₀ calculations

All statistical analyses were performed using Graphpad Prism 7. One-way analysis of variance (ANOVA) followed with Tukey's multiple comparisons test was employed to compare the mean values (from the formulations) with each other. Statistically significant differences were assumed when $p < 0.05$. The level of confidence was set as 95%. All values are expressed as their mean \pm standard error of mean (SE) (cell studies) or mean \pm standard deviation (SD) (all other studies). IC₅₀ was calculated in GraphPad Prism using the non-linear regression equation log (inhibitor) vs. response (three parameters) or log (inhibitor) vs. response -variable slope (four parameters).

2.3.3. Results

2.3.3.1. Monomer analysis

2.3.3.1.1. FT-IR and NMR

2.3.3.1.1.1. ω -Pentadecalactone (PDL)

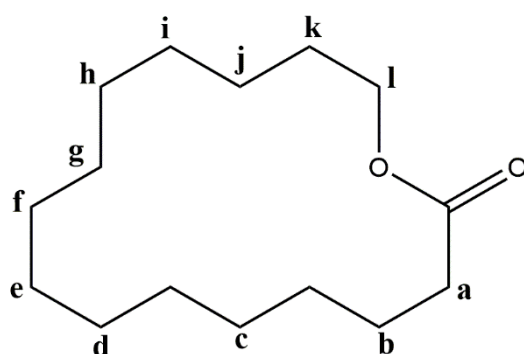


Figure 2-6 Structure of ω -pentadecalactone

FT-IR ν max: 3469, 2924, 2853, 2686, 1731, 1461, 1378, 1348, 1284, 1248, 1242, 1235, 1157, 1108, 1070, 1060, 1054, 1013, 964, 880 cm^{-1} . ^1H NMR (300

MHz, CDCl₃) δ 4.15 – 4.10 (m, 2H, H-l), 2.35 – 2.29 (m, 2H, h-a), 1.70 – 1.57 (m, 4H, H-b,k), 1.44 – 1.26 (m, 20H, H-c-j).

2.3.3.1.1.2. Divinyl adipate (DVA)

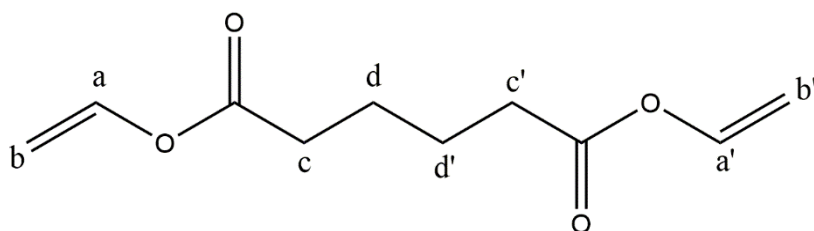


Figure 2-7 Structure of divinyl adipate

FT-IR ν max: 3466, 3095, 3047, 2993, 2963, 2953, 2914, 2883, 1736, 1641, 1407 cm^{-1} . ¹H NMR (300 MHz, CDCl₃) δ 7.31 – 7.23 (m, 2H, H-a, a'), 4.88 (dd, J = 14.0, 1.6 Hz, 2H, H-b), 4.57 (dd, J = 6.3, 1.6 Hz, 2H, H-b'), 2.47 – 2.37 (m, 4H, H-c,c'), 1.77 – 1.67 (m, 4H, d,d').

2.3.3.1.1.3. Glycerol

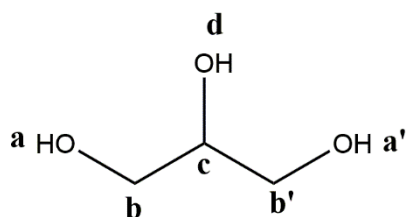


Figure 2-8 Structure of glycerol

FT-IR ν max: 3255, 2929, 2877, 1026 cm^{-1} . ¹H NMR (300 MHz, Deuterium Oxide) δ 3.84 – 3.76 (m, 1H, H-c), 3.70 – 3.53 (m, 4H, H-b,b').

2.3.3.1.1.4. Poly(ethylene glycol) methyl ether (mPEG₂₀₀₀)

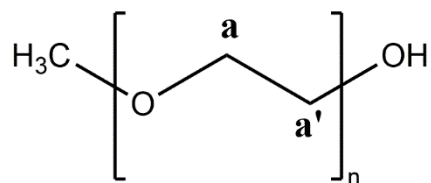


Figure 2-9 Structure of mPEG₂₀₀₀

FT-IR ν max: 2900, 1120 cm⁻¹. ¹H NMR (300 MHz, CDCl₃) δ 3.64 (s, 182H, H-a,a').

2.3.3.2. *Polymer analysis*

2.3.3.2.1. Molecular weight – GPC

Mwts of polymers were ascertained from a standard curve (**Figure 2-10**) made from the polystyrene standards.

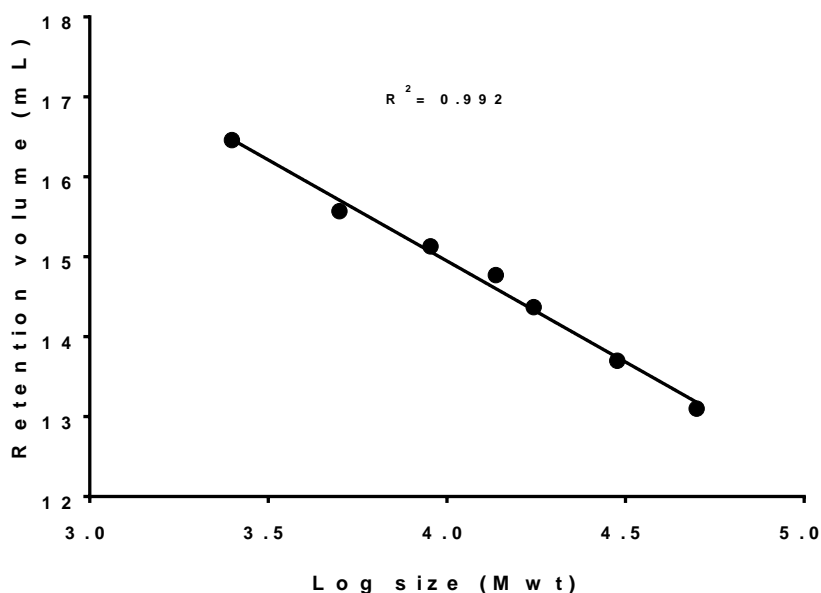


Figure 2-10 Polymer standard curve using GPC ($R^2=0.992$) $n=3$

2.3.3.2.1.1. PGA-co-PDL

The PGA-co-PDL polymer with a monomer ratio of 1:1:1 was a white powder. GPC analysis of the polymer revealed a MWt of 16.5 KDa with respect to (wrt) polystyrene standards.

2.3.3.2.1.2. PGA-co-PDL-PEG₂₀₀₀

The PGA-co-PDL-PEG₂₀₀₀ with a monomer ratio of 1:1:1:0.01 was a fine white powder. GPC analysis of the polymer revealed a MWt of 21.4 KDa wrt polystyrene standards.

2.3.3.2.1.3. PLGA

The PLGA polymer was a fine white powder that was reported to have a MWt of between 7 and 17KDa. GPC analysis of the polymer revealed a MWt of 14.9 KDa wrt polystyrene standards.

2.3.3.2.1.4. mPEG-PLGA

The mPEG-PLGA polymer was a hard, white block. The monomers were reported to have an average MWt of 2KDa (PEG) and 11.5 KDa (PLGA). GPC analysis of the polymer revealed a MWt of 30.4 KDa wrt polystyrene standards.

2.3.3.2.2. Chemical structure – FT-IR and NMR

2.3.3.2.2.1. PGA-co-PDL

Both FT-IR and NMR (**Figure 2-12**) were utilised for structural confirmation. FT-IR spectroscopy was used to analyse the end groups of the polymer, in order to confirm the completion of the reaction and formation of the product.

The FT-IR spectrum of PGA-co-PDL showed a trough at 3455 cm^{-1} which specifies an O-H bond and a sharp peak signifying a carbonyl stretch at 1727 cm^{-1} (**Figure 2-11**). Additionally, the lack of characteristic bands linked to the terminal vinyl groups of DVA at 1650 cm^{-1} (**Figure 2-7**) confirms the complete consumption of monomers during polymerisation.

The monomer ratio was estimated by using the $^1\text{H-NMR}$ integration method (Kolhe *et al.*, 2004).

PGA-co-PDL – theoretical molar ratio (1:1:1)

- a. Number of $-\text{CH}_2$ protons at $\delta\ 2.43 - 2.21 = 4$ protons = 1 molecule of DVA
- b. Number of $-\text{CH}_2$ protons at $\delta\ 4.20 - 3.99 = 4$ protons = 1 molecule of glycerol
- c. Number of $-\text{CH}_2$ protons at $\delta\ 4.20 - 3.99, 2.43 - 2.21, 1.69 - 1.57$ and $1.27 = 28$ protons = 1 molecule of PDL

PGA-co-PDL – calculated molar ratio (1:1:1)

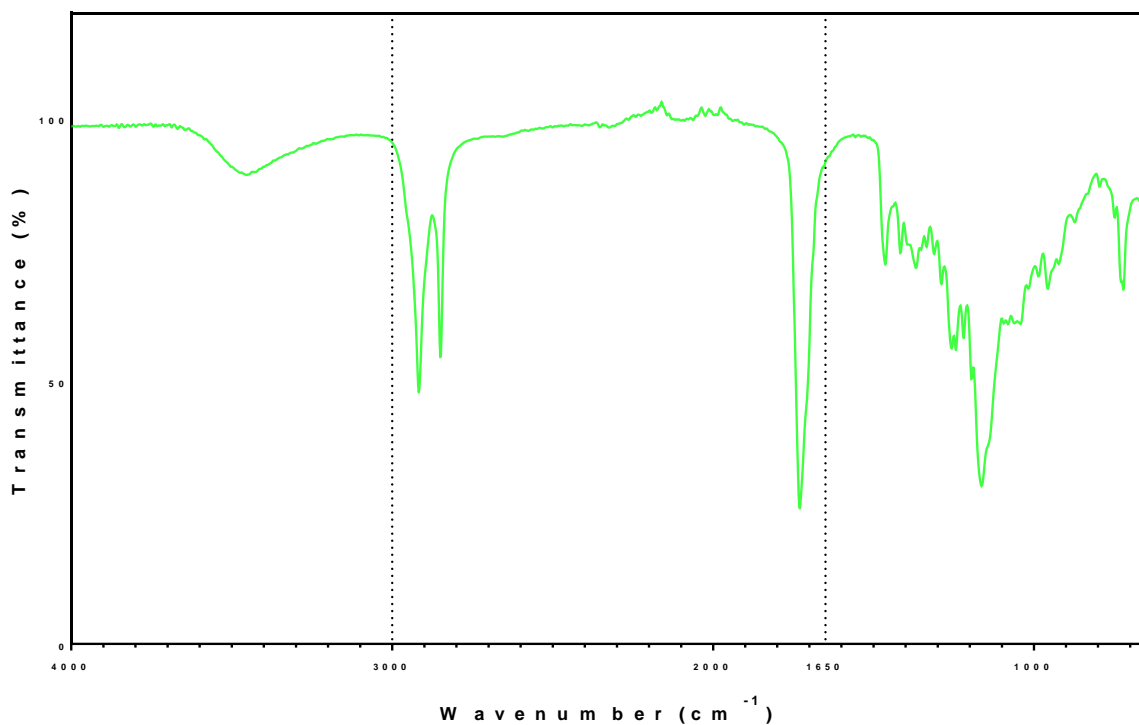


Figure 2-11 FT-IR spectrum of PGA-co-PDL

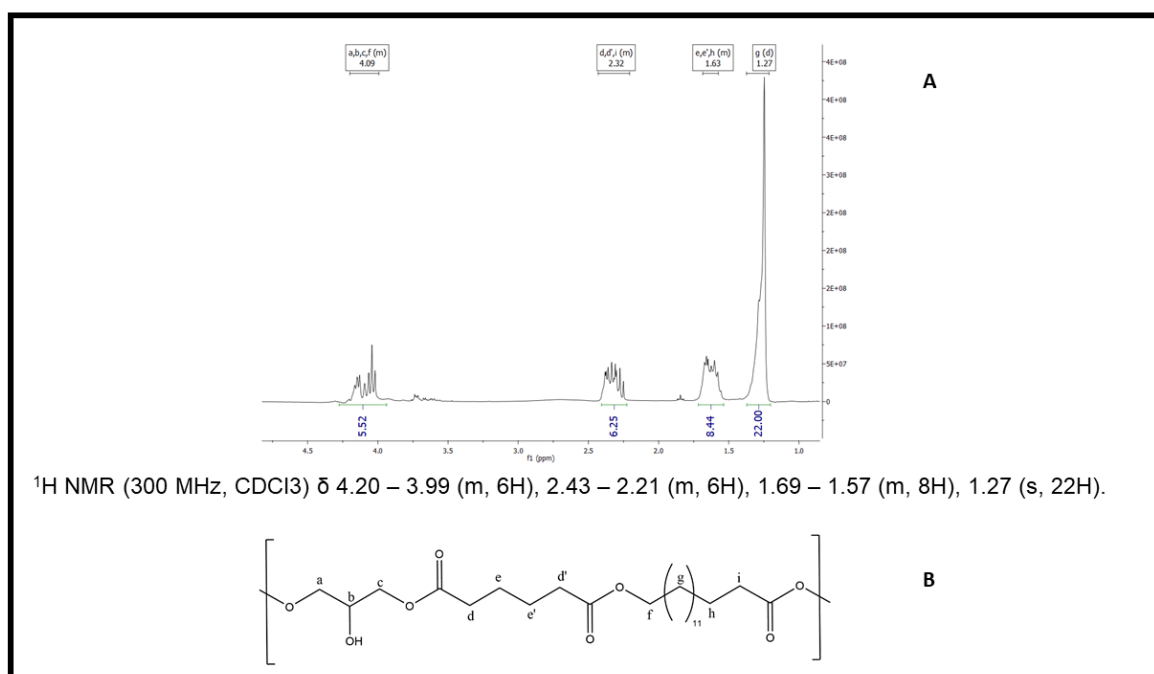


Figure 2-12 $^1\text{H-NMR}$ spectrum (A) and structure of PGA-co-PDL (B) with protons labelled

2.3.3.2.2.2. PGA-co-PDL-PEG₂₀₀₀

Both FT-IR and NMR (**Figure 2-14**) was again used for the structural confirmation of the PGA-co-PDL-PEG₂₀₀₀ copolymer. The FT-IR spectrum was used to analyse the end groups of the polymer, in order to confirm the completion of the reaction and formation of the product. The FT-IR spectrum of PGA-co-PDL-PEG₂₀₀₀, like the one for PGA-co-PDL, showed a trough at 3455 cm⁻¹ which specifies an O-H bond and a sharp peak signifying a carbonyl stretch at 1727 cm⁻¹ (**Figure 2-13**). Additionally, the lack of characteristic bands linked to the terminal vinyl groups of DVA at 1650 cm⁻¹ (**Figure 2-7**) confirms the complete consumption of monomers during polymerisation. Additionally, the singlet peak on the NMR (**Figure 2-14**) showed that there was integration of the PEG monomer.

The monomer ratio was estimated by using the ¹H-NMR integration method (Kolhe *et al.*, 2004).

PGA-co-PDL-PEG₂₀₀₀ – theoretical molar ratio (1:1:1:0.01)

- a. Number of -CH₂ protons at δ 2.42 – 2.24 = 4 protons = 1 molecule of DVA
- b. Number of -CH₂ protons at δ 4.19 – 4.00 = 4 protons = 1 molecule of glycerol
- c. Number of -CH₂ protons at δ 4.19 – 4.00, 2.42 – 2.24, 1.72 – 1.54, 1.26 = 26 protons = 0.93 molecule of PDL
- d. Number of -CH₂ protons at δ 3.64 = 1 proton = 0.005 molecule of PEG₂₀₀₀

PGA-co-PDL-PEG₂₀₀₀ – calculated molar ratio (1:1:0.93:0.005)

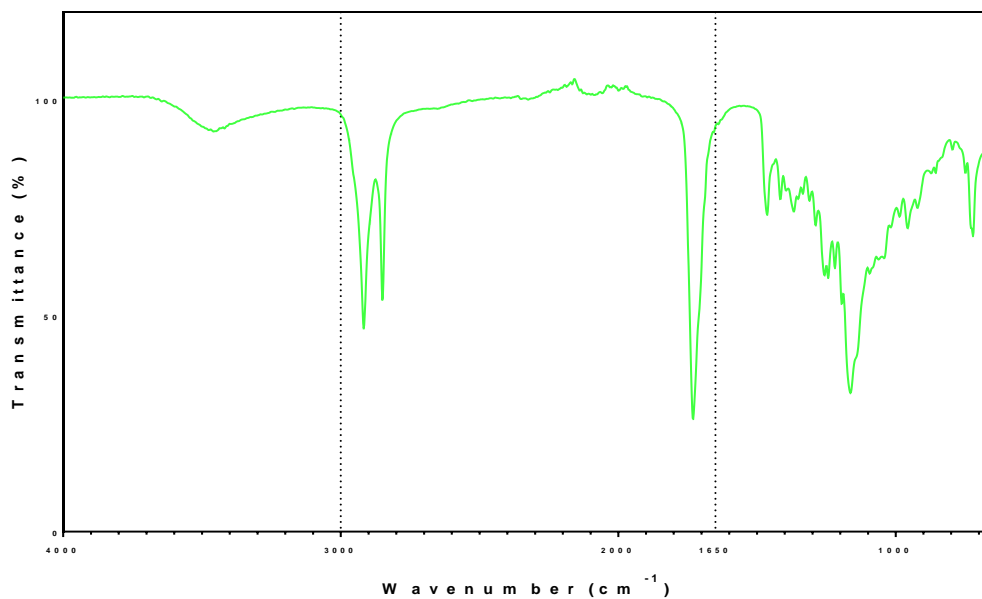


Figure 2-13 FT-IR spectrum of PGA-co-PDL-PEG₂₀₀₀

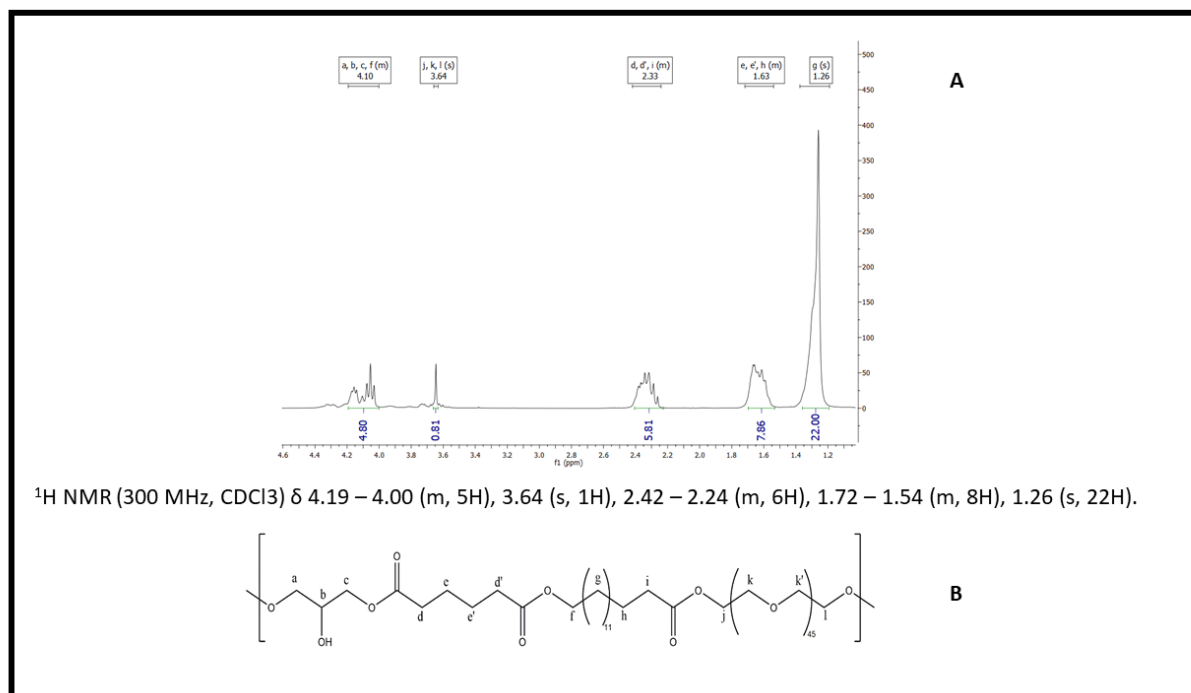


Figure 2-14 ¹H-NMR spectrum (A) and structure of PGA-co-PDL-PEG₂₀₀₀ (B) with protons labelled

2.3.3.2.2.3. PLGA

Both FT-IR (**Figure 2-15**) and NMR (**Figure 2-16**) gave similar results to previous reports (Carvalho and Erbetta, 2012). This analysis was done to confirm the structure of the purchased polymer. The equations provided in (Carvalho and Erbetta, 2012) were used to determine the monomer make-up of the PLGA copolymer (**Equations 2-4, 2-5**):

$$\% D, L - lactide\ monomer = \frac{(CH3\ 1.56\ ppm\ integral\ area \div 3)}{((CH3\ 1.56\ ppm\ integral\ area \div 3) + (CH2\ 4.73\ ppm\ integral\ area \div 2))} \times 100\% \quad \text{Equation 2-4}$$

$$\% glycolide\ monomer = \frac{(CH2\ 4.73\ ppm\ integral\ area \div 2)}{((CH3\ 1.56\ ppm\ integral\ area \div 3) + (CH2\ 4.73\ ppm\ integral\ area \div 2))} \times 100\% \quad \text{Equation 2-5}$$

The results from **Equations 2-4, 2-5** showed that the PLGA copolymer consisted of a 50:50 blend (*D,L*-lactide: glycolide).

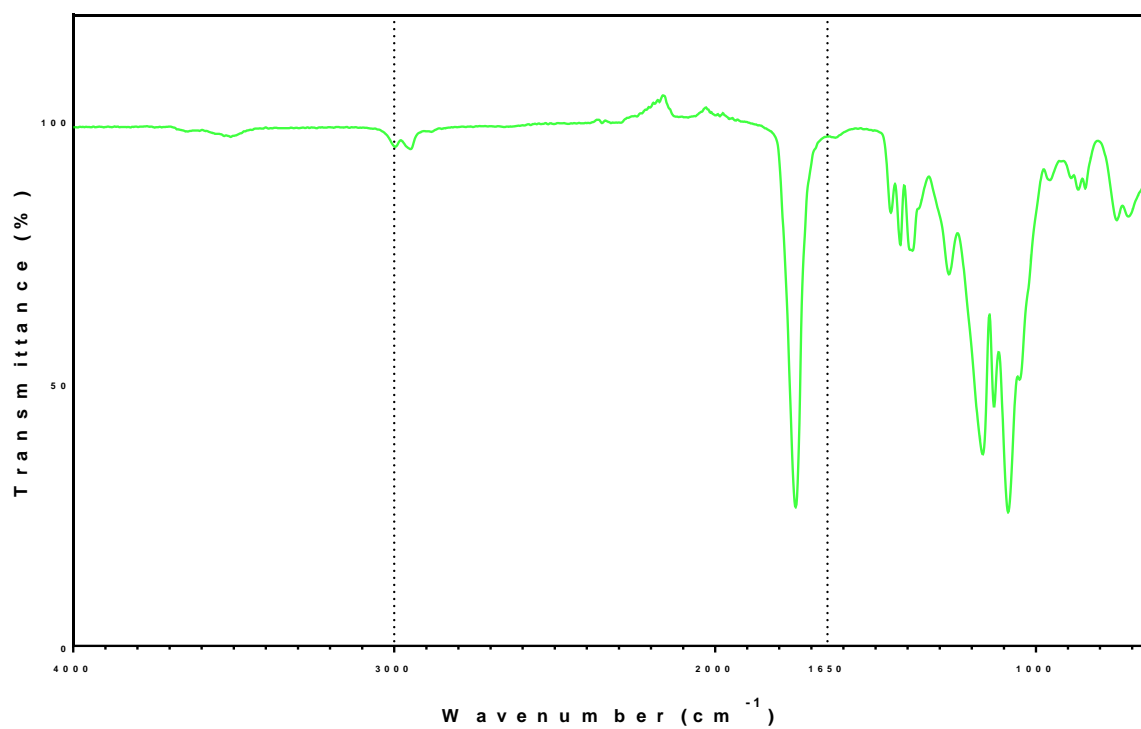


Figure 2-15 FT-IR spectrum of PLGA

¹H NMR (300 MHz, CDCl₃) δ 5.38 – 5.06 (m, 1H), 4.73 (d, J = 3.9 Hz, 2H),
1.56 (d, J = 7.5 Hz, 3H).

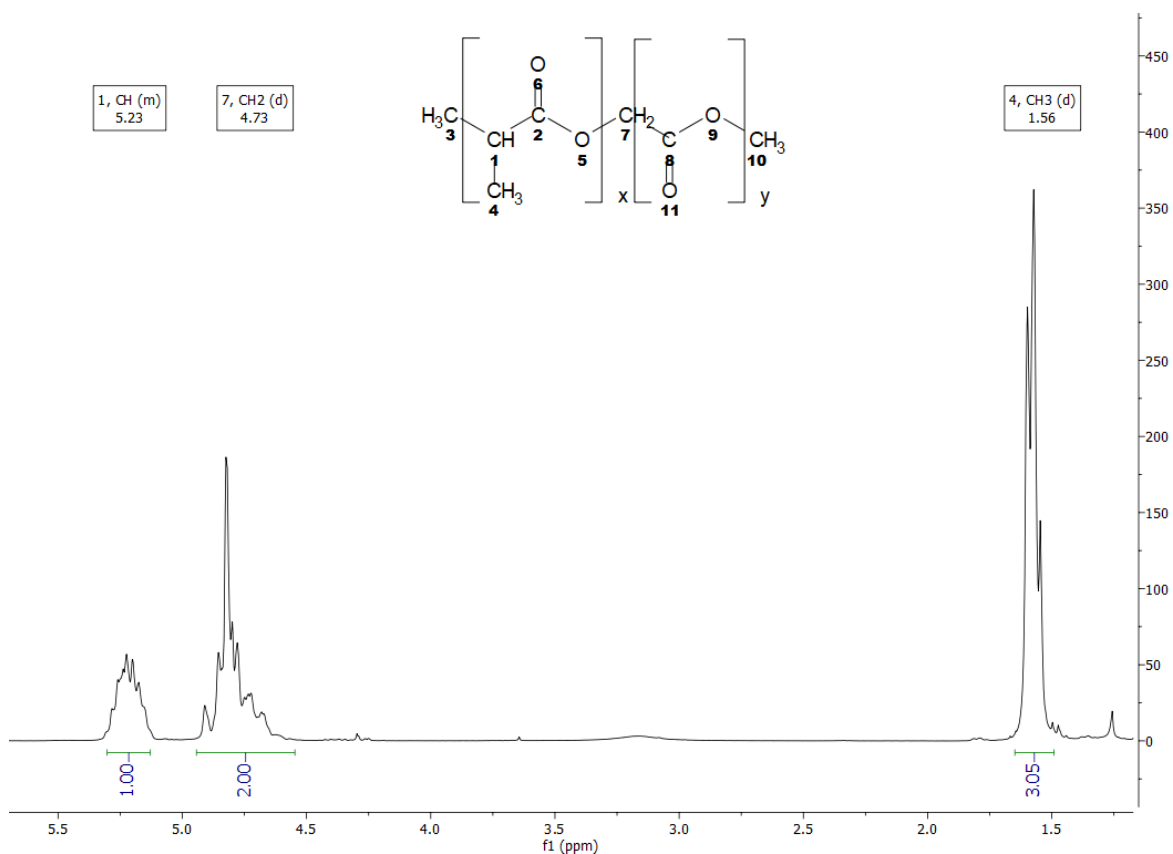


Figure 2-16 ¹H-NMR spectrum of PLGA

2.3.3.2.2.4. mPEG-PLGA

Both FT-IR (**Figure 2-17**) and NMR (**Figure 2-18**) gave similar results to previous reports (Pereira *et al.*, 2016). This analysis was done to confirm the structure of the purchased polymer. The ¹H-NMR for PEG-PLGA has the same peaks as PLGA, with the addition of a new peak at 3.64 ppm corresponding to the methylene groups present in PEG. The peaks for the monomers of PLGA, *D,L*-lactide and glycolide correspond to the peaks at 1.58 ppm and peaks at 4.82 ppm & 5.22 ppm, respectively (Koopaei *et al.*, 2012). The relationship between the peak areas and the number of protons was used to calculate the molar amount of each monomer of the copolymer.

D,L -lactide = δ 1.58-1.64 = 3/7.5 = 40%

Glycolide = δ 4.58-4.95, 5.22 = 3/7.5 = 40%

PLGA = 6/7.5 = 80%

PEG = δ 3.64 = 1.5/7.5 = 20%

The FT-IR structure for PEG-PLGA is similar to the PLGA FT-IR spectrum, which is due to the low amount of PEG present in the copolymer (20% w/w), which is similar to values reported by the manufacturer (17%).

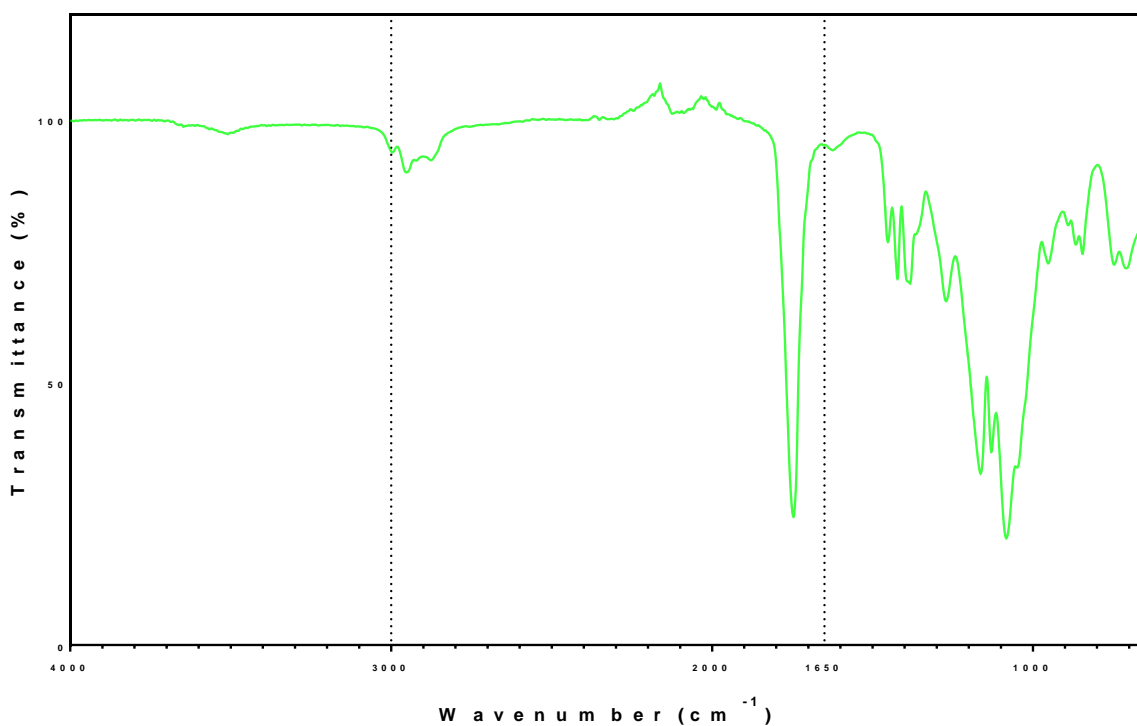


Figure 2-17 FT-IR spectrum of PEG-PLGA

¹H NMR (300 MHz, CDCl₃) δ 5.22 (tdd, 1H), 4.95 – 4.58 (m, 2H), 3.64 (s, 1.5H), 1.64 – 1.58 (m, 3H).

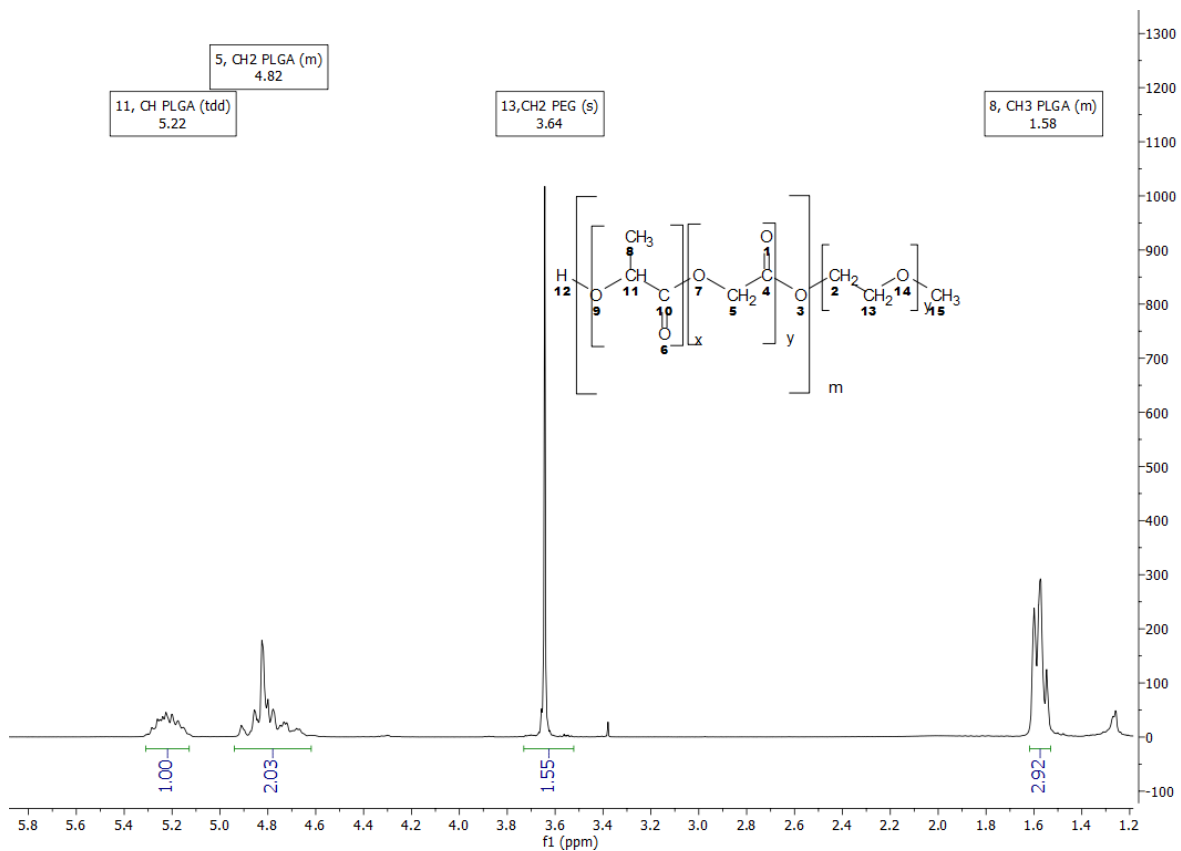


Figure 2-18 ¹H-NMR spectrum of mPEG-PLGA

2.3.3.2.3. Thermal analysis – DSC

2.3.3.2.3.1. PGA-co-PDL

The T_m (melting point) of PGA-co-PDL (**Figure 2-19**) as determined by DSC was 58.5 °C, which is similar to 55.3 °C previously reported (Tawfeek *et al.*, 2011).

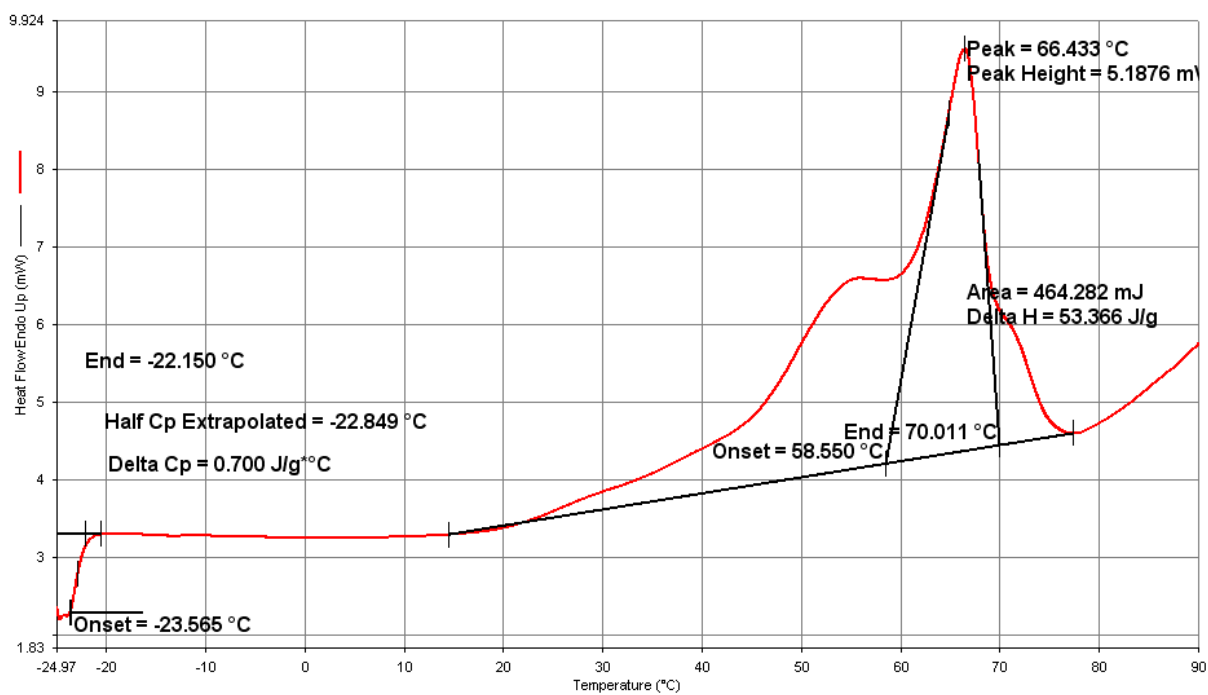


Figure 2-19 DSC of PGA-co-PDL

2.3.3.2.3.2. PGA-co-PDL-PEG₂₀₀₀

The T_m (melting point) of PGA-co-PDL-PEG₂₀₀₀ (**Figure 2-20**) as determined by DSC was 44.9 °C.

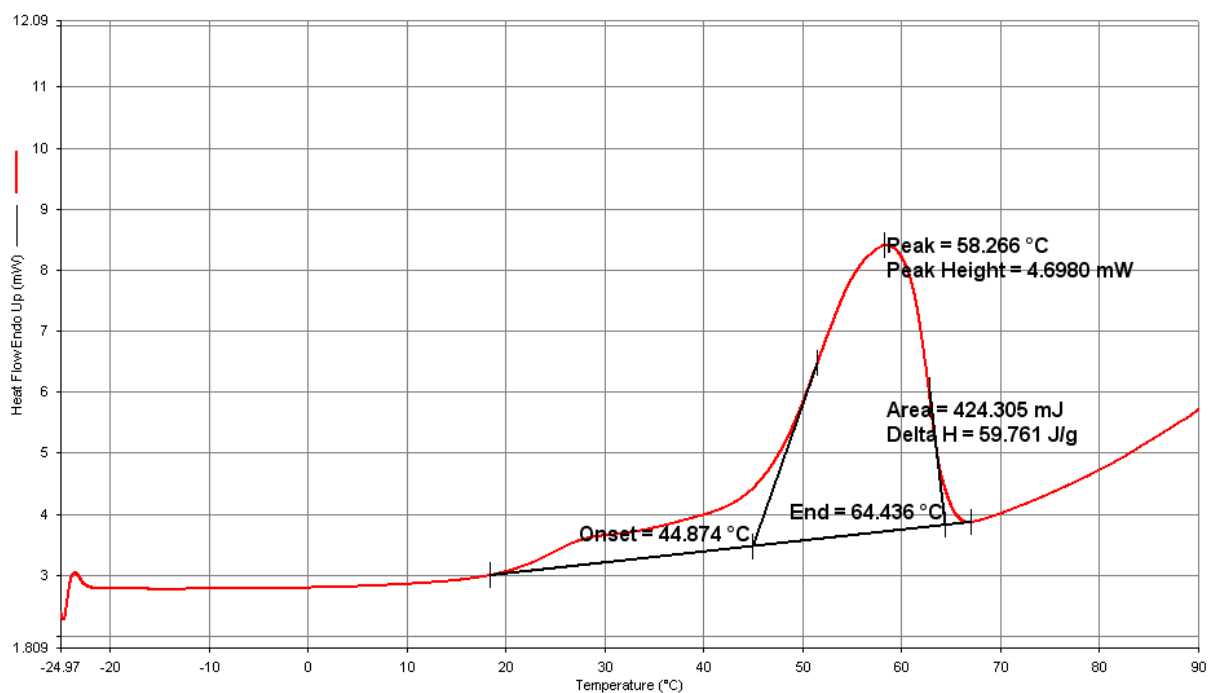


Figure 2-20 DSC of PGA-co-PDL-PEG₂₀₀₀

2.3.3.2.3.3. PLGA

The absence of a melting transition phase (**Figure 2-21**) infers that the analysed copolymers are amorphous, which is in agreement with the literature. PLGA containing less than 85% glycolide are amorphous (Carvalho and Erbetta, 2012).

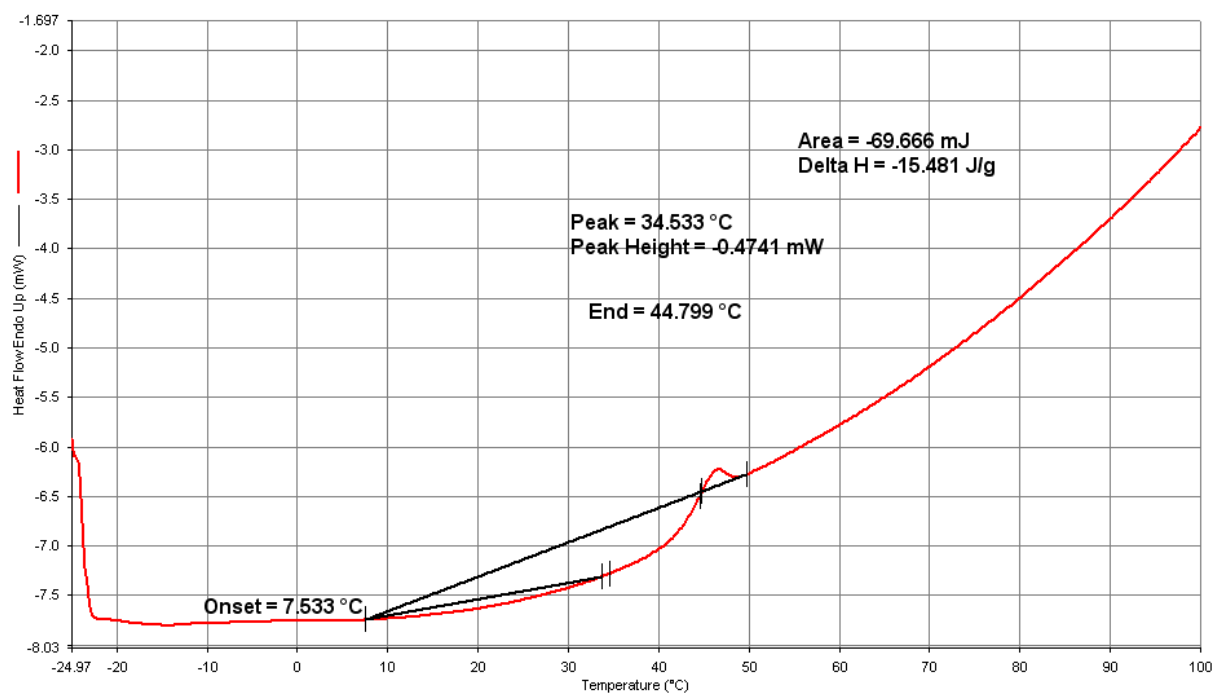


Figure 2-21 DSC of PLGA

2.3.3.2.3.4. mPEG-PLGA

Transition temperature at 241-246 °C according to the manufacturer.

2.3.3.3. Nanoparticle analysis

2.3.3.3.1. Particle size, polydispersity index (PDI), and zeta potential

Results from the zetasizer showing the particle size, polydispersity index, and zeta potential of all four different types of NPs. NPs of PGA-co-PDL-PEG₂₀₀₀, PLGA, and mPEG-PLGA are all under 205 nm, while PGA-co-PDL NPs were between 220 and 252 nm (**Table 2-1**). All NPs were highly negatively charged with good polydispersity, indicating high stability and good size distribution, respectively.

Table 2-1 Particle size, PDI, and zeta potential of NPs before and after centrifugation

Polymer	Formulation	Before centrifugation			After centrifugation		
		Size (d.nm)	PDI	Zeta potential (mV)	Size (d.nm)	PDI	Zeta potential (mV)
PGA-co-PDL	BNP	200 ± 5	0.120 ± 0.040	-9.06 ± 0.22	252 ± 9	0.293 ± 0.043	-30.00 ± 1.11
	5% RNP	205 ± 1	0.142 ± 0.002	-7.25 ± 0.31	229 ± 5	0.257 ± 0.032	-28.70 ± 0.05
	10% RNP	210 ± 5	0.091 ± 0.024	-4.25 ± 0.21	221 ± 5	0.219 ± 0.008	-30.27 ± 0.31
PGA-co-PDL-PEG ₂₀₀₀	BNP	188 ± 4	0.130 ± 0.031	-20.50 ± 0.98	190 ± 6	0.126 ± 0.011	-32.17 ± 0.47
	5% RNP	192 ± 2	0.091 ± 0.043	-19.17 ± 1.31	199 ± 5	0.126 ± 0.032	-31.80 ± 0.66
	10% RNP	208 ± 2	0.106 ± 0.047	-21.17 ± 1.33	200 ± 6	0.112 ± 0.040	-32.33 ± 1.61
PLGA	BNP	205 ± 1	0.125 ± 0.021	-12.97 ± 0.21	195 ± 5	0.257 ± 0.033	-35.37 ± 1.44
	5% RNP	201 ± 7	0.128 ± 0.018	-12.03 ± 0.06	202 ± 10	0.294 ± 0.002	-28.27 ± 1.27
	10% RNP	204 ± 2	0.170 ± 0.043	-10.78 ± 0.82	202 ± 5	0.290 ± 0.018	-30.40 ± 195
mPEG-PLGA	BNP	211 ± 7	0.353 ± 0.008	-18.57 ± 0.23	204 ± 5	0.285 ± 0.013	-36.37 ± 0.58
	5% RNP	198 ± 1	0.248 ± 0.020	-17.80 ± 1.65	197 ± 6	0.249 ± 0.024	-37.40 ± 0.17
	10% RNP	191 ± 6	0.276 ± 0.028	-22.00 ± 0.78	184 ± 4	0.230 ± 0.013	-36.97 ± 1.40

2.3.3.3.2. Drug loading and encapsulation efficiency (EE%)

2.3.3.3.2.1. Drug loading and encapsulation efficiency

Drug loading (DL) of the various polymeric NPs was calculated using a standard curve (**Figure 2-22**). The lowest concentration at which resveratrol can be detected (LOD) or quantified (LOQ) with acceptable precision and accuracy was calculated from the standard deviation (SD) of the response and the slope obtained from the linear regression of a specific calibration curve (0.5 µg/mL – 7.5 µg/mL) in the low-end region of the proposed range (ICH, 2005). The LOD and LOQ was calculated as 0.2 and 0.6 µg/mL, respectively. PGA-co-PDL NPs showed a drug loading capacity of 1.75 to 4 times that of its nearest competitor (PGA-co-PDL-PEG₂₀₀₀) for 10% RNP and 5% RNP, respectively (**Table 2-2**). PGA-co-PDL-PEG₂₀₀₀ showed an increase in EE% between 5% RNP and 10% RNP, while the other 3 formulations showed a decrease in EE% between 5% RNP and 10% RNP.

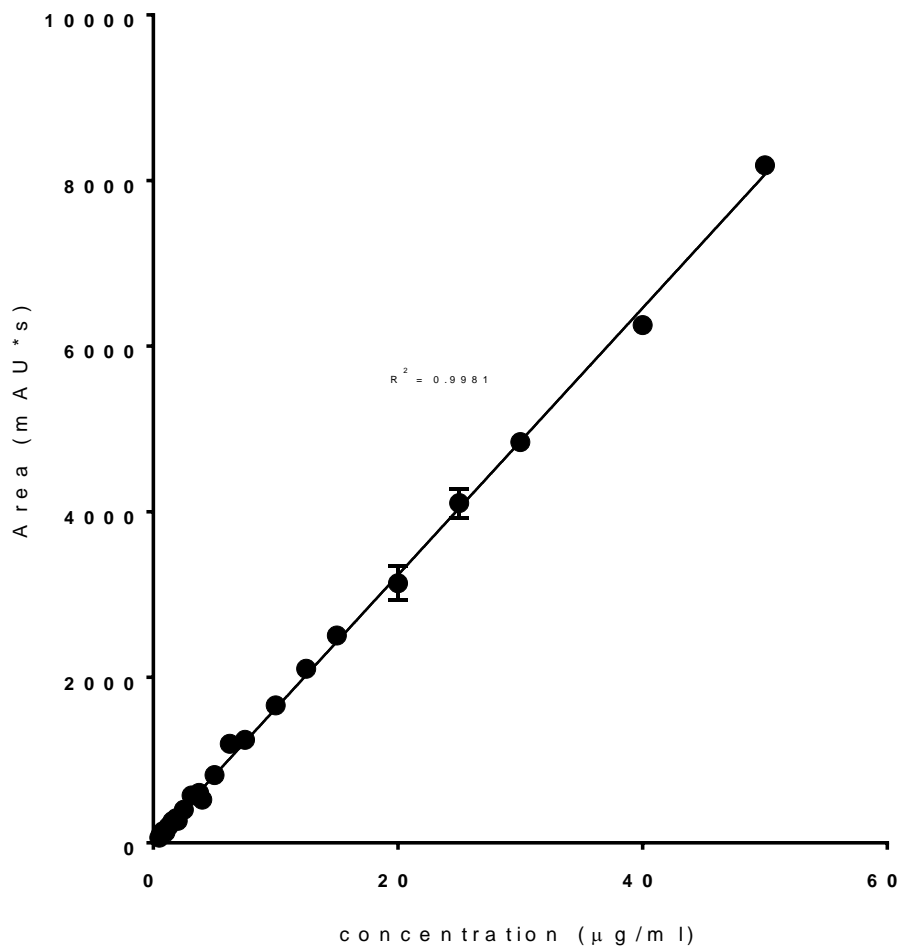


Figure 2-22 Resveratrol standard curve ($R^2=0.9981$) with SD as error bars (n=3)

Table 2-2 Drug loading and encapsulation efficiency of 5% resveratrol-loaded NPs (RNP) and 10% RNP of various polymeric NPs

Polymer	Formulation	Drug loading ($\mu\text{g}/\text{mg}$)*	encapsulation efficiency (%)
PGA-co-PDL	5% RNP	39 ± 0.12	78 ± 0.24
	10% RNP	70 ± 0.89	70 ± 0.89
PGA-co-PDL-PEG ₂₀₀₀	5% RNP	10 ± 0.39	20 ± 0.78
	10% RNP	40 ± 2.32	40 ± 2.32
PLGA	5% RNP	10 ± 0.13	20 ± 0.27
	10% RNP	14 ± 0.39	14 ± 0.39
PEG-PLGA	5% RNP	10 ± 0.24	20 ± 0.48
	10% RNP	13 ± 0.33	13 ± 0.33

* $\mu\text{g}/\text{mg}$ – concentration of resveratrol in micrograms in 1 milligram of polymeric nanoparticles

2.3.3.3.3. PGA-co-PDL NPs stability

2.3.3.3.3.1. Size and zeta potential at 4°C

The short-term stability of the PGA-co-PDL NPs (BNP, 5% RNP, and 10% RNP) was investigated for up to 28 days when stored at 4°C. With the BNP there was no statistically significant difference in the particle size compared to the initial preparation over the course of the stability study at 4°C ($p > 0.05$), apart from days 9 ($p < 0.0001$), 23 ($p < 0.005$), and 28 ($p < 0.0001$) (**Figure 2-23**). For zeta potential there was a lot more variation with days 3, 6, 8, 9, 13, 15, 19, 20, 27, and 28 showing statistically significant differences ($p < 0.005$)

compared to the day 1 sample with the rest of the days showing no statistically significant differences ($p > 0.05$) (**Figure 2-24**). For 5% RNP there was no statistically significant difference in the particle size compared to the initial preparation over the course of the stability study at 4°C ($p > 0.05$), apart from day 22 ($p < 0.05$) (**Figure 2-23**). For zeta potential, the same sample showed statistically significant differences ($p < 0.0001$) compared to the day 1 sample (**Figure 2-24**). The 10% RNP showed no statistically significant difference in the particle size compared to the initial preparation over the course of the stability study at 4°C ($p > 0.05$) (**Figure 2-23**). The zeta potential showed statistically significant differences ($p < 0.0001$) for all days compared to the day 1 sample (**Figure 2-24**).

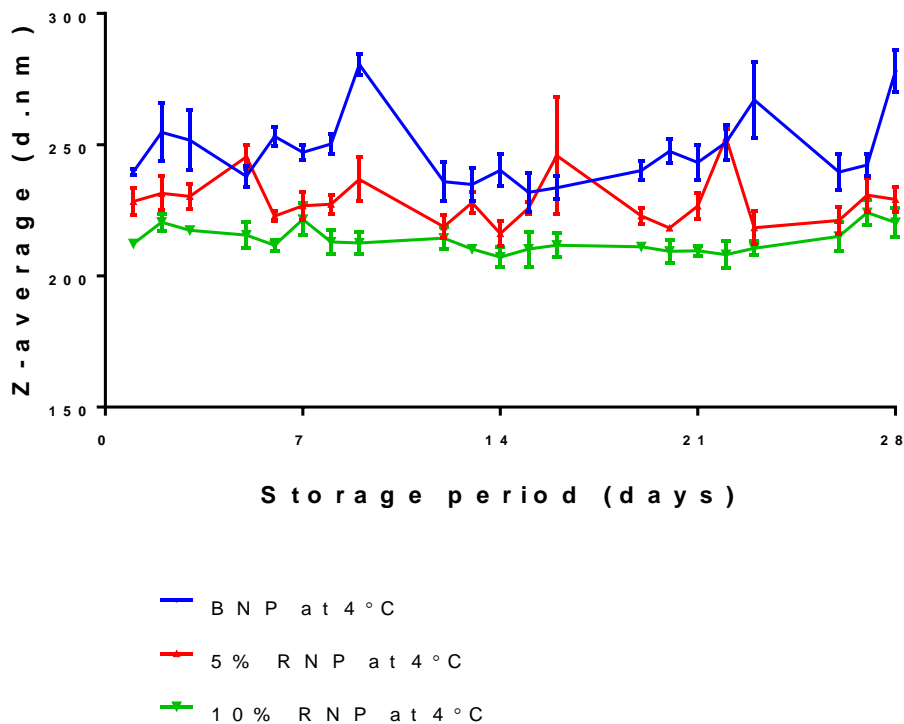


Figure 2-23 Effect of storage time on size of PGA-co-PDL NPs in water stored at 4°C ± SD (n=3)

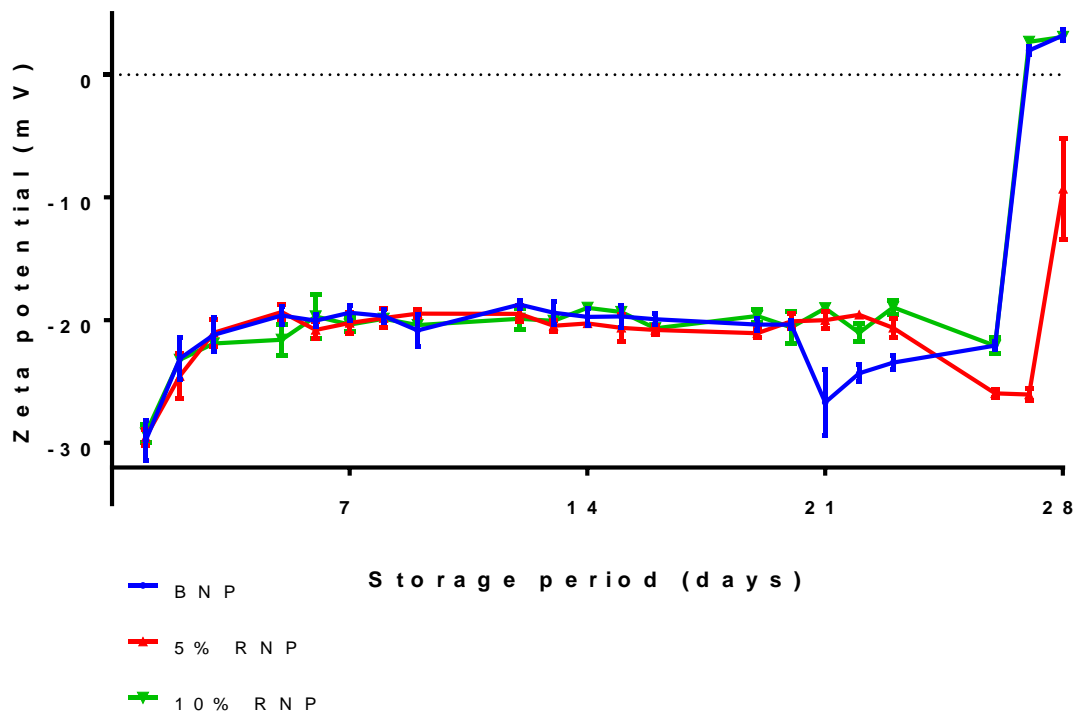


Figure 2-24 Effect of storage time on zeta potential of PGA-co-PDL NPs in water stored at 4°C ± SD (n=3)

2.3.3.3.3.2. Size when NPs are stored at 37 °C

The short-term stability of blank PGA-co-PDL NPs (BNP, 5% RNP, and 10% RNP) was investigated for up to 28 days when stored at 37°C in water (**Figure 2-25**). There was no statistically significant difference in the particle size of BNP compared to the initial preparation over the course of the stability study at 37°C in water ($p > 0.05$), apart from days 2 ($p < 0.0001$), 17 ($p < 0.005$), 18 ($p < 0.05$), 21 ($p < 0.0001$), 23-25 ($p < 0.0001$). The 5% RNP stored in water showed greater statistical significance ($p < 0.05$) compared to the initial sample with only days 17, 18, 24, and 24 showing no statistical significance ($p > 0.05$). 10% RNP in water was similar with all days showing statistical significance ($p <$

0.05) compared to the initial sample with only days 17, 18, and 28 showing no statistical significance ($p > 0.05$).

The short-term stability of blank PGA-co-PDL NPs (BNP, 5% RNP, and 10% RNP) were investigated for up to 18 days when stored at 37°C in cell culture media (**Figure 2-26**). For the first 4 days of the BNP in media at 37 °C, there was no statistically significant difference ($p > 0.05$), but for the rest of the days 5-18 there were statistically significant differences ($p < 0.0001$) compared to the day 1 sample. There was no statistically significant difference ($p > 0.05$) between days 1-4 and 9-11, but there were statistically significant differences ($p < 0.05$) for the other days compared to the initial sample for 5% RNP in media. 10% RNP in media showed no statistically significant difference ($p > 0.05$) between days 1-4, 8, 9, and 11, but the other days showed statistically significant differences ($p < 0.0001$) compared to the initial sample.

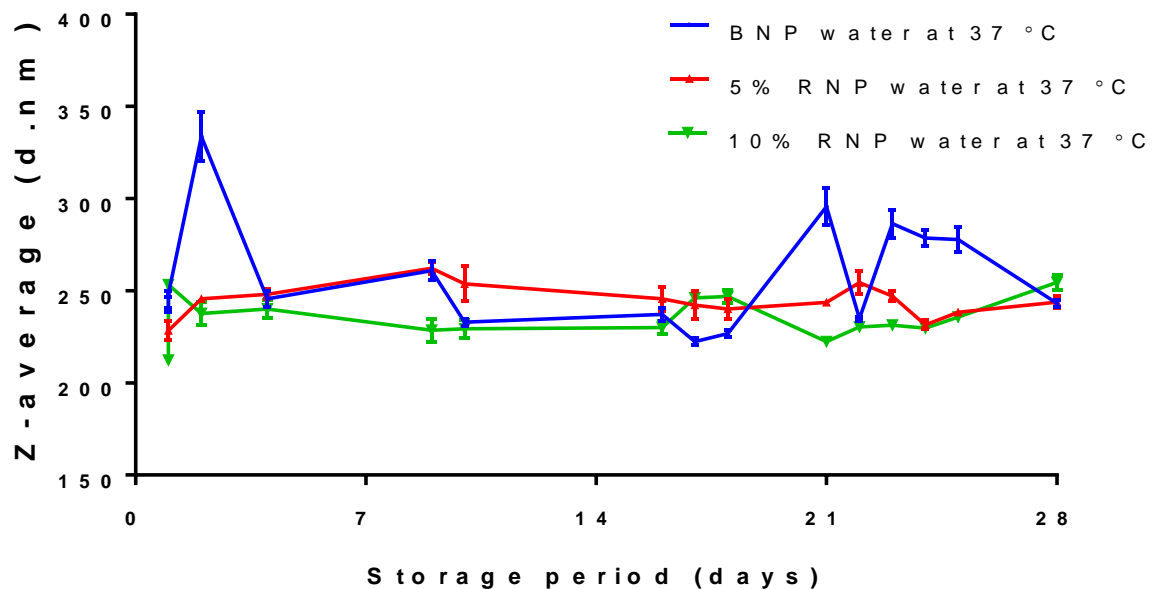


Figure 2-25 Effect of storage time on size of PGA-co-PDL NPs stored at 37°C in water \pm SD (n=3)

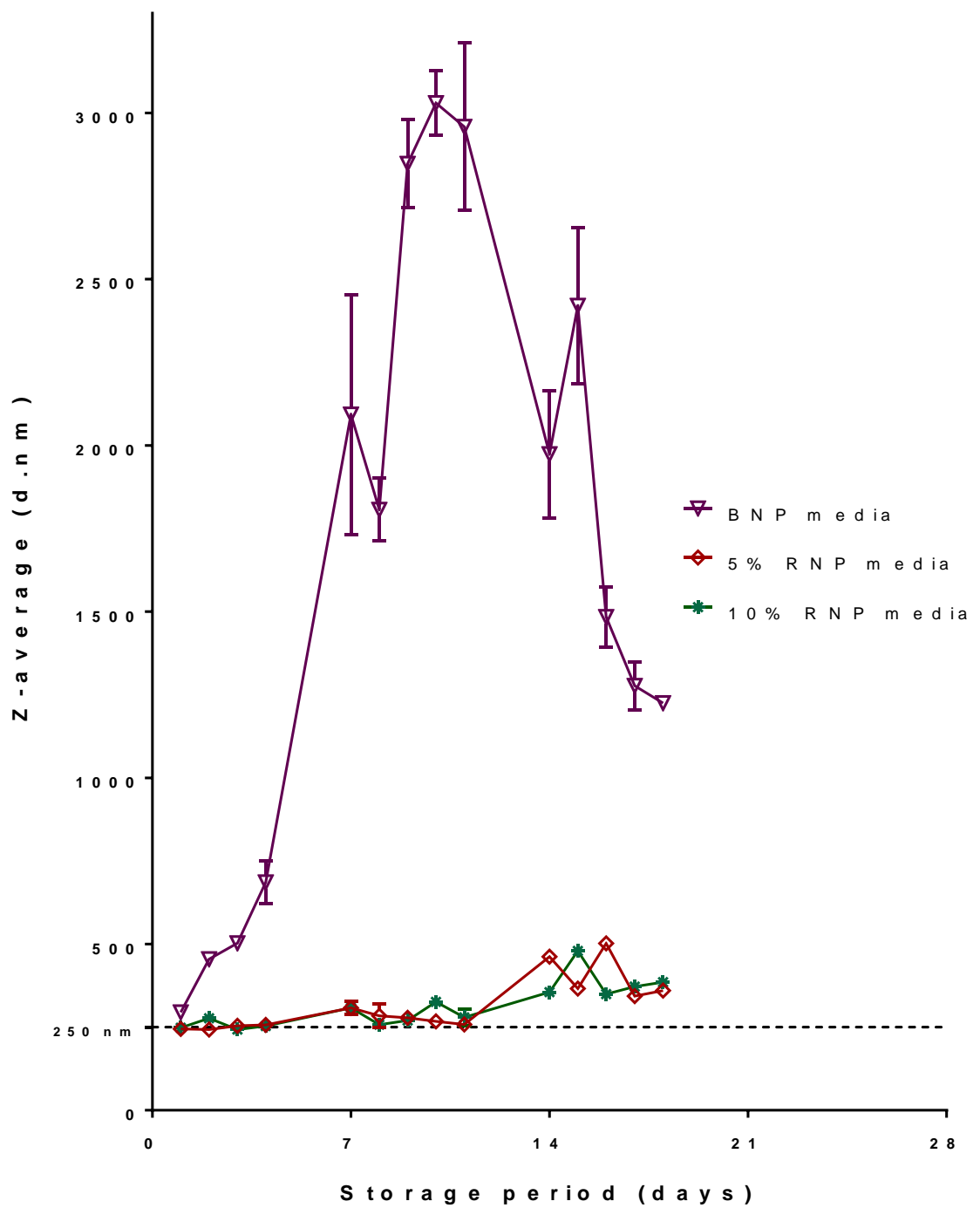


Figure 2-26 Effect of storage time on size of PGA-co-PDL NPs stored at 37°C in media \pm SD (n=3)

2.3.3.3.4. Release study of PGA-co-PDL

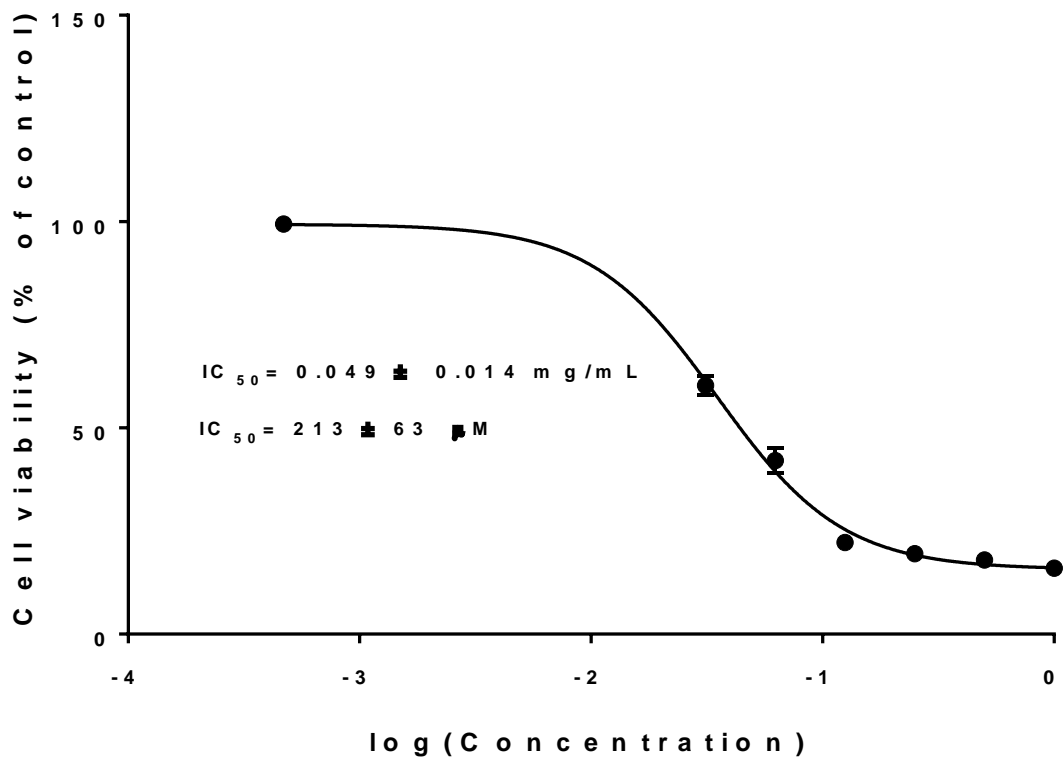
A burst release of resveratrol from 5% RNP and 10% RNP was observed with $17 \pm 0.04 \mu\text{g}$ and $25 \pm 0.02 \mu\text{g}$ released at time point zero, respectively. The amount of resveratrol released from 5% RNP and 10% RNP was $36 \pm 0.03 \mu\text{g}$ and $69 \pm 0.04 \mu\text{g}$ after 30 and 60 minutes, respectively. There were no resveratrol peaks detected after this time.

2.3.3.3.5. Cell viability studies of PGA-co-PDL

2.3.3.3.5.1. Alamar Blue (resazurin sodium salt)

2.3.3.3.5.1.1. *Determining the IC_{50} of free-resveratrol*

Figure 2-27 consists of a representative Log concentration-viability response curve of 1 experiment since with an accompanying table that gives the results of all 3 experiments. The relative 50% inhibitory concentration (IC_{50}) for free-resveratrol on Calu 3 cells after 24 hours was shown to be $0.049 \pm 0.014 \text{ mg/mL}$ (**Figure 2-27**). This is equivalent to $213 \pm 63 \mu\text{M}$. It should be stated that one of the results was quite different to the other two, leading to a huge SE. If the calculations were based on two replicates that were very similar in value, the IC_{50} would have been $150 \pm 3 \mu\text{M}$.



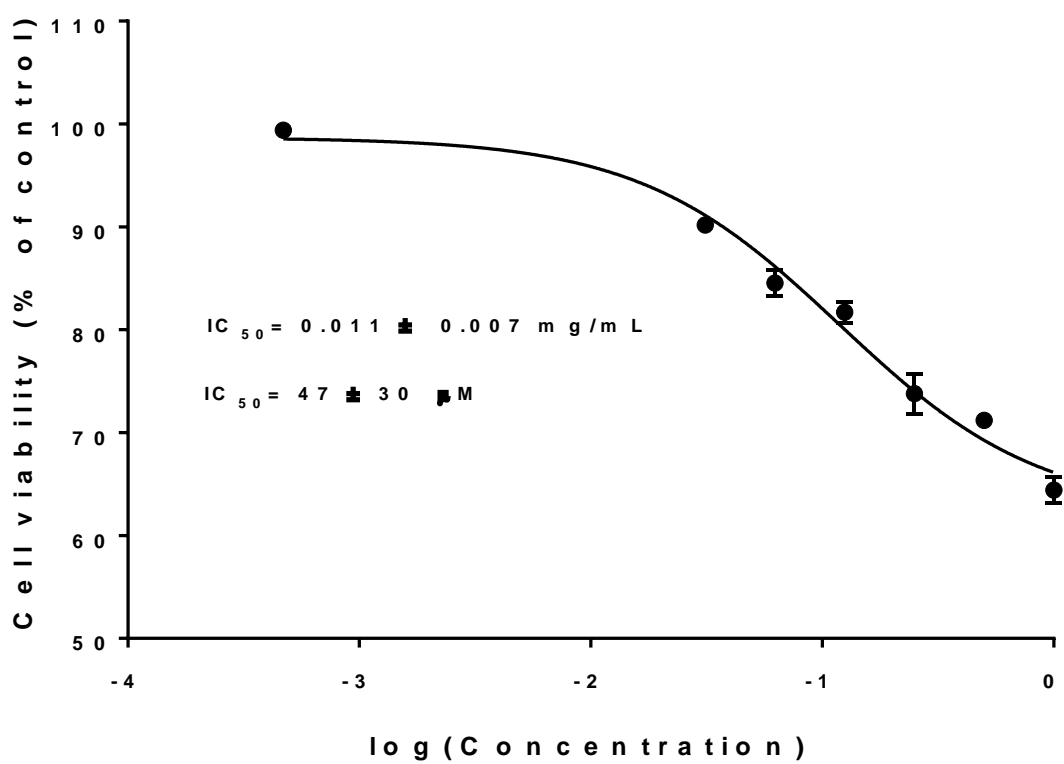
Experiment	R-square	IC50	
		mg/mL	μM
1	0.968	0.077	338
2	0.991	0.035	153
3	0.974	0.034	147

Figure 2-27 Representative Log concentration-viability response curve showing effects of free-resveratrol using Alamar blue assay ± SE

2.3.3.3.5.1.2. Determining IC_{50} of resveratrol loaded into PGA-co-PDL NPs

2.3.3.3.5.1.2.1. 5% Resveratrol-loaded NPs

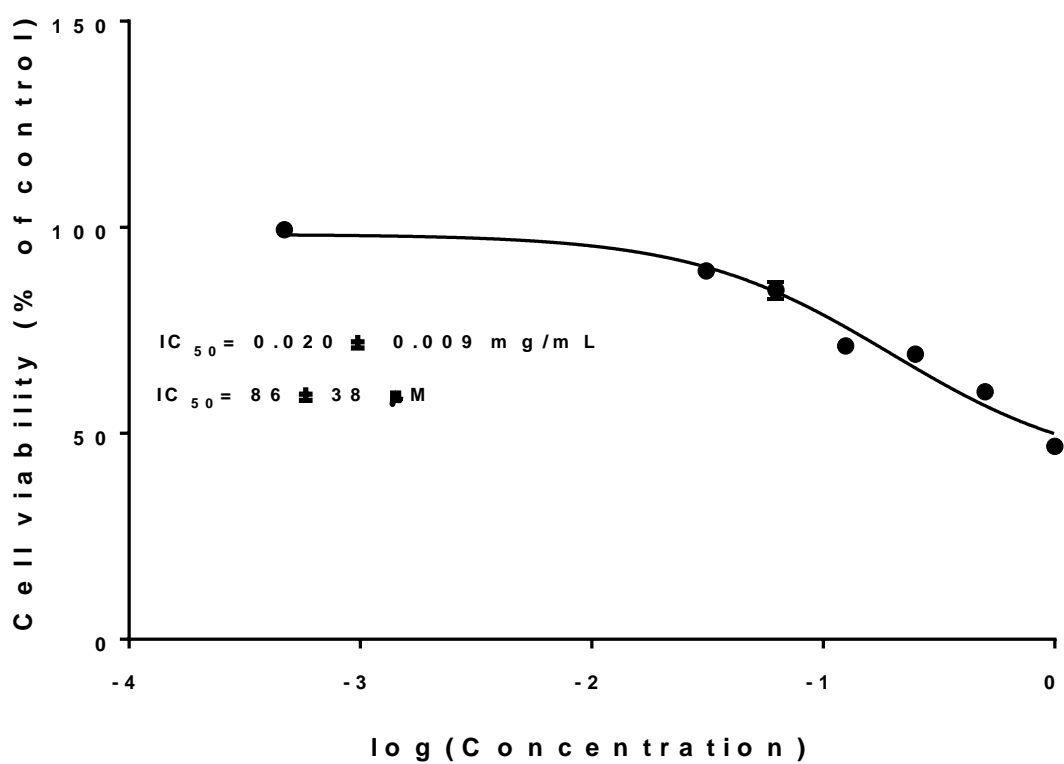
Figure 2-28 consists of a representative Log concentration-viability response curve of 1 experiment since with an accompanying table that gives the results of all 3 experiments. The IC_{50} for 5% resveratrol-encapsulated NPs (5% RNPs) on Calu 3 cells after 24 hours was shown to be 0.276 ± 0.175 mg/mL (**Figure 2-28**). Using the drug loading results (**Table 2-2**), it was determined that the amount of resveratrol present would be 0.011 ± 0.007 mg. This means that the IC_{50} for resveratrol encapsulated into 5% RNPs was 47 ± 30 μ M. It should be stated that one of the results was quite different to the other two, leading to a huge SE. If the calculations were based on two replicates that were very similar in value, the IC_{50} would have been 17 ± 3 μ M.



Experiment	R-square	IC50	
		mg/mL	μM
1	0.909	0.024	107
2	0.964	0.005	20
3	0.907	0.003	14

Figure 2-28 Representative Log concentration-viability response curve showing effects of 5% resveratrol-loaded NPs using Alamar blue assay ± SE

Figure 2-29 consists of a representative Log concentration-viability response curve of 1 experiment since with an accompanying table that gives the results of all 3 experiments. The IC_{50} for 10% resveratrol-encapsulated NPs (10% RNPs) on Calu 3 cells after 24 hours was shown to be 0.279 ± 0.123 mg/mL (**Figure 2-29**). Using the drug loading results (**Table 2-2**), it was determined that the amount of resveratrol present would be 0.020 ± 0.009 mg. This means that the IC_{50} for resveratrol encapsulated into 10% RNPs is 86 ± 38 μ M. It should be stated that one of the results was quite different to the other two, leading to a huge SE. If the calculations were based on two replicates that were very similar in value, the IC_{50} would have been 48 ± 12 μ M.



Experiment	R-square	IC50	
		mg/mL	μM
1	0.951	0.037	160
2	0.962	0.014	60
3	0.943	0.008	37

Figure 2-29 Representative Log concentration-viability response curve showing effects of 10% resveratrol-loaded NPs using Alamar blue assay ± SE

2.3.3.3.5.1.2.3. Percentage changes in IC₅₀

The 5% RNPs and 10% RNPs formulations decreased the IC₅₀ as compared to free-resveratrol by 78±7% and 60±7%, respectively (**Table 2-3**).

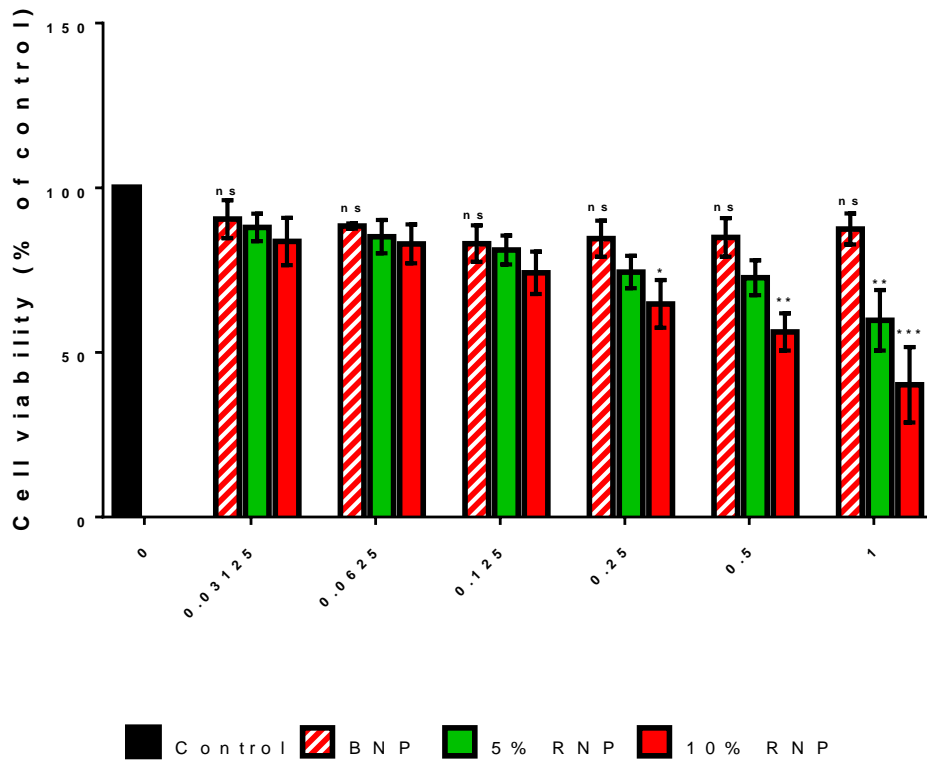
Table 2-3 Percentage changes in IC₅₀ for resveratrol-encapsulated NPs compared to free resveratrol

Formulation	IC ₅₀ (μM)				Percent change in IC ₅₀ (%)	
	Experiments				Average	SE
	1	2	3	Average		
Free-resveratrol	338	153	147	213	0	0
5% RNP	107	20	14	47	78	7
10% RNP	160	60	37	86	60	7

2.3.3.3.5.1.3. Effect of resveratrol-loaded NPs vs blank NPs on Calu 3 cells

The BNP (0.03125-1 mg/mL) showed good cytocompatibility in Calu 3 cells (**Figure 2-30**). The viability of the cells treated with BNP at a concentration of 1 mg/mL was 87.5±4.7% after 24-hour exposure. There was no statistically significant difference between the viability of cells treated with BNP up to 1mg/ml and the control cells treated with the vehicle alone (p> 0.99, ANOVA, Tukey's comparison).

However, the 5% RNP and 10% RNP decreased the viability of Calu 3 cells in a concentration-dependent manner (**Figure 2-30**). There was a statistically significant difference between 5% RNP and BNP at a concentration of 1 mg/mL (p<0.005). There were also statistically significant differences between 10% RNPs and BNPs at concentrations 0.25 (p<0.05), 0.5 (p<0.005) and 1 mg/mL (p<0.001).



ns	no significance between control and BNP
*	P< 0.05 indicates a significant difference between sample and corresponding BNP
**	P< 0.005 indicates a significant difference between sample and corresponding BNP
***	P< 0.001 indicates a significant difference between sample and corresponding BNP

Figure 2-30 Calu 3 cell viability as determined by Alamar blue assay after 24-hour exposure to blank nanoparticles (BNP), 5% resveratrol-loaded PGA-co-PDL nanoparticles (5% RNP), and 10% resveratrol-loaded PGA-co-PDL nanoparticles (10% RNP). Data represent mean \pm standard error of mean for n=3 independent experiments.

2.3.3.3.5.2. LDH assay

2.3.3.3.5.2.1. 48-hour treatment

The LDH assay showed that both the BNP (300 μ M) and 10% RNP (300 μ M) caused a statistically significant increase in LDH release compared with the control ($p < 0.05$) after 48-hour exposure (**Figure 2-31**). However, there was no statistically significant difference between the BNP (300 μ M) and 10% RNP (300 μ M) ($p > 0.9999$).

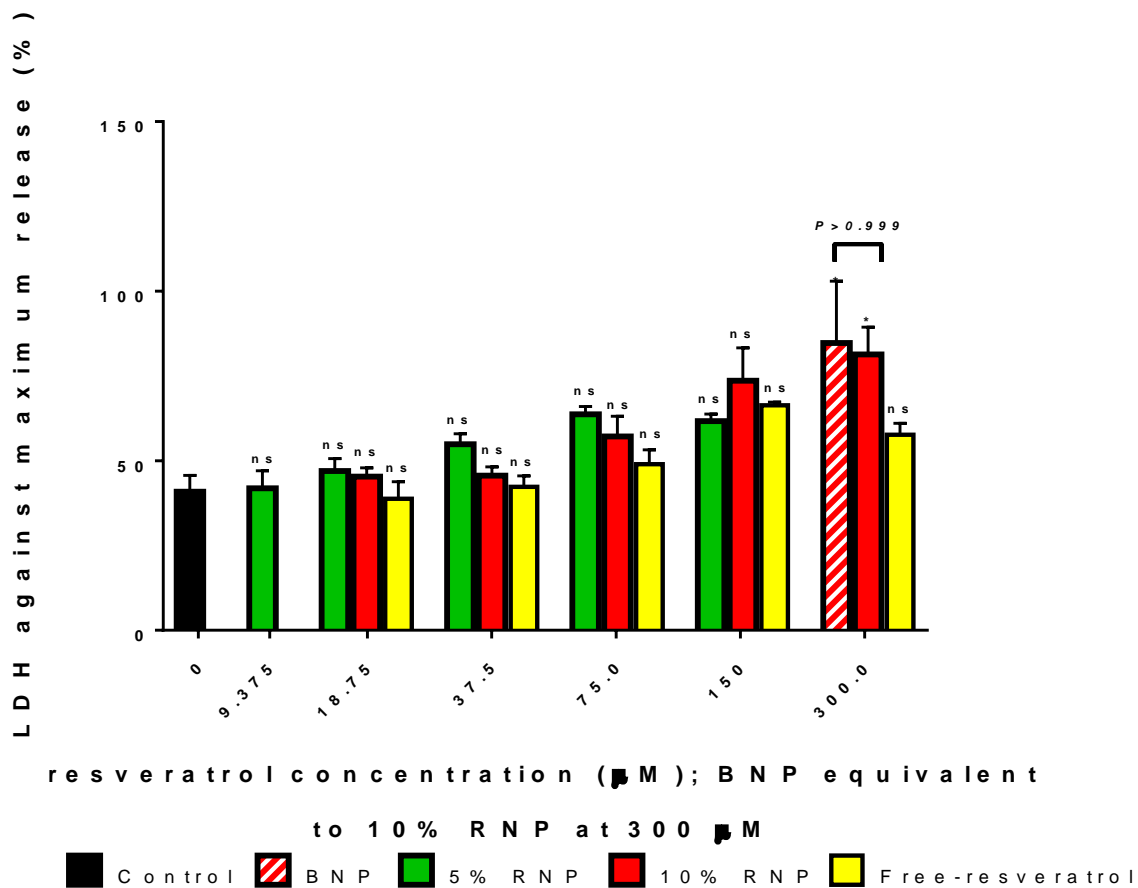


Figure 2-31 The effects of blank PGA-co-PDL nanoparticles (BNP), 5% resveratrol-loaded PGA-co-PDL nanoparticles (5% RNP), 10% resveratrol-loaded PGA-co-PDL nanoparticles (10% RNP), and free-resveratrol on LDH release in Calu 3 cells after 48 hours. Data represent mean \pm standard error of mean for n=3 independent experiments.

2.3.3.3.5.2.2. 72-hour treatment

The LDH assay showed that the BNP (300 μ M) caused a statistically significant increase in LDH release compared with the control ($p < 0.05$) after 72-hour exposure (**Figure 2-32**). 5% RNP (150 μ M) caused a statistically significant increase in LDH release compared with the control ($p < 0.0005$) after 72-hour exposure. 10% RNP, 300 μ M and 150 μ M, caused a statistically significant increase in LDH release compared with the control ($p < 0.0001$ and $p < 0.005$, respectively) after 48-hour exposure. Moreover, there was a statistically significant difference ($p > 0.005$) between the BNP (300 μ M) and 10% RNP (300 μ M), which could indicate that the LDH release could be due to encapsulated resveratrol since the polymer content of both formulations are equal.

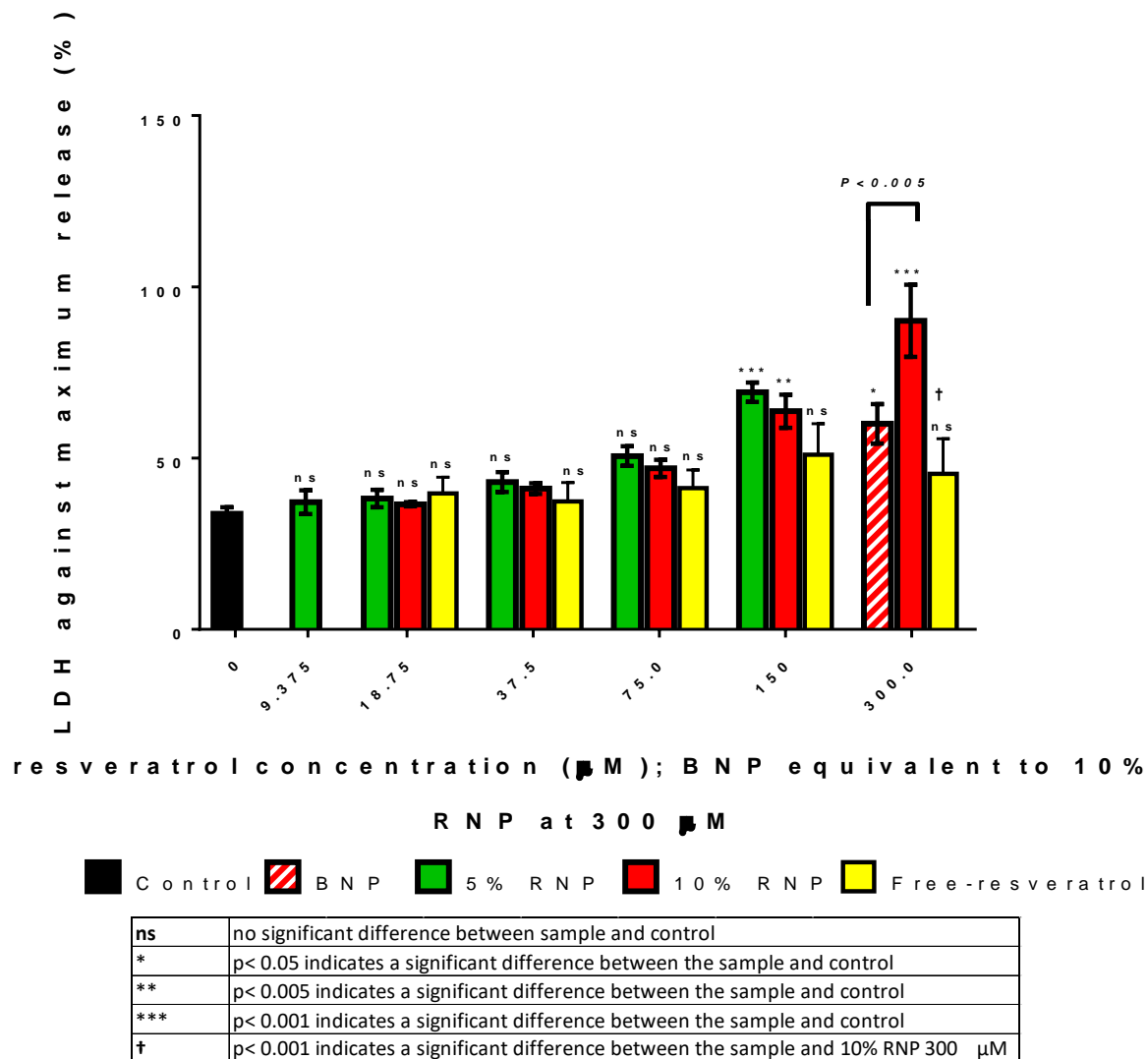


Figure 2-32 The effects of blank PGA-co-PDL nanoparticles (BNP), 5% resveratrol-loaded PGA-co-PDL nanoparticles (5% RNP), 10% resveratrol-loaded PGA-co-PDL nanoparticles (10% RNP), and free-resveratrol on LDH release in Calu 3 cells after 72 hours. Data represent mean \pm standard error of mean of n=3 independent experiments

2.3.4. Discussion

2.3.4.1. Polymer synthesis and analysis

PGA-co-PDL and PGA-co-PDL-PEG₂₀₀₀ were synthesised via ring opening polymerisation and polycondensation as described in literature (Namekawa, Uyama and Kobayashi, 2000; Thompson *et al.*, 2006). The polymers were synthesised via polymerisation of PDL (**Figure 2-6**), DVA (**Figure 2-7**), and glycerol (**Figure 2-8**) for PGA-co-PDL (**Figure 2-1**), with mPEG₂₀₀₀ (**Figure 2-9**) added to obtain PGA-co-PDL-PEG₂₀₀₀ (**Figure 2-2**). The polymerisation is enzyme-dependent with the highest yield of polymer obtained when using a lipase enzyme obtained from *Candida antarctica* (Namekawa, Uyama and Kobayashi, 2000; Kim, D.Y., Wu, X. and Dordick, 2003; Sivalingam and Madras, 2004). The hydrolytic enzyme, commercially available as Novozyme 435®, has regio-selectivity for primary hydroxyl groups and has been shown to be over 90% selective in this reaction (Kline, Beckman and Russell, 1998; Thompson *et al.*, 2006; Kobayashi, 2009). Increasing the ratio of glycerol:PDL, due to the increase in free hydroxyl groups, would increase the hydrophilicity of the PGA-co-PDL and PGA-co-PDL-PEG₂₀₀₀ polymers (Thompson *et al.*, 2006). PGA-co-PDL is soluble in both non-polar solvents, such as DCM, chloroform, THF, and diethyl ether, as well as polar solvents, such as phosphate buffer at pH 7.4. This could be due to the hydroxyl group present on the polymer from the glycerol monomer (Thompson *et al.*, 2006). However, it should be noted that PGA-co-PDL is more hydrophobic than hydrophilic (Tawfeek, 2013; Tawfeek *et al.*, 2013). Increasing the contact time of the lipase enzyme with the polymer leads to an increase in the molecular weight of the polymer (Kunda, Alfagih, Dennison, Tawfeek, *et al.*, 2015) up to 24 hours, after

which the dominating hydrolytic reaction leads to a decrease in polymer molecular weight (Kline, Beckman and Russell, 1998; Thompson *et al.*, 2006). Thus, complete removal of the enzyme from the reacted copolymers is an important step in controlling the size of the polymer and subsequent degradation (Thompson *et al.*, 2006). Kunda *et al.* illustrated this, where PGA-co-PDL synthesis of 24 and 6 hours resulted in polymers of 24 KDa and 14.7 KDa, respectively, which is similar to the 16.5 KDa PGA-co-PDL polymer produced in this study in 6.5 hours (Kunda, Alfagih, Dennison, Tawfeek, *et al.*, 2015). The ¹H-NMR analysis showed that the PGA-co-PDL polymer consisted of a 1:1:1 ratio of the three monomers and previous studies have shown that the PGA-co-PDL polymer is a random mixture of these monomers (Thompson *et al.*, 2006; Gaskell *et al.*, 2008). This is due to the nature of the polymerisation reaction. Namekawa *et al.*, showed that the reaction begins with the coupling of DVA to glycerol and then the ring-opening of PDL is initiated by the OH of either glycerol or the DVA-glycerol (Namekawa, Uyama and Kobayashi, 2000). Since the DVA can react with either glycerol or, the recently opened, PDL, multiple possibilities for the attachment of the monomers exist. Similarly, for the PGA-co-PDL-PEG₂₀₀₀ polymer, after the ring-opening, the OH of the mPEG can be the starting point of the polymer chain (Azhari *et al.*, 2018). However, the mPEG only possesses a single free hydroxyl group (**Figure 2-9**). Therefore, it can only be attached to the end of the polymer backbone (Tawfeek, 2013; Ghasemi *et al.*, 2018). Thus, the feed ratio of mPEG can dictate the length of the polymer i.e. too much mPEG can lead to the formation of small chains, while too little mPEG can lead to longer chains or some chains absent any mPEG

Interestingly, studies by Perkins showed that PGA-co-PDL-PEG₂₀₀₀ synthesis over 5 hours, using the same molar feed ratio as in this study, produced a polymer of 13.5 KDa, while the polymer produced in this current study in 6.5 hours was almost double the size at 21.4 KDa (Perkins, 2015). Moreover, previous studies showed a reduction in the molecular weight of the PGA-co-PDL polymer with mPEG polymerisation to form PGA-co-PDL-PEG (Tawfeek, 2013; Perkins, 2015). However, increasing mPEG molecular weight leads to an increase in molecular weight of polymer at the expense of PDL concentration (Iftikhar, 2011; Perkins, 2015). The reason for this seems to be that the reaction medium becomes biphasic with polar molecules, PEG and glycerol, being one phase and non-polar, lactone, the other phase (Poojari and Clarson, 2010; Iftikhar, 2011). The attachment of PEG, a hydrophilic, non-ionic polymer, to a molecule is known as PEGylation and is used to enhance the pharmaceutical properties of various molecules or drugs (Turecek *et al.*, 2016). PEGylation has been used to shield NPs from opsonisation and phagocytosis, thereby, increasing the circulation time of the NPs (Partikel *et al.*, 2019; Wani, Raza and Khan, 2019). PEG reduces the muco-adhesion of a particle, allowing the quick diffusion of the particles through the low viscosity interstitial fluids between mucin fibres (Huckaby and Lai, 2018). Polymerisation with mPEG₂₀₀₀ increases the hydrophilicity of the polymer (Hong, Hu and Yuan, 2006; Saini and Sinha, 2019). Opsonisation occurs on negative and hydrophobic surfaces such as those found on PLGA polymer based NPs (Carvalho and Erbetta, 2012). The PLGA, purchased from Sigma, was confirmed as a 50:50 blend of *D,L*-lactide:glycolide (**Figure 2-3**). *D,L*-lactide increases the hydrophobicity of PLGA, leading to less water absorption

and less degradation, while glycolide increases the hydrophilicity which increases water absorption and degradation (Keles *et al.*, 2015; Sharma *et al.*, 2016). However, the 50:50 blend PLGA shows the fastest degradation rate of all PLGA blends (Makadia and Siegel, 2011; Kapoor *et al.*, 2015). PEGylation of PLGA, such as the mPEG-PLGA purchased from Sigma (**Figure 2-4**) has been shown to increase hydrophilicity and reduce opsonisation. The difference in polymer hydrophilicity/hydrophobicity, along with the solubility and molecular weight can all influence the encapsulation and release of the encapsulated drug (Pagels and Prud'Homme, 2015).

2.3.4.2. *Polymeric nanoparticle synthesis and analysis*

All polymeric NPs were prepared using a (w1/o/w2) double emulsion/solvent evaporation method previously optimised for the preparation of PGA-co-PDL blank NPs of 200 nm (after centrifugation) (Kunda, Alfagih, Dennison, Tawfeek, *et al.*, 2015). Studies suggest that particles < 200 nm are ideal since they show increased uptake compared to larger particles with the ability to evade detection and removal by alveolar macrophages and also shows rapid penetration of the respiratory mucus (Dandekar *et al.*, 2010; Schuster *et al.*, 2013; Youngren-Ortiz *et al.*, 2017; Dabbagh *et al.*, 2018).

2.3.4.2.1. *Size and charge*

This is the first-time resveratrol has been encapsulated into PGA-co-PDL and PGA-co-PDL-PEG₂₀₀₀ NPs. The NPs prepared from PGA-co-PDL-PEG₂₀₀₀, mPEG-PLGA, and PLGA were all under 205 nm (**Table 2-1**). Although, the method was optimised for PGA-co-PDL blank NPs (BNP), it was statistically larger ($p < 0.0001$) than the BNP of the three other polymers. Moreover, at 252 ± 9 nm, the PGA co-PDL BNP was statistically larger than the PGA-co-PDL

5% RNP ($p < 0.005$) and 10% RNP ($p < 0.0001$). However, these sizes are still acceptable for internalisation via caveolae-mediated endocytosis (Rejman *et al.*, 2004; Panariti, Misericocchi and Rivolta, 2012; Prabha *et al.*, 2016; Behzadi *et al.*, 2017; Foroozandeh and Aziz, 2018). The NPs of the four polymers were all negative between -28 and -37 mV with no discernible pattern between BNP, 5% RNP, and 10% RNP (**Table 2-1**). The negative zeta potential of the polymers can be attributed to the coating with PVA (Ranjan *et al.*, 2011; Shagholani, Ghoreishi and Mousazadeh, 2015). The resveratrol did not have an impact on the zeta potential of the NPs which has been confirmed in literature (Neves *et al.*, 2016). The high zeta potential (-30 mV) can confer physical stability due the electrostatic repulsions between particles which will help to avoid flocculation and aggregation of the NPs (Neves *et al.*, 2016).

2.3.4.2.2. Drug loading and encapsulation efficiency (EE%)

The polymers showed the following order with regards to drug loading and encapsulation efficiency (EE%): PGA-co-PDL > PGA-co-PDL- PEG₂₀₀₀ > PLGA > PLGA-PEG. Where drug loading is defined by the ratio between the mass of the API (in this case resveratrol) and the drug carrier (in this case polymer) (Shen *et al.*, 2017b) Meanwhile, the encapsulation efficiency is the ratio between the mass of the API inside the particle (drug loading) and the mass of the API in the feed, which is determined by several factors including the solubility of the polymer in the organic solvent, concentration of the polymer, ratio of drug to polymer, and rate of removal of organic solvent (Tayade and Kale, 2004; Jyothi *et al.*, 2010; Shen *et al.*, 2017a).

As expected, the drug loading significantly increased between the 5% RNP and 10% RNP of all four polymers, with the PGA-co-PDL NPs having the

highest drug loading at $39 \pm 0.12 \mu\text{g}$ and $70 \pm 0.89 \mu\text{g}$ ($p < 0.0001$), respectively. However, although the drug loading (mass of resveratrol inside NPs) increased between the 5% RNP and 10% RNP, the EE% decreased between the 5% RNP and 10% RNP of PLGA, mPEG-PLGA, PGA-co-PDL. Similarly, Wan et al. observed that increasing the mass of resveratrol in the formulation of PLGA-NPs, initially increased the drug loading and EE% (Wan et al., 2018) However, further increases in the mass of resveratrol, although increasing the drug loading, showed a decrease in EE% , which was attributed to the excessive amount of resveratrol causing destabilisation of the formed resveratrol-loaded PLGA-NPs when PLGA reached saturation (Wan et al., 2018). The PGA-co-PDL-PEG₂₀₀₀ 5% RNP and 10% RNP showed both an increase in drug loading and EE%, which could indicate that the optimal amount of resveratrol had not been reached for this polymer.

Resveratrol is not very soluble in water (0.05 mg/mL) and normally a single o/w emulsion method would be used for such hydrophobic drugs (Robinson, Mock and Liang, 2015; Sharma et al., 2016). However, previous studies have shown the suitability of w1/o/w2 double emulsions for encapsulation of resveratrol, due to the increased protection offered (Hemar et al., 2010; Matos et al., 2014; Wang et al., 2017). One study found that the encapsulation efficiency and drug loading of resveratrol-loaded PLGA NPs formulated using double emulsion w1/o/w2, where w1 was resveratrol and PLGA dissolved in DCM, was $48.7 \pm 6.9 \%$ and $8.2 \pm 0.5\%$ (w/w), respectively (Shen et al., 2018). This is more than twice than that obtained in this study (**Table 2-2**). Resveratrol-loaded PEG-PLGA NPs prepared using a double emulsion solvent evaporation method showed an encapsulation efficiency of 68.2% and

drug loading of 8.34% (w/w), which is a lower drug loading but an encapsulation efficiency more than 3 times than what was achieved in this study (Li *et al.*, 2016) (**Table 2-2**). However, it is worth noting that the methods used to formulate the PLGA NPs and PEG-PLGA NPs in those studies was optimised for those specific NPs, while the solvent evaporation method used in this current study was optimised for size of PGA-co-PDL NPs. Also, most studies dissolve resveratrol into ethanol or acetone and used that mixture as the first water phase (w1) or together with the polymer in ethyl acetate (Sanna *et al.*, 2015; Li *et al.*, 2016). Whereas, in this study the resveratrol was added together with the polymer into the DCM. This could explain the discrepancy of results and why the PGA-co-PDL NPs had the highest encapsulation. Therefore, if the formulation parameters were optimised for each polymer, the EE% might have been better, however, the aim was to do a direct comparison at this stage. Hence, the same set of formulation parameters were used. Solvents in which the polymer is less soluble in, which will cause the polymer to solidify faster, can be used to increase the drug loading/encapsulation (Thompson *et al.*, 2007). In order to obtain a stable double emulsion, the primary emulsion (w1/o) must be stable, which is dependent on the droplet size, amounts of dispersed and continuous phase, and the affinity of the emulsifier for both phases (Matos *et al.*, 2014). The emulsifier in this study was polyvinyl alcohol), a highly hydrophilic surfactant (Park *et al.*, 2018). A high concentration of hydrophilic surfactants decrease encapsulation due to oil film rupture and leaking of the inner water droplets (Matos *et al.*, 2014).

The drug loading capacity of NPs are important since a higher drug loading has several benefits. A higher drug loading means that less excipient (in this

case polymer) is used to deliver the same dosage of the active pharmaceutical agent (API). It would be desirable to have a high drug loading and there is evidence to suggest that drug loading of 9% (w/w) seems more beneficial than a higher one (Chu *et al.*, 2013). The drug loading of PGA-co-PDL was 0.07 ± 0.009 mg/mg or $7\pm 0.9\%$ (w/w). Due to the high drug loading and encapsulation efficiency of PGA-co-PDL NPs, they were subsequently analysed further.

2.3.4.2.3. Stability studies

The PGA-co-PDL NPs (BNP, 5% RNP and 10% RNP) showed good stability for size and charge in water stored at both 4 °C and 37 °C over the 28 days. However, the stability of the three formulations in media at 37 °C showed a definite increase in the size of the NPs, especially the BNP, which went from 294.6 ± 2 nm on Day 1 to 454.6 ± 12 nm on Day 2, and on Day 7 it rose to a statistically significant ($p < 0.0001$) 2093 ± 360 nm. The dramatic increase in the size of the NP in media is most likely attributed to the NPs forming complexes with the proteins present in the cell culture medium (Schulze *et al.*, 2008; Maiorano *et al.*, 2010; Moore *et al.*, 2019).

2.3.4.2.4. Release studies

The release study for PGA-co-PDL NPs was done in PBS at 37 °C. Two methods were used in order to assess the release of resveratrol from these formulations. Both methods had the same release profile. Interestingly, using **Equation 2-3**, it was found that between 44 and 36 % of resveratrol is immediately released upon contact with the release media from 5% RNP and 10% RNP, respectively. This may be attributed to resveratrol located on the surface of the NPs (Huang and Brazel, 2001; Kamaly *et al.*, 2016) The

percentage of resveratrol released ranged from 92-99% after 30 and 60 minutes for 5% RNP and 10% RNP, respectively. It would be ideal to have a more sustained drug delivery system in order to maintain the local drug concentration at a constant level, decreasing side effects, reducing dosing frequency and increasing patient compliance (Hsu *et al.*, 2015; Patel and Patel, 2015). There are several potential causes of a burst release profile including formulation conditions, heterogeneity of matrices, properties of the drug, and percolation limited diffusion (Huang and Brazel, 2001; Peppas and Narasimhan, 2014). During the formulation process some of the drug may not encapsulate inside the matrix of the nanoparticle and instead get trapped on the surface of the nanoparticle which is then immediately released upon contact with a release medium (Huang and Brazel, 2001; Kamaly *et al.*, 2016). During a drying process, such as with freeze-drying or spray drying, the water present in the NPs tends to move to the surface of the NPs and evaporates. Drugs may move along with water to the surface of the nanoparticles through convection which could lead to burst release of the drug (Huang and Brazel, 2001; Kamaly *et al.*, 2016). This is interesting since the NPs were freeze-dried before doing the release study. Perhaps, the release study should have been performed without drying, but this would reduce the accuracy of the weighing of the NPs. There are many factors that influence drug release rate, including drug solubility, molecular weight and size, particle size and shape, polymer properties (solubility, etc.), formulation processing technique, excipients, etc. (Varma *et al.*, 2004). PGA-co-PDL NPs may have given the best encapsulation efficiency, but the other polymers may have given a better release profile. PLGA NPs have shown burst release, however, PEGylation has shown to slow

down the release profile of PLGA and could perhaps do the same for PGA-co-PDL- PEG₂₀₀₀ (Hsu *et al.*, 2015).

2.3.4.3. *Cell viability studies*

The detection of cell viability is the most generally used parameter to assess cytotoxicity (Kroll *et al.*, 2009). Cell viability is a measure of healthy, living cells in a given population (Adan, Kiraz and Baran, 2016). Assays based on cell viability include those detecting mitochondrial activity, such as 3-(4,5-dimethylthiazol-2-yl)-2,5-diphenyltetrazolium bromide (MTT) and Alamar blue, or membrane integrity, such as LDH (which assesses necrotic or late apoptotic cell death) (Mitjans, Nogueira-Librelo and Vinardell, 2018). Many of these *in vitro* assays used to test the cytotoxicity of NPs were made for the hazard characterisation of chemicals which differ tremendously from NPs (Kroll *et al.*, 2009; Dhawan and Sharma, 2010). Several features of NPs, such as high adsorption capacity, catalytic activity, hydrophobicity, optical and magnetic properties, and surface charge, may interfere with the assays on top of the concern that *in vitro* testing cannot mimic the complexity of *in vivo* testing in animal models or the human body (Kroll *et al.*, 2009; Sukhanova *et al.*, 2018). Evidence suggests that there is no correlation between *in vitro* and *in vivo* pulmonary toxicity of NPs (Sayes, Reed and Warheit, 2007; Warheit, Sayes and Reed, 2009; Sayes, 2020). The colorimetric MTT assay is used to detect mitochondrial activity in the conversion of the yellow tetrazolium, MTT, to a purple water-insoluble formazan (Kroll *et al.*, 2009). This assay has been used in cytotoxicity studies of various NPs (Kroll *et al.*, 2009). Carbon and PLGA-polyethylene oxide (PLGA-PEO) NPs have been shown to alter the light

absorption of this assay, skewing the results of the assay (Wörle-Knirsch, Pulskamp and Krug, 2006; Belyanskaya *et al.*, 2007; Guadagnini *et al.*, 2015). The LDH assay works on the principle that the cytosolic enzyme, LDH, is present in many cells and that upon plasma membrane damage, it gets released into the cell culture medium. Extracellular LDH then catalyses the conversion of lactate to pyruvate via the reduction of NAD⁺ to NADH (Decker and Lohmann-Matthes, 1988; Fotakis and Timbrell, 2006; Han *et al.*, 2011). Diaphorase, NADH dehydrogenase, utilises NADH to reduce a tetrazolium salt (INT) to a red formazan product which can be measured to determine the amount of LDH released into the cell culture medium. Trace metal-containing NPs and silver NPs have been shown to interfere with the LDH assay (Suska *et al.*, 2005; Han *et al.*, 2011). Differentiating between healthy, necrotic, and apoptotic cells can be achieved by the detection of externalised phosphatidylserine on the cell surface (Zwicker *et al.*, 2019). Phosphatidylserine, usually located on the inside of the plasma membrane of a healthy cell, is exposed on the surface of an apoptotic cell (Koopman *et al.*, 1994; Shlomovitz, Speir and Gerlic, 2019). Annexin V, a Ca²⁺-dependent phospholipid-binding protein, has high affinity for phosphatidylserine and, when fluorescently-labelled, can be employed to detect apoptotic cells (Fleisher and Oliveira, 2019; Zwicker *et al.*, 2019). However, Annexin V, due to a broken plasma membrane, will bind to the phosphatidylserine on the inner side of the plasma membrane of necrotic cells, producing a false negative result (Kroll *et al.*, 2009; Crowley, Marfell, Scott and Waterhouse, 2016). Therefore, co-staining with propidium iodide, which will solely stain necrotic cells, is necessary to distinguish between necrotic and apoptotic cells

(Crowley, Marfell, Scott, Boughaba, *et al.*, 2016). Gold NPs adsorbed the propidium iodide and entered healthy cells, leading to false positives for necrosis (Shukla *et al.*, 2005). The neutral red assay is based on the principle that viable cells will exclusively accumulate the neutral red dye in lysosomes through non-ionic passive diffusion, where it can be quantified via fluorescence or absorption measurement (Gomez Perez *et al.*, 2017). Carbon NPs induced adsorption of the dye, manipulating the ability of the assay to assess cell viability (Casey *et al.*, 2007). There are many studies showing the interference of metallic and carbon-based NPs, but not many have looked at the interference of polymeric NPs (Warheit, Sayes and Reed, 2009; Ong *et al.*, 2014).

MTT assay and staining with Calcein AM and propidium iodide, and CellTiter-Glo assay were used to assess the cytotoxicity of the PGA-co-PDL NPs. The CellTiter-Glo assay uses luminescence to measure the cell viability by quantifying the amount of ATP (Sakamuru, Attene-Ramos and Xia, 2016). None of these assays gave consistent results (results not shown). Studies recommend using at least two different methods to assess cytotoxicity, in order to verify the results (Matuszak *et al.*, 2016). Therefore, two cell viability assays were used to assess the efficacy of PGA-co-PDL NPs as a delivery system.

Alamar Blue (resazurin sodium salt) involves the reduction of resazurin (blue and nonfluorescent) by healthy cells to resorufin, which is pink and highly fluorescent (Brien *et al.*, 2000). The reduction is said to be due to the enzymatic actions of mitochondrial, cytosolic, and microsomal enzymes (Vega-Avila and Pugsley, 2011; Rampersad, 2012; Munshi, Twining and Dahl, 2014). Whereas Alamar Blue determines the degree of cytotoxicity by

measuring the number of viable cells that remain after exposure to the treatment, the LDH assay evaluates the cytotoxicity by measuring the amount of cytoplasmic enzyme (i.e. LDH) released after being exposed to the treatment (i.e. measures the amount of cell death).

For the Alamar Blue assay, the Calu 3 cells were treated with various concentrations of BNP, 5% RNP, 10% RNP, and free-resveratrol for 24 hours. The IC₅₀ was determined from a concentration-response sigmoid curve of experimentally-derived cytotoxicity data plotted in GraphPad Prism. The PGA-co-PDL BNP was shown to possess good cytocompatibility, with none of the tested concentrations reducing the cell viability to less than 85% (**Figure 2-30**). Therefore, no IC₅₀ could be calculated for the PGA-co-PDL BNP since there was no significant reduction in viability. These results are consistent with those previously shown by studies of PGA-co-PDL NPs/microparticles on A549 and normal human bronchial epithelial (16HBE14o-) cells (Tawfeek *et al.*, 2011; Kunda, 2014). MTT assay results of PGA-co-PDL NPs (1.25 mg/mL) on A549 cells showed a 70.84 ± 6.99% cell viability after 24 hours (Kunda, 2014). Similarly, spray-dried PGA-co-PDL microparticles with no excipients were exposed to 16HBE14o- cells and it showed a cell viability of 87.14 ± 3.40% even at 5 mg/mL after 24 hours (Tawfeek, 2013). These results suggest that PGA-co-PDL NPs is a good delivery system that does not have an inherent cytotoxic effect. The Alamar blue assay showed that the 5% RNP, 10% RNP, and free-resveratrol had a concentration-dependent cytotoxic effect on the cell viability of the Calu 3 cells (**Figures 2-27, 2-28, 2-29**). The IC₅₀ after 24 hours of treatment with the free resveratrol was 0.049 ± 0.014 mg/mL or 213 ± 63 µM (**Figure 2-27**). Trotta *et al* observed that Calu 3 cells were less

sensitive to resveratrol. Resveratrol was well-tolerated and non-toxic to Calu 3 cells at concentrations as high as 160 μM , even after 72 hours, with cell viability being maintained above 95% (Trotta *et al.*, 2015). This gives credence to the high IC_{50} for resveratrol obtained in this study. In this study, it was found that the IC_{50} values of the 5% RNP and 10% RNP were $47 \pm 30 \mu\text{M}$ (**Figure 2-28**) and $86 \pm 38 \mu\text{M}$ (**Figure 2-29**), respectively. When compared to the IC_{50} of the free-resveratrol, it is evident that the delivery system caused a maximum decrease in IC_{50} of 78% (**Table 2-3**). This indicates that the PGA-co-PDL NPs are more effective in exposing the resveratrol to the cells than the free-resveratrol. This seems to be true even for the well-established anticancer drugs, such as doxorubicin and paclitaxel. One study found that doxorubicin NPs and paclitaxel NPs decreased their respective IC_{50} values by 8 times and 9 times, respectively, as compared to the free-drug in P-glycoprotein-overexpressing human ovarian carcinoma cells (Dong *et al.*, 2009). Phenolic compounds such as quercetin have also showed decreases in IC_{50} (higher cytotoxicity efficacy) when loaded into NPs. Quercetin loaded into solid lipid NPs reduced its 24 hours IC_{50} in MCF-7 cells by 50%, as compared with free quercetin (Niazvand *et al.*, 2019). Similarly, resveratrol-loaded glycyrrhizic acid-conjugated human serum albumin NPs decreased the IC_{50} after 48 hours by 35% as compared to free-resveratrol in HepG2 cells (M. Wu *et al.*, 2017). Another study found that resveratrol-loaded gelatin NPs decreased the IC_{50} after 24 hours by 50% compared with free resveratrol in NCI-H460 non-small cell lung cancer cells (Karthikeyan *et al.*, 2013).

The ANOVA and subsequent Tukey's comparison revealed that there was no statistical difference ($p > 0.99$) between the BNP and the untreated cells

(negative control) (**Figure 2-30**). This means that for these sets of experiments, the BNP-treated Calu 3 cells were physiologically similar to the negative control cells. As explained earlier, this bodes well for the BNP as a delivery system and implies that the cytotoxicity seen in the 5% RNP and 10% RNP treated cells were due to the resveratrol loaded into these NPs. The 5% RNP and 10% RNP decreased the cell viability of Calu 3 cells in a concentration-dependent manner (**Figure 2-30**). Compared to BNP, the 5% RNP and 10% RNP caused significant decreases in cell viability at 1 mg/mL ($p < 0.005$) and 0.25-1 mg/mL ($p < 0.05$), respectively. This further suggests that the cytotoxicity of the 5% RNP and 10% RNP was due to the resveratrol and not the PGA-co-PDL NPs, since the same amount of polymer was present in the 1 mg/mL BNP, 1 mg/mL 5% RNP and 1 mg/mL 10% RNP. The reduction in cell viability also shows that, despite the burst release of resveratrol during the release study, it would seem that the PGA-co-PDL NPs effectively delivered the resveratrol to the cells.

For the LDH assay the cells were treated for both 48 hours and 72 hours. Preliminary tests showed that no real difference in cytotoxicity was noticeable at 24 hours (data not shown). In order to accommodate the necessary controls on the treatment plate for the LDH assay, it was decided that the most efficient way was to have a single BNP concentration that corresponded to the highest amount of polymer present in the concentrations of the 10% RNP, i.e. 300 μ M. Both BNP and 10% RNP, at 300 μ M, increased LDH release to the same extent after 48h ($p < 0.05$), whereas, after 72 h, while both BNP and 10% RNP still increased LDH release, the LDH release by 10% RNP was greater than that of BNP ($p < 0.005$) (**Figures 2-31, 2-32**). This could indicate that the LDH

release could be due to encapsulated resveratrol, since the polymer contents of both formulations were equal. Moreover, the free-resveratrol did not cause a significant increase in LDH release compared to the control at both 48 and 72 hours ($p>0.05$). However, at 72 hours, the 10% RNP at 300 μM caused a significant increase in LDH release compared to free-resveratrol at the same concentration ($p<0.001$). This shows the improvement in the efficacy of resveratrol using PGA-co-PDL NPs as a delivery system.

Together, the results showed that resveratrol encapsulated into PGA-co-PDL NPs reduced Calu 3 cell viability in a concentration- and time-dependent manner. These results are consistent with results obtained by a previous study in which resveratrol (0-100 μM) administered to A549 and CH27 human lung carcinoma cells was found to cause a concentration-dependent increase in LDH leakage (Weng *et al.*, 2009). However, as NPs are not able to be inhaled into the lungs, the resveratrol-loaded NPs will need to be spray-dried into nanocomposite microparticles (Elsayed and AbouGhaly, 2016; Rezazadeh *et al.*, 2018). This is the focus of the next chapter.

2.3.5. Conclusion

In this study, a comparison of four different polymers used for the formulation of resveratrol-containing NPs and characterised in terms of size, charge, drug loading and encapsulation efficiency was undertaken. PGA-co-PDL NPs were chosen as the most effective due to the higher encapsulation efficiency obtained. Subsequent cell viability tests (Alamar blue) of PGA-co-PDL NPs showed that the blank PGA-co-PDL NPs had no inherent cytotoxic effect on the Calu 3 cells. More importantly, it demonstrated that the PGA-co-PDL-encapsulated resveratrol was more effective than free-resveratrol, reducing the IC₅₀ by 78%. Furthermore, the LDH assay confirmed that the cytotoxic effects were due to the resveratrol encapsulated inside the NPs and not the delivery system itself. Together, these results demonstrated that the resveratrol-encapsulated PGA-co-PDL NPs has a concentration- and time-dependent cytotoxic effect on Calu 3 cells.

This study showed the potential of resveratrol-encapsulated PGA-co-PDL NPs to treat cancer and hence further studies towards the incorporation of the PGA-co-PDL NPs into micron-sized nanocomposite microparticles via spray drying to enable pulmonary delivery of the NPs were subsequently undertaken.

3 CHAPTER 3: Formulation of Resveratrol Loaded PGA-co-PDL Nanoparticles into Aerosolisable Microcarriers

3.1. Introduction

Inhalable chemotherapy, which involves the local administration of chemotherapy to the lungs, offer a promising alternative to intravenous administration (Abdelaziz *et al.*, 2018). There are many advantages to delivering drugs via the lungs for both local and systemic treatment, including high bioavailability, since the first pass metabolism is bypassed, rapid onset of action due to direct targeting at the disease site (lung cancer cells), self-administration (dry powder inhalation devices) and non-invasiveness (increased patient compliance) (Sung, Pulliam and Edwards, 2007; Mahmud and Discher, 2011; Thorley and Tetley, 2013; Lee *et al.*, 2015).

In chapter 2, PGA-co-PDL NPs were demonstrated to be an effective delivery system for resveratrol. However, the size of the NPs (approximately 200 nm) poses a problem for pulmonary delivery (Pilcer and Amighi, 2010). The NPs will therefore be incorporated into nanocomposite microparticles (NCMPs) using spray drying to obtain the ideal particle size range of 1-5 μm for lung deposition (**Figure 3-1**) (Rezazadeh *et al.*, 2018). Spray drying is an established technique for the production of particles which involves the transformation of a fluid material into dried particles, by means of a gaseous hot drying medium (Cal and Sollohub, 2010). The spray drying process involves using excipients which have several functions including, enhancing the flowability of drug particles to ease filling of the dry powder inhaler (DPI), enhancing dispersion of drug particles during emission, muco-adhesion in case of chitosan and decreasing concentration of the drug to facilitate accurate delivery of the dose (Peng *et al.*, 2016).

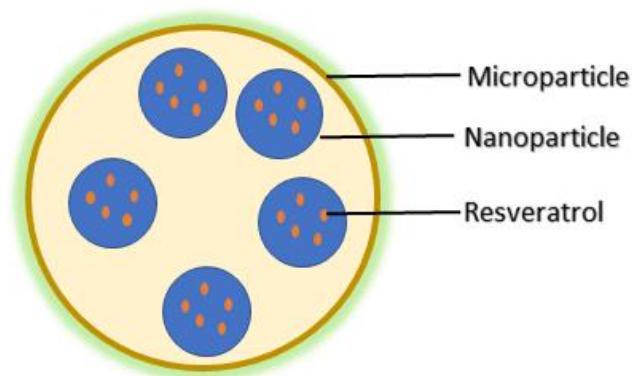


Figure 3-1 Illustration of nanocomposite microparticle containing resveratrol-loaded nanoparticles

L-leucine is a hydrophobic amino acid which has been well-established as a dispersion enhancer (Takeuchi *et al.*, 2018). It translocates to the surface of the particles after spray drying and decreases the interaction forces between particles (Nieto-Orellana *et al.*, 2018). Chitosan is a natural polycationic linear polysaccharide, that has been shown to be mucoadhesive, non-immunogenic and non-toxic (Cheung *et al.*, 2015). It forms electrostatic interactions with the sialic groups of mucins in the mucus layer (Hejjaji, Smith and Morris, 2018; Collado-gonz, Gonz and Goycoolea, 2019). A bioadhesive polymer such as chitosan is capable of prolonging the presence of the formulation in the lungs, thus increasing the efficacy of a formulation. Clarithromycin-loaded microparticles were formulated via spray drying with L-leucine and chitosan (Dimer *et al.*, 2015). The spray dried microparticles had a good yield ($60.7 \pm$

2.3%) with a drug loading of $36.0 \pm 1.4\%$ w/w, a high FPF of $73.3 \pm 2.3\%$, and a mass median aerodynamic diameter (MMAD) of $1.8 \mu\text{m}$ (Dimer *et al.*, 2015). Interestingly, the deposition of the spray-dried microparticles was assessed using Pharmaceutical Aerosol Deposition Device on Cell Cultures (PADD OCC) using Calu-3 cells. The PADD OCC system comprises of three components, namely, the air flow control unit, the aerosolisation unit, and the deposition unit, which are all connected by silicon tubes (Hein *et al.*, 2011). The system was designed to imitate the entire aerosol drug delivery process, including aerosol generation, aerosol deposition onto pulmonary epithelial cells, and drug transport across this biological barrier, to help investigate new aerosol formulations in the early stage development (Hein *et al.*, 2010). Using the PADD OCC system, it was shown that $8.7 \mu\text{g}/\text{cm}^2$ of the spray dried microparticles deposited on Calu 3 cells were transported to the basolateral compartment after 24 hours (Dimer *et al.*, 2015).

3.2. Aims and Objectives

The aim of this study was to develop NCMPs for the dry powder delivery of resveratrol PGA-co-PDL NPs to the lung.

The objectives of the study were:

1. Incorporate BNP, 5% RNP, and 10% RNP into NCMPs via spray drying using L-leucine and chitosan as excipients:
 - a. Investigate size and charge of NPs recovered from NCMPs.
 - b. Analyse the NCMPs for yield, drug loading, encapsulation efficiency, and the release of resveratrol from NCMPs.

c. Study the *in vitro* aerosolisation deposition and cell toxicity of the NCMPs.

3.3. Materials and Methods

3.3.1. Materials

Microparticle synthesis: L-leucine and low molecular weight chitosan were purchased from Sigma-Aldrich, UK.

Polymer synthesis and cell culture: Same as in chapter 2.

3.3.2. Methods

3.3.2.1. *Polymeric nanoparticle synthesis and analysis*

PGA-co- PDL was synthesised and analysed as described previously, in chapter 2, section 2.3.2.1.1.

3.3.2.2. *Polymeric nanoparticle formulation*

Blank (BNP), 5%- (5% RNP), and 10%-resveratrol loaded PGA-co-PDL NPs (10% RNP) were prepared and analysed according to the methods described in Chapter 2, sections 2.3.2.3-4.

3.3.2.3. *Nanocomposite microparticle formulation*

3.3.2.3.1. *Spray drying*

The NPs were formulated into NCMP using a Büchi B-290 mini spray-dryer (Büchi Labortechnik, Flawil, Switzerland). The spray-dryer was equipped with a nozzle atomiser with a nozzle orifice featuring a diameter of 0.7 mm. The parameters for the spray drying process were optimised previously (Almurshedi, 2018) using; a feed rate of 10% (corresponding to 2.5 mL/min), an atomising air flow of 400 L/h, aspirator capacity of 100%, and an inlet temperature of 100 °C (corresponding outlet temperature of 47-50 °C). The

spray-dryer had a high-performance cyclone (Büchi Labortechnik, Flawil, Switzerland) attached, to facilitate the removal of the dry NCMPs from the air stream.

The polymeric NPs were incorporated into NCMPs using L-leucine (LEU) and low molecular weight chitosan (CHI) as microcarriers at a nanoparticle to microcarrier ratio (w/w) of 1:1.5:1 (NPs:LEU:CHI). This ratio was chosen since it showed good results in a previous study (Almurshedi, 2018). L-leucine and chitosan were dissolved under stirring in distilled water (10 mL) or acetic acid (0.1%) aqueous solution (10 mL), respectively. A quantity of PGA-co-PDL NPs was dispersed in the solution containing L-leucine with stirring at 25 °C for 1 min. The chitosan solution was then added to the mixture of L-leucine and NPs, which made the feed solution for spray drying. After spray drying, the NCMPs were collected and stored inside a desiccator under vacuum until needed.

3.3.2.4. *Nanocomposite microparticle analysis*

3.3.2.4.1. Yield

The yield was defined as the difference between the combined weight of the NPs and microcarriers and the weight of the dry powder collected at the end of the spray drying process multiplied by 100 % (w/w) (n=3) as illustrated in **Equation 3-1**.

$$\text{Yield (\%)} = \frac{\text{weight of dry powder collected after spray drying (mg)}}{\text{weight of NPs and microcarriers before spray drying (mg)}} \times 100 \quad \text{Equation 3-1}$$

3.3.2.4.2. Particle size and zeta potential

The spray dried NCMPs (5 mg) were dispersed in deionised water (dH₂O; 5 mL), vortexed for 5 minutes and an aliquot (2 mL) was pipetted into a cuvette; the size, PDI, and charge was measured as reported in chapter 2, section 2.3.2.4.1 on a Malvern Zetasizer Nano at 25 °C (n=3).

3.3.2.4.3. Morphology

Scanning electron microscopy (SEM, FEI Quanta™ 200 ESEM, The Netherlands) was used to visualise the morphology and size of the spray-dried NCMPs. The samples were prepared by layering the powder on a conductive carbon tab mounted on aluminium stubs (pin stubs, 13 mm). A sputter coater (EmiTech K 550X Gold Sputter Coater, 25 mA for 3 min) was then utilised to coat the samples with palladium (10-15 nm).

3.3.2.4.4. Moisture content

The moisture content of the spray-dried NCMPs was ascertained by using thermo gravimetric analysis (TGA, TA instruments TGA Q50, UK). An open platinum TGA pan was loaded with samples (4-15 mg). The pan was suspended from a microbalance and heated from 25-650 °C at a rate of 10 °C/min. The moisture content of the sample was analysed from the mass loss recorded from 25-120 °C using the equipped software (TA Universal Analysis 2000 software).

3.3.2.4.5. Drug loading and encapsulation efficiency (EE)

Each formulation (NCMP-BNP, NCMP-5% RNP, and NCMP-10% RNP) was weighed (4-12 mg) and dissolved in 0.1% acetic acid (aqueous; 1 mL). This mixture was sonicated for 5 minutes using an ultrasonic bath (Ultrawave, UK)

to burst open the NCMPs. Methanol (1 mL) was then added to the sonicated mixture and sonication was repeated for 5 minutes using the ultrasonic bath in order for the released resveratrol to enter into the methanol, since the resveratrol is more soluble in methanol than the 0.1% aqueous acetic acid. The resultant solution was filtered through Captiva Econofilter PTFE 13 mm 0.45 μm (Agilent Technologies, USA) into 2mL crimp vials (Agilent Technologies, USA).

High performance liquid chromatography (HPLC) (1200 series; Agilent Technologies, USA) using a YMC-Triart C18 150 x 4.6 mm I.D. S-5 μm , 12 nm column (YMC Co. LTD., Japan) was used to determine the amount of resveratrol encapsulated in the NCMPs. The samples previously prepared and loaded into the crimp vials were placed into the HPLC tray. The samples (20 μL) were injected into the system running a mobile phase of methanol:water (51:49%; v/v) at a flow rate of 0.54 mL/min. The variable wavelength detector (VWD; Agilent Technologies, USA) was set at 306 nm. The NCMP-BNP was used as a control.

Previously, resveratrol (0.122 $\mu\text{g}/\text{mL}$ -1000 $\mu\text{g}/\text{mL}$) was run on the HLPC using the same parameters as above. The results of the area under the curve was plotted against the various concentrations to obtain a calibration curve. This calibration curve was used to determine the amount of resveratrol encapsulated in the NCMPs.

3.3.2.4.6. Release study

NCMP-BNP, NCMP-5% RNP, and NCMP-10% RNP (10 mg) were placed in separate sealed Falcon tubes containing PBS (10 mL; pH 7.4). The tubes were placed on a Grant-Bio PTR-35 multi-function rotator (Grant Instruments, UK) stirring at 30 rpm in a Stuart S160 incubator (Stuart Equipment, UK) at 37 °C. At pre-determined intervals, the tubes were removed from stirring and centrifuged using a Hermle Z400 centrifuge (Hermle LaborTechnik, Germany) at 5000 rpm for 10 minutes. Afterwards, an aliquot (1 mL) of the supernatant was removed and replaced with a fresh aliquot of PBS (1 mL). The supernatant was analysed via HPLC for resveratrol content using the method described in chapter 2, section 2.3.2.4.2. The cumulative resveratrol release (CRR) was calculated using **Equation 3-2**.

$$CRR \% = \frac{\text{Cumulative resveratrol release}}{\text{resveratrol loaded}} \times 100 \% \quad \text{Equation 3-2}$$

3.3.2.4.7. *In vitro* aerosolisation studies

The mass median aerodynamic diameter (MMAD) of the spray-dried NCMPs was determined by using a Next Generation Impactor (NGI; Copley Scientific, Nottingham, UK).

The NGI consists of 8 stages (stage 8 being filter paper) with various cut-off diameters. At 60 L/min, the 7 stages have the following diameters: stage 1 (8.06 µm); stage 2 (4.46 µm); stage 3 (2.82 µm); stage 4 (1.66 µm); stage 5 (0.94 µm); stage 6 (0.55 µm); and stage 7 (0.34 µm)(Marple *et al.*, 2003).

The NGI was equipped with a stainless-steel induction port (USP throat adaptor) and pre-separator (which was filled with 15 mL dH₂O). The removable

impactor cups under each stage was coated with 1% tween 80: methanol solution to remove particle bounce (Hamishehkar *et al.*, 2018). The impactor cups were weighed before and after each run to determine the particle mass deposited.

All three formulations of spray-dried NCMPs were weighed and manually loaded into hydroxypropyl methylcellulose capsules (size 3) (3 capsules, each corresponding to 10-15 mg spray-dried powder). The loaded capsules were placed inside a Cyclohaler® (Teva Pharmaceutical Industries Ltd.) that was attached to a mouthpiece adaptor (Copley Scientific, UK) connected to the induction port to form an airtight seal.

Three capsules were loaded and released for each sample and experiments were done in triplicate. The overall dose for each sample was about 30 mg. A Copley HCP5 vacuum pump (Copley Scientific, UK) and a Copley TPK 2000 critical flow controller (Copley Scientific, UK) were used to establish a flow rate of 60 L/min in order to simulate the flow rate in a healthy adult lung. A Copley DFM 2000 flow meter (Copley Scientific, UK) was employed to ensure the correct flow rate before each experiment.

The samples were drawn from the Cyclohaler® through the induction port into the NGI for 4 seconds per run.

The MMAD and the geometric standard deviation (GSD) were determined using online software (<http://www.mmadcalculator.com>). The emitted dose (ED), respirable fraction (RF), and fine particle fraction (FPF) were calculated using **Equations 3-3, 3-4, 3-5** (Stocke *et al.*, 2015):

$$ED \% = \frac{\text{Initial mass in capsules} - \text{Final mass in capsules}}{\text{Initial mass in capsules}} \times 100 \% \quad \text{Equation 3-3}$$

$$RF \% = \frac{\text{Mass of particles on stages 2-7}}{\text{Total particle mass on all stages}} \times 100 \% \quad \text{Equation 3-4}$$

$$FPF \% = \frac{\text{Mass of particles on stages 2-7}}{\text{Initial mass in capsules}} \times 100 \% \quad \text{Equation 3-5}$$

3.3.2.5. Cell culture

Human lung adenocarcinoma cell line (Calu-3) was grown in Minimum Essential Medium Eagle (MEM) media supplemented with 10 % foetal bovine serum (FBS), 1 % L-glutamine, 1% penicillin-streptomycin, 1% MEM Non-essential amino acids and 1% sodium pyruvate in a 75 cm² tissue culture flask incubated in a humidified incubator at 37 °C with 5% CO₂.

3.3.2.5.1. Cell toxicity studies

The Pierce™ LDH Cytotoxicity Assay Kit (ThermoFisher Scientific, UK) was used to determine the *in vitro* cytotoxicity of the NCMPs. Lactate dehydrogenase (LDH) is a soluble cytoplasmic enzyme that is present in almost all cells and is released into the extracellular space when the plasma membrane is damaged (Burd and Usategui-Gomez, 1973). The LDH cytotoxicity assay works by detecting this LDH being released into the cell culture medium using a tetrazolium dye. The conversion happens in a two-step process. Firstly, reduced nicotinamide adenine dinucleotide (NADH) is produced by LDH when it catalyses the oxidation of lactate to pyruvate. Secondly, the newly formed NADH in the presence of an electron acceptor converts the tetrazolium salt into a coloured formazan product that can be detected using a spectrophotometer (Korzeniewski and Callewaert, 1983). The linearity of the assay allows for calculating the percentage of necrotic cells

in a sample. An established protocol was used to run the assay and analyse the data (Chan, Moriwaki and De Rosa, 2013).

The LDH assay was performed exactly as is described in chapter 2, section 2.3.2.6.2. However, the cells were treated with NCMPs and free-resveratrol at concentrations of 0-5.75 mg/mL for 48 hours.

3.3.2.6. *Statistical analyses*

All statistical analyses were performed using GraphPad Prism 7. One-way analysis of variance (ANOVA) followed by Tukey's multiple comparisons test was employed to compare the formulations with each other. Statistically significant differences were assumed when $p < 0.05$. The level of confidence was set as 95%. All values are expressed as their mean \pm standard error of mean (cell studies) or mean \pm standard deviation (all other studies).

3.3.3. Results

3.3.3.1. *Nanocomposite microparticle analysis*

3.3.3.1.1. Yield

Using **Equation 3-1**, it was found that the yield ranged from 31.8-73.2% across the three formulations in the following order NCMP-BNP ($73.2 \pm 29.9\%$) > NCMP-5% RNP ($56.5 \pm 10.4\%$) > NCMP-10% RNP ($31.8 \pm 18.0\%$). There was no statistically significant difference ($p > 0.5$) between the three NCMPs.

3.3.3.1.2. Particle size and zeta potential

The size of the NPs recovered from the spray-dried NCMPs after re-dispersion in dH₂O was 1322 ± 306 nm and PDI 0.432 ± 0.220 for the NCMP-BNP, 1207 ± 443 nm and PDI 0.241 ± 0.06 for the NCMP-5% RNP, and 1744 ± 925 nm

and PDI 0.524 ± 0.424 for the NCMPs-10% RNP (**Figure 3-2**). All recovered NPs were statistically larger compared to the pre-spray-dried formulations.

The surface zeta potential of the reconstituted nanoparticles recovered all changed to positive, likely due to the added chitosan (**Figure 3-3**).

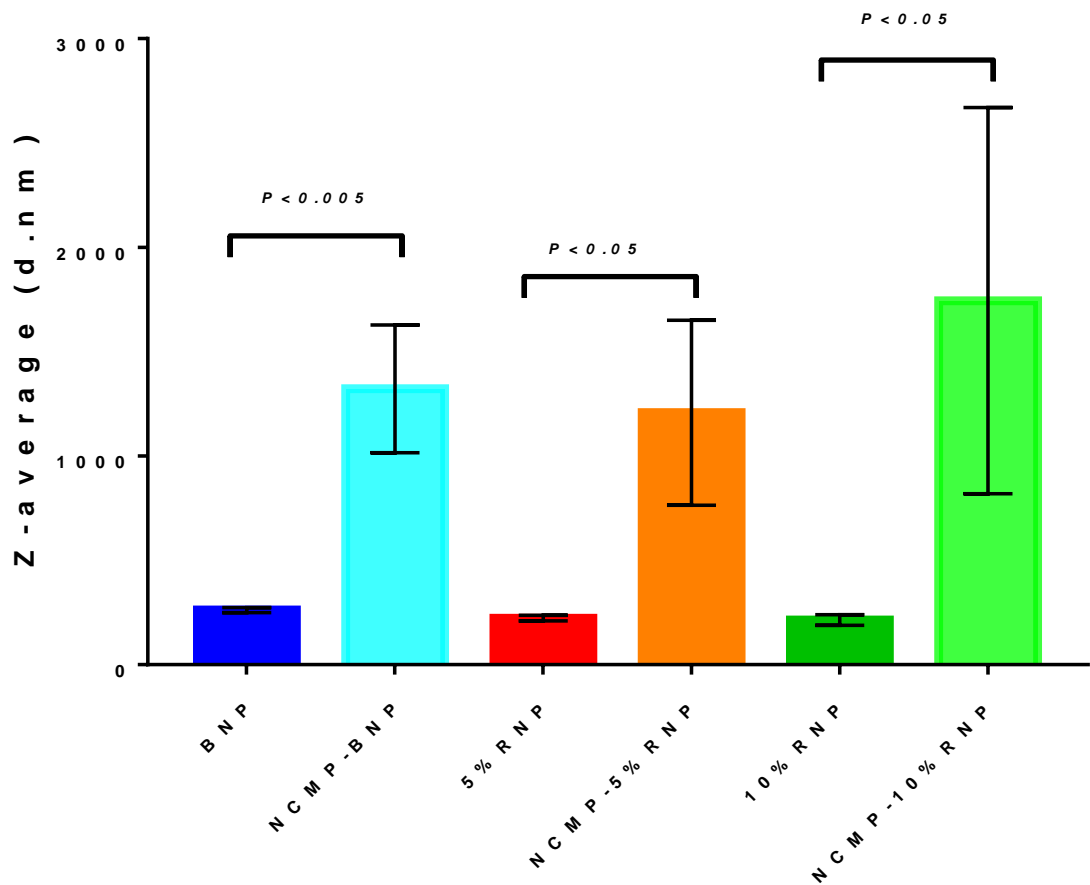


Figure 3-2 Size of PGA-co-PDL nanoparticles vs PGA-co-PDL nanoparticles reconstituted from nanocomposite microparticles in distilled water, n=3. Unpaired t-test was used to compare each pair of means as shown.

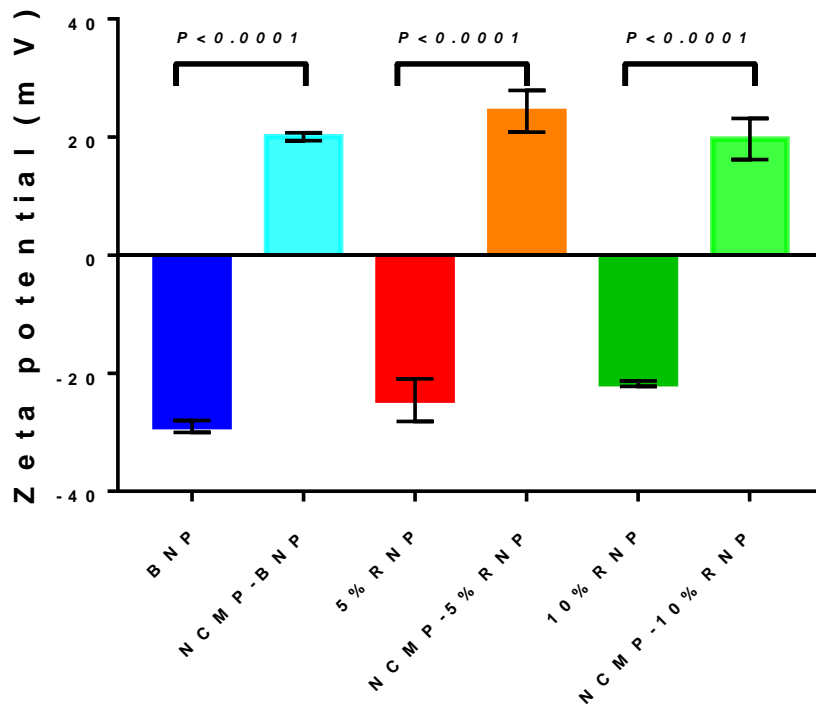


Figure 3-3 Charge of PGA-co-PDL nanoparticles vs reconstituted PGA-co-PDL nanoparticles from nanocomposite microparticles in distilled water, $n=3$. Unpaired t-test was used to compare each pair of means as shown.

3.3.3.1.3. Morphology

The surface morphology of the NCMPs were assessed using SEM. The NCMPs had a wrinkly surface with noticeable cavities/indentations in the middle of the particles (**Figure 3-4**). There was a heterogenous size distribution ranging from $<1 \mu\text{m}$ to $> 8 \mu\text{m}$ (**Figure 3-4**).

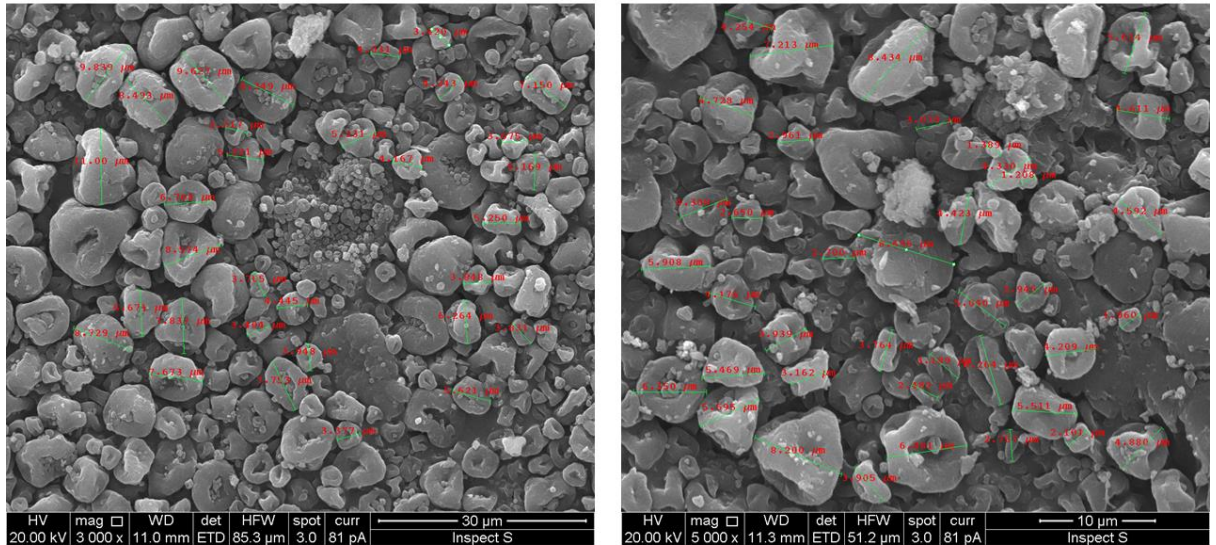


Figure 3-4 SEM images of NCMP-BNPs. Pictures were taken at 3000x and 5000x magnifications

3.3.3.1.4. Moisture content

The moisture content of the NCMPs was determined using TGA and the thermograms show that the spray-dried NCMPs contained a residual moisture content of $4.695 \pm 1.769\%$ w/w (NCMP-BNP), $4.441 \pm 1.078\%$ w/w (NCMP-5% RNP), and $4.896 \pm 0.762\%$ w/w (NCMP-10% RNP) (n=2) (**Figure 3-5**).

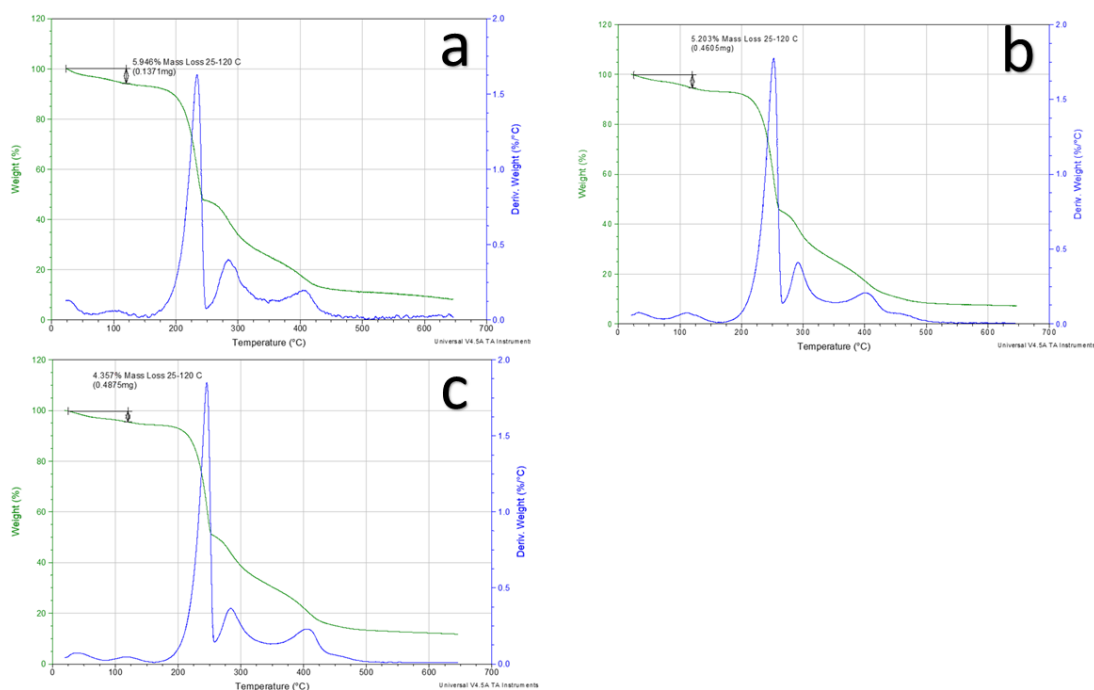


Figure 3-5 Thermogram of (a) NCMP-BNP, (B) NCMP-5% RNP, and (c) NCMP-10% RNP

3.3.3.1.5. Drug loading and encapsulation efficiency (EE%)

The drug loading and encapsulation efficiency (**Table 3-1**) of the NCMPs were calculated using a standard curve (**Figure 3-6**). The lowest concentration at which resveratrol can be detected (LOD) or quantified (LOQ) were calculated as 0.061 and 0.18 $\mu\text{g}/\text{mL}$, respectively.

Theoretical drug loading (TDL) was calculated using the **Equation 3-6**:

$$TDL = \frac{\text{Weight of resveratrol (mg) in NPs added}}{\text{Combined weight of NPs, Leucine, and Chitosan (mg)}} \quad \text{Equation 3-6}$$

$$5\% \text{ RNP (TDL)} = \frac{1.56 \text{ mg}}{140 \text{ mg}} = 11.14 \mu\text{g}/\text{mg}$$

$$10\% \text{ RNP (TDL)} = \frac{2.8 \text{ mg}}{140 \text{ mg}} = 20 \mu\text{g}/\text{mg}$$

EE% was calculated using **Equation 3-7**.

$$EE\% = \frac{\text{Drug loading calculated from standard curve } (\mu\text{g})}{TDL (\mu\text{g})} \times 100 \quad \text{Equation 3-7}$$

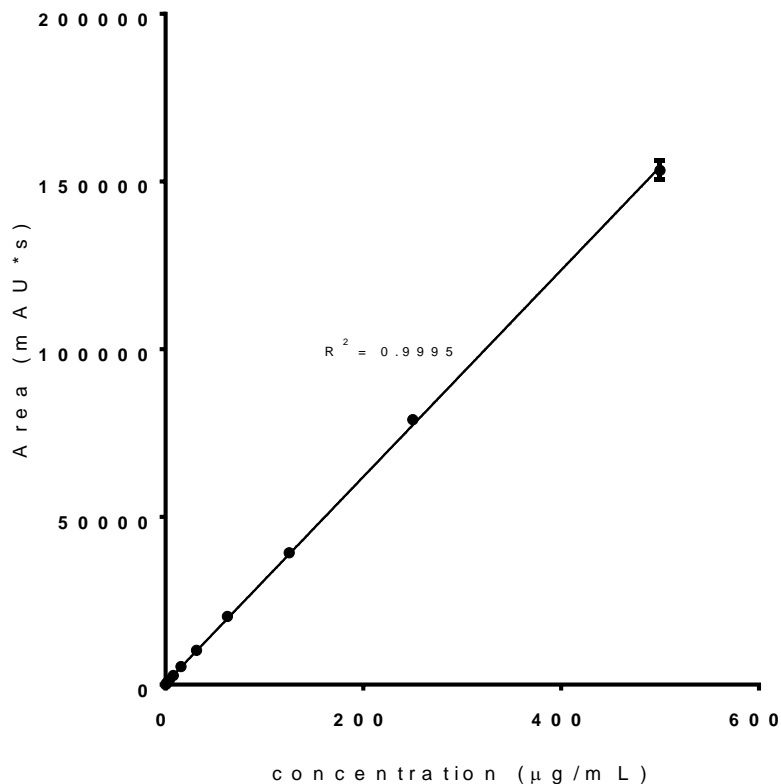


Figure 3-6 Resveratrol standard curve using HPLC ($R^2=0.9995$)
n=3

Table 3-1 Drug loading and encapsulation efficiency of NCMP-5% RNP and NCMP-10% RNP

Formulation	Drug loading (µg/mg)*	encapsulation efficiency (%)
NCMP-5% RNP	2.23 ± 0.01	20.00 ± 0.04
NCMP-10% RNP	7.97 ± 0.01	39.85 ± 0.05

* µg/mg – concentration of resveratrol in micrograms per 1 milligram of NCMPs

3.3.3.1.6. Release study

The percentage cumulative resveratrol released *in vitro* from the NCMPs, calculated using **Equation 3-2**, showed that only 20-25% of resveratrol was released over 24 hours (**Figure 3-7**). The percentage of resveratrol released after 15 minutes was $6.4 \pm 0.04\%$ and $3.5 \pm 0.03\%$, 1 hour was $17.9 \pm 0.20\%$ and $13.3 \pm 0.07\%$, 4 hours was $22.7 \pm 0.25\%$ and $18.2 \pm 0.09\%$, and after 24 hours $25.8 \pm 0.25\%$ and $21.5 \pm 0.1\%$ for NCMP-5% RNP and 10% NCMP-10% RNP, respectively.

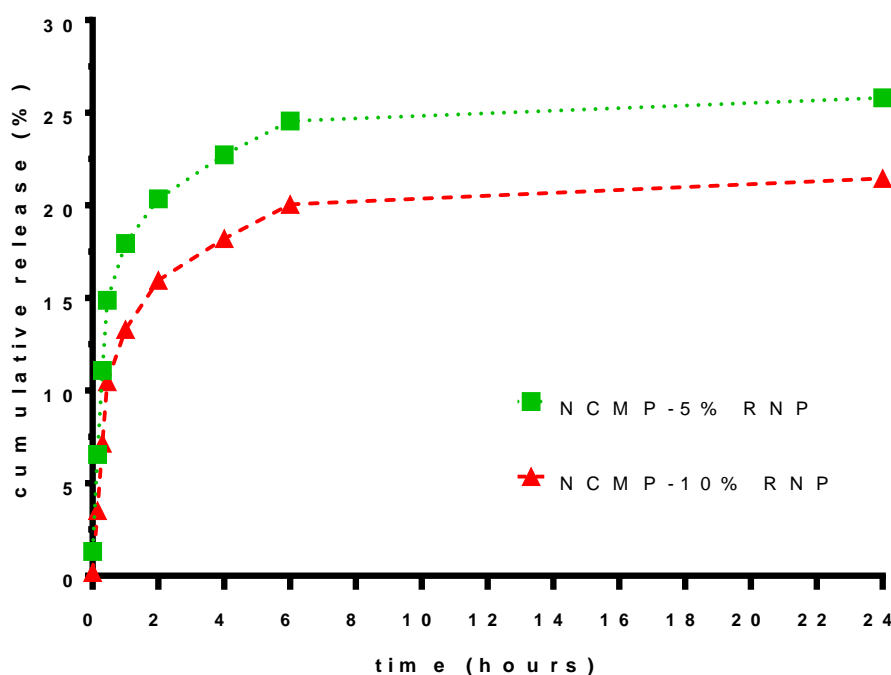


Figure 3-7 *In vitro* release profile of NCMPs-5% RNP and NCMPs-10% RNP in PBS (pH 7.4) at 37 °C

3.3.3.1.7. *In vitro* aerosolisation studies

The ED of all three NCMPs was above 98%. The RF was $72 \pm 3.4\%$, $74 \pm 4.5\%$, $70 \pm 1.7\%$ for NCMP-BNP, NCMP-5% RNP, and NCMP-10% RNP, respectively (**Table 3-2**). The FPF and its corresponding mass relates to the percentage and amount of the formulation that would reach the lower echelons of the lungs (Stages 2-7 in **Figure 3-8**). NCMP-BNP had an FPF and corresponding mass of $38.9 \pm 7.2\%$ and 7 ± 1.3 mg (per capsule). Meanwhile, the NCMP-5% RNP and NCMP-10% RNP had an FPF and mass of $46.7 \pm 5.7\%$ and 6 ± 0.9 mg and $39.8 \pm 4.8\%$ and 7 ± 0.84 mg, respectively. The MMAD of NCMP-BNP, NCMP-5% RNP, and NCMP-10% RNP were 3.96 ± 0.69 μm (n=4), 3.11 ± 0.51 μm (n=4), and 3.59 ± 0.43 (n=3), respectively. These results all suggest that the majority of the ED of the formulations are to be delivered to the lower bronchi-alveolar regions of the lungs.

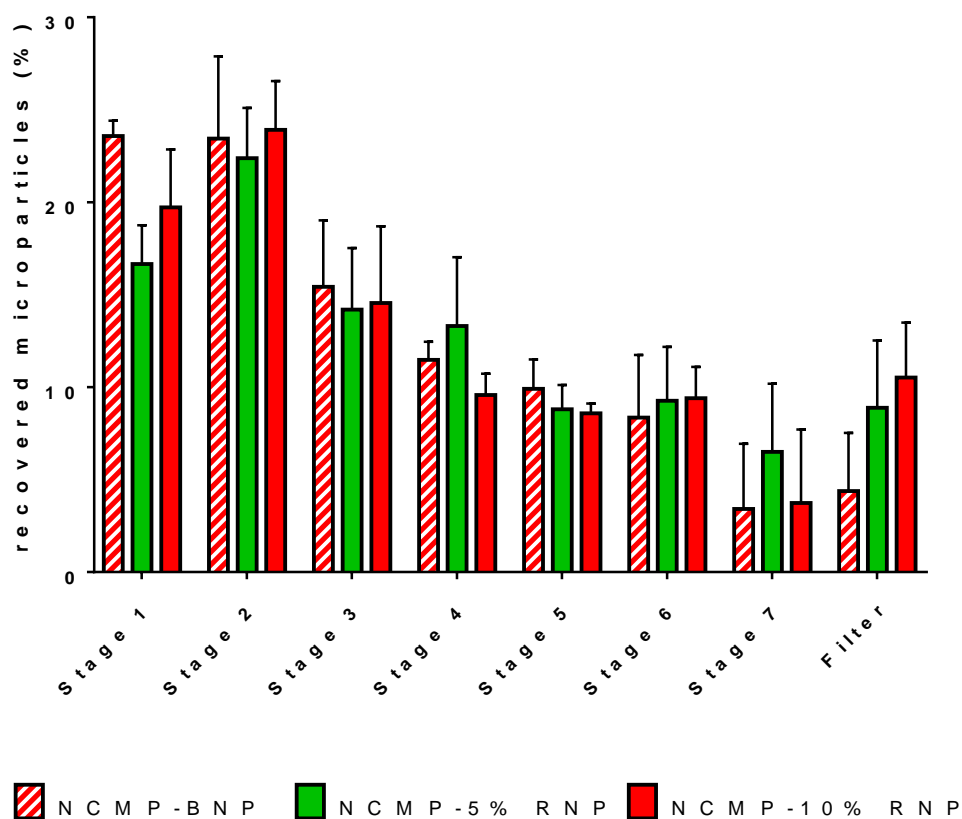


Figure 3-8 Percentage of NCMPs deposited at each stage of the NGI n=4

Table 3-2 Emitted Dose, Respirable Fraction, and Fine Particle Fraction of NCMP-BNP, NCMP-5% RNP, and NCMP-10% RNP

NCMPs	Emitted Dose (%)	Respirable Fraction (%)	Fine Particle Fraction (%)
NCMP-BNP	98.7 ± 0.8	72.0 ± 3.4	38.9 ± 7.2
NCMP-5% RNP	98.9 ± 1.3	74.5 ± 4.5	46.7 ± 5.7
NCMP-10% RNP	98.7 ± 1.9	69.8 ± 1.7	39.8 ± 4.8

3.3.3.1.8. Cell viability studies

3.3.3.1.8.1. LDH assay

There was no statistically significant difference ($p > 0.05$) between the three NCMPs tested and the control (**Figure 3-9**). At 2.5 mg/mL, the NCMP-BNP induced an LDH release of 56 ± 21 % compared to the maximum LDH release by cell lysis. At higher concentrations, 2.8 mg/mL, the NCMP-5% RNP and NCMP-10% RNP resulted in lower LDH release, 43 ± 20 % and 34 ± 10 %, respectively. This indicates that the NCMP-BNP caused more cell damage than the NCMP-5% RNP and NCMP-10% RNP. However, it should be noted that this experiment was fraught with problems and the NCMPs may have caused interference with the assay that confounded the results.

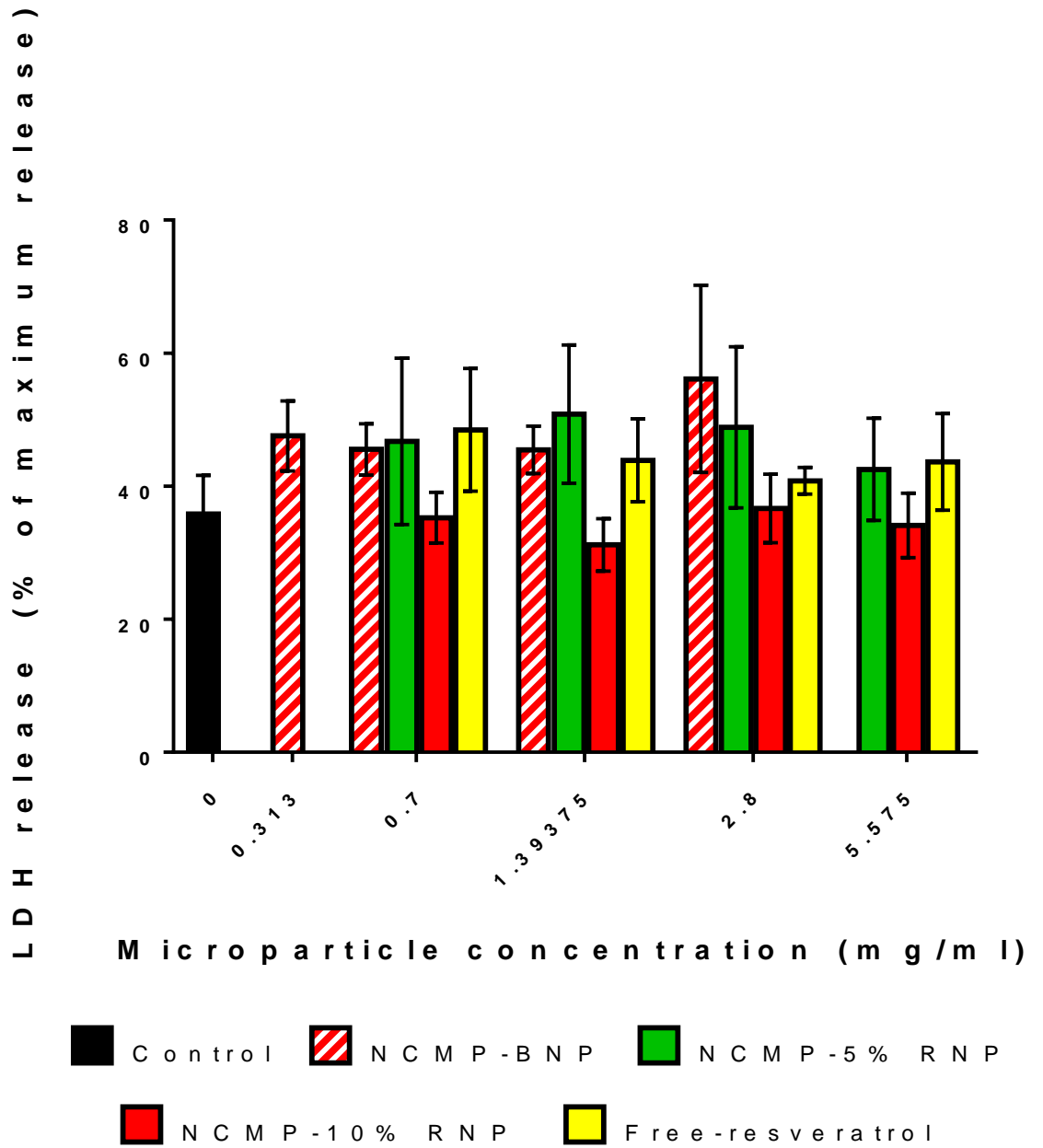


Figure 3-9 The effect of NCMP-5% RNP and NCMP-10% RNP on LDH release in Calu 3 cells after 48 hours

3.3.4. Discussion

The aim of this study was to develop NCMPs for the dry powder delivery of resveratrol PGA-co-PDL NPs to the lung. PGA-co-PDL NPs with a diameter in the region of 250 nm , would be readily uptaken into the cells, but they are incapable of depositing directly into the lungs since they would be exhaled without settling in the alveoli (Pilcer and Amighi, 2010; Florence, 2012). In order to be inhaled and efficiently deposited into the lungs, particles need to have an aerodynamic diameter in the range of 1-5 μm (Yildiz-Peköz *et al.*, 2018). Thus, the PGA-co-PDL NPs optimised in Chapter 2 had to be formulated into NCMPs for pulmonary administration by dry powder inhalation.

NCMPs were formed via spray drying using L-leucine and chitosan as excipients. L-leucine, a hydrophobic amino acid, is beneficial as an excipient due to its ability to reduce the aggregation of particles produced via spray drying (Takeuchi *et al.*, 2018). L-leucine has been shown to increase the FPF (Takeuchi *et al.*, 2018). Chitosan is a natural polycationic linear polysaccharide, that has been shown to be mucoadhesive, non-immunogenic and non-toxic (Cheung *et al.*, 2015). It forms electrostatic interactions with the sialic groups of mucins in the mucus layer (Hejjaji, Smith and Morris, 2018; Collado-gonz, Gonz and Goycoolea, 2019). Chitosan was shown to modify the release profile of drugs in spray-dried formulations (Learoyd *et al.*, 2008) Leucine and chitosan in combination was shown to enhance the dispersibility and modify the drug release profile of dry powder formulations of hydrophilic terbutaline sulfate, and hydrophobic beclomethasone dipropionate (Learoyd *et al.*, 2009). In this study, it was anticipated that spray drying the PGA-co-PDL NPs with L-leucine (aerosolisation enhancer) and chitosan (drug release

modifier) would result in NCMPs that showed good dispersibility, would adhere to the mucosal surface of the lungs and upon dispersion the NPs would deliver a sustained drug release profile.

The yield of the spray-dried NCMPs had the following order NCMP-BNP ($73.2 \pm 29.9 \%$) > NCMP-5% RNP ($56.5 \pm 10.4 \%$) > NCMP-10% RNP ($31.8 \pm 18.0 \%$). There was no statistically significant difference between the three NCMPs ($p > 0.05$). This may be due to the difficulty in removal of the powder from the sides of the cyclone, due to some of the liquid droplets attaching to the inside wall of the drying chamber and cyclone of the spray-dryer and the difficulty in removal of chitosan. Vancomycin hydrochloride-encapsulated chitosan microspheres were prepared via spray drying with different chitosan: drug ratios (Cevher *et al.*, 2006). The low yields were attributed to liquid droplets attaching to the inside of the wall of main chamber of the spray-dryer (Cevher *et al.*, 2006). Similarly, liquid droplets attaching to the inner chambers of the spray dryer was also blamed for the decreased yield for liposomes spray-dried into NCMPs with chitosan and L-leucine as excipients (Almurshedi, 2018).

After deposition into the lung, the NCMPs are thought to disperse, releasing the drug-loaded NPs within the alveoli (Tomoda *et al.*, 2008). The size of the NPs recovered from the spray-dried NCMPs after re-dispersion in dH₂O were statistically larger than before spray drying ($p < 0.05$) (**Figure 3-2**). Some studies found that NPs recovered from the NCMPs were 10–20% bigger and others found it was 30% bigger than the original NPs (Sham *et al.*, 2004; Chaubal and Popescu, 2008). Preparation of 5% and 10% TAS-103 -PLGA NPs via single-emulsion solvent evaporation resulted in NPs of 201 nm and

211 nm, respectively (Tomoda *et al.*, 2009). The NPs were spray-dried into NCMPs using trehalose dihydrate as an excipient (Tomoda *et al.*, 2009). When the NCMPs containing 5% and 10% TAS-103 -PLGA NPs were dispersed in distilled water, the NCMPs decomposed and yielded NPs of 231 and 241 nm, respectively (Tomoda *et al.*, 2009). Gelatin and polybutylcyanoacrylate (PBCA) NPs were prepared with a mean particle sizes of 242 ± 17 and 173 ± 59 nm, respectively (Sham *et al.*, 2004). After spray drying with lactose, the particles were dispersed in water and the mean particle sizes of the gelatin and PBCA NPs increased to 319 ± 58 and 231 ± 33 nm, respectively (Sham *et al.*, 2004). PGA-co-PDL Blank NPs and BSA adsorbed NPs were spray-dried in NCMPs using L-leucine (Kunda, 2014). The size of the NPs recovered from the NCMPs was 210 ± 16 and 223 ± 2 nm compared to 204 ± 3 and 299 ± 32 nm before spray drying for PGA-co-PDL Blank NPs and BSA adsorbed NPs, respectively. pH sensitive liposomes (PSL NPs) were prepared with an average size range of 42-57 nm (Almurshedi, 2018). After spray drying with L-leucine (1.5 w/w) and various concentrations of low molecular weight chitosan (0.5-2 w/w), the recovered PSL NPs, 62.4-89.4 nm, were larger than the original PSL NPs (Almurshedi, 2018). Increased chitosan concentration resulted in an increase in recovered PSL NPs size (Almurshedi, 2018). Trehalose dihydrate and lactose are readily soluble in water and although L-leucine is hydrophobic, it can disperse in water, which will explain the recovery of NPs from NCMPs using these excipients (Lipiäinen *et al.*, 2018; Sansone *et al.*, 2018; Focaroli *et al.*, 2019). On the other hand, chitosan swells (forming a gel) when exposed to an aqueous medium, which could explain the

increased size of the NPs recovered from the NCMPs spray-dried with chitosan (Aranaz *et al.*, 2017).

The surface zeta potential of the reconstituted NPs recovered were all positive where-as the NPs had been negatively charged before spray drying (**Figure 3-3**). This positive change is most likely due to the chitosan, a cationic polysaccharide, coating the NPs (Ranjan *et al.*, 2011; Muhsin *et al.*, 2016). Similar results were found previously when liposomes were spray-dried into NCMPs using L-leucine and chitosan. It was found that the reconstituted liposomes tended to move towards a more positive zeta potential as the concentration of chitosan increased (Almurshedi, 2018).

The morphological analysis via SEM showed particles that had wrinkly/corrugated surfaces with noticeable cavities/indentations in the middle of the particles (**Figure 3-3**). These cavities are caused by L-leucine possessing the ability to migrate to the surface of the particle droplet during the rapid atomisation phase of spray drying. Being hydrophobic, L-leucine, blocks water from adsorbing onto the surface of the particle which produces the cavities upon drying (Merchant *et al.*, 2014). This shape is thought to reduce the cohesion forces, because of the reduced contact area (Chew and Chan, 2001; Irvine, Afrose and Islam, 2018). L-leucine was shown to produce this morphology when used as an excipient for spray-dried PGA-co-PDL NCMPs (Kunda, Alfagih, Dennison, Somavarapu, *et al.*, 2015). The same surface morphology with pitted particles were obtained when liposomes were spray-dried with the same ratio of L-leucine and chitosan, 1.5:1 (Almurshedi, 2018). It was shown that only when the L-leucine:chitosan ratio increased to 1.5:2, did the particles start to become smoother and the pitting was less

pronounced (Almurshedi, 2018). This was further shown when levofloxacin spray-dried with L-leucine (20% w/w) resulted in broken particles with deep pitting, but the levofloxacin spray dried with octanoyl chitosan (20% w/w) and L-leucine (5% w/w) showed a smoother particle with no evidence of the pitting (Merchant *et al.*, 2014). The reduction in the pitting of the particles can be attributed to the chitosan increasing the viscosity of the feed solution, counteracting the ability of the L-leucine to displace the water on the surface of the droplet. It was found that microspheres produced using a low viscosity grade of chitosan showed a wrinkly surface morphology compared to microspheres prepared using a high viscosity grade which had a smooth surface (He, Davis and Illum, 1996). Increased feed viscosity, due to increased concentrations of chitosan, has also been implicated in increased particle sizes, lower encapsulation efficiency, and decreased drug release (Jarudilokkul, Tongthammachat and Boonamnuayvittaya, 2011; Cho *et al.*, 2014).

The resveratrol content of the NCMP-5% RNP and NCMP-10% RNP was 2.23 µg and 7.79 µg, respectively (**Table 3-1**). This is between 20-40 % of the amount predicted in **Equation 3-6**. This encapsulation efficiency is low and this could be attributed to the NPs. In chapter 2, it was shown that the PGA-co-PDL 5% RNP and 10% RNP had burst release profiles, with up to 44 % of resveratrol released immediately upon contact with the release medium. This was attributed to some resveratrol not encapsulating inside the nanoparticle during the formulation process, but instead being trapped on the surface of the nanoparticle, which is then immediately released upon contact with a release medium (Huang and Brazel, 2001; Kamaly *et al.*, 2016). This process might

also occur during the NCMPs formulation process, when the NPs are placed inside the distilled water or acetic acid (0.1%) aqueous solution of L-leucine and chitosan.

In chapter 2, it was shown that the encapsulation efficiency of the PGA-co-PDL 5% RNP and 10% RNP were quite high at 78 and 70 %, respectively. Therefore, increasing the encapsulation efficiency of the NPs might not be feasible to increase the amount of drug inside of the NCMPs, especially since the encapsulation efficiency of the NPs is lowering with increased amount of drug added (as shown in chapter 2, **Table 2-2**). However, since the amount of drug inside of the NCMPs are increasing with a higher drug loading in the NPs, it could be argued that increasing the ratio of NPs would increase the encapsulation efficiency of the NCMPs, up to a certain point (**Table 3-1**)

In chapter 2, the results from the release study for the PGA-co-PDL NPs showed no further release after 1 hour. During this study, the respective release profiles of the NCMP-5% RNP and NCMP-10% RNP were analysed. Both formulations had a very slow cumulative release of resveratrol (CRR) (**Figure 3-7**). The CRR was calculated from **Equation 3-2** with 100% represented by the initial drug loading (**Table 3-1**). The percentage of resveratrol released after 15 minutes was $6.4 \pm 0.04\%$ and $3.5 \pm 0.03\%$, 1 hour was $17.9 \pm 0.20\%$ and $13.3 \pm 0.07\%$, 4 hours was $22.7 \pm 0.25\%$ and $18.2 \pm 0.09\%$, and after 24 hours $25.8 \pm 0.25\%$ and $21.5 \pm 0.1\%$ for NCMP-5% RNP and NCMP-10% RNP, respectively. The release rate went from 13-18 % in the first hours then slowed to 3-4 % further release over the last 20 hours. This could be attributed to two things. Firstly, the amount of resveratrol encapsulated inside the NCMPs used in the release study could have differed,

largely, from the amount displayed in **Table 3-1**. This could have been ascertained by bursting the particles after 24 hours and analysing it via HPLC to check if there was any resveratrol left. Secondly, this could be due to a reduction in resveratrol release due the NPs being within a chitosan matrix (Liu *et al.*, 2019). Previous studies have shown that the ratio of chitosan is inversely proportional to the release rate of a drug from a formulation (Almurshedi, 2018). Apart from the increased viscosity, it is suggested that the hydrophilic nature of the chitosan present in the microparticle causes it to swell when it comes into contact with the water, which produces a gel layer that the drug has to diffuse through (Aranaz *et al.*, 2017). This gel diffusion results in the sustained release profile. Logically, the greater the concentration of chitosan, the greater the thickness of the gel the drug has to diffuse through, which ultimately leads to a greater drug retention and slower release profile (Thein-Han *et al.*, 2004). There are three mechanisms for the release of a drug through the NCMPs, including release from the surface of polymeric NPs, diffusion through the swollen gel like layer, and release of the drug due to erosion of the polymer. In the majority of cases, the release of the drug is due to a combination of these mechanisms (Soares *et al.*, 2016). Both the NCMP-5% RNP and NCMP-10% RNP produced curves that fit the Higuchi model best ($R^2=0.95$). This may suggest that the resveratrol has to diffuse through the NPs and the chitosan gel layer in order to be released. Thus, tweaking the chitosan ratio and overall viscosity could be used to control the particle sizes, drug encapsulation efficiency, and drug release profile.

Chitosan has a greater affinity for water and tends to absorb the water into its matrix protecting it during the spray drying process and resulting in a higher

final moisture content (Merchant *et al.*, 2014). TGA thermograms showed that the spray-dried formulations contained a residual moisture content between 4.6-4.9% (**Figure 3-5**). These results are comparable to previous studies using L-leucine as an excipient, which showed a moisture content between 0.5-5% (Nieto-Orellana *et al.*, 2018). Since the spray-dried formulations used in this study only contained 29% w/w chitosan compared with 43% w/w L-leucine, its water absorption may have been less pronounced.

The results from the *in vitro* aerosolisation studies using the NGI, showed all three NCMPs had a good ED, RF, and FPF. The ED of all three formulations were above 98% and the NCMP-BNP, NCMP-5% RNP, and NCMP-10% RNP had an RF of $72 \pm 3.4\%$, $74 \pm 4.5\%$, $70 \pm 1.7\%$, respectively (**Table 3-2**). The high ED can be attributed to the inclusion of L-leucine as a dispersibility enhancer (Rabbani and Seville, 2005; Learoyd *et al.*, 2008). The efficiency of drug deposition in the lower respiratory tract is characterised by the FPF (Yildiz-Peköz *et al.*, 2018). The three NCMPs had an FPF of $38.9 \pm 7.2\%$, $46.7 \pm 5.7\%$ and $39.8 \pm 4.8\%$, respectively. These results are higher than the FPF range of 10-20% provided by conventional DPIs (Suarez and Hickey, 2000; Meenach *et al.*, 2013; Yildiz-Peköz *et al.*, 2018). Previous data have suggested that the higher the ratio of chitosan to L-leucine, the lower the FPF (Almurshedi, 2018). The MMAD of all three NCMPs were between 3.1-4 μm . These results place the three NCMPs within ideal range of 1-5 μm for particles to be able to deposit in the deep regions of the lung (El-Sherbiny and Smyth, 2012; Elsayed and AbouGhaly, 2016; Rezazadeh *et al.*, 2018). It seems that the use of L-leucine enhanced the dispersibility of the formulations, but the excipients together produced a low FPF, which may suggest aggregation of

the particles. Kunda *et al.*, spray-dried bovine serum albumin (BSA) adsorbed PGA-co-PDL NPs within L-leucine (1:1.5 w/w), at the same ratio and using the same spray-dryer parameters as in this study (Kunda, Alfagih, Dennison, Tawfeek, *et al.*, 2015). The spray drying resulted in a yield of 42.35 ± 3.17 % and the *in vitro* release study showed an initial burst release of 30.15 ± 2.33 % with 95.15 ± 1.08 % BSA released over 48 hours (Kunda, Alfagih, Dennison, Tawfeek, *et al.*, 2015). These results are comparable to some of the results from this study, however, the MMAD was 1.21 ± 0.67 μm , which was much lower than what was achieved in this current study with both L-leucine and chitosan as excipients (Kunda, Alfagih, Dennison, Tawfeek, *et al.*, 2015).

The LDH assay was performed to assess the cytotoxic effects of the NCMPs on Calu 3 cells. Although in chapter 2 the cell viability studies produced some promising results, the cell viability results from the NCMPs were inconclusive. There seemed to be no discernible pattern with the NCMP-BNP and NCMP-10% RNP. This could have been due, at least in part, to the wide variabilities (indicated by large standard error of the mean values) recorded for some of the data sets. There has been increasing concern with regards to reproducibility in biomedical research (Prinz, Schlange and Asadullah, 2011; Errington *et al.*, 2014; Freedman *et al.*, 2015; Baker and Penny, 2016). It could also be that due to the low release rate of resveratrol from the particles, the cytotoxic effect obtained with the NPs, as shown in chapter 2, was not fully replicable in 48 hours. Therefore, a longer incubation period may need to be investigated in the future. As with NPs mentioned in chapter 2, the NCMPs could be interfering with the LDH assay in various ways (Han *et al.*, 2011; Kong *et al.*, 2011; Oostingh *et al.*, 2011; Sukhanova *et al.*, 2018). Certain

microparticles have been found to interfere with the MTT and LDH assays (Laaksonen *et al.*, 2007; Korhonen *et al.*, 2016) It is imperative that optimisation of the cell culture assay takes place. Some of the steps that need to be taken include optimisation of seeding cell density (Che, Wang and Li, 2009). It is essential to ensure that the cells are still in the growth phase at the end of the assay (Wright Muelas *et al.*, 2018). Chitosan, although biocompatible, has been shown to be cytotoxic and it would be worthwhile to assess the effects of both the chitosan and L-leucine, individually and combined, on the Calu 3 cells using the LDH assay (Cheung *et al.*, 2015; Patrulea *et al.*, 2015).

3.3.5. Conclusion

The aim of this study was to develop NCMPs for the dry powder delivery of resveratrol PGA-co-PDL NPs to the lung. The PGA-co-PDL NPs synthesised in chapter 2 were able to be incorporated into NCMPs using L-leucine and chitosan as excipients. The highest yield of the resveratrol-loaded NCMPs was the NCMP-5% RNP at 56.5 ± 10.4 %. The recovered NPs from the NCMPs showed an increase in size with a change from negative to positive, due to chitosan. The NCMPs improved on the release rate by enabling a slow release profile over a 24-hour period.

In chapter 2, the resveratrol-loaded PGA-co-PDL NPs showed a concentration- and time-dependent cytotoxic effect on Calu 3 cells and reduced the IC₅₀ of resveratrol by 78%, however, further studies are required to assess whether this effect is reproducible within a dry powder required for pulmonary delivery.

4 CHAPTER 4: The functionalisation of PGA-co-PDL using a modified glycerol

4.1. Introduction

Polymeric nanoparticles (NPs) allow for the encapsulation of drugs inside a protective polymeric matrix. NPs have been shown to be a suitable delivery system for several drugs against various cancers including colon, liver, lung and prostate (Karthikeyan *et al.*, 2013; Jung *et al.*, 2015; J. Wu *et al.*, 2017; Nassir *et al.*, 2018). In Chapter 2, the ability of resveratrol loaded PGA-co-PDL NPs to cause a concentration- and time-dependent decrease in Calu 3 cell viability was demonstrated. The resveratrol loaded PGA-co-PDL NPs showed a decrease in the IC₅₀ of the resveratrol by 78%. These studies illustrate the potential of polymeric NPs as a resveratrol delivery system, but there was no elucidation of the mechanism of uptake of the NPs into cancer cells. The mechanism of uptake of NPs by cells is a core determinant of the NPs biodistribution and toxicity (Foroozandeh and Aziz, 2018). Polar or charged species, such as NPs, cannot passively traverse the cell membrane, but rather have to make use of endocytosis.

Endocytosis is an energy-dependent process used for internalising ions and biomolecules by cells (Iversen, Skotland and Sandvig, 2011). There are two major categories of endocytosis, namely, phagocytosis and pinocytosis (Sahay, Alakhova and Kabanov, 2010). Phagocytosis involves the internalisation of debris, bacteria or other solutes larger than 0.5 µm by specialised phagocytes, such as dendritic cells, macrophages, and neutrophils (Zhao and Stenzel, 2018). Pinocytosis has four subclassifications, namely, clathrin-mediated endocytosis, caveolae-mediated endocytosis, clathrin- and caveolae-independent endocytosis and micropinocytosis (Foroozandeh and Aziz, 2018). Micropinocytosis involves the non-specific uptake of fluids and

particles together into the cell (Oh and Park, 2014). Clathrin- and caveolae-mediated endocytosis involves the use of receptors and clathrin- and caveolae-independent endocytosis involves cells lacking both clathrin- and caveolae (Oh and Park, 2014). The nanoparticle (NP) properties seem to determine the type of endocytosis employed. Clathrin-mediated endocytosis were shown to be the pathway for internalisation of polymer based NPs (Foroozandeh and Aziz, 2018). Clathrin-mediated endocytosis seems to be preferred when NPs are < 200 nm, and for particles > 200 nm caveolae-mediated endocytosis came into effect (Rejman *et al.*, 2004; Prabha *et al.*, 2016). Apart from size, there are several other factors that impact NP uptake by cells, including shape, surface charge, hydrophobicity, and surface functionality (Behzadi *et al.*, 2017). Visualisation of the cellular uptake using, for example, confocal microscopy requires a fluorescent delivery system or drug (Kenesei *et al.*, 2016). However, if the delivery system or drug does not possess intrinsic fluorescence, a fluorescent agent has to be added. Fluorescent molecules may be encapsulated within the delivery system, but in order to accurately assess the uptake of the particle, the fluorescent ligand needs to be chemically conjugated to either the parent polymer or the surface of the NP (Peng and Chiu, 2015; Kenesei *et al.*, 2016; Chatterjee *et al.*, 2017).

The main objective of nanomedicines is to enhance the treatment efficacy and using targeted NPs goes a long way in realising this objective. Targeted drug delivery systems aim to enhance efficacy through the accumulation of the drug at the specific site of interest, thereby decreasing toxicity throughout the rest of the body (Cheng *et al.*, 2015). There are two types of targeting, passive and active. Passive targeting involves exploitation of certain characteristics of

tumours. For example, the blood vessels of many solid tumours possess characteristics that are unique and not usually observed in healthy tissue, such as, extensive angiogenesis leading to increased blood supply, increased vascular permeability due to vascular mediators and defective vascular architecture, and reduced lymphatic drainage from the interstitial spaces of tumour tissues (Maeda, 2001). These characteristics are known as the Enhanced Permeability and Retention (EPR) effect. Active targeting involves, for example, the incorporation of a ligand onto the surface of NPs that specifically binds to a particular target site such as, peritumoural and intratumoural blood vessels, the extracellular matrix, tumour cells or intracellular targets (Wilhelm *et al.*, 2016). Ligands that can be used to target cancer cells include antibodies, aptamers, nucleic acids, peptides, sugars, and other small molecules (Bertrand *et al.*, 2014; Bazak *et al.*, 2015).

The attachment of moieties onto the polymer backbone or NP surface requires the presence of functional groups within the polymer. The polymerisation of poly(lactic-co-glycolic) acid (PLGA), from lactic and glycolic acid, results in the formation of one hydroxyl end group (Martins *et al.*, 2018). Hydrolytic degradation of the PLGA in an aqueous environment yields PLGA with one hydroxyl and one carboxylic acid end group, which may be functionalised (Souza, Dorati and Deluca, 2014; Kapoor *et al.*, 2015). A monoclonal antibody (mAb) targeting membrane proteins of MCF-7 cells was covalently attached to the free carboxylic end group of the PLGA NPs, using 1-ethyl-3-(3-dimethylaminopropyl)-carbodiimide (EDC) (Kocbek *et al.*, 2007). EDC facilitates conjugations of molecules containing a primary amine and a carboxylic group (Kocbek *et al.*, 2007). MCF-10A neoT cells, which like MCF-

7, originate from human breast epithelial cells, were co-cultured with Caco-2 human colon adenocarcinoma cells. The mAb-labelled PLGA NPs were localised exclusively to the MCF-10A neoT cells, while the uncoated PLGA NPs were found in both cell lines (Kocbek *et al.*, 2007). Wang *et al.*, exploited the affinity of wheat germ agglutinin (WGA) to recognise and rapidly bind to N-acetylglucosamine and sialic acid residues expressed on colon cells, leading to internalisation (Wang, Ho and Lim, 2010). The free carboxyl end group on PLGA NPs were used to covalently conjugate fluorescently-labelled WGA (fWNPs) and fluorescently-labelled bovine serum albumin (fBNPs) (Wang, Ho and Lim, 2010). The fWNPs and fBNPs were assessed for uptake against two human colon cancer cells lines (Caco-2 and HT-29) and one human colon fibroblast (CCD-18Co). The fWNPs showed a 12-fold higher uptake in Caco-2 cells compared to fBNPs (Wang, Ho and Lim, 2010). Moreover, the fWNPs showed a selective affinity for the cancer cell lines, Caco-2 and HT-29, over the normal cell line, CCD-18Co (Wang, Ho and Lim, 2010). Similar functionality can be achieved in polymers containing glycerol, due to the free secondary hydroxyl group present on glycerol (You *et al.*, 2010; Zhang and Grinstaff, 2014).

Chemical moieties can be attached to a functionalised polymer backbone or end group using click chemistry. Click chemistry refers to a group of chemical reactions that meet strict conditions including being, “ modular, wide in scope, give very high yields, generate only inoffensive by-products that can be removed by nonchromatographic methods, and be stereospecific“ (Kolb, Finn and Sharpless, 2001). Click chemistry reactions include, cycloaddition reactions, nucleophilic ring-opening reactions, non-aldol type carbonyl

chemistry, and carbon-carbon additions (Kolb and Sharpless, 2003). In biomedical research, click chemistry has been employed in lead discovery, optimisation, as well as tagging of proteins, nucleotides, and whole organisms (Kolb and Sharpless, 2003). One of the cycloaddition reactions, metal catalysed azide/alkyne 'click' reaction (also termed copper-catalysed azide-alkyne cycloaddition (CuAAC)), has shown wide application in the field of polymer science (Binder and Sachsenhofer, 2008; Binder, 2019). The CuAAC reaction has a high efficiency, high tolerance of functional groups, and solvent insensitivity (Binder and Sachsenhofer, 2007). This reaction was used to label intact Cowpea mosaic virus particles with fluorescein (Wang *et al.*, 2003). Similarly, click chemistry also offers a quick and simplistic way to modify the surfaces of nanocarriers with fluorescent tags or targeting ligands (Voigt *et al.*, 2019). Surface modification can be implemented pre-, intra-, or post-preparation (Voigt *et al.*, 2019). A tetrazine fluorophore was clicked onto polyethylene glycol (PEG) and hyperbranched polyglycerol (hbPG)-modified liposomes via CuAAC reaction to determine the intra- and extracellular fate of the liposomes (Voigt *et al.*, 2019). Poly(styrene-co-maleic anhydride) (PSMA) was used to functionalise semiconducting polymer dots (Pdots) made from a highly fluorescent semiconducting polymer poly[(9,9-dioctylfluorenyl-2,7-diyl)-co-(1,4-benzo-{2,1',3}-thiadiazole)] (PFBT) (Wu *et al.*, 2010). The resulting carboxyl-functionalised Pdots were reacted with amine-azido via the standard carboxyl-amine coupling catalysed by EDC (Wu *et al.*, 2010). The azide-functionalised Pdots were then able to click onto alkyne-functionalised silica nanoparticles via CuAAC to convert the optically inert silica particles into highly fluorescent probes (Wu *et al.*, 2010). An alkyne-functionalised homopolymer

of *D,L*-lactide (hexyn-pDLLA) was synthesised via ring opening polymerisation and coupled with azide-NIR10 via CuAAC reaction to obtain the fluorescent-labelled polymer (Rahimian *et al.*, 2015). The fluorescent-labelled polymers were formulated into ovalbumin-loaded polymeric NPs using double emulsion-solvent evaporation method and assessed for cellular uptake in Albino BL/6 mice using fluorescence spectroscopy (Rahimian *et al.*, 2015).

In this chapter, glycerol will be modified to possess a pendant alkyne group and enzymatically polymerised with divinyl adipate (DVA) and ω -pentadecalactone (PDL) to produce an alkynal functionalised PGA-co-PDL. Subsequently, click chemistry will be used to attach a fluorescent azide to the modified PGA-co-PDL.

4.2. Aims and Objectives

The aim of this study was to design and synthesise functionalised PGA-co-PDL to enable the attachment of fluorescent ligands for the fluorescent detection of NPs within cells.

The main objectives were to:

- a. Evaluate the feasibility for using click chemistry for polymer modification.
- b. Synthesise a modified glycerol containing an alkyne group.
- c. Polymerisation of alkyne-glycerol containing PGA-co-PDL.
- d. Attach a fluorescent azide to the polymer backbone alkyne groups.

4.3. Materials and Methods

4.3.1. Materials

Polymer synthesis: Same as in chapter 2.

Synthesis of modified glycerol (2-(prop-2-yn-1-yloxy)propane-1,3-diol):

Benzaldehyde, n-hexane, and p-toluenesulfonic acid monohydrate (PTSA) were bought from Acros Organics (Fisher Scientific, UK.). Glycerol, 2-Phenyl-1,3-dioxan-5-ol, N,N-Diisopropylethylamine (DIPEA), Glacial acetic acid (AcOH) and sodium hydride (NaH) were purchased from Sigma-Aldrich. Diethyl ether (HPLC grade) and Toluene (HPLC grade) were purchased from Fisher Scientific, UK. Propargyl bromide was obtained from Alfa Aesar (Thermo Fisher Scientific, UK). All chemicals were used as received unless otherwise indicated.

Instruments: FT-IR spectra were obtained using Agilent Technologies MicroLab FTIR software running on an Agilent Technologies Cary 630 FTIR Spectrometer-IR spectrometer (Agilent, USA). The spectra were collected from 650-4000 cm^{-1} at a resolution of 4 cm^{-1} . NMR analyses were performed using either a Bruker 300 MHz (operating at 300.18 MHz for ^1H and 75.48 MHz for ^{13}C) or a Bruker 600 MHz (operating at 600.31 MHz for ^1H , 150.95 MHz for ^{13}C) NMR spectrometers. Coupling constants (J) are reported in Hertz (Hz) and significant multiplicities are described by singlet (s), doublet (d), triplet (t), quartet (q), doublet of doublets (dd), or multiplet (m). Mass spectra were acquired on a Water's LCT Micromass LCT mass spectrometer equipped with an electrospray ionisation (ESI) source and time of flight (ToF) detector (Water's, US). Analyses were carried out on sample solutions in methanol (1

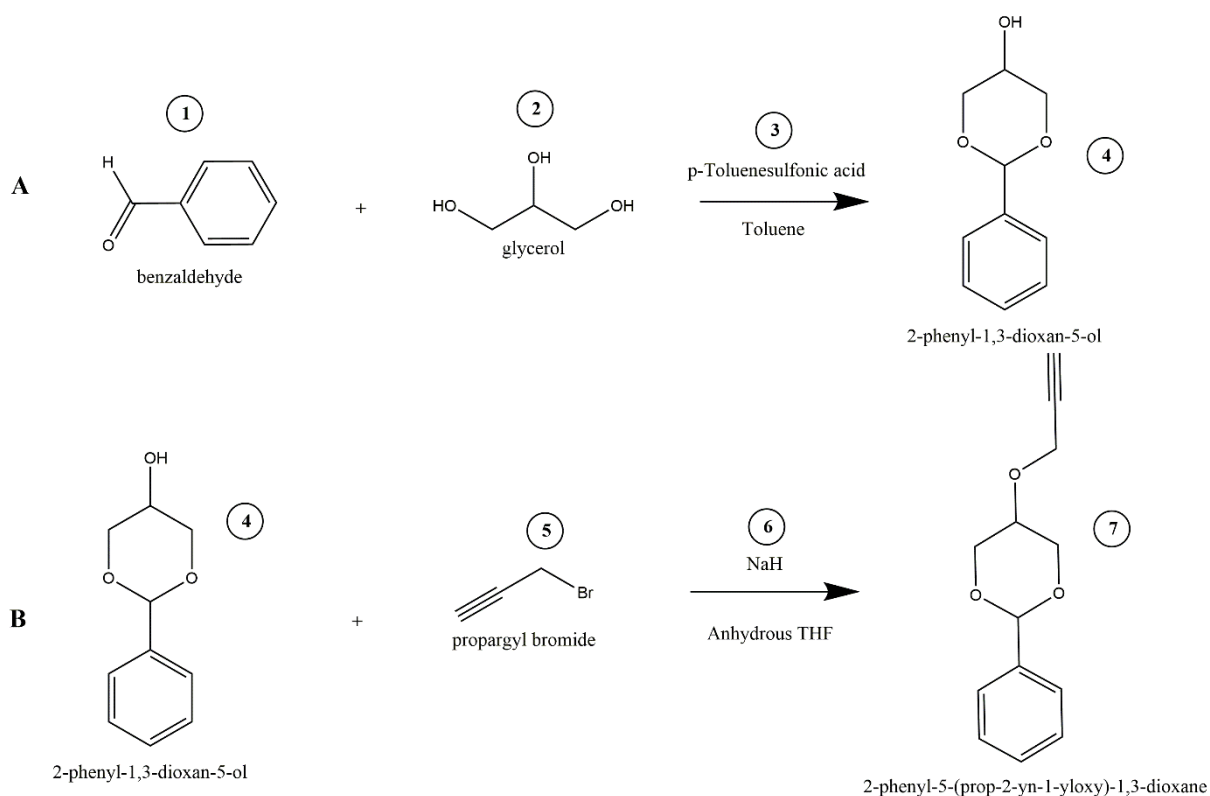
ppb). GPC analysis was performed as in chapter 2, section 2.3.2.2.1. Molecular weights of polymers were ascertained from a standard curve ($R^2=0.9891$).

4.3.2. Methods

4.3.2.1. *Synthesis of glycerol (2-(prop-2-yn-1-yloxy)propane-1,3-diol)*

4.3.2.1.1. Stage 1: synthesis of 2-phenyl-[1,3]-dioxan-5-ol

A 500 mL round bottom flask was charged with benzaldehyde (9 g, 84.81 mmol), glycerol (9 g, 97.73 mmol), PTSA (60 mg, 3.15 mmol), and toluene (300 mL). This flask was placed onto a heating mantle on a hot plate stirrer at 125 °C equipped with a Dean-Stark apparatus for the removal of water produced during the reaction. This reaction was allowed to run to completion (i.e., when no water was collected in the Dean-Stark). (**Scheme 4-1A**). The resulting product (2-phenyl-[1,3]-dioxan-5-ol) was purified using column chromatography (n-hexane:diethyl ether 3:7) and then analysed using NMR.



Scheme 4-1 Synthesis of (A) 2-phenyl-[1,3]-dioxan-5-ol and (B) 2-phenyl-5-(prop-2-yn-1-yloxy)-1,3-dioxane

4.3.2.1.2. Stage 2: synthesis of 2-phenyl-5-(prop-2-yn-1-yloxy)-1,3-dioxane

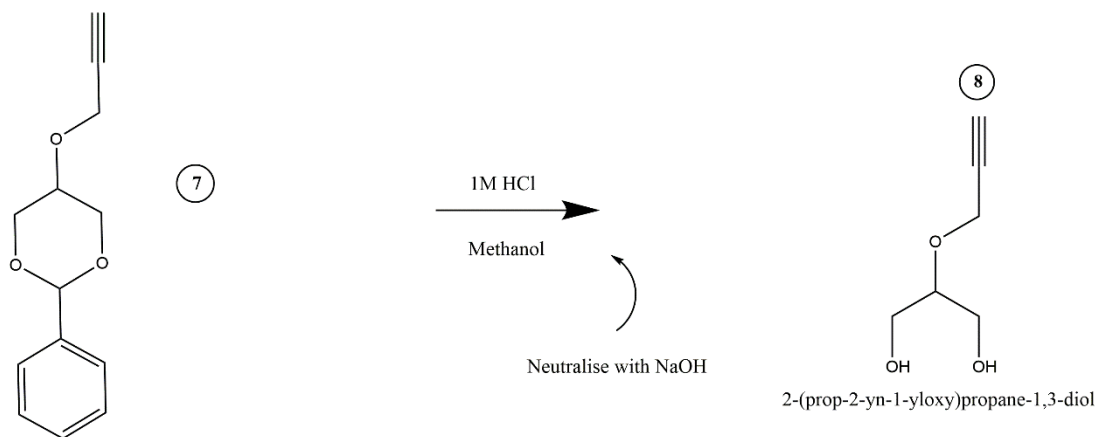
A 250 mL round bottom flask was charged with 60% w/w sodium hydride in mineral oil (0.18 g, 4.44 mmol) and anhydrous THF (40 mL) and stirred vigorously at 0 °C under nitrogen. 2-phenyl-[1,3]dioxan-5-ol (0.40 g, 2.22 mmol) was added to this mixture and allowed to react for 30 minutes (**Scheme 4-1B**). Then an 80% w/w solution of propargyl bromide in toluene (0.42 mL, 4.44 mmol) was added dropwise and the progress of the reaction was monitored by thin layer chromatography (TLC; n-hexane:diethyl ether 1:1).

After 24 hours, the suspension was then filtered using Buchner filtration with one layer of filter paper (Whatman GF/A). The filtrate was then transferred to a 100 mL round-bottom flask with DCM (30 mL) and the solution was

concentrated via rotary evaporation at 40 °C @ 120 rpm (Laborota 4000, Heidolph Instruments attached to a Divac pump). The concentrated product was dissolved in n-hexane (3 mL) and the solution was warmed in a water bath (70 °C). Diethyl ether was added dropwise until the product was completely dissolved. The solution was allowed to cool inside the fume cupboard and the crystals formed as the solution underwent cooling. The desired product was obtained as a white crystalline solid, which was washed with cold n-hexane.

4.3.2.1.3. Stage 3: synthesis of 2-(prop-2-yn-1-yloxy)propane-1,3-diol

A 50 mL round bottom flask was charged with 2-phenyl-5-(prop-2-yn-1-yloxy)-1,3-dioxane (0.46 g, 2.06 mmol), methanol (10 mL) and 1 M aqueous hydrochloric acid (10 mL) and stirred vigorously (500 rpm) while being allowed to react at room temperature for 2 hours. Then 1 M aqueous sodium hydroxide was added dropwise until the reaction mixture resulted neutral to litmus paper. (**Scheme 4-2**). The resulting solution was extracted with n-hexane in a separating funnel. The organic layer was concentrated via rotary evaporation at 40 °C @ 120 rpm. The solid residue was taken in chloroform and the resulting suspension was filtered through cotton wool to remove the excess sodium chloride salt. The solvent was evaporated at reduced pressure and the resulting solid was used without further purification.



2-phenyl-5-(prop-2-yn-1-yloxy)-1,3-dioxane

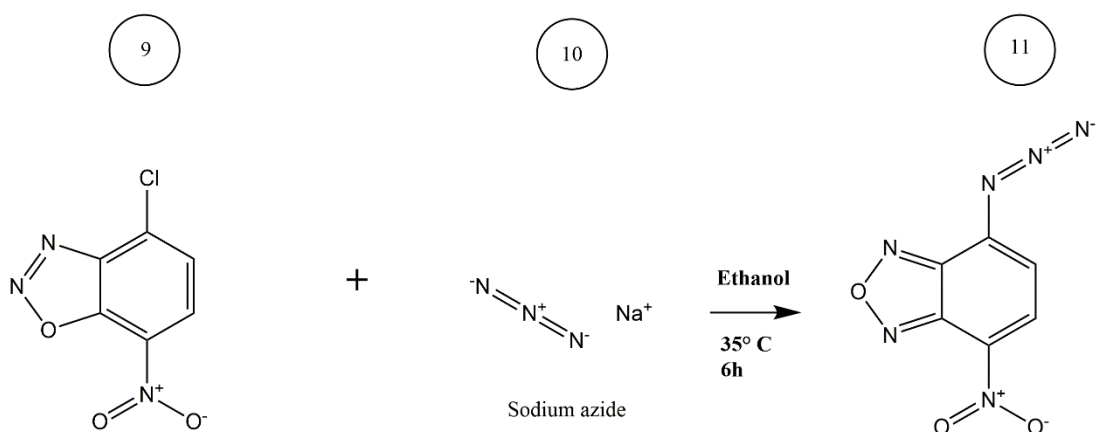
Scheme 4-2 Synthesis of 2-(prop-2-yn-1-yloxy)propane-1,3-diol

4.3.2.2. Synthesis of NBD azide

4-Azido-7-nitro-2,1,3-benzoxadiazole (NBD-azide) was obtained according to the method described by Lord et al. (**Scheme 4-3**) (Lord *et al.*, 2010).

A 50 mL round bottom flask containing a stirring bar was charged with NBD chloride (1.50 g, 7.52 mmol), sodium azide (0.54 g, 8.30 mmol), and ethanol (15 mL). The mixture was left stirring at 35° C for 6 hours. After 6 hours, the solution was poured into ice water, forming a precipitate. The precipitate was

filtered using Buchner filtration and washed with distilled water. The resulting product and starting materials were analysed via NMR and FT-IR.



4-Chloro-7-nitro-1,2,3-benzoxadiazole

4-Azido-7-nitro-2,1,3-benzoxadiazole

Scheme 4-3 Synthesis of 4-Azido-7-nitro-2,1,3-benzoxadiazole (NBD-azide)

4.3.2.3. *Polymer synthesis*

To determine if 2-(prop-2-yn-1-yloxy)propane-1,3-diol could be incorporated into the PGA-co-PDL polymer, a series of PGA-co-PDL polymers were synthesised at 1.25 mmol scale using various ratios of 2-(prop-2-yn-1-yloxy)propane-1,3-diol and glycerol (**Table 4-1**). For convenience, PGA-co-PDL synthesised with 2-(prop-2-yn-1-yloxy)propane-1,3-diol and glycerol will be called alkyne-PGA-co-PDL.

Table 4-1 Ratios of glycerol or 2-(prop-2-yn-1-yloxy)propane-1,3-diol integrated into various polymers

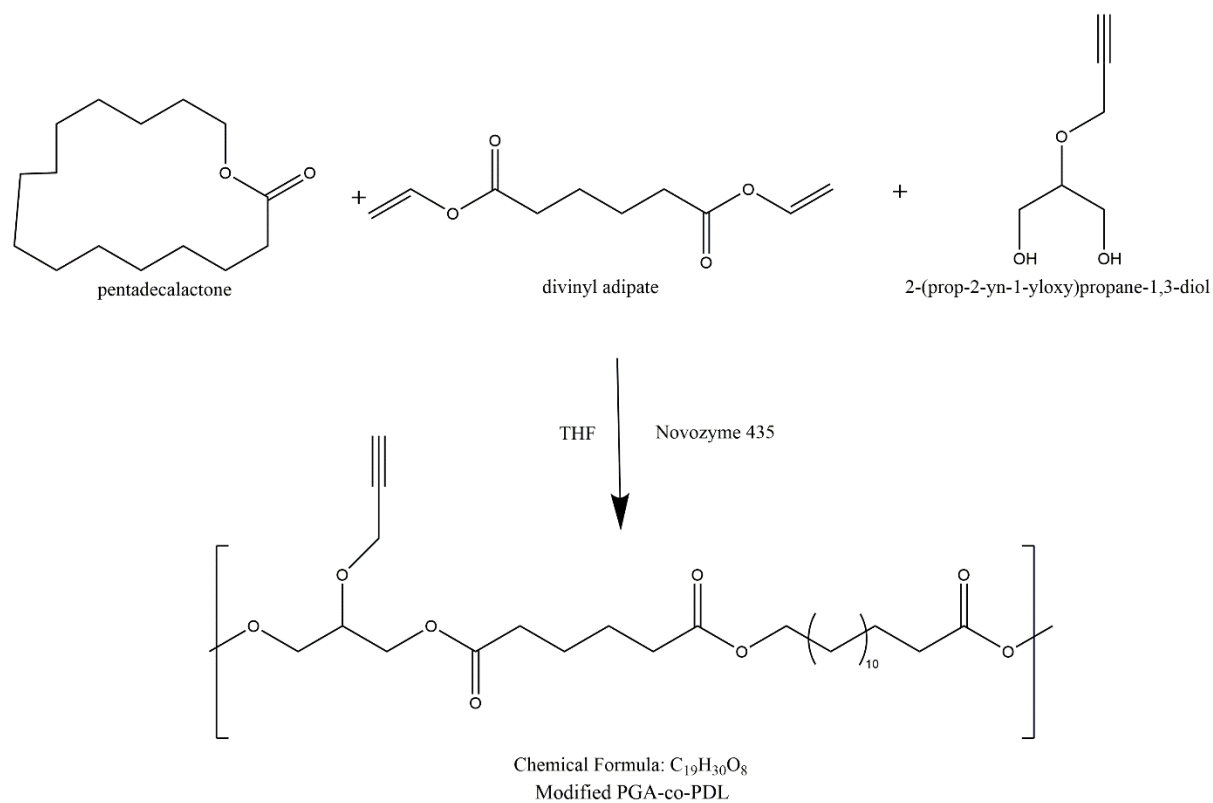
1.25 mmol Polymer	ratio	
	2-(prop-2-yn-1-yloxy)propane-1,3-diol	Glycerol
PGA-co-PDL	0	100
Alkyne-PGA-co-PDL	100	0
50% alkyne-PGA-co-PDL	50	50
10% alkyne-PGA-co-PDL	10	90

4.3.2.3.1. PGA-co-PDL

The 1.25 mmol scale PGA-co-PDL polymer was synthesised as previously described (Chapter 2, section 2.3.2.1.) but on a 1.25 mmol scale using PDL (1.25 mmol; 0.30 g), DVA (1.25 mmol; 0.247), glycerol (1.25 μ mol; 0.115 g) THF (15 mL) and lipase acrylic resin enzyme (0.85 mg; Sigma Aldrich, UK) was added to the mixture.

4.3.2.3.2. Alkyne-PGA-co-PDL

The Alkyne-PGA-co-PDL polymer was synthesised as above but replacing the glycerol with 2-(prop-2-yn-1-yloxy)propane-1,3-diol (1.25 μ mol; 0.16 g) (**Scheme 4-4**).



Scheme 4-4 Synthesis of alkyne-PGA-co-PDL

4.3.2.3.3. 50 % alkyne-PGA-co-PDL

The 50% alkyne-PGA-co-PDL polymer was synthesised as in 4.3.2.3.1., but with both the glycerol (0.625 μ mol; 0.058 g) and 2-(prop-2-yn-1-yloxy)propane-1,3-diol (0.625 μ mol; 0.081 g).

4.3.2.3.4. 10 % alkyne-PGA-co-PDL

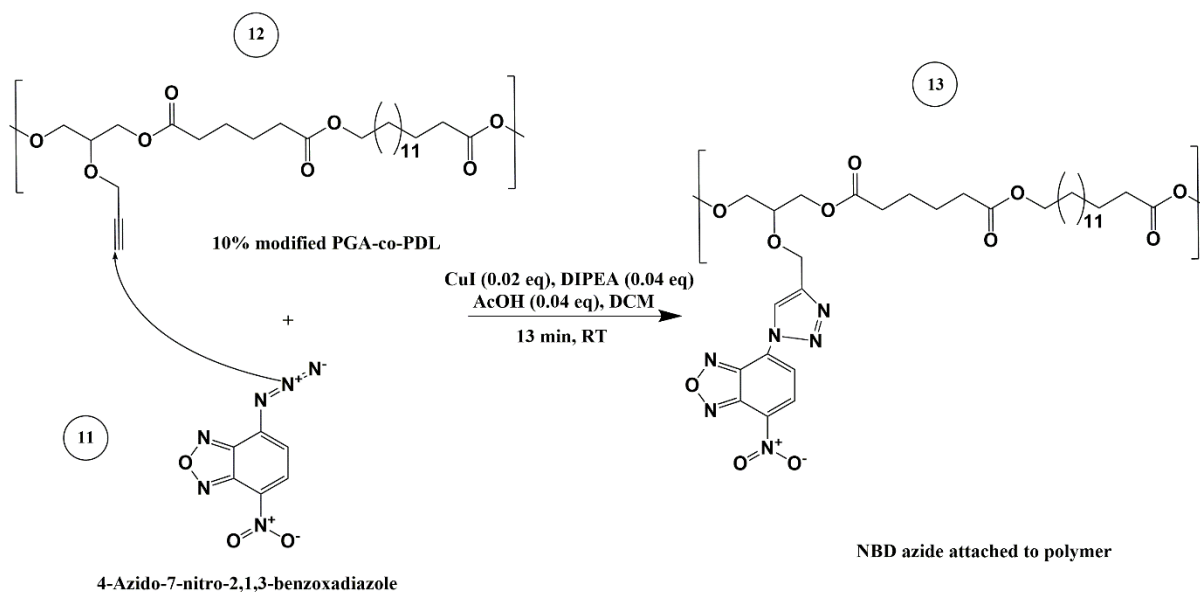
The 10% alkyne-PGA-co-PDL polymer was synthesised as in 4.3.2.3.1., but with both the glycerol (1.125 μ mol; 0.104 g) and 2-(prop-2-yn-1-yloxy)propane-1,3-diol (0.125 μ mol; 0.016 g).

4.3.2.4. Metal catalysed azide-alkyne 'click' reaction

4.3.2.4.1. NBD azide reacted with 10 % alkyne-PGA-co-PDL

The 'click' reaction between sodium azide and 10 % alkyne-PGA-co-PDL was carried out according to the procedure described by Shao et al., with some modifications (**Scheme 4-5**) (Shao *et al.*, 2011).

A 50 mL round bottom flask containing a stirring bar was charged with copper iodide (3.80 mg, 0.02 mmol), DIPEA (6.97 mL, 0.04 mmol), and AcOH (2.29 mL, 0.04 mmol) in DCM (2 mL). Then, the 10% alkyne-PGA-co-PDL (2.56 mg, 1.00 mmol) and NBD azide (0.22 mg, 1.05 mmol) were added to the mixture at room temperature. The resulting mixture was allowed to react for 13 minutes. Then, the reaction mixture was first washed with 1% aqueous hydrochloric acid and then with deionised H₂O. The organic phase was dried using magnesium sulphate. The resulting product was then dissolved in DCM (2 mL) and placed in a Falcon 15 mL conical centrifuge tube (Fisher Scientific, UK) together with methanol (12 mL) to help with precipitation of the polymer. The solution was centrifuged using a Hermle Z400 centrifuge (Hermle LaborTechnik, Germany) at 5000 rpm for 10 minutes. The resulting NPs were dispersed in DCM (2 mL) and methanol added to a fresh Falcon 15 mL conical centrifuge tube and the centrifugation repeated. The resulting NPs were dispersed and centrifuged a third time. The resulting NPs after 3 washes were analysed via NMR and FT-IR.



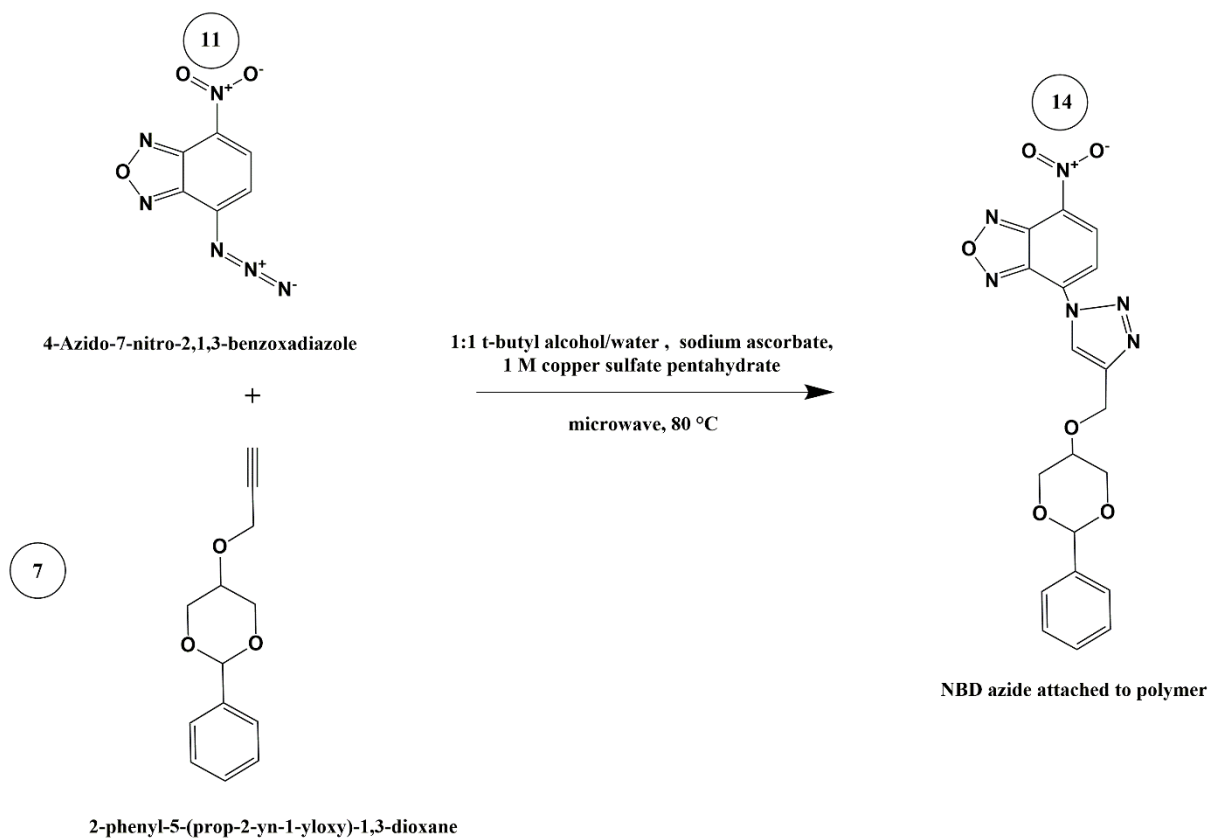
Scheme 4-5 CuAAC reaction of NBD azide with 10 % alkyne-PGA-co-PDL

4.3.2.4.2. NBD azide reacted with 2-phenyl-5-(prop-2-yn-1-yloxy)-1,3-dioxane

The microwave ‘click’ reaction between NBD azide and 2-phenyl-5-(prop-2-yn-1-yloxy)-1,3-dioxane was adopted from the literature (**Scheme 4-6**) (Trujillo *et al.*, 2019).

A 35 mL microwave vessel containing a stirring bar was charged with NBD azide (0.043 g, 0.21 mmol), 1:1 t-butyl alcohol/water (2 mL), 2-phenyl-5-(prop-2-yn-1-yloxy)-1,3-dioxane (0.046 g, 0.21 mmol), 1 M copper sulphate pentahydrate (10 μ L), and sodium ascorbate (2.5 mg) were added. The vessel was capped and heated in the CEM Discover SP microwave instrument (CEM, UK). The vessel was heated to 80 $^{\circ}$ C and held at that temperature for 10 minutes. The vessel was vented and cooled to about 50 $^{\circ}$ C. The cap was removed from the vessel and it was further cooled by the addition of ice water (2 mL). Then, 10% aqueous ammonia (5 mL) was added to the vessel and it

was stirred for 5 minutes. The reaction mixture was washed with a solution of ethyl acetate (3 × 10 mL). The organic phase was dried using magnesium sulphate and the solvent was evaporated under reduced pressure. The resulting product was analysed via NMR and FT-IR.



Scheme 4-6 CuAAC reaction of NBD azide with 2-phenyl-5-(prop-2-yn-1-yloxy)-1,3-dioxane

4.3.3. Results

4.3.3.1. Synthesis of modified glycerol

4.3.3.1.1. Stage 1: synthesis of 2-phenyl-[1,3]-dioxan-5-ol

The synthesis of 2-phenyl-[1,3]-dioxan-5-ol (**4**) resulted in the formation of a fluffy white powder. The mass of 2-phenyl-[1,3]dioxan-5-ol obtained was 3.089 g (20 % yield). ESI-MS, calculated for $C_{10}H_{12}O_3$ - m/z 180.2, found - m/z 203.1 ($M + Na^+$). FT-IR ν max: 3267.0, 3091.8, 3065.7, 2970.6, 2864.4, 1494.6, 1451.7, 1384.7, 1077.2 cm^{-1} . 1H NMR (300 MHz, $CDCl_3$) δ 7.53 – 7.47 (m, 2H, H-e,i), 7.42 – 7.35 (m, 3H, H-f,g,h), 5.56 (s, 1H, H-b), 4.23 – 4.09 (m, 4H, H-a,a'), 3.64 (d, 1H, H-c), 3.03 (d, 1H, H-d) (**Figure 4-1**). ^{13}C NMR (75 MHz, $CDCl_3$) δ 137.9, 129.1, 128.3, 125.9, 101.7, 72.3, 64.0.

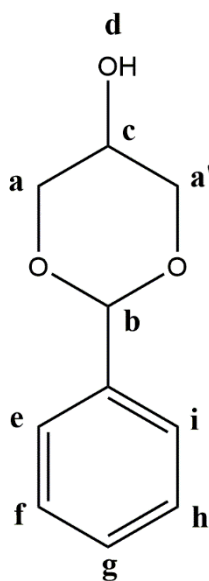


Figure 4-1 Structure of 2-phenyl-[1,3]-dioxan-5-ol with protons labelled for NMR

4.3.3.1.2. Stage 2: synthesis of 2-phenyl-5-(prop-2-yn-1-yloxy)-1,3-dioxane

The synthesis of 2-phenyl-5-(prop-2-yn-1-yloxy)-1,3-dioxane (**7**) resulted in a similar white powder as 2-phenyl-[1,3]-dioxan-5-ol. Yield from the production of 2-phenyl-5-(prop-2-yn-1-yloxy)-1,3-dioxane was found to be 0.363 g (75 %). ESI-MS, calculated for $C_{10}H_{14}O_3$ - m/z 218.25, found - m/z 241.1 ($M + Na^+$). FT-IR ν max: 3293.1, 3035.9, 2976.2, 2952.0, 2918.5, 2853.2, 2113.4, 1384.7, 1343.7, 1321.3, 1282.2 cm^{-1} . 1H NMR (600 MHz, $CDCl_3$) δ 7.50 (dd, 2H, H-e,i), 7.37 – 7.30 (m, 3H, H-f,g,h), 5.56 (s, 1H, H-b), 4.36 (dd, 4H, a,a'), 4.08 (dd, 2H, H-j), 3.64 (p, 1H, H-c), 2.43 (t, 1H, H-k) (**Figure 4-2**). ^{13}C NMR (75 MHz, $CDCl_3$) δ 138.0, 128.9, 128.2, 126.1, 101.4, 79.4, 74.9 68.8, 68.7, 55.6.

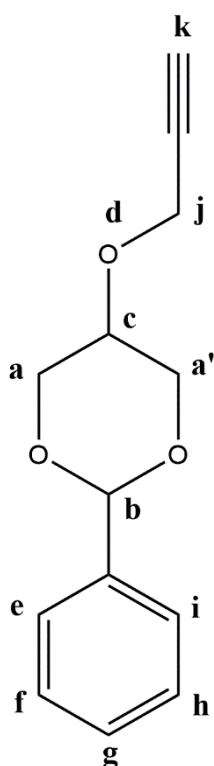


Figure 4-2 Structure of 2-phenyl-5-(prop-2-yn-1-yloxy)-1,3-dioxane with protons labelled for NMR

4.3.3.1.3. Stage 3: synthesis of 2-(prop-2-yn-1-yloxy)propane-1,3-diol

The synthesis of 2-(prop-2-yn-1-yloxy)propane-1,3-diol (**8**) produced a viscous liquid similar in colour to glycerol. Yield from the production of 2-(prop-2-yn-1-yloxy)propane-1,3-diol was found to be 0.176 g instead of the theoretical 0.268 g. The reaction thus gave a yield of 66 %. ESI-MS, calculated for $C_6H_{10}O_3$ - m/z 130.14, found - m/z 153.08 ($M + Na^+$). FT-IR ν max: 3360.1, 3281.9, 2922.2, 2115.2, 1636.3, 1446.2, 1397.7, 1345.5, 1099.5 cm^{-1} . 1H NMR (300 MHz, $CDCl_3$) δ 4.24 (d, 2H, H-j), 3.86 (s, 2H, H-l,m), 3.73 – 3.54 (m, 5H, H-a,a',c), 2.52 (t, 1H, H-k) (**Figure 4-3**). ^{13}C NMR (75 MHz, $CDCl_3$) δ 79.9, 79.3, 74.9, 61.9, 57.3.

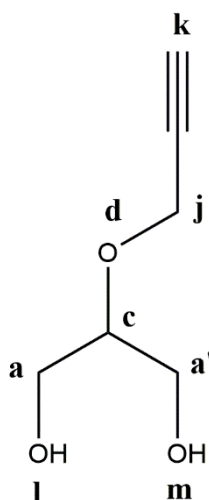


Figure 4-3 Structure of 2-(prop-2-yn-1-yloxy)propane-1,3-diol with protons labelled for NMR

4.3.3.2. Synthesis of NBD azide

The synthesis of NBD azide (**11**) resulted in the formation a yellow powder. Yield from the production of NBD azide was 1.36 g instead of the theoretical 1.54 g. The reaction thus gave a yield of 88 %. FT-IR ν max: 2111.5 cm^{-1} (N_3). ^1H NMR (300 MHz, CDCl_3) δ 8.51 (d, $J = 6.1$ Hz, 1H), 7.09 (d, 1H) ^{13}C NMR (75 MHz, CDCl_3) δ 143.6, 138.1, 132.1, 114.9.

4.3.3.3. Polymer synthesis

4.3.3.3.1. PGA-co-PDL

The PGA-co-PDL synthesis resulted in a white, flaky powder, that was too low in yield to quantify, monomer composition calculated (1:1:1). Mw: 2.2 KDa. FT-IR ν max: 3432.9, 2915.3, 2847.8, 1729.5, 1463.2, 1463.2, 1365.9, 1160.8, 1040.0, 719.9 cm^{-1} . ^1H NMR (300 MHz, CDCl_3) δ 4.25 – 3.98 (m, 4H, H-a,c), 3.77 – 3.54 (m, 1H, H-i), 2.45 – 2.21 (m, 5H, H-d,d',i), 1.77 – 1.52 (m, 7H, H-e,e',h), 1.27 (d, 22H, H-g) (**Figure 4-4**).

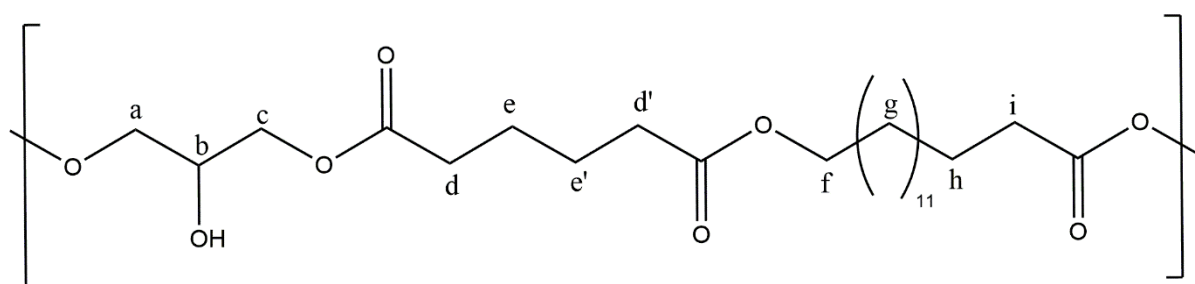


Figure 4-4 Structure of 1.25 mmol PGA-co-PDL with protons labelled for NMR

4.3.3.3.2. alkyne-PGA-co-PDL

The alkyne-PGA-co-PDL synthesis resulted in a viscous liquid that did not solidify upon drying, monomer composition calculated (1:1:1). Mw: 2.5 KDa. FT-IR ν max: 3267.0, 2915.3, 2847.8, 1729.5, 1463.2, 1463.2, 1365.9, 1160.8, 1040.0, 719.9 cm^{-1} . ^1H NMR (300 MHz, CDCl_3) δ 4.34 – 3.92 (m, 7H), 2.54 – 2.26 (m, 7H), 1.77 – 1.54 (m, 8H), 1.32 (s, 26H) (**Figure 4-5**).

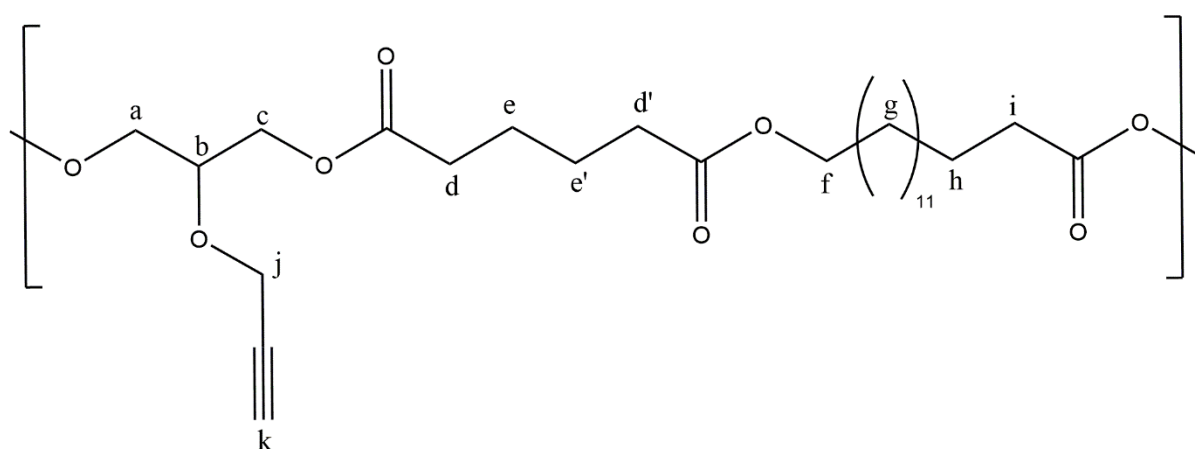


Figure 4-5 Structure of 1.25 mmol alkyne-PGA-co-PDL with protons labelled for NMR

4.3.3.3.3. 50 % alkyne-PGA-co-PDL

The 50% alkyne-PGA-co-PDL synthesis resulted in a white crystallised powder, but too low to quantify, monomer composition calculated (1:1:1). FT-IR ν max: 3425.4, 3265.2, 2916.6, 2849.6, 2115.3, 1729.5, 1462.9, 1416.4, 1395.9, 1366.1, 1334.4, 1162.9, 1047.4, 721.2 cm^{-1} . ^1H NMR (300 MHz, CDCl_3) δ 4.39 – 3.95 (m, 8H), 3.88 – 3.56 (m, 2H), 2.43 – 2.24 (m, 8H), 1.74 – 1.54 (m, 8H), 1.27 (d, $J = 5.5$ Hz, 22H).

4.3.3.3.4. 10 % alkyne-PGA-co-PDL

The 10% alkyne-PGA-co-PDL synthesis resulted in a white crystallised powder, but too low to quantify, monomer composition calculated (1:1:1). FT-IR ν max: 3393.7, 2916.6, 2849.6, 1729.5, 1462.9, 1194.6, 721.3. ^1H NMR (300 MHz, CDCl_3) δ 4.34 – 3.98 (m), 3.80 – 3.55 (m), 2.45 – 2.22 (m), 1.76 – 1.51 (m), 1.45 – 1.16 (m).

4.3.4. Discussion

The aim of this study was to functionalise PGA-co-PDL with a fluorescent ligand, in order to visual the uptake of the NPs synthesised from the polymer. Ligands can either be attached to the polymer surface before NP formation or afterwards onto the surface of the nanoparticle (Nicolas *et al.*, 2013) The enzyme, Lipase B, that is used for the polymerisation of glycerol is regiospecific to primary hydroxyl groups and hence, PGA-co-PDL contains a free secondary hydroxyl group, which can be exploited to facilitate functionality (You *et al.*, 2010; Jan *et al.*, 2013).

Thompson *et al.*, conjugated the free carboxyl group of ibuprofen to the free hydroxyl group of PGA-co-PDL (Thompson *et al.*, 2008). The microparticles synthesised from the ibuprofen-conjugated PGA-co-PDL showed a reduced burst release and slower release rate compared to microspheres containing unconjugated ibuprofen (Thompson *et al.*, 2009). One drawback was storage in a humid environment resulted in the hydrolysis of the ester linkages of the conjugated material, leading to an increase in burst release (Thompson *et al.*, 2009). Click chemistry offers a modular approach allowing for stable binding

with various moieties (Hein, Liu and Wang, 2008; Juríček *et al.*, 2009). A polymer or nanoparticle presenting an azide or alkyne on the surface will be able to undergo copper-catalysed azide–alkyne cycloaddition (CuAAC) reaction with various ligands (Binder, 2019; Voigt *et al.*, 2019). Glycerol has been shown to possess diverse chemistry allowing for azide functionalisation (Zhang and Grinstaff, 2014; Gładysz, Ruszkowski and Milecki, 2018)

The azide functionalisation of glycerol was achieved in a three-step process (**Scheme 4-1 and Scheme 4-2**). Protection of both primary hydroxyl groups was achieved by reaction with benzaldehyde and production of cyclic acetal (Vrbková, Dračínský and Holý, 2007). As in previous studies, both the 5 and 6-membered ring products were generated, but compound **4** was isolated using column chromatography (**Scheme 4-1**) (Wang, Hawley and DeAthos, 2003; Gładysz, Ruszkowski and Milecki, 2018). The FT-IR spectrum of compound **4** showed an O-H trough between 3400-3200 cm^{-1} due to the presence of the terminal alcohol. It also showed a C-H stretches for the bonds in the benzene ring (3075-3030 cm^{-1}) and the C-H bonds located in the cyclohexane attached to the aromatics (2985-2860 cm^{-1}). There was also evidence of C-C stretching in the ring (1400-1500 cm^{-1}). The low yield (20 %) was comparable to that reported previously (Gładysz, Ruszkowski and Milecki, 2018). Due to the low yield obtained, 2-phenyl-[1,3]-dioxan-5-ol was purchased and used for all subsequent reactions.

The following step saw the introduction of the alkyne group in the form of propargyl bromide reacted onto the unprotected hydroxyl group, resulting in compound **7** with a good yield of 75% (**Scheme 4-1**). This is slightly lower than previous reports of 82% yield (Cattiaux *et al.*, 2018). However, it should be

noted that the work up for the 82% yield differed as it was purified via column chromatography and not crystallisation as employed in this study. The FT-IR spectrum of compound **7** showed the O-H trough between 3400-3200 cm^{-1} notably absent. Instead there was the C-H stretch at 3295 cm^{-1} corresponding to the terminal alkyne. There was also another peak corresponding to the $\text{-C}\equiv\text{C-}$ stretch. The rest of the peaks C-H aromatic (3100- 3030 cm^{-1}), C-H alkyl bonds (2990-2840 cm^{-1}) and C-C stretching in the ring (1400-1500 cm^{-1}) were all similar to the FT-IR spectrum of compound **4**.

The next step was to cleave the benzylidene acetal protective group, to allow further functionalisation of the hydroxyl group (**Scheme 4-2**). The two-step process for deprotection involved using hydrochloric acid and methanol to obtain the desired compound **9**, consistent with literature (Gładysz, Ruszkowski and Milecki, 2018). The reaction gave a yield of 66%, which is similar to the yield of 67% reported in literature (Cattiaux *et al.*, 2018). The FT-IR of compound **8** showed the notable return of the O-H trough (3500-3322 cm^{-1}), but this time it corresponds with the two terminal OH bonds. There was also the alkyne-C-H stretch (3289 cm^{-1}) attached to the O-H trough and a notable absence of the C-H peaks corresponding to the C-H bonds in the aromatic ring. This showed the removal of the aromatic ring. There was also the retainment of the C-H stretch (2950-2850 cm^{-1}) corresponding to the C-H bonds located on the opened cyclohexane and the $\text{-C}\equiv\text{C-}$ stretch (2113 cm^{-1}).

(**Figure 4-6a**) and 1.25 mmol alkyne-PGA-co-PDL (**Figure 4-7a**) with regards to the absence of the OH trough (absence of glycerol) and presence of a weak peak at 3267 cm^{-1} corresponding to the alkyne C-H stretch which suggests that the alkyne group is present instead of the glycerol as in the case of the normal PGA-co-PDL. There is a gradual re-emergence of the OH trough and disappearance of the alkyne C-H stretch as the concentration of glycerol increased in respect to compound **8** for the 100%, 50%, and 10% alkyne-PGA-co-PDL (**Figure 4-7a-c**). This is logical since there will be a gradual increase in the concentration of glycerol in the polymers.

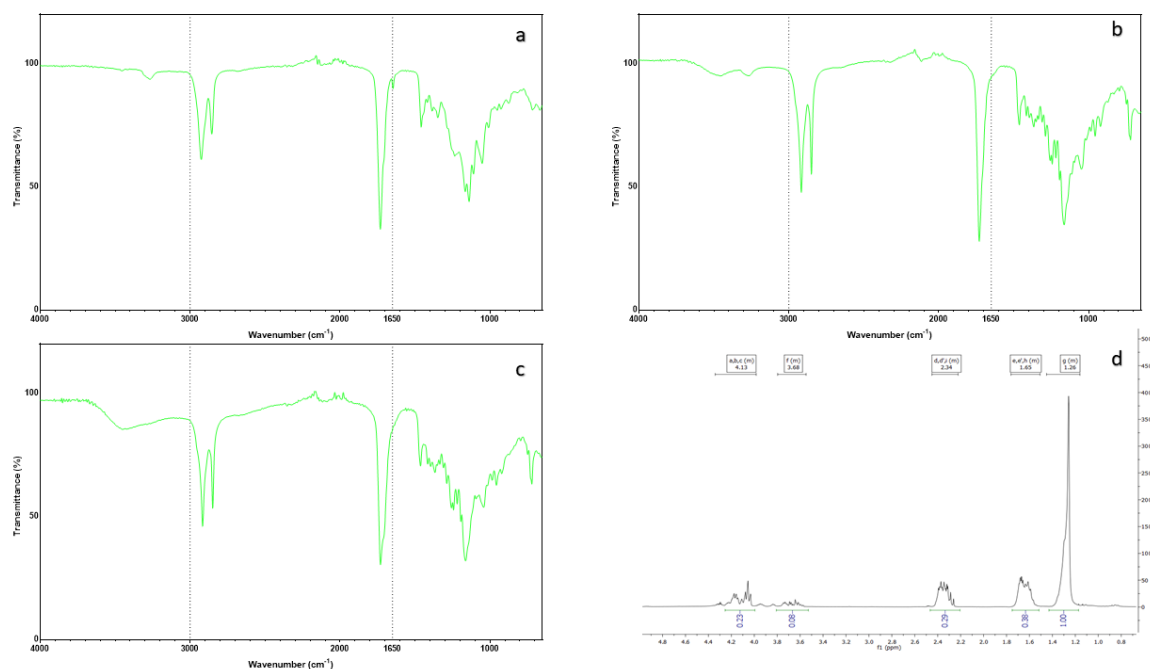


Figure 4-7 FT-IR of (a) alkyne-PGA-co-PDL, (b) 50 % alkyne-PGA-co-PDL and (c) 10 % alkyne-PGA-co-PDL showing the gradual re-emergence of the hydroxyl trough and (d) ¹H-NMR of 10 % alkyne-PGA-co-PDL

Compound **11**, NBD azide, was produced by the reaction of compound **9** and **10**, with a yield of 88% (**Scheme 4-4**). This yield is slightly lower than the 94% reported in literature (Lord *et al.*, 2010). Nitrobenzoxadiazole (NBD) fluorophores, such as NDB azide, have become useful as small molecule labels used in chemical biology and bioanalytical studies (Key and Cairo, 2011). NDB azide can be photoactivated allowing the visualisation of particles conjugated to it (Tobimatsu *et al.*, 2014). The good photostability and photoconversion efficiency of NBD azide facilitates long term fluorescence observation that may otherwise lead to photobleaching (Lord *et al.*, 2010; Minoshima and Kikuchi, 2017). The FT-IR of NBD azide showed a distinctive peak at 2111.5 cm^{-1} (**Figure 4-8a**).

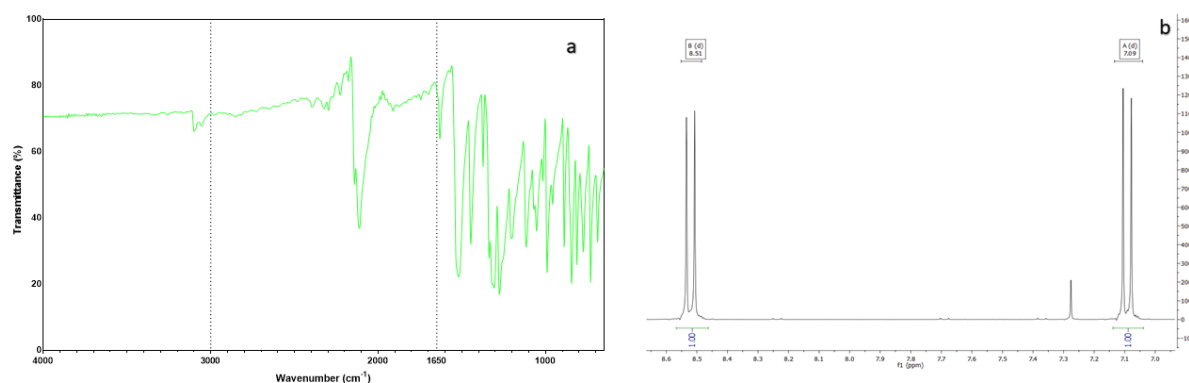


Figure 4-8 (a) FT-IR and (b) ¹H-NMR of NDB azide

The NBD azide and the 10 % alkyne-PGA-co-PDL were reacted via a CuAAC reaction (**Scheme 4-5**). The reaction consists of a three-step catalytic cycle, namely the formation of Cu (I) acetylide, cycloaddition, and protonation of C-Cu bond (Shao *et al.*, 2011). The FT-IR of the reaction product did not have the characteristic peak at 2111.5 cm^{-1} associated with the NBD azide (**Figure 4-9a**). This could be due to the low percentage (10%) of alkyne available to

bind with NBD azide, which could lead to a low signal to noise ratio for such a small molecule in a big polymer. However, the $^1\text{H-NMR}$ did not show peaks at 7.6 ppm and 8.2 ppm, associated with the binding of NBD azide (**Figure 4-9b**). Together this suggests that the NBD azide did not successfully bind to the polymer. There is concern regarding conjugation onto high molecular weight polymers, due to reduced accessibility to reactive sites stemming from higher viscosity and potential folding of larger polymers (Pickens *et al.*, 2018). Suggested solutions include, adding denaturing agents such as DMSO, diluting reaction mixtures, or raising temperature and increasing reaction times (Pickens *et al.*, 2018).

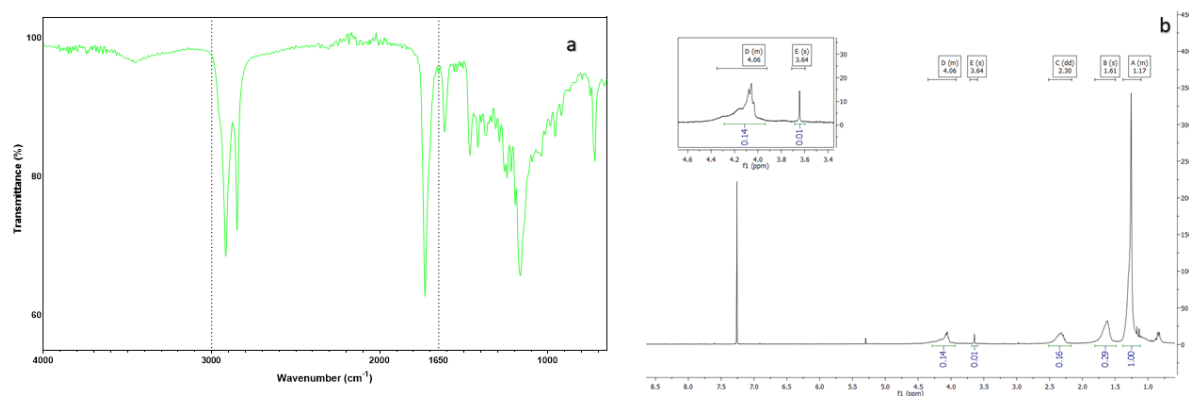


Figure 4-9 (a) FT-IR and (b) $^1\text{H-NMR}$ spectra of the CuAAC reaction between NBD azide and 10 % alkyne-PGA-co-PDL

It was then decided to attach the NDB azide to compound **7** using a microwave method CuAAC reaction (**Scheme 4-6**) (Trujillo *et al.*, 2019). The NMR of the crude product was similar to the NMR of the original compound **7** which indicates that the reaction was not successful (**Figure 4-10**). The low concentrations of the reactants are most likely the cause of the reactions not working (Presolski, Hong and Finn, 2011). It would be beneficial to scale-up

the production of compound **7** in order to have a higher concentration with which to run the reaction.

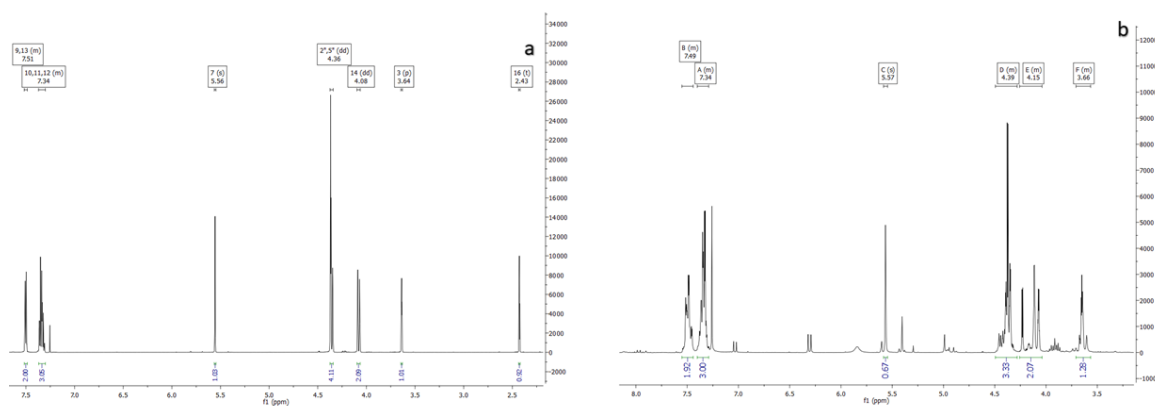


Figure 4-10 $^1\text{H-NMR}$ of (a) 2-phenyl-5-(prop-2-yn-1-yloxy)-1,3-dioxane and (b) CuAAC reaction between 2-phenyl-5-(prop-2-yn-1-yloxy)-1,3-dioxane and NBD azide

4.3.5. Conclusion

In summary, the three-step reactions to modify glycerol to contain an alkyne moiety was successful. This was the first time 2-(prop-2-yn-1-yloxy)propane-1,3-diol was used in the polymerisation of PGA-co-PDL. The polymerisation showed moderate success at integration of the modified glycerol (2-(prop-2-yn-1-yloxy)propane-1,3-diol) into the polymer. The study was, therefore, able to meet the objectives of modifying glycerol to contain an alkyne group and then using it to synthesise a polymer containing the alkyne group. However, for the click chemistry to be successful, a higher concentration of reactants such as 2-phenyl-5-(prop-2-yn-1-yloxy)-1,3-dioxane is needed. Thus, future studies need to scale up the production of these reactants.

5 CHAPTER 5: General discussion and future work

5.1. Overview

Lung cancer has grown from an obscure disease in the 19th century to the deadliest cancer today (Witschi, 2001; Cancer Research UK, 2019). Chemotherapy is the current first line therapy for advanced stages of lung cancer, but has numerous limitations and side effects (Corrie, 2011; Rubio-Gonzalez *et al.*, 2018). Several nanocarrier delivery systems have been developed to improve drug delivery to cancer cells in order to help overcome the limitations of systemic chemotherapy (Arora and Jaglan, 2016; Vittorio *et al.*, 2017). Nanocarriers, including polymeric nanoparticles (NPs) and microparticles (MPs), are currently being researched or on the market for cancer treatment (Luque-Michel *et al.*, 2017; Abdelaziz *et al.*, 2018). Phenolic compounds, such as resveratrol, caused apoptosis and decreased tumour growth in both *in vitro* and *in vivo* models; however, resveratrol suffers from bioavailability issues (Yin *et al.*, 2013; Huminiecki and Horbańczuk, 2018; Santos *et al.*, 2019). Nanocarriers can be utilised to encapsulate the resveratrol and help overcome the poor bioavailability (Davidov-Pardo and McClements, 2014; Singh and Pai, 2014). Pulmonary delivery for lung cancer permits non-invasive circumvention of first pass metabolism and local accumulation of the drug at the tumour site to reduce the potential of systemic toxicity (Youngren-Ortiz *et al.*, 2017). The size of the NPs (< 1µm) renders them incapable of depositing directly into the lungs since they are exhaled without settling. A solution to this is to incorporate the NPs into nanocomposite microparticles (NCMPs) using spray drying. The aim of this project was to formulate and characterise NCMPs of resveratrol-loaded PGA-co-PDL NPs as a treatment for lung cancer by dry powder pulmonary delivery.

5.1.1. Formulation of polymeric nanoparticles

Four different polymers were used to synthesise polymeric NPs. Poly(*D,L*-lactide-co-glycolide) (PLGA) and Poly(ethylene glycol) methyl ether-block-poly(lactide-co-glycolide) (mPEG-PLGA) were purchased from Sigma. Whereas the poly(glycerol adipate-co- ω -pentadecalactone) (PGA-co-PDL) and Poly(ethylene glycol methyl ether)-PGA-co-PDL (PGA-co-PDL-PEG₂₀₀₀) were synthesised via ring opening polymerisation and polycondensation according to methods described in literature (Namekawa, Uyama and Kobayashi, 2000; Thompson *et al.*, 2006).

Polymeric NPs can be used as a versatile drug delivery system; however, their drug loading, *in vivo* distribution, and cell uptake are largely influenced by their size (Hickey *et al.*, 2015; Huang and Zhang, 2018). Polymeric NPs between 100-200 nm are desirable since these particles are ideal for uptake and evasion of the alveolar macrophages and they show rapid penetration through the respiratory mucus (Dabbagh *et al.*, 2018; Wei *et al.*, 2018). Variations in NP size could negatively influence their biodistribution, leading to loss of therapeutic efficacy. Thus, it is important to control the size of the NPs during the manufacturing process (Huang and Zhang, 2018; Wei *et al.*, 2018).

In this study, a modified water-in-oil-in water ($w_1/o/w_2$) double emulsion evaporation method was used. This method was previously optimised to produce PGA-co-PDL NPs of 200 nm (Kunda, Alfagih, Dennison, Tawfeek, *et al.*, 2015). Although this method was optimised for PGA-co-PDL NPs, it was decided to use this method to formulate the other polymeric NPs as well. This was done to allow a more like-for-like comparison of particles. Therefore, it was surprising to discover that the PGA-co-PDL NPs were consistently > 205

nm, while the NPs of the other three polymers (PGA-co-PDL-PEG₂₀₀₀, PLGA, and PEG-PLGA) were all < 205 nm. Several parameters were shown to affect polymeric NPs made using the double emulsion solvent evaporation method, including molecular weight (MWt) of polymer, organic solvent volume, aqueous volume, internal aqueous concentration, sonication time, stirrer speed, and external aqueous concentration (Kunda, Alfagih, Dennison, Tawfeek, *et al.*, 2015). The MWt of the polymer was ranked as the third most important factor controlling particle size, with an increased MWt corresponding to an increase in particle size (Kunda, Alfagih, Dennison, Tawfeek, *et al.*, 2015). In this current study, all the parameters were the same, except for the MWt of the polymers. Some studies agree that an increased MWt of the polymer results in increases in the size of the corresponding NPs. The size of PLGA NPs increased when the MWt of the PLGA polymers were increased from 14.5 kDa (90.9 ± 2.8 nm) to 213 kDa (143 ± 1.9 nm) (Mittal *et al.*, 2007). However, other studies found opposite results. PLA polymers of 17.5 kDa, 50 kDa, and 90 kDa corresponded with PLA NPs of 250 ± 13 nm, 227 ± 9 nm, and 205 ± 8 nm, respectively (Zambaux *et al.*, 1999). Another study also found that low MWt (9.3 kDa) PLA produced bigger NPs than high MWt (150 kDa) PLA at 235 ± 58 nm and 111 ± 32 nm, respectively (Palacio, Orozco and López, 2011). Contrarily, MPs prepared using the double emulsion solvent evaporation method showed a direct relationship between polymer size and microparticle size (Bragagni *et al.*, 2013). PLA polymers, 10-18 kDa, 18-28 kDa, and 209 kDa synthesised microparticles of 32, 40, and 68 μ m, respectively (Bragagni *et al.*, 2013). These studies suggest that direct comparison between particle size and MWt can only be done between the

same polymers. Certainly, this is what was noticed in this current study. The polymers showed the following order with regard to MWt: mPEG-PLGA > PGA-co-PDL-PEG₂₀₀₀ > PGA-co-PDL > PLGA; while the NPs had this order of size: PGA-co-PDL > mPEG-PLGA > PLGA > PGA-co-PDL-PEG₂₀₀₀.

Resveratrol, 5% and 10% (w/w), were encapsulated into NPs prepared from the four polymers. PGA-co-PDL has previously been studied for the delivery of proteins, vaccines and non-steroidal anti-inflammatory drugs, (Gaskell *et al.*, 2008; Tawfeek, 2013; Kunda, Alfagih, Dennison, Tawfeek, *et al.*, 2015; Tawfeek *et al.*, 2017), but this was the first attempt at encapsulating resveratrol into PGA-co-PDL NPs for lung cancer therapy. The PGA-co-PDL not only produced NPs of the largest size, but also the highest encapsulation efficiency (EE%). The PGA-co-PDL 5% resveratrol-loaded NPs (5% RNP) and 10% resveratrol-loaded NPs (10% RNP) had an EE% of $78 \pm 0.24\%$ and $70 \pm 0.89\%$, respectively. The second highest EE% was PGA-co-PDL-PEG₂₀₀₀ 10% RNP at $40 \pm 2.32\%$. The polydispersity index (PDI) values of the PGA-co-PDL, PGA-co-PDL PEG₂₀₀₀, and PLGA polymeric NPs were less than 0.14 with the PEG-PLGA NPs being less than 0.35, all indicating a very narrow size distribution (Danaei *et al.*, 2018). The NPs from all the polymers presented a high zeta potential (-30 mV), which can contribute to physical stability, thus, preventing flocculation and aggregation of the NPs (Neves *et al.*, 2016).

As mentioned before, the double emulsion evaporation method used in this study was optimised with PGA-co-PDL. Thus, it is possible that improved NPs could have been obtained with the other polymers using different formulation parameters. In this study, the resveratrol was co-dissolved with the polymer in DCM (representing first water phase (w1)) where-as most studies dissolved

resveratrol into ethanol or acetone and used that mixture as w1 (Sanna *et al.*, 2015; Li *et al.*, 2016). Dissolving the resveratrol in ethanol as w1, allowed Li *et al.* to produce PEG-PLGA NPs with an EE% of 68.2% compared to the EE% for PEG-PLGA NPs of $20 \pm 0.48\%$ found in this current study (Li *et al.*, 2016). Ideally, one would want to optimised the formulation parameters for each polymer, but in this study a direct comparison between polymers wanted to be made, hence the use of the same parameters for all polymers. That said, the PGA-co-PDL blank NPs (BNP), 5% RNP and 10% RNP were taken forward to cytotoxicity studies.

5.1.2. Cytotoxicity studies

The efficacy of PGA-co-PDL NPs as a drug delivery system for resveratrol compared to free-resveratrol was assessed using the Alamar blue and LDH assays on Calu 3 cells.

The Alamar blue assay showed that the PGA-co-PDL BNP possessed good cytocompatibility, with none of the tested concentrations (up to 1 mg/mL) reducing the cell viability to less than 85% after 24 hours. Comparable results were found on A549 cells with PGA-co-PDL BNP, 1.25 mg/mL, showing a cell viability of 70% according to the MTT assay (Kunda, 2014). The ANOVA and subsequent Tukey's comparison revealed that there was no statistical difference between the cell viability of the BNP-treated and the untreated cells (negative control) ($p > 0.99$). Thus, providing the concentration of PGA-co-PDL NPs is constant, all cytotoxic effects can be attributed to the encapsulated resveratrol. Furthermore, the Alamar blue assay showed that 5% RNP, 10%

RNP, and free-resveratrol had a concentration-dependent cytotoxic effect on the cell viability of the Calu 3 cells. The IC_{50} after 24 hours of treatment with the free-resveratrol was $213 \pm 63 \mu\text{M}$. Meanwhile, the IC_{50} values of the 5% RNP and 10% RNP after 24 hours were $47 \pm 30 \mu\text{M}$ and $86 \pm 38 \mu\text{M}$, respectively. These results demonstrate that using PGA-co-PDL NPs as a delivery system reduced the IC_{50} of resveratrol on Calu 3 cells after 24 hours by up to 78%. This is a greater effect than reported by Karthikeyan *et al*, who reported that the IC_{50} of resveratrol in NCI-H460 cells after 24 hours decreased by 50% when loaded into gelatin NPs (Karthikeyan *et al.*, 2013), although we recognise that the sensitivities of different cell types to the same toxic agent could be different.

The LDH assay was used on the Calu 3 cells to give further credence to the results obtained using the Alamar blue assay. The resveratrol-loaded PGA-co-PDL NPs were again tested against free-resveratrol at 24, 48 and 72 hours. Preliminary tests showed that there were no noticeable differences between the cytotoxicity profiles at 24 hours. However, the LDH results for 48 hours and 72 hours showed a concentration- and time-dependant increase in LDH release for the resveratrol-loaded PGA-co-PDL NPs and the free-resveratrol. The free-resveratrol did not show a significant difference from the control ($p>0.05$). Meanwhile, at 72 hours, the $300 \mu\text{M}$ 10% RNP caused a significant difference in LDH release compared to the control ($p<0.001$) and the $300 \mu\text{M}$ BNP ($p<0.005$). This suggests that the LDH release was due to the resveratrol encapsulated into the PGA-co-PDL NPs.

5.1.3. Spray drying of resveratrol-loaded nanoparticles into NCMPs

The PGA-co-PDL NPs were spray-dried, using L-leucine and chitosan as excipients, to produce NCMP carriers suitable for pulmonary delivery via DPI.

The NCMPs were produced with a yield ranging from 32-73%. The large variance in yield was attributed to the difficulty in the removal of the powder from the sides of the cyclone, due to some of the liquid droplets attaching to the inside wall of the drying chamber and cyclone of the spray dryer. This has been noted in other studies particularly when using chitosan as an excipient (Cevher *et al.*, 2006; Almurshedi, 2018). Morphological studies showed that the particles possessed wrinkly/corrugated surfaces with noticeable cavities/indentations in the middle of the particles. Studies suggest that this is due to the hydrophobic nature of L-leucine preventing water from adsorbing onto the surface of the particle which produces the cavities upon drying (Merchant *et al.*, 2014). Several other studies have noted these cavities, which aid in dispersibility of the particles, when using L-leucine (Kunda, Alfagih, Dennison, Somavarapu, *et al.*, 2015).

Aerosolisation studies using an NGI showed that the NCMPs had a MMAD between 3.1-4 μm , which is within the ideal range of 1-5 μm for particles to be able to deposit in the lung (El-Sherbiny and Smyth, 2012; Elsayed and AbouGhaly, 2016; Rezazadeh *et al.*, 2018). The NCMPs had a high ED >98% and RF 70-74%, but a low FPF 39-47%, which showed that L-leucine may have enhanced the dispersibility, but together the excipients produced a low FPF, which may suggest aggregation of the particles. Almurshedi reported that as the chitosan:L-leucine ratio increases, the FPF decreases (Almurshedi, 2018).

Once deposited into the lung, the NCMPs need to swell and/or disperse to release the enclosed NPs, in order for the cells to take-up the NPs (Tomoda *et al.*, 2008). In this study, the size of the NPs released from the NCMPs, after dispersion in distilled water, was larger than before spray drying ($p < 0.05$). Spray drying with water dispersant excipients, such as trehalose and lactose, tends to allow for recovery of NPs that are 10-30% bigger than before spray drying (Sham *et al.*, 2004; Chaubal and Popescu, 2008; Tomoda *et al.*, 2009). However, rather than dispersing, chitosan tends to form a gel upon contact with an aqueous medium, which could hinder the release of the entrapped NPs (Aranaz *et al.*, 2017). This gel formation can also be attributed to the NCMPs modifying the release profile of the NPs (Liu *et al.*, 2019). Before spray drying, all the resveratrol loaded into the NPs was released within 60 minutes, but after spray drying only 18% of the resveratrol was released after 60 minutes. After 24 hours, the NCMP showed a resveratrol release of 25%.

5.1.4. Polymer modification through click chemistry

Polymeric NPs have been used as a drug delivery system for various drugs against several cancers including colon, liver, lung and prostate (Karthikeyan *et al.*, 2013; Jung *et al.*, 2015; J. Wu *et al.*, 2017; Nassir *et al.*, 2018). Most NPs use the unique characteristics of tumours, known as the EPR effect, to passively target the cancer cells (Kobayashi, Watanabe and Choyke, 2013; J. Wu *et al.*, 2017). However, attaching ligands, such as antibodies, that can specifically bind to a particular target site on a tumour cell, would allow for active targeting (Wilhelm *et al.*, 2016). Further attachment of a fluorescent ligand would help with visualisation of the entry of the NPs into the cells (Robin and O'Reilly, 2015; Jiang *et al.*, 2018).

Glycerol was modified to 2-(prop-2-yn-1-yloxy)propane-1,3-diol, which possesses an alkyne group, using known methods (Vrbková, Dračinský and Holý, 2007; Gładysz, Ruszkowski and Milecki, 2018). The 2-(prop-2-yn-1-yloxy)propane-1,3-diol was used in various ratios alongside glycerol, PDL and DVA in the polymerisation reaction to PGA-co-PDL possessing a pendant alkyne group on the polymer backbone. This was the first time a modified glycerol possessing an alkyne group was used to polymerise this polymer.

It was found that as the ratio of 2-(prop-2-yn-1-yloxy)propane-1,3-diol to glycerol increased in the polymer, there was a noticeable decrease and eventual absence of the OH trough, which is characteristic of the pendant hydroxyl group on the glycerol molecule. The trough was replaced by an alkyne C-H stretch, which suggested that the 2-(prop-2-yn-1-yloxy)propane-1,3-diol was incorporated into the polymer.

A type of click chemistry, CuAAC reaction, was used to react the alkyne group on the PGA-co-PDL polymer to the azide group of the NBD azide, which was synthesised earlier. NBD azide is a fluorophore that can be photoactivated to allow the visualisation of particles conjugated to it (Tobimatsu *et al.*, 2014). The CuAAC reaction is normally highly efficient, but the lack of the characteristic peak on the FT-IR spectrum associated with NDB azide suggested the reaction was unsuccessful (Castro, Rodríguez and Albericio, 2016). The polymer used for the reaction only contained 10% 2-(prop-2-yn-1-yloxy)propane-1,3-diol (w/w), which means that there was a low concentration of alkyne groups on which the NBD azide could bind. This problem may be amplified by the concern that further reduction of binding site accessibility may

occur with folding of larger polymers (Pickens *et al.*, 2018). These two problems together could explain the lack of success of the reaction.

It was decided to attempt the CuAAC reaction on a smaller azide, 2-phenyl-5-(prop-2-yn-1-yloxy)-1,3-dioxane. This was derived from glycerol with the secondary hydroxyl groups protected with benzaldehyde, which contains the alkyne group and was reacted with the NBD azide. Neither the NMR nor the FT-IR spectra indicated that the reaction was successful. Although, the yield of the reactions to produce the 2-(prop-2-yn-1-yloxy)propane-1,3-diol was high (>60 %), the scale was very low. This meant that the polymerisation reaction had to be reduced and the click reactions had to be done on a small scale using low concentrations, which can influence the success of a reaction (Presolski, Hong and Finn, 2011). These are all issues that need to be addressed in future studies.

5.2. Future work

Although progress has been made towards a drug delivery system for resveratrol, the work is not completed. Some additional studies can be performed to build on the successes achieved in this current work, in order to help improve the drug delivery system.

5.2.1. Optimisation and validation of cytotoxicity studies

The cytotoxicity studies performed using the NPs need to be validated, while the studies performed using the NCMPs have to be optimised.

As mentioned throughout this thesis, NPs possess unique characteristics that have been found to cause interference with various cytotoxicity assays (Kroll *et al.*, 2009; Sukhanova *et al.*, 2018). Although previous studies have shown more interference from carbon or metallic based NPs, at least one study has mentioned polymeric NPs causing interference (Belyanskaya *et al.*, 2007; Casey *et al.*, 2007; Guadagnini *et al.*, 2015). In this study, it was noticed that the PGA-co-PDL NPs did not yield consistent results in the cytotoxicity assays used. Furthermore, the results from the NCMPs were inconclusive. Some considerations needed in the cytotoxicity assessment of NPs are as follows:

It is recommended that the physicochemical characterisations of the NPs/NCMPs are fully assessed prior to commencement of cytotoxicity testing (Kong *et al.*, 2011). Furthermore, the components of the NPs/NCMPs should be tested, separately, for any interference with the assay components, in the presence and absence of cells (Ong *et al.*, 2014). The PGA-co-PDL NPs showed a good cytotoxicity profile, but when the NCMPs were tested there was no distinctive trend noticed. This could have been caused by the components of the NCMPs, i.e. the chitosan and L-leucine, either separately or synergistically. Only by testing the various components can this be identified. The NCMPs were also tested at a higher concentration than the NPs and this could have increased the chance of interference (Ong *et al.*, 2014). NPs/NCMPs concentration should be limited in the final sample. Therefore,

the choice of cytotoxicity assay is important and it is recommended that at least two different assays are used (Matuszak *et al.*, 2016).

Once the right assays are established where NPs/NCMPs showed no interference, it is recommended that the cytotoxicity studies performed in this study are repeated, in order to achieve reproducibility and thus reliability of data. Furthermore, assessment of the NPs/NCMPs both in human lung cancer cell lines and human non-cancerous cell lines would be beneficial.

5.2.2. Increase scale of click chemistry

A high concentration might be a problem for cytotoxicity studies, but the low concentrations used for the click chemistry reactions caused the reactions to be unsuccessful (Presolski, Hong and Finn, 2011).

This part of the project would benefit from having it performed on a bigger scale to offset some of the low yields obtained by some reactions. Reactions between a small molecule, like the fluorescent moiety used in this study, and a high molecular weight polymer have some difficulties due to the nature of polymers (Pickens *et al.*, 2018). It would be wise to optimise the click chemistry reaction on the smaller molecules that present the azide and alkyne groups. This optimised reaction can then be used to “click” the azide molecule onto the polymer presenting with the alkyne moiety. Alternatively, the NBD azide can be attached to the modified glycerol prior to the polymerisation reaction.

5.3. Conclusion

In this thesis, resveratrol was encapsulated into PLGA, mPEG-PLGA, PGA-co-PDL-PEG₂₀₀₀, and PGA-co-PDL NPs. All NPs were under 252 nm with good PDI (<0.353) and a high zeta potential (> -30 mV). The PGA-co-PDL NPs showed the best EE% at $78 \pm 0.24\%$ and $70 \pm 0.89\%$ and drug loading of $39 \pm 0.12 \mu\text{g}/\text{mg}$ and $70 \pm 0.89 \mu\text{g}/\text{mg}$ for 5% RNP and 10% RNP, respectively. These two NPs showed a burst release profile, with no resveratrol detected after 60 minutes in a release medium. The Alamar blue and LDH assays showed that the PGA-co-PDL 5% RNP and 10 % RNP had a dose- and time-dependent cytotoxic effect on Calu 3 cells. The resveratrol-loaded PGA-co-PDL NPs reduced the IC₅₀ of resveratrol after 24 hours by up to 78%. The selected NPs was then incorporated into NCMP using L-leucine and chitosan using spray drying. The NCMP formulations had a high ED >98 % and RF 70-74%, but a low FPF 39-47%. The MMAD was in the ideal range of 1-5 μm to facilitate lung deposition. Moreover, the NCMP seemed to modify the release profile of the NPs, presenting a sustained release of resveratrol over 24 hours. Glycerol was successfully modified to contain an alkyne moiety and was used to polymerise novel PGA-co-PDL with the alkyne moiety present. Further studies need to be done in order to build on these successes.

6 References

Abdelaziz, H. M. *et al.* (2018) 'Inhalable particulate drug delivery systems for lung cancer therapy: Nanoparticles, microparticles, nanocomposites and nanoaggregates', *Journal of Controlled Release*. Elsevier, 269, pp. 374–392. doi: 10.1016/j.jconrel.2017.11.036.

Adan, A., Kiraz, Y. and Baran, Y. (2016) 'Cell proliferation and cytotoxicity assays', *Current pharmaceutical biotechnology*. Bentham Science Publishers, 17(14), pp. 1213–1221. doi: 10.2174/13892010176661608081605.

Ahmadi, Z., Mohammadinejad, R. and Ashrafizadeh, M. (2019) 'Drug delivery systems for resveratrol, a non-flavonoid polyphenol: Emerging evidence in last decades', *Journal of Drug Delivery Science and Technology*, 51, pp. 591–604. doi: 10.1016/j.jddst.2019.03.017.

Al-Mansour, Z., Pang, L. and Bathini, V. (2019) 'Novel Cancer Therapeutics in Geriatrics: What is Unique to the Aging Patient?', *Drugs & Aging*. Springer International Publishing, 36(1), pp. 1–11. doi: 10.1007/s40266-018-0619-2.

Al-Nasiry, S. *et al.* (2007) 'The use of Alamar Blue assay for quantitative analysis of viability, migration and invasion of choriocarcinoma cells', *Human Reproduction*. Narnia, 22(5), pp. 1304–1309. doi: 10.1093/humrep/dem011.

Albuquerque, R. V. *et al.* (2015) 'In vitro protective effect and antioxidant mechanism of resveratrol induced by dapsone hydroxylamine in human cells', *PLoS ONE*, 10(8). doi: 10.1371/journal.pone.0134768.

Alexiou, C. *et al.* (2000) 'Locoregional Cancer Treatment with Magnetic Drug Targeting Locoregional Cancer Treatment with Magnetic Drug Targeting 1',

(4), pp. 6641–6648.

Almeida, L. *et al.* (2009) 'Pharmacokinetic and safety profile of trans-resveratrol in a rising multiple-dose study in healthy volunteers', *Molecular Nutrition & Food Research*, 53(S1), pp. S7–S15. doi: 10.1002/mnfr.200800177.

Almurshedi, A. S. (2018) *Development of afatinib lipid nanoparticles targeting non small cell lung cancer*. Liverpool John Moores University.

Altice, C. K. *et al.* (2017) 'Financial Hardships Experienced by Cancer Survivors: A Systematic Review.', *Journal of the National Cancer Institute*. Oxford University Press, 109(2). doi: 10.1093/jnci/djw205.

Amoabediny, G. *et al.* (2018) 'Overview of preparation methods of polymeric and lipid-based (niosome, solid lipid, liposome) nanoparticles: A comprehensive review Overview of preparation methods of polymeric and lipid-based (niosome, solid lipid, liposome) nanoparticles: A comprehensiv', *International Journal of Polymeric Materials and Polymeric Biomaterials*, 67(6), pp. 383–400. doi: 10.1080/00914037.2017.1332623.

Anand, P. *et al.* (2008) 'Cancer is a Preventable Disease that Requires Major Lifestyle Changes', *Pharmaceutical Research*. Springer US, 25(9), pp. 2097–2116. doi: 10.1007/s11095-008-9661-9.

Appleby, J. (2019) 'What's the point of waiting time targets if they can't be met', *BMJ (Online)*, 364(February), pp. 1–4. doi: 10.1136/bmj.l845.

Aranaz, I. *et al.* (2017) 'Chitosan spray-dried microparticles for controlled delivery of venlafaxine hydrochloride', *Molecules*, 22(11), pp. 1–13. doi:

10.3390/molecules22111980.

Arora, D. and Jaglan, S. (2016) 'Nanocarriers based delivery of nutraceuticals for cancer prevention and treatment: A review of recent research developments', *Trends in Food Science & Technology*. Elsevier, 54, pp. 114–126. doi: 10.1016/J.TIFS.2016.06.003.

Aslantürk, Ö. S. (2018) 'In Vitro Cytotoxicity and Cell Viability Assays: Principles, Advantages, and Disadvantages', in *Genotoxicity - A Predictable Risk to Our Actual World*. InTech. doi: 10.5772/intechopen.71923.

Azarmi, S., Roa, W. H. and Löbenberg, R. (2008) 'Targeted delivery of nanoparticles for the treatment of lung diseases', *Advanced Drug Delivery Reviews*. Elsevier, 60(8), pp. 863–875. doi: 10.1016/j.addr.2007.11.006.

Azhari, Z. *et al.* (2018) 'Short poly(ethylene glycol) block initiation of poly(l-lactide) di-block copolymers: a strategy for tuning the degradation of resorbable devices', *Polymer International*, 67(6), pp. 726–738. doi: 10.1002/pi.5563.

Baker, M. and Penny, D. (2016) 'Is there a reproducibility crisis?', *Nature*, 533(7604), pp. 452–454. doi: 10.1038/533452A.

Barrow, A. and Pandit, J. J. (2014) 'Lung ventilation and the physiology of breathing', *Surgery (Oxford)*. Elsevier, 32(5), pp. 221–227. doi: 10.1016/J.MPSUR.2014.02.010.

Bazak, R. *et al.* (2015) 'Cancer active targeting by nanoparticles: a comprehensive review of literature', *Journal of Cancer Research and Clinical Oncology*, 141(5), pp. 769–784. doi: 10.1007/s00432-014-1767-3.

Behzadi, S. *et al.* (2017) 'Cellular uptake of nanoparticles: Journey inside the cell', *Chemical Society Reviews*. Royal Society of Chemistry, 46(14), pp. 4218–4244. doi: 10.1039/c6cs00636a.

Belyanskaya, L. *et al.* (2007) 'The reliability and limits of the MTT reduction assay for carbon nanotubes-cell interaction', *Carbon*, 45, pp. 2643–2648. doi: 10.1016/j.carbon.2007.08.010.

Bertrand, N. *et al.* (2014) 'Cancer Nanotechnology: The impact of passive and active targeting in the era of modern cancer biology', *Advanced drug delivery reviews*. NIH Public Access, 66, p. 2. doi: 10.1016/J.ADDR.2013.11.009.

Bestvina, C. M. *et al.* (2014) *Patient-Oncologist Cost Communication, Financial Distress, and Medication Adherence*. Available at: <https://ascopubs.org/doi/pdfdirect/10.1200/jop.2014.001406> (Accessed: 18 May 2019).

Bhimani, J. *et al.* (2019) 'The impact of new cancer drug therapies on site specialised cancer treatment activity in a UK cancer network 2014–2018', *Journal of Oncology Pharmacy Practice*. SAGE PublicationsSage UK: London, England, p. 107815521983944. doi: 10.1177/1078155219839445.

Binder, W. H. (2019) 'The Past 40 Years of Macromolecular Sciences: Reflections on Challenges in Synthetic Polymer and Material Science', *Macromolecular Rapid Communications*. Wiley-VCH Verlag. doi: 10.1002/marc.201800610.

Binder, W. H. and Sachsenhofer, R. (2007) "'Click" chemistry in polymer and materials science', *Macromolecular Rapid Communications*, pp. 15–54. doi: 10.1002/marc.200600625.

Binder, W. H. and Sachsenhofer, R. (2008) ‘“Click” chemistry in polymer and material science: An Update’, *Macromolecular Rapid Communications*, pp. 952–981. doi: 10.1002/marc.200800089.

Boocock, D. J. *et al.* (2007) ‘Phase I Dose Escalation Pharmacokinetic Study in Healthy Volunteers of Resveratrol, a Potential Cancer Chemopreventive Agent’, *Cancer Epidemiol Biomarkers Prev*, 16(6), pp. 1246–52. doi: 10.1158/1055-9965.EPI-07-0022.

Borriello, A. *et al.* (2014) ‘Resveratrol: From basic studies to bedside’, *Cancer Treatment and Research*. Edited by V. Zappia *et al.* Springer, Berlin, Heidelberg, 159, pp. 167–184. doi: 10.1007/978-3-642-38007-5_10.

Bragagni, M. *et al.* (2013) ‘Selection of PLA polymers for the development of injectable prilocaine controlled release microparticles: Usefulness of thermal analysis’, *International Journal of Pharmaceutics*, 441(1–2), pp. 468–475. doi: 10.1016/j.ijpharm.2012.11.007.

Bray, F. *et al.* (2018) ‘Global Cancer Statistics 2018: GLOBOCAN Estimates of Incidence and Mortality Worldwide for 36 Cancers in 185 Countries’, *CA CANCER J CLIN*, 68, pp. 394–424. doi: 10.3322/caac.21492.

Brien, J. O. *et al.* (2000) ‘Investigation of the Alamar Blue (resazurin) fluorescent dye for the assessment of mammalian cell cytotoxicity’, *European journal of biochemistry*, 267(17), pp. 5421–5426. Available at: <http://www.ncbi.nlm.nih.gov/pubmed/10951200>.

Bu, L. *et al.* (2013) ‘Trans-resveratrol loaded chitosan nanoparticles modified with biotin and avidin to target hepatic carcinoma’, *International Journal of Pharmaceutics*, 452(1–2), pp. 355–362. doi: 10.1016/j.ijpharm.2013.05.007.

Bupa (2011) *Cancer diagnosis and treatment: a 2021 projection*. Available at: www.bupa.com (Accessed: 11 May 2019).

Burd, J. F. and Usategui-Gomez, M. (1973) 'A colorimetric assay for serum lactate dehydrogenase', *Clinica Chimica Acta*. Elsevier, 46(3), pp. 223–227. doi: 10.1016/0009-8981(73)90174-5.

Burki, T. K. (2019) 'NHS England statistics and long-term plan', *The Lancet Oncology*. Elsevier Ltd, 20(2), p. 187. doi: 10.1016/s1470-2045(19)30008-7.

Cal, K. and Sollohub, K. (2010) 'Spray Drying Technique. I: Hardware and Process Parameters', *Journal of pharmaceutical sciences*, 99(2), pp. 575–586. doi: 10.1002/jps.21886.

Callahan, C. and Brintzenhofeszoc, K. (2015) 'Financial Quality of Life for Patients With Cancer: An Exploratory Study', *Journal of Psychosocial Oncology*, 33(4), pp. 377–394. doi: 10.1080/07347332.2015.1045679.

Cancer Research UK (2017) *Full team ahead: understanding the UK non-surgical cancer treatments workforce*. Available at: https://www.cancerresearchuk.org/sites/default/files/full_team_ahead-exec_summary.pdf (Accessed: 14 May 2019).

Cancer Research UK (2019) *Lung cancer statistics*. Available at: <https://www.cancerresearchuk.org/health-professional/cancer-statistics/statistics-by-cancer-type/lung-cancer#heading-One> (Accessed: 10 March 2019).

Carletto, B. *et al.* (2016) 'Resveratrol-loaded nanocapsules inhibit murine melanoma tumor growth', *Colloids and Surfaces B: Biointerfaces*. Elsevier

B.V., 144, pp. 65–72. doi: 10.1016/j.colsurfb.2016.04.001.

Carvalho, D. and Erbetta, C. (2012) 'Synthesis and Characterization of Poly(D,L-Lactide-co-Glycolide) Copolymer', *Journal of Biomaterials and Nanobiotechnology*. Scientific Research Publishing, 03(02), pp. 208–225. doi: 10.4236/jbnb.2012.32027.

Casey, A. *et al.* (2007) 'Spectroscopic analysis confirms the interactions between single walled carbon nanotubes and various dyes commonly used to assess cytotoxicity', *Carbon*, 45(7), pp. 1425–1432. doi: 10.1016/j.carbon.2007.03.033.

Castro, V., Rodríguez, H. and Albericio, F. (2016) 'CuAAC: An Efficient Click Chemistry Reaction on Solid Phase', *ACS Combinatorial Science*, 18(1), pp. 1–14. doi: 10.1021/acscombsci.5b00087.

Cattiaux, L. *et al.* (2018) 'New branched amino acids for high affinity dendrimeric DC-SIGN ligands', *Bioorganic & Medicinal Chemistry*. Pergamon, 26(5), pp. 1006–1015. doi: 10.1016/J.BMC.2017.12.036.

Cevher, E. *et al.* (2006) 'Characterization of biodegradable chitosan microspheres containing vancomycin and treatment of experimental osteomyelitis caused by methicillin-resistant *Staphylococcus aureus* with prepared microspheres', *International Journal of Pharmaceutics*, 317(2), pp. 127–135. doi: 10.1016/j.ijpharm.2006.03.014.

Chan, F. K.-M., Moriwaki, K. and De Rosa, M. J. (2013) 'Detection of necrosis by release of lactate dehydrogenase activity.', *Methods in molecular biology (Clifton, N.J.)*. NIH Public Access, 979, pp. 65–70. doi: 10.1007/978-1-62703-290-2_7.

Chatterjee, M. *et al.* (2017) 'A novel approach to fabricate dye-encapsulated polymeric micro- and nanoparticles by thin film dewetting technique', *Journal of Colloid and Interface Science*. Elsevier Inc., 506, pp. 126–134. doi: 10.1016/j.jcis.2017.07.023.

Chaubal, M. V. and Popescu, C. (2008) 'Conversion of nanosuspensions into dry powders by spray drying: A case study', *Pharmaceutical Research*, 25(10), pp. 2302–2308. doi: 10.1007/s11095-008-9625-0.

Che, P., Wang, L. and Li, Q. (2009) 'The development, optimization and validation of an assay for high throughput antiviral drug screening against dengue virus', *International Journal of Clinical and Experimental Medicine*, 2(4), pp. 363–373.

Cheng, C. J. *et al.* (2015) 'A holistic approach to targeting disease with polymeric nanoparticles.', *Nature reviews. Drug discovery*. NIH Public Access, 14(4), pp. 239–47. doi: 10.1038/nrd4503.

Cheredy, K. K., Payen, V. L. and Pr at, V. (2018) 'PLGA polymer: From a classic drug carrier to a novel therapeutic activity contributor', *Journal of Controlled Release*. Elsevier, 289(January 2019), pp. 10–13. doi: 10.1016/j.jconrel.2018.09.017.

Cheung, R. C. F. *et al.* (2015) *Chitosan: An update on potential biomedical and pharmaceutical applications*, *Marine Drugs*. doi: 10.3390/md13085156.

Chew, N. Y. K. and Chan, H. K. (2001) 'Use of solid corrugated particles to enhance powder aerosol performance', *Pharmaceutical Research*, 18(11), pp. 1570–1577. doi: 10.1023/A:1013082531394.

Chimento, A. *et al.* (2019) 'Progress to Improve Oral Bioavailability and Beneficial Effects of Resveratrol', *International Journal of Molecular Sciences*. Multidisciplinary Digital Publishing Institute, 20(6), p. 1381. doi: 10.3390/ijms20061381.

Chishti, N. *et al.* (2019) 'Preparation, Optimization, and In Vivo Evaluation of Nanoparticle-Based Formulation for Pulmonary Delivery of Anticancer Drug', *Medicina*. Multidisciplinary Digital Publishing Institute, 55(6), p. 294. doi: 10.3390/medicina55060294.

Cho, A. R. *et al.* (2014) 'Preparation of Chitosan-TPP Microspheres as Resveratrol Carriers', *Journal of Food Science*, 79(4), pp. 568–576. doi: 10.1111/1750-3841.12395.

Chou, T.-C. and Talalay, P. (1984) 'Quantitative analysis of dose-effect relationships: the combined effects of multiple drugs or enzyme inhibitors', *Advances in Enzyme Regulation*, 22, pp. 27–55. doi: 10.1016/0065-2571(84)90007-4.

Chu, K. S. *et al.* (2013) 'Nanoparticle drug loading as a design parameter to improve docetaxel pharmacokinetics and efficacy.', *Biomaterials*. NIH Public Access, 34(33), pp. 8424–9. doi: 10.1016/j.biomaterials.2013.07.038.

CLIC Sargent (2019) *Cancer costs again : The financial and emotional impact of relapse and secondary cancer*. Available at: https://www.clicsargent.org.uk/wp-content/uploads/2019/01/Cancer_costs_again_Policy-Report_A4.pdf (Accessed: 18 May 2019).

Collado-gonz, M., Gonz, Y. and Goycoolea, F. M. (2019) 'Interaction Between

Chitosan and Mucin : Fundamentals and Applications’, *Biomimetics*, 4(2), pp. 1–20.

Corrie, P. G. (2011) ‘Cytotoxic chemotherapy: Clinical aspects’, *Medicine*. Elsevier Ltd, 39(12), pp. 717–722. doi: 10.1016/j.mpmed.2011.09.012.

Crisp, N. *et al.* (2014) ‘Chemotherapy at home: Keeping patients in their “natural habitat”’, *Canadian Oncology Nursing Journal*, 24(2), pp. 89–94. doi: 10.5737/1181912x2428994.

Crowley, L. C., Marfell, B. J., Scott, A. P., Boughaba, J. A., *et al.* (2016) ‘Dead cert: Measuring cell death’, *Cold Spring Harbor Protocols*, 2016(12), pp. 1064–1072. doi: 10.1101/pdb.top070318.

Crowley, L. C., Marfell, B. J., Scott, A. P. and Waterhouse, N. J. (2016) ‘Quantitation of apoptosis and necrosis by annexin V binding, propidium iodide uptake, and flow cytometry’, *Cold Spring Harbor Protocols*, 2016(11), pp. 953–957. doi: 10.1101/pdb.prot087288.

d’Angelo, I. *et al.* (2015) ‘Overcoming barriers in *Pseudomonas aeruginosa* lung infections: Engineered nanoparticles for local delivery of a cationic antimicrobial peptide’, *Colloids and Surfaces B: Biointerfaces*. Elsevier B.V., 135, pp. 717–725. doi: 10.1016/j.colsurfb.2015.08.027.

Dabbagh, A. *et al.* (2018) ‘Critical Parameters for Particle-Based Pulmonary Delivery of Chemotherapeutics’, *Journal of Aerosol Medicine and Pulmonary Drug Delivery*. Mary Ann Liebert, Inc. 140 Huguenot Street, 3rd Floor New Rochelle, NY 10801 USA , 31(3), pp. 139–154. doi: 10.1089/jamp.2017.1382.

Danaei, M. *et al.* (2018) ‘Impact of particle size and polydispersity index on the

clinical applications of lipidic nanocarrier systems', *Pharmaceutics*. MDPI AG.
doi: 10.3390/pharmaceutics10020057.

Dandekar, P. *et al.* (2010) 'Pulmonary Targeting of Nanoparticle Drug Matrices', 23(6), pp. 343–353.

Davidov-Pardo, G. and McClements, D. J. (2014) 'Resveratrol encapsulation: Designing delivery systems to overcome solubility, stability and bioavailability issues', *Trends in Food Science and Technology*. Elsevier Ltd, 38(2), pp. 88–103. doi: 10.1016/j.tifs.2014.05.003.

Decker, T. and Lohmann-Matthes, M. L. (1988) 'A quick and simple method for the quantitation of lactate dehydrogenase release in measurements of cellular cytotoxicity and tumor necrosis factor (TNF) activity', *Journal of Immunological Methods*, 115(1), pp. 61–69. doi: 10.1016/0022-1759(88)90310-9.

Dekali, S. *et al.* (2014) 'Assessment of an in vitro model of pulmonary barrier to study the translocation of nanoparticles', *Toxicology Reports*. Elsevier, 1, pp. 157–171. doi: 10.1016/J.TOXREP.2014.03.003.

Deshmukh, R., Wagh, P. and Naik, J. (2016) 'Solvent evaporation and spray drying technique for micro- and nanospheres/particles preparation: A review', *Drying Technology*. Taylor & Francis, 34(15), pp. 1758–1772. doi: 10.1080/07373937.2016.1232271.

Dhawan, A. and Sharma, V. (2010) 'Toxicity assessment of nanomaterials: Methods and challenges', *Analytical and Bioanalytical Chemistry*, 398(2), pp. 589–605. doi: 10.1007/s00216-010-3996-x.

Dias, M. *et al.* (2017) 'Lung cancer in never-smokers—what are the differences?', *Acta Oncologica*. Taylor and Francis Ltd, 56(7), pp. 931–935. doi: 10.1080/0284186X.2017.1287944.

Dimer, F. *et al.* (2015) 'Inhalable Clarithromycin Microparticles for Treatment of Respiratory Infections', *Pharmaceutical Research*, 32(12), pp. 3850–3861. doi: 10.1007/s11095-015-1745-8.

Dolovich, M. B. *et al.* (2019) 'Biophysical model to predict lung delivery from a dual bronchodilator dry-powder inhaler', *International Journal of Pharmaceutics: X*. Elsevier, 1, p. 100018. doi: 10.1016/J.IJPX.2019.100018.

Dolovich, M. B. and Dhand, R. (2011) 'Aerosol drug delivery: Developments in device design and clinical use', *The Lancet*. Elsevier Ltd, 377(9770), pp. 1032–1045. doi: 10.1016/S0140-6736(10)60926-9.

Dong, X. *et al.* (2009) 'Doxorubicin and paclitaxel-loaded lipid-based nanoparticles overcome multidrug resistance by inhibiting P-glycoprotein and depleting ATP.', *Cancer research*. NIH Public Access, 69(9), pp. 3918–26. doi: 10.1158/0008-5472.CAN-08-2747.

Duan, J. *et al.* (2019) 'The red wine component ellagic acid induces autophagy and exhibits anti-lung cancer activity in vitro and in vivo', *Journal of Cellular and Molecular Medicine*, 23(1), pp. 143–154. doi: 10.1111/jcmm.13899.

Ebi, H. *et al.* (2009) 'Relationship of Deregulated Signaling Converging onto mTOR with Prognosis and Classification of Lung Adenocarcinoma Shown by Two Independent *In silico* Analyses', *Cancer Research*. American Association for Cancer Research, 69(9), pp. 4027–4035. doi: 10.1158/0008-5472.CAN-08-3403.

El-Sherbiny, I. M. and Smyth, H. D. C. (2012) 'Controlled release pulmonary administration of curcumin using swellable biocompatible microparticles.', *Molecular pharmaceutics*. NIH Public Access, 9(2), pp. 269–80. doi: 10.1021/mp200351y.

Elsayed, I. and AbouGhaly, M. H. H. (2016) 'Inhalable nanocomposite microparticles: preparation, characterization and factors affecting formulation', *Expert Opinion on Drug Delivery*. Taylor & Francis, 13(2), pp. 207–222. doi: 10.1517/17425247.2016.1102224.

Elshaer, M. *et al.* (2018) 'Resveratrol: An overview of its anti-cancer mechanisms', *Life Sciences*, 207(June), pp. 340–349. doi: 10.1016/j.lfs.2018.06.028.

Errington, T. M. *et al.* (2014) 'An open investigation of the reproducibility of cancer biology research', *eLife*, 3, pp. 1–9. doi: 10.7554/eLife.04333.

Esfanjani, A. F., Assadpour, E. and Jafari, S. M. (2018) 'Improving the bioavailability of phenolic compounds by loading them within lipid-based nanocarriers', *Trends in Food Science & Technology*. Elsevier, 76, pp. 56–66. doi: 10.1016/J.TIFS.2018.04.002.

Evans, J. M. *et al.* (2016) 'A multi-method review of home-based chemotherapy', *European journal of cancer care*, 25(5), pp. 883–902. doi: 10.1111/ecc.12408.

Ezendam, N. P. M. *et al.* (2014) 'Chemotherapy-induced peripheral neuropathy and its impact on health-related quality of life among ovarian cancer survivors: Results from the population-based PROFILES registry', *Gynecologic Oncology*. Academic Press, 135(3), pp. 510–517. doi:

10.1016/J.YGYNO.2014.09.016.

Fantini, M. *et al.* (2015) 'In vitro and in vivo antitumoral effects of combinations of polyphenols, or polyphenols and anticancer drugs: perspectives on cancer treatment.', *International journal of molecular sciences*. Multidisciplinary Digital Publishing Institute (MDPI), 16(5), pp. 9236–82. doi: 10.3390/ijms16059236.

Farooq, M. A. *et al.* (2019) 'Nanocarrier-mediated co-delivery systems for lung cancer therapy: recent developments and prospects', *Environmental Chemistry Letters*. Springer International Publishing, pp. 1–19. doi: 10.1007/s10311-019-00897-7.

Feitelson, M. A. *et al.* (2015) 'Sustained proliferation in cancer: Mechanisms and novel therapeutic targets', *Seminars in Cancer Biology*. Academic Press, 35, pp. S25–S54. doi: 10.1016/J.SEMCANCER.2015.02.006.

Feng, Y., Zhou, J. and Jiang, Y. (2016) 'Resveratrol in lung cancer - A systematic review', *Journal of B.U.ON.*, 21(4), pp. 950–953.

Fiegel, J. *et al.* (2003) 'Large Porous Particle Impingement on Lung Epithelial Cell Monolayers—Toward Improved Particle Characterization in the Lung', *Pharmaceutical Research*. Kluwer Academic Publishers-Plenum Publishers, 20(5), pp. 788–796. doi: 10.1023/A.

Fleisher, T. A. and Oliveira, J. B. (2019) 'Flow cytometry', in *Clinical Immunology*. Fifth Edit. Elsevier, pp. 1239–1251. doi: 10.1016/B978-0-7020-6896-6.00092-2.

Florence, A. T. (2012) "Targeting" nanoparticles: The constraints of physical laws and physical barriers', *Journal of Controlled Release*. Elsevier B.V.,

164(2), pp. 115–124. doi: 10.1016/j.jconrel.2012.03.022.

Focaroli, S. *et al.* (2019) 'A Design of Experiment (DoE) approach to optimise spray drying process conditions for the production of trehalose/leucine formulations with application in pulmonary delivery', *International Journal of Pharmaceutics*. Elsevier B.V., 562, pp. 228–240. doi: 10.1016/j.ijpharm.2019.03.004.

Foroozandeh, P. and Aziz, A. A. (2018) 'Insight into Cellular Uptake and Intracellular Trafficking of Nanoparticles.', *Nanoscale research letters*. Springer, 13(1), p. 339. doi: 10.1186/s11671-018-2728-6.

Foster, K. A. *et al.* (2000) 'Characterization of the Calu-3 cell line as a tool to screen pulmonary drug delivery', *International Journal of Pharmaceutics*. Elsevier, 208(1–2), pp. 1–11. doi: 10.1016/S0378-5173(00)00452-X.

Fotakis, G. and Timbrell, J. A. (2006) 'In vitro cytotoxicity assays: Comparison of LDH, neutral red, MTT and protein assay in hepatoma cell lines following exposure to cadmium chloride', *Toxicology Letters*, 160(2), pp. 171–177. doi: 10.1016/j.toxlet.2005.07.001.

Francioso, A. *et al.* (2014) 'Improved Stability of trans-Resveratrol in Aqueous Solutions by Carboxymethylated (1,3/1,6)-beta-d-Glucan', *J Agric Food Chem*, 62(7), pp. 1520–1525. doi: 10.1021/jf404155e.

Freedman, L. P. *et al.* (2015) 'Reproducibility: Changing the policies and culture of cell line authentication', *Nature Methods*. Nature Publishing Group, 12(6), pp. 493–497. doi: 10.1038/nmeth.3403.

Freites-Martinez, A. *et al.* (2019) 'Assessment of Quality of Life and Treatment

Outcomes of Patients with Persistent Postchemotherapy Alopecia', *JAMA Dermatology*, 155(6), pp. 724–728. doi: 10.1001/jamadermatol.2018.5071.

Gambini, J. *et al.* (2015) 'Properties of Resveratrol: In Vitro and In Vivo Studies about Metabolism, Bioavailability, and Biological Effects in Animal Models and Humans ', *Oxidative Medicine and Cellular Longevity*, 2015, pp. 1–13. doi: 10.1155/2015/837042.

Gaskell, E. E. *et al.* (2008) 'Encapsulation and release of α -chymotrypsin from poly(glycerol adipate-co- ω -pentadecalactone) microparticles', *Journal of Microencapsulation*, 25(3), pp. 187–195. doi: 10.1080/02652040701848775.

Gaul, R. *et al.* (2018) 'Nanotechnology approaches to pulmonary drug delivery: Targeted delivery of small molecule and gene-based therapeutics to the lung', *Design of Nanostructures for Versatile Therapeutic Applications*. William Andrew Publishing, pp. 221–253. doi: 10.1016/B978-0-12-813667-6.00006-1.

Gemine, R. E. *et al.* (2019) 'Longitudinal study to assess impact of smoking at diagnosis and quitting on 1-year survival for people with non-small cell lung cancer', *Lung Cancer*. Elsevier, 129, pp. 1–7. doi: 10.1016/J.LUNGCAN.2018.12.028.

Ghasemi, R. *et al.* (2018) 'MPEG-PLA and PLA-PEG-PLA nanoparticles as new carriers for delivery of recombinant human Growth Hormone (rhGH)', *Scientific Reports*. Nature Publishing Group, 8(1). doi: 10.1038/s41598-018-28092-8.

Ghasemian, E. *et al.* (2016) 'Inhaled sildenafil nanocomposites: lung accumulation and pulmonary pharmacokinetics*', *Pharmaceutical*

Development and Technology. Taylor & Francis, 21(8), pp. 961–971. doi: 10.3109/10837450.2015.1086369.

Gładysz, M., Ruszkowski, P. and Milecki, J. (2018) 'Synthesis and cytotoxic activity of novel acyclic nucleoside analogues with functionality in click chemistry', *Nucleosides, Nucleotides and Nucleic Acids*, 37(1), pp. 53–66. doi: 10.1080/15257770.2017.1417598.

Godugu, C. *et al.* (2013) 'Inhalation delivery of Telmisartan enhances intratumoral distribution of nanoparticles in lung cancer models.', *Journal of controlled release: official journal of the Controlled Release Society*. NIH Public Access, 172(1), pp. 86–95. doi: 10.1016/j.jconrel.2013.06.036.

Gomez Perez, M. *et al.* (2017) 'Neutral Red versus MTT assay of cell viability in the presence of copper compounds', *Analytical Biochemistry*. Elsevier Inc, 535, pp. 43–46. doi: 10.1016/j.ab.2017.07.027.

Gordon, L. G. *et al.* (2009) 'Fuel, beds, meals and meds: out-of-pocket expenses for patients with cancer in rural Queensland', in *Cancer Forum*. The Cancer Council Australia, p. 204.

Grainger, C. I. *et al.* (2006) 'Culture of Calu-3 cells at the air interface provides a representative model of the airway epithelial barrier', *Pharmaceutical Research*, 23(7), pp. 1482–1490. doi: 10.1007/s11095-006-0255-0.

Guadagnini, R. *et al.* (2015) 'Toxicity screenings of nanomaterials: Challenges due to interference with assay processes and components of classic in vitro tests', *Nanotoxicology*, 9(S1), pp. 13–24. doi: 10.3109/17435390.2013.829590.

Guo, X. *et al.* (2014) 'Inhalable microspheres embedding chitosan-coated PLGA nanoparticles for 2-methoxyestradiol', *Journal of Drug Targeting*, 22(5), pp. 421–427. doi: 10.3109/1061186X.2013.878944.

Hamishehkar, H *et al.* (2018) *The effect of different coating materials on the prevention of powder bounce in the next generation impactor*, *Research in Pharmaceutical Sciences*. Available at: <http://www.rpsjournal.net> (Accessed: 13 April 2019).

Han, X. *et al.* (2011) 'Validation of an LDH assay for assessing nanoparticle toxicity', *Toxicology*, 287(1–3), pp. 99–104. doi: 10.1016/j.tox.2011.06.011.

Han, Z. *et al.* (2012) 'MicroRNA-622 functions as a tumor suppressor by targeting K-Ras and enhancing the anticarcinogenic effect of resveratrol', *Carcinogenesis*. Narnia, 33(1), pp. 131–139. doi: 10.1093/carcin/bgr226.

Harborne, J. B. (1991) 'THE CHEMICAL BASIS OF PLANT DEFENSE', *Plant defenses against mammalian herbivory*. CRC Press, p. 45.

Harborne, J. B. (1999) 'Classes and functions of secondary products from plants', *Chemicals from plants*. Imperial College Press London, pp. 1–25.

Hashemzaei, M. *et al.* (2017) 'Anticancer and apoptosis-inducing effects of quercetin in vitro and in vivo', *Oncology Reports*. Spandidos Publications, 38(2), pp. 819–828. doi: 10.3892/or.2017.5766.

He, P., Davis, S. S. and Illum, L. (1996) 'Chitosan microspheres prepared by spray drying method', *European Journal of Pharmaceutical Sciences*, 4, p. S173. doi: 10.1016/s0928-0987(97)86523-2.

Hein, C. D., Liu, X. M. and Wang, D. (2008) 'Click chemistry, a powerful tool

for pharmaceutical sciences', *Pharmaceutical Research*, pp. 2216–2230. doi: 10.1007/s11095-008-9616-1.

Hein, S. *et al.* (2010) 'The Pharmaceutical Aerosol Deposition Device on Cell Cultures (PADD OCC) in vitro system: Design and experimental protocol', *ATLA Alternatives to Laboratory Animals*, 38(4), pp. 285–295. doi: 10.1177/026119291003800408.

Hein, S. *et al.* (2011) 'A new Pharmaceutical Aerosol Deposition Device on Cell Cultures (PADD OCC) to evaluate pulmonary drug absorption for metered dose dry powder formulations', *European Journal of Pharmaceutics and Biopharmaceutics*. Elsevier B.V., 77(1), pp. 132–138. doi: 10.1016/j.ejpb.2010.10.003.

Hejjaji, E. M. A., Smith, A. M. and Morris, G. A. (2018) 'Evaluation of the mucoadhesive properties of chitosan nanoparticles prepared using different chitosan to tripolyphosphate (CS: TPP) ratios', *International Journal of Biological Macromolecules*. Elsevier B.V., 120, pp. 1610–1617. doi: 10.1016/j.ijbiomac.2018.09.185.

Heleno, S. A. *et al.* (2015) 'Bioactivity of phenolic acids: Metabolites versus parent compounds: A review', *Food Chemistry*. Elsevier Ltd, 173, pp. 501–513. doi: 10.1016/j.foodchem.2014.10.057.

Hemar, Y. *et al.* (2010) 'Encapsulation of resveratrol using Water-in-Oil-in-Water double emulsions', *Food Biophysics*, 5(2), pp. 120–127. doi: 10.1007/s11483-010-9152-5.

Hertel, S. P., Winter, G. and Friess, W. (2015) 'Protein stability in pulmonary drug delivery via nebulization', *Advanced Drug Delivery Reviews*. Elsevier

B.V., 93, pp. 79–94. doi: 10.1016/j.addr.2014.10.003.

Hesketh, P. *et al.* (2004) 'Chemotherapy-induced alopecia: psychosocial impact and therapeutic approaches', *Supportive Care in Cancer*. Springer-Verlag, 12(8), pp. 543–549. doi: 10.1007/s00520-003-0562-5.

Hickey, J. W. *et al.* (2015) 'Control of polymeric nanoparticle size to improve therapeutic delivery.', *Journal of controlled release: official journal of the Controlled Release Society*. NIH Public Access, 219, pp. 536–547. doi: 10.1016/j.jconrel.2015.10.006.

Hong, Y., Hu, F. Q. and Yuan, H. (2006) 'Effect of PEG2000 on drug delivery characterization from solid lipid nanoparticles', *Pharmazie*, 61(4), pp. 312–315.

Hoppentocht, M. *et al.* (2014) 'Technological and practical challenges of dry powder inhalers and formulations', *Advanced Drug Delivery Reviews*. Elsevier, 75, pp. 18–31. doi: 10.1016/J.ADDR.2014.04.004.

Hsu, M. N. *et al.* (2015) 'Sustained release of hydrophobic drugs by the microfluidic assembly of multistage microgel/poly (lactic-co-glycolic acid) nanoparticle composites', *Biomicrofluidics*. American Institute of Physics Inc., 9(5). doi: 10.1063/1.4916230.

Hu, C. M. J., Aryal, S. and Zhang, L. (2010) 'Nanoparticle-assisted combination therapies for effective cancer treatment', *Therapeutic Delivery*, pp. 323–334. doi: 10.4155/tde.10.13.

Huang, W. and Zhang, C. (2018) 'Tuning the Size of Poly(lactic-co-glycolic Acid) (PLGA) Nanoparticles Fabricated by Nanoprecipitation', *Biotechnology*

Journal, 13(1), pp. 1–8. doi: 10.1002/biot.201700203.

Huang, X. and Brazel, C. S. (2001) 'On the importance and mechanisms of burst release in matrix-controlled drug delivery systems', *Journal of Controlled Release*, 73(2–3), pp. 121–136. doi: 10.1016/S0168-3659(01)00248-6.

Huckaby, J. T. and Lai, S. K. (2018) 'PEGylation for enhancing nanoparticle diffusion in mucus', *Advanced Drug Delivery Reviews*. Elsevier B.V., pp. 125–139. doi: 10.1016/j.addr.2017.08.010.

Huminiecki, L. and Horbańczuk, J. (2018) 'The functional genomic studies of resveratrol in respect to its anti-cancer effects', *Biotechnology Advances*. Elsevier, 36(6), pp. 1699–1708. doi: 10.1016/J.BIOTECHADV.2018.02.011.

Hunt, D. *et al.* (2018) 'Modelling the implications of reducing smoking prevalence: the public health and economic benefits of achieving a “tobacco-free” UK', *Tob Control*, 27, pp. 129–135. doi: 10.1136/tobaccocontrol-2016-053507.

van den Hurk, C. J. G. *et al.* (2015) 'Measurement of chemotherapy-induced alopecia—time to change', *Supportive Care in Cancer*. Springer Berlin Heidelberg, 23(5), pp. 1197–1199. doi: 10.1007/s00520-015-2647-3.

ICH (2005) *VALIDATION OF ANALYTICAL PROCEDURES: TEXT AND METHODOLOGY* Q2(R1). Available at: https://www.ich.org/fileadmin/Public_Web_Site/ICH_Products/Guidelines/Quality/Q2_R1/Step4/Q2_R1__Guideline.pdf (Accessed: 11 May 2019).

Iftikhar, A. (2011) *Enzymatic synthesis and evaluation of biodegradable polyesters for microparticulate drug delivery*. Liverpool John Moores

University.

International Agency for Research on Cancer (2018) *Globocan 2018*. Available at: <http://gco.iarc.fr/today> (Accessed: 10 March 2019).

Iqbal, M. *et al.* (2015) 'Double emulsion solvent evaporation techniques used for drug encapsulation', *International Journal of Pharmaceutics*. Elsevier, 496(2), pp. 173–190. doi: 10.1016/J.IJPHARM.2015.10.057.

Irvine, J., Afrose, A. and Islam, N. (2018) 'Formulation and delivery strategies of ibuprofen: challenges and opportunities', *Drug Development and Industrial Pharmacy*, 44(2), pp. 173–183. doi: 10.1080/03639045.2017.1391838.

Islam, M. S. *et al.* (2017) 'Pulmonary aerosol transport and deposition analysis in upper 17 generations of the human respiratory tract', *Journal of Aerosol Science*. Pergamon, 108, pp. 29–43. doi: 10.1016/J.JAEROSCI.2017.03.004.

De luliis, F. *et al.* (2015) 'Taxane induced neuropathy in patients affected by breast cancer: Literature review', *Critical Reviews in Oncology/Hematology*. Elsevier, 96(1), pp. 34–45. doi: 10.1016/J.CRITREVONC.2015.04.011.

Iversen, T., Skotland, T. and Sandvig, K. (2011) 'Endocytosis and intracellular transport of nanoparticles: Present knowledge and need for', *Nano today*, 6(2), pp. 176–185. doi: 10.1016/j.nantod.2011.02.003.

Ivey, J. W., Vehring, R. and Finlay, W. H. (2015) 'Understanding pressurized metered dose inhaler performance', *Expert Opinion on Drug Delivery*, 12(6), pp. 901–916. doi: 10.1517/17425247.2015.984683.

Jan, S. U. *et al.* (2013) 'Synthesis, conjugation and evaluation of some novel polymers and their micro particles for sustained release drug formulations',

Pak. J. Pharm. Sci, 26(4), pp. 741–746.

Jarudilokkul, S., Tongthammachat, A. and Boonamnuyavittaya, V. (2011) 'Preparation of chitosan nanoparticles for encapsulation and release of protein', *Korean Journal of Chemical Engineering*, 28(5), pp. 1247–1251. doi: 10.1007/s11814-010-0485-z.

Jensen, D. K. *et al.* (2012) 'Design of an inhalable dry powder formulation of DOTAP-modified PLGA nanoparticles loaded with siRNA', *Journal of Controlled Release*, 157(1), pp. 141–148. doi: 10.1016/j.jconrel.2011.08.011.

Jiang, R. *et al.* (2018) 'Facile construction and biological imaging of cross-linked fluorescent organic nanoparticles with aggregation-induced emission feature through a catalyst-free azide-alkyne click reaction', *Dyes and Pigments*. Elsevier Ltd, 148, pp. 52–60. doi: 10.1016/j.dyepig.2017.09.005.

Jung, K. H. *et al.* (2015) 'Resveratrol-loaded polymeric nanoparticles suppress glucose metabolism and tumor growth in vitro and in vivo', *International Journal of Pharmaceutics*. Elsevier B.V., 478(1), pp. 251–257. doi: 10.1016/j.ijpharm.2014.11.049.

Juríček, M. *et al.* (2009) 'A novel modular approach to triazole-functionalized phthalocyanines using click chemistry', *Journal of Organic Chemistry*, 74(1), pp. 21–25. doi: 10.1021/jo802078f.

Jyothi, N. V. N. *et al.* (2010) 'Microencapsulation techniques, factors influencing encapsulation efficiency', *Journal of Microencapsulation*, 27(3), pp. 187–197. doi: 10.3109/02652040903131301.

Kamaly, N. *et al.* (2016) 'Degradable Controlled-Release Polymers and

Polymeric Nanoparticles: Mechanisms of Controlling Drug Release.', *Chemical reviews*. NIH Public Access, 116(4), pp. 2602–63. doi: 10.1021/acs.chemrev.5b00346.

Kaminskas, L. M. *et al.* (2014) 'Pulmonary administration of a doxorubicin-conjugated dendrimer enhances drug exposure to lung metastases and improves cancer therapy', *Journal of Controlled Release*. Elsevier B.V., 183, pp. 18–26. doi: 10.1016/j.jconrel.2014.03.012.

Kanehira, Y. *et al.* (2016) 'Tumor distribution and anti-tumor effect of doxorubicin following intrapulmonary administration to mice with metastatic lung tumor', *Journal of Drug Delivery Science and Technology*. Elsevier Ltd, 33(14), pp. 143–148. doi: 10.1016/j.jddst.2016.04.001.

Kang, D. *et al.* (2019) 'Permanent Chemotherapy-Induced Alopecia in Patients with Breast Cancer: A 3-Year Prospective Cohort Study', *The Oncologist*, 24(3), pp. 414–420. doi: 10.1634/theoncologist.2018-0184.

Kantarjian, H. and Patel, Y. (2017) 'High cancer drug prices 4 years later-Progress and prospects', *Cancer*. John Wiley & Sons, Ltd, 123(8), pp. 1292–1297. doi: 10.1002/cncr.30545.

Kapoor, D. N. *et al.* (2015) 'PLGA: A unique polymer for drug delivery', *Therapeutic Delivery*, 6(1), pp. 41–58. doi: 10.4155/tde.14.91.

Karthikeyan, S. *et al.* (2013) 'Anticancer activity of resveratrol-loaded gelatin nanoparticles on NCI-H460 non-small cell lung cancer cells', *Biomedicine & Preventive Nutrition*. Elsevier, 3(1), pp. 64–73. doi: 10.1016/J.BIONUT.2012.10.009.

Karthikeyan, S., Hoti, S. L. and Prasad, N. R. (2015) 'Resveratrol loaded gelatin nanoparticles synergistically inhibits cell cycle progression and constitutive NF-kappaB activation, and induces apoptosis in non-small cell lung cancer cells', *Biomedicine & Pharmacotherapy*. Elsevier Masson, 70, pp. 274–282. doi: 10.1016/J.BIOPHA.2015.02.006.

Keles, H. *et al.* (2015) 'Investigation of factors influencing the hydrolytic degradation of single PLGA microparticles', *Polymer Degradation and Stability*. Elsevier Ltd, 119, pp. 228–241. doi: 10.1016/j.polymdegradstab.2015.04.025.

Kenesei, K. *et al.* (2016) 'Enhanced detection with spectral imaging fluorescence microscopy reveals tissue- and cell-type-specific compartmentalization of surface-modified polystyrene nanoparticles', *Journal of Nanobiotechnology*. BioMed Central, 14(1), pp. 1–14. doi: 10.1186/s12951-016-0210-0.

Key, J. A. and Cairo, C. W. (2011) 'Identification of fluorogenic and quenched benzoxadiazole reactive chromophores', *Dyes and Pigments*. Elsevier Ltd, 88(1), pp. 95–102. doi: 10.1016/j.dyepig.2010.05.007.

Kim, D.Y., Wu, X. and Dordick, J. S. (2003) 'Generation of environmentally compatible polymer libraries via combinatorial biocatalysis.', in *Biocatalysis in Polymer Science*. American Chemical Society, pp. 34–49.

Kim, P. (2007) 'Cost of cancer care: The patient perspective', *Journal of Clinical Oncology*, 25(2), pp. 228–232. doi: 10.1200/JCO.2006.07.9111.

Kline, B. J., Beckman, E. J. and Russell, A. J. (1998) 'One-Step Biocatalytic Synthesis of Linear Polyesters with Pendant Hydroxyl Groups', *Journal of the*

American Chemical Society, 120(37), pp. 9475–9480. doi: 10.1021/ja9808907.

Kobayashi, H., Watanabe, R. and Choyke, P. L. (2013) 'Improving conventional enhanced permeability and retention (EPR) effects; what is the appropriate target?', *Theranostics*. Ivyspring International Publisher, 4(1), pp. 81–9. doi: 10.7150/thno.7193.

Kobayashi, S. (2009) 'Recent developments in lipase-catalyzed synthesis of polyesters', *Macromolecular Rapid Communications*, 30(4–5), pp. 237–266. doi: 10.1002/marc.200800690.

Kocbek, P. *et al.* (2007) 'Targeting cancer cells using PLGA nanoparticles surface modified with monoclonal antibody', *Journal of Controlled Release*, 120(1–2), pp. 18–26. doi: 10.1016/j.jconrel.2007.03.012.

Kolb, H. C., Finn, M. G. and Sharpless, K. B. (2001) 'Click Chemistry: Diverse Chemical Function from a Few Good Reactions', *Angewandte Chemie International Edition*. John Wiley & Sons, Ltd, 40(11), pp. 2004–2021. doi: 10.1002/1521-3773(20010601)40:11<2004::AID-ANIE2004>3.0.CO;2-5.

Kolb, H. C. and Sharpless, K. B. (2003) 'The growing impact of click chemistry on drug discovery', *Drug Discovery Today*. doi: 10.1016/S1359-6446(03)02933-7.

Kolhe, P. *et al.* (2004) 'Hyperbranched Polymer-Drug Conjugates with High Drug Payload for Enhanced Cellular Delivery', *Pharmaceutical Research*, 21(12), pp. 2185–2195. Available at: <https://link.springer.com/content/pdf/10.1007/s11095-004-7670-x.pdf> (Accessed: 3 July 2018).

Kong, B. *et al.* (2011) 'Experimental considerations on the cytotoxicity of nanoparticles.', *Nanomedicine (London, England)*. NIH Public Access, 6(5), pp. 929–41. doi: 10.2217/nnm.11.77.

Koopaei, M. N. *et al.* (2012) 'Enhanced antibacterial activity of roxithromycin loaded pegylated poly lactide-co-glycolide nanoparticles', *DARU, Journal of Pharmaceutical Sciences*, 20(1). doi: 10.1186/2008-2231-20-92.

Koopman, G. *et al.* (1994) 'Annexin V for flow cytometric detection of phosphatidylserine expression on B cells undergoing apoptosis', *Blood. Am Soc Hematology*, 84(5), pp. 1415–1420.

Korhonen, E. *et al.* (2016) 'Cytotoxicity assessment of porous silicon microparticles for ocular drug delivery', *European Journal of Pharmaceutics and Biopharmaceutics*. Elsevier B.V., 100, pp. 1–8. doi: 10.1016/j.ejpb.2015.11.020.

Korzeniewski, C. and Callewaert, D. M. (1983) 'An enzyme-release assay for natural cytotoxicity', *Journal of Immunological Methods*. Elsevier, 64(3), pp. 313–320. doi: 10.1016/0022-1759(83)90438-6.

Kradin, R. L. (2017) 'Anatomy of the Lung', in Kradin, R. L. (ed.) *Understanding Pulmonary Pathology*. Academic Press, pp. 5–19. doi: 10.1016/B978-0-12-801304-5.00002-2.

Kreft, M. E. *et al.* (2015) 'The characterization of the human cell line Calu-3 under different culture conditions and its use as an optimized in vitro model to investigate bronchial epithelial function', *European Journal of Pharmaceutical Sciences*. Elsevier, 69, pp. 1–9. doi: 10.1016/j.ejps.2014.12.017.

Kroll, A. *et al.* (2009) 'Current in vitro methods in nanoparticle risk assessment: limitations and challenges.', *European journal of pharmaceutics and biopharmaceutics: official journal of Arbeitsgemeinschaft für Pharmazeutische Verfahrenstechnik e.V.* Elsevier B.V., 72(2), pp. 370–7. doi: 10.1016/j.ejpb.2008.08.009.

Kumari, A., Yadav, S. K. and Yadav, S. C. (2010) 'Biodegradable polymeric nanoparticles based drug delivery systems', *Colloids and Surfaces B: Biointerfaces*. Elsevier, 75(1), pp. 1–18. Available at: <https://www.sciencedirect.com/science/article/pii/S0927776509004111> (Accessed: 18 July 2018).

Kunda, N. K. *et al.* (2013) 'Nanocarriers targeting dendritic cells for pulmonary vaccine delivery', *Pharmaceutical Research*, 30(2), pp. 325–341. doi: 10.1007/s11095-012-0891-5.

Kunda, N. K. (2014) *Dry powder inhalation of pneumococcal vaccine using polymeric nanoparticles as carriers*. Liverpool John Moores University.

Kunda, N. K., Alfagih, I. M., Dennison, S. R., Tawfeek, H. M., *et al.* (2015) 'Bovine Serum Albumin Adsorbed PGA-co-PDL Nanocarriers for Vaccine Delivery via Dry Powder Inhalation', *Pharmaceutical Research*, 32(4), pp. 1341–1353. doi: 10.1007/s11095-014-1538-5.

Kunda, N. K., Alfagih, I. M., Dennison, S. R., Somavarapu, S., *et al.* (2015) 'Dry powder pulmonary delivery of cationic PGA-co-PDL nanoparticles with surface adsorbed model protein', *International Journal of Pharmaceutics*. Elsevier, 492(1–2), pp. 213–222. doi: 10.1016/j.ijpharm.2015.07.015.

Laaksonen, T. *et al.* (2007) 'Failure of MTT as a toxicity testing agent for

mesoporous silicon microparticles', *Chemical Research in Toxicology*, 20(12), pp. 1913–1918. doi: 10.1021/tx700326b.

Lakshmi, S. *et al.* (2019) 'In vitro and in vivo studies of 5,7-dihydroxy flavones isolated from *Alpinia galanga* (L.) against human lung cancer and ascetic lymphoma', *Medicinal Chemistry Research*. Springer US, 28(1), pp. 39–51. doi: 10.1007/s00044-018-2260-3.

Learoyd, T. P. *et al.* (2008) 'Modified release of beclometasone dipropionate from chitosan-based spray-dried respirable powders', *Powder Technology*, 187(3), pp. 231–238. doi: 10.1016/j.powtec.2008.02.015.

Learoyd, T. P. *et al.* (2009) 'Sustained delivery by leucine-modified chitosan spray-dried respirable powders', *International Journal of Pharmaceutics*, 372(1–2), pp. 97–104. doi: 10.1016/j.ijpharm.2009.01.017.

Lee, W.-H. *et al.* (2015) 'Inhalation of nanoparticle-based drug for lung cancer treatment: Advantages and challenges', *Asian Journal of Pharmaceutical Sciences*. Elsevier, 10(6), pp. 481–489. doi: 10.1016/J.AJPS.2015.08.009.

Li, J. *et al.* (2016) 'Polyethyleneglycol-Modified Poly(D,L-lactide-co-glycolide) Loaded Resveratrol Nanoparticles Characterization and Their Anti-cancer Activities', *Journal of Nanoscience and Nanotechnology*, 16(9), pp. 9477–9481. doi: 10.1166/jnn.2016.12368.

Lipiäinen, T. *et al.* (2018) 'Comparison of melibiose and trehalose as stabilising excipients for spray-dried β -galactosidase formulations', *International Journal of Pharmaceutics*, 543(1–2), pp. 21–28. doi: 10.1016/j.ijpharm.2018.03.035.

Liu, K. *et al.* (2017) 'Paclitaxel and quercetin nanoparticles co-loaded in

microspheres to prolong retention time for pulmonary drug delivery.', *International journal of nanomedicine*. Dove Press, 12, pp. 8239–8255. doi: 10.2147/IJN.S147028.

Liu, Q. *et al.* (2019) 'Influence of stabilizer type and concentration on the lung deposition and retention of resveratrol nanosuspension-in-microparticles', *International Journal of Pharmaceutics*. Elsevier B.V., 569, p. 118562. doi: 10.1016/j.ijpharm.2019.118562.

Loira-Pastoriza, C., Todoroff, J. and Vanbever, R. (2014) 'Delivery strategies for sustained drug release in the lungs', *Advanced Drug Delivery Reviews*. Elsevier B.V., 75, pp. 81–91. doi: 10.1016/j.addr.2014.05.017.

Lord, S. J. *et al.* (2010) 'Azido Push–Pull Fluorogens Photoactivate to Produce Bright Fluorescent Labels †', *The Journal of Physical Chemistry B*. NIH Public Access, 114(45), pp. 14157–14167. doi: 10.1021/jp907080r.

Lucas, I. and Kolodziej, H. (2015) 'Trans-Resveratrol Induces Apoptosis through ROS-Triggered Mitochondria-Dependent Pathways in A549 Human Lung Adenocarcinoma Epithelial Cells', *Planta Medica*. Georg Thieme Verlag KG, 81(12/13), pp. 1038–1044. doi: 10.1055/s-0035-1546129.

Luo, Q. *et al.* (2019) 'Lung cancer mortality in Australia in the twenty-first century: How many lives can be saved with effective tobacco control?', *Lung Cancer*. Elsevier, 130, pp. 208–215. doi: 10.1016/J.LUNGCAN.2019.02.028.

Luque-Michel, E. *et al.* (2017) 'Clinical advances of nanocarrier-based cancer therapy and diagnostics', *Expert Opinion on Drug Delivery*. Taylor & Francis, 14(1), pp. 75–92. doi: 10.1080/17425247.2016.1205585.

Maeda, H. (2001) 'The enhanced permeability and retention (EPR) effect in tumor vasculature: The key role of tumor-selective macromolecular drug targeting', *Advances in Enzyme Regulation*, 41(1), pp. 189–207. doi: 10.1016/S0065-2571(00)00013-3.

Maguire, R. *et al.* (2018) 'Development and preliminary testing of a brief clinical tool to enable daily monitoring of chemotherapy toxicity: The Daily Chemotherapy Toxicity self-Assessment Questionnaire', *European Journal of Cancer Care*, 27(6), pp. 1–10. doi: 10.1111/ecc.12890.

Mahmud, A. and Discher, D. E. (2011) 'Lung vascular targeting through inhalation delivery: Insight from filamentous viruses and other shapes', *IUBMB Life*, pp. 607–612. doi: 10.1002/iub.481.

Maiorano, G. *et al.* (2010) 'Effects of cell culture media on the dynamic formation of protein-nanoparticle complexes and influence on the cellular response', *ACS Nano*, 4(12), pp. 7481–7491. doi: 10.1021/nn101557e.

Makadia, H. K. and Siegel, S. J. (2011) 'Poly Lactic-co-Glycolic Acid (PLGA) as biodegradable controlled drug delivery carrier', *Polymers*, 3(3), pp. 1377–1397. doi: 10.3390/polym3031377.

Malcolmson, R. J. and Embleton, J. K. (1998) 'Dry powder formulations for pulmonary delivery', *Pharmaceutical Science and Technology Today*, 1(9), pp. 394–398. doi: 10.1016/S1461-5347(98)00099-6.

Mansour, H. M., Rhee, Y.-S. and Wu, X. (2009) 'Nanomedicine in pulmonary delivery.', *International journal of nanomedicine*. Dove Press, 4, pp. 299–319. Available at: <http://www.ncbi.nlm.nih.gov/pubmed/20054434> (Accessed: 19 July 2018).

Marple, V. A. *et al.* (2003) *Next Generation Pharmaceutical Impactor (A New Impactor for Pharmaceutical Inhaler Testing). Part I: Design*, *JOURNAL OF AEROSOL MEDICINE*. Available at: <https://pdfs.semanticscholar.org/c58a/a74fb96080cf4a507751e67add3c9fa767e4.pdf> (Accessed: 30 April 2019).

Martins, C. *et al.* (2018) 'Functionalizing PLGA and PLGA Derivatives for Drug Delivery and Tissue Regeneration Applications', *Advanced Healthcare Materials*, 7(1), pp. 1–24. doi: 10.1002/adhm.201701035.

Masood, F. (2016) 'Polymeric nanoparticles for targeted drug delivery system for cancer therapy', *Materials Science and Engineering C*. Elsevier B.V., 60, pp. 569–578. doi: 10.1016/j.msec.2015.11.067.

Matos, M. *et al.* (2014) 'Preparation of water-in-oil-in-water (W1/O/W2) double emulsions containing trans-resveratrol', *Colloids and Surfaces A: Physicochemical and Engineering Aspects*. Elsevier B.V., 442, pp. 69–79. doi: 10.1016/j.colsurfa.2013.05.065.

Matuszak, J. *et al.* (2016) 'Nanoparticles for intravascular applications: Pcharacterization and cytotoxicity testing', *Nanomedicine*, 11(6), pp. 597–616. doi: 10.2217/nnm.15.216.

McKenzie, H. *et al.* (2011) 'Chemotherapy outpatients' unplanned presentations to hospital: a retrospective study', *Supportive Care in Cancer*. Springer-Verlag, 19(7), pp. 963–969. doi: 10.1007/s00520-010-0913-y.

Meenach, S. A. *et al.* (2013) 'Characterization and aerosol dispersion performance of advanced spray-dried chemotherapeutic PEGylated phospholipid particles for dry powder inhalation delivery in lung cancer',

European Journal of Pharmaceutical Sciences. Elsevier B.V., 49(4), pp. 699–711. doi: 10.1016/j.ejps.2013.05.012.

Menon, J. U. *et al.* (2014) 'Polymeric nanoparticles for pulmonary protein and DNA delivery', *Acta Biomaterialia*. Elsevier, 10(6), pp. 2643–2652. doi: 10.1016/J.ACTBIO.2014.01.033.

Merchant, Z. *et al.* (2014) 'Engineering hydrophobically modified chitosan for enhancing the dispersion of respirable microparticles of levofloxacin', *European Journal of Pharmaceutics and Biopharmaceutics*. Elsevier B.V., 88(3), pp. 816–829. doi: 10.1016/j.ejpb.2014.09.005.

Minoshima, M. and Kikuchi, K. (2017) 'Photostable and photoswitching fluorescent dyes for super-resolution imaging', *Journal of Biological Inorganic Chemistry*, 22(5), pp. 639–652. doi: 10.1007/s00775-016-1435-y.

Mitjans, M., Nogueira-Librelo, D. R. and Vinardell, M. P. (2018) 'Nanotoxicity In Vitro: Limitations of the Main Cytotoxicity Assays', in *Nanotoxicology*. CRC Press, pp. 171–192.

Mittal, G. *et al.* (2007) 'Estradiol loaded PLGA nanoparticles for oral administration: Effect of polymer molecular weight and copolymer composition on release behavior in vitro and in vivo', *Journal of Controlled Release*, 119(1), pp. 77–85. doi: 10.1016/j.jconrel.2007.01.016.

Mols, F. *et al.* (2014) 'Chemotherapy-induced peripheral neuropathy and its association with quality of life: a systematic review', *Supportive Care in Cancer*. Springer Berlin Heidelberg, 22(8), pp. 2261–2269. doi: 10.1007/s00520-014-2255-7.

Monteillier, A. *et al.* (2018) 'Intranasal administration of resveratrol successfully prevents lung cancer in A/J mice', *Scientific Reports*. Nature Publishing Group, 8(1), p. 14257. doi: 10.1038/s41598-018-32423-0.

Moore, T. L. *et al.* (2019) 'Nanoparticle administration method in cell culture alters particle-cell interaction', *Scientific Reports*. Springer US, 9(1), pp. 1–9. doi: 10.1038/s41598-018-36954-4.

Muhsin, M. D. A. *et al.* (2016) 'Effects of Chemical Conjugation of L-Leucine to Chitosan on Dispersibility and Controlled Release of Drug from a Nanoparticulate Dry Powder Inhaler Formulation', *Molecular Pharmaceutics*, 13(5), pp. 1455–1466. doi: 10.1021/acs.molpharmaceut.5b00859.

Muller, A. G. *et al.* (2019) 'Delivery of natural phenolic compounds for the potential treatment of lung cancer', *DARU Journal of Pharmaceutical Sciences*. Springer, p. 1. doi: 10.1007/s40199-019-00267-2.

Munshi, S., Twining, R. C. and Dahl, R. (2014) 'Alamar blue reagent interacts with cell-culture media giving different fluorescence over time: Potential for false positives', *Journal of Pharmacological and Toxicological Methods*. Elsevier Inc., 70(2), pp. 195–198. doi: 10.1016/j.vascn.2014.06.005.

Muralidharan, P. *et al.* (2015) 'Inhalable nanoparticulate powders for respiratory delivery', *Nanomedicine: Nanotechnology, Biology and Medicine*, 11(5), pp. 1189–1199. doi: 10.1016/j.nano.2015.01.007.

Nachlas, M. M. *et al.* (1960) 'The determination of lactic dehydrogenase with a tetrazolium salt', *Analytical Biochemistry*, 1(4–5), pp. 317–326. doi: 10.1016/0003-2697(60)90029-4.

Nagavarma, B. V. N. *et al.* (2012) 'Different techniques for preparation of polymeric nanoparticles- A review', *Asian Journal of Pharmaceutical and Clinical Research*, 5(SUPPL. 3), pp. 16–23.

Namekawa, S., Uyama, H. and Kobayashi, S. (2000) 'Enzymatic synthesis of polyesters from lactones, dicarboxylic acid divinyl esters, and glycols through combination of ring-opening polymerization and polycondensation.', *Biomacromolecules*, 1(3), pp. 335–338. doi: 10.1021/bm000030u.

Nassir, A. M. *et al.* (2018) 'Resveratrol-loaded PLGA nanoparticles mediated programmed cell death in prostate cancer cells', *Saudi Pharmaceutical Journal*. Elsevier, 26(6), pp. 876–885. Available at: <https://linkinghub.elsevier.com/retrieve/pii/S1319016418300720> (Accessed: 10 October 2018).

Neves, A. R. *et al.* (2016) 'Nanoscale delivery of resveratrol towards enhancement of supplements and nutraceuticals', *Nutrients*. MDPI AG, 8(3). doi: 10.3390/nu8030131.

NHS (2011) *Cancer survival rates 'threatened by rising cost' - NHS*. Available at: <https://www.nhs.uk/news/cancer/cancer-survival-rates-threatened-by-rising-cost/> (Accessed: 18 May 2019).

Niazvand, F. *et al.* (2019) 'Effects of Quercetin-loaded nanoparticles on MCF-7 human breast cancer cells', *Medicina (Lithuania)*, 55(4), pp. 1–15. doi: 10.3390/medicina55040114.

Nicolas, J. *et al.* (2013) 'Design, functionalization strategies and biomedical applications of targeted biodegradable/biocompatible polymer-based nanocarriers for drug delivery', *Chemical Society Reviews*, 42(3), pp. 1147–

1235. doi: 10.1039/c2cs35265f.

Nieto-Orellana, A. *et al.* (2018) 'Dry-powder formulations of non-covalent protein complexes with linear or miktoarm copolymers for pulmonary delivery', *International Journal of Pharmaceutics*. Elsevier, 540(1–2), pp. 78–88. doi: 10.1016/J.IJPHARM.2018.02.008.

Nursing Times (2002) *Home chemotherapy: NHS and independent sector collaboration*, *Nursing Times*. Available at: <https://www.nursingtimes.net/home-chemotherapy-nhs-and-independent-sector-collaboration/206425.article> (Accessed: 18 May 2019).

O'Brien, J. *et al.* (2000) 'Alamar blue,O'brain et al, 2000.pdf', *The Federation of European Biochemical Societies Journal*, pp. 5421–6. Available at: <http://www.ncbi.nlm.nih.gov/pubmed/10951200>.

O'Neill, C. and Wallis, C. (2009) 'Home healthcare: Emerging evidence for NHS commissioners', *Journal of Care Services Management*. Taylor & Francis, 3(4), pp. 357–363. doi: 10.1179/csm.2009.3.4.357.

Ochsner, A. (1973) 'My first recognition of the relationship of smoking and lung cancer', *Preventive Medicine*, 2(4), pp. 611–614. doi: 10.1016/0091-7435(73)90059-5.

Oh, N. and Park, J.-H. (2014) 'Endocytosis and exocytosis of nanoparticles in mammalian cells.', *International journal of nanomedicine*. Dove Press, 9 Suppl 1(Suppl 1), pp. 51–63. doi: 10.2147/IJN.S26592.

Ong, K. J. *et al.* (2014) 'Widespread nanoparticle-assay interference: Implications for nanotoxicity testing', *PLoS ONE*, 9(3). doi:

10.1371/journal.pone.0090650.

Ong, P. and Ost, D. (2017) 'Lung cancer epidemiologic changes: Implications in diagnosis and therapy', *Interventions in Pulmonary Medicine*, pp. 323–332. doi: 10.1007/978-3-319-58036-4_20.

Oostingh, G. J. *et al.* (2011) 'Problems and challenges in the development and validation of human cell-based assays to determine nanoparticle-induced immunomodulatory effects', *Particle and Fibre Toxicology*. BioMed Central, 8(1), p. 8. doi: 10.1186/1743-8977-8-8.

Ostuni, R. *et al.* (2015) 'Macrophages and cancer: From mechanisms to therapeutic implications', *Trends in Immunology*. Elsevier Ltd, 36(4), pp. 229–239. doi: 10.1016/j.it.2015.02.004.

Pagels, R. F. and Prud'Homme, R. K. (2015) 'Polymeric nanoparticles and microparticles for the delivery of peptides, biologics, and soluble therapeutics', *Journal of Controlled Release*. Elsevier, 219, pp. 519–535. doi: 10.1016/j.jconrel.2015.09.001.

Palacio, J., Orozco, V. H. and López, B. L. (2011) 'Effect of the molecular weight on the physicochemical properties of poly(lactic acid) nanoparticles and on the amount of ovalbumin adsorption', in *Journal of the Brazilian Chemical Society*, pp. 2304–2311. doi: 10.1590/s0103-50532011001200010.

Panariti, A., Miserocchi, G. and Rivolta, I. (2012) 'The effect of nanoparticle uptake on cellular behavior: disrupting or enabling functions?', *Nanotechnology, science and applications*. Dove Press, 5, pp. 87–100. doi: 10.2147/NSA.S25515.

Park, M. J. *et al.* (2018) 'Hydrophilic polyvinyl alcohol coating on hydrophobic electrospun nanofiber membrane for high performance thin film composite forward osmosis membrane', *Desalination*. Elsevier, 426(October 2017), pp. 50–59. doi: 10.1016/j.desal.2017.10.042.

Parkin, D. M., Boyd, L. and Walker, L. C. (2011) '16. The fraction of cancer attributable to lifestyle and environmental factors in the UK in 2010', *British Journal of Cancer*. Nature Publishing Group, 105(S2), pp. S77–S81. doi: 10.1038/bjc.2011.489.

Partikel, K. *et al.* (2019) 'Effect of nanoparticle size and PEGylation on the protein corona of PLGA nanoparticles', *European Journal of Pharmaceutics and Biopharmaceutics*. Elsevier, 141(November 2018), pp. 70–80. doi: 10.1016/j.ejpb.2019.05.006.

Patel, B., Patel, J. and Chakraborty, S. (2014) 'Review of Patents and Application of Spray Drying in Pharmaceutical, Food and Flavor Industry', *Recent Patents on Drug Delivery & Formulation*, 8(1), pp. 63–78. doi: 10.2174/1872211308666140211122012.

Patel, J. and Patel, A. (2015) 'Artificial Neural Networking in Controlled Drug Delivery', in *Artificial Neural Network for Drug Design, Delivery and Disposition*. Elsevier Inc., pp. 195–218. doi: 10.1016/B978-0-12-801559-9.00010-7.

Patel, K. R. *et al.* (2011) 'Clinical trials of resveratrol', *Ann. N.Y. Acad. Sci*, 1215(1), pp. 161–169. doi: 10.1111/j.1749-6632.2010.05853.x.

Patrulea, V. *et al.* (2015) 'Chitosan as a starting material for wound healing applications', *European Journal of Pharmaceutics and Biopharmaceutics*, 97,

pp. 417–426. doi: 10.1016/j.ejpb.2015.08.004.

Peddireddy, V. (2016) 'Lung cancer incidence in never smokers: Genetic and gender basis', *Gene Reports*. Elsevier, 4, pp. 198–207. doi: 10.1016/J.GENREP.2016.06.003.

Peng, H. S. and Chiu, D. T. (2015) 'Soft fluorescent nanomaterials for biological and biomedical imaging', *Chemical Society Reviews*, 44(14), pp. 4699–4722. doi: 10.1039/c4cs00294f.

Peng, R.-M. *et al.* (2018) 'Oral delivery system enhanced the bioavailability of stilbenes: Resveratrol and pterostilbene', *BioFactors*, 44(1), pp. 5–15. doi: 10.1002/biof.1405.

Peng, T. *et al.* (2016) 'Influence of physical properties of carrier on the performance of dry powder inhalers', *Acta Pharmaceutica Sinica B*. Elsevier, 6(4), pp. 308–318. doi: 10.1016/J.APSB.2016.03.011.

Peppas, N. A. and Narasimhan, B. (2014) 'Mathematical models in drug delivery: How modeling has shaped the way we design new drug delivery systems', *Journal of Controlled Release*. Elsevier B.V., 190, pp. 75–81. doi: 10.1016/j.jconrel.2014.06.041.

Peppercorn, J. (2014) 'The financial burden of cancer care: Do patients in the US know what to expect?', *Expert Review of Pharmacoeconomics and Outcomes Research*, 14(6), pp. 835–842. doi: 10.1586/14737167.2014.963558.

Pereira, E. D. *et al.* (2016) 'Influence of PLGA and PLGA-PEG on the dissolution profile of oxaliplatin', *Polímeros*. ABPol, 26(2), pp. 137–143. doi:

10.1590/0104-1428.2323.

Perkins, E. (2015) *Synthesis of PGA-co-PDL-co- PEG Co-polymers for Potential Use in Drug Delivery Applications*. Liverpool John Moores University.

Pickens, C. J. *et al.* (2018) 'Practical Considerations, Challenges, and Limitations of Bioconjugation via Azide-Alkyne Cycloaddition', *Bioconjugate Chemistry*, 29(3), pp. 686–701. doi: 10.1021/acs.bioconjchem.7b00633.

Pilcer, G. and Amighi, K. (2010) 'Formulation strategy and use of excipients in pulmonary drug delivery', *International Journal of Pharmaceutics*. Elsevier, 392(1–2), pp. 1–19. doi: 10.1016/J.IJPHARM.2010.03.017.

Pilleron, S. *et al.* (2018) 'Global cancer incidence in older adults, 2012 and 2035: A population-based study'. doi: 10.1002/ijc.31664.

Poojari, Y. and Clarson, S. J. (2010) 'Lipase catalyzed synthesis and thermal properties of poly(dimethylsiloxane)-poly(ethylene glycol) amphiphilic block copolymers', *Journal of Inorganic and Organometallic Polymers and Materials*, 20(1), pp. 46–52. doi: 10.1007/s10904-009-9304-6.

Prabha, S. *et al.* (2016) 'Effect of size on biological properties of nanoparticles employed in gene delivery', *Artificial Cells, Nanomedicine and Biotechnology*, 44(1), pp. 83–91. doi: 10.3109/21691401.2014.913054.

Presolski, S. I., Hong, V. P. and Finn, M. G. (2011) 'Copper-Catalyzed Azide-Alkyne Click Chemistry for Bioconjugation', *Current Protocols in Chemical Biology*. John Wiley & Sons, Inc., 3(4), pp. 153–162. doi: 10.1002/9780470559277.ch110148.Copper-Catalyzed.

Prinz, F., Schlange, T. and Asadullah, K. (2011) 'Believe it or not: How much

can we rely on published data on potential drug targets?', *Nature Reviews Drug Discovery*. Nature Publishing Group, 10(9), pp. 712–713. doi: 10.1038/nrd3439-c1.

Raaschou-Nielsen, O. *et al.* (2011) 'Lung Cancer Incidence and Long-Term Exposure to Air Pollution from Traffic', *Environmental Health Perspectives*, 119(6), pp. 860–865. doi: 10.1289/ehp.1002353.

Raaschou-Nielsen, O. *et al.* (2013) 'Air pollution and lung cancer incidence in 17 European cohorts: prospective analyses from the European Study of Cohorts for Air Pollution Effects (ESCAPE)', *The Lancet Oncology*. Elsevier, 14(9), pp. 813–822. doi: 10.1016/S1470-2045(13)70279-1.

Rabbani, N. R. and Seville, P. C. (2005) 'The influence of formulation components on the aerosolisation properties of spray-dried powders', *Journal of Controlled Release*, 110(1), pp. 130–140. doi: 10.1016/j.jconrel.2005.09.004.

Rahimian, S. *et al.* (2015) 'Near-infrared labeled, ovalbumin loaded polymeric nanoparticles based on a hydrophilic polyester as model vaccine: In vivo tracking and evaluation of antigen-specific CD8+ T cell immune response', *Biomaterials*. Elsevier, 37, pp. 469–477. doi: 10.1016/J.BIOMATERIALS.2014.10.043.

Rampersad, S. N. (2012) 'Multiple applications of alamar blue as an indicator of metabolic function and cellular health in cell viability bioassays', *Sensors (Switzerland)*, 12(9), pp. 12347–12360. doi: 10.3390/s120912347.

Ranjan, A. P. *et al.* (2011) 'A sustained release formulation of chitosan modified PLCL:poloxamer blend nanoparticles loaded with optical agent for

animal imaging', *Nanotechnology*, 22(29). doi: 10.1088/0957-4484/22/29/295104.

Rauf, A. *et al.* (2018) 'Resveratrol as an anti-cancer agent: A review', *Critical Reviews in Food Science and Nutrition*. Taylor & Francis, 58(9), pp. 1428–1447. doi: 10.1080/10408398.2016.1263597.

Ray, L. (2019) 'Polymeric Nanoparticle-Based Drug/Gene Delivery for Lung Cancer', *Nanotechnology-Based Targeted Drug Delivery Systems for Lung Cancer*. Academic Press, pp. 77–93. doi: 10.1016/B978-0-12-815720-6.00004-6.

Reis, C. P. *et al.* (2006) 'Nanoencapsulation I. Methods for preparation of drug-loaded polymeric nanoparticles', *Nanomedicine: Nanotechnology, Biology, and Medicine*, 2, pp. 8–21. doi: 10.1016/j.nano.2005.12.003.

Rejman, J. *et al.* (2004) 'Size-dependent internalization of particles via the pathways of clathrin- and caveolae-mediated endocytosis', *Biochemical Journal*, 377(1), pp. 159–169. doi: 10.1042/BJ20031253.

Rezazadeh, M. *et al.* (2018) 'Preparation and Characterization of Spray-Dried Inhalable Powders Containing Polymeric Micelles for Pulmonary Delivery of Paclitaxel in Lung Cancer', *Journal of Pharmacy & Pharmaceutical Sciences*, 21(1s), p. 200. doi: 10.18433/jpps30048.

Robin, M. P. and O'Reilly, R. K. (2015) 'Strategies for preparing fluorescently labelled polymer nanoparticles', *Polymer International*, 64(2), pp. 174–182. doi: 10.1002/pi.4842.

Robinson, K., Mock, C. and Liang, D. (2015) 'Pre-formulation studies of

resveratrol', *Drug Development and Industrial Pharmacy*. Taylor and Francis Ltd., 41(9), pp. 1464–1469. doi: 10.3109/03639045.2014.958753.

Rodrigues, T. C. *et al.* (2018) 'Mucosal immunization with PspA (Pneumococcal surface protein A)-adsorbed nanoparticles targeting the lungs for protection against pneumococcal infection.', *PloS one*. Public Library of Science, 13(1), p. e0191692. doi: 10.1371/journal.pone.0191692.

Rubio-Gonzalez, B. *et al.* (2018) 'Pathogenesis and treatment options for chemotherapy-induced alopecia: a systematic review', *international journal of dermatology*, 57, pp. 1417–1424. doi: 10.1111/ijd.13906.

Saha, B. *et al.* (2018) 'Resveratrol analogue, trans-4,4'-dihydroxystilbene (DHS), inhibits melanoma tumor growth and suppresses its metastatic colonization in lungs', *Biomedicine and Pharmacotherapy*. Elsevier, 107(August), pp. 1104–1114. doi: 10.1016/j.biopha.2018.08.085.

Sahay, G., Alakhova, D. Y. and Kabanov, A. V (2010) 'Endocytosis of nanomedicines.', *Journal of controlled release: official journal of the Controlled Release Society*. NIH Public Access, 145(3), pp. 182–95. doi: 10.1016/j.jconrel.2010.01.036.

Saini, B. and Sinha, M. K. (2019) 'Effect of hydrophilic poly(ethylene glycol) methyl ether additive on the structure, morphology, and performance of polysulfone flat sheet ultrafiltration membrane', *Journal of Applied Polymer Science*, 136(10), pp. 1–14. doi: 10.1002/app.47163.

Sakamuru, S., Attene-Ramos, M. S. and Xia, M. (2016) 'Mitochondrial membrane potential assay', in *High-Throughput Screening Assays in Toxicology*. Springer, pp. 161–172. doi: 10.1007/978-1-4939-6346-1.

Samet, J. M. *et al.* (2009) 'Lung cancer in never smokers: clinical epidemiology and environmental risk factors', *Clinical Cancer Research*, 15(18), pp. 5626–5671. doi: 10.1158/1078-0432.CCR-09-0376.

Sanchez, L., Yi, Y. and Yu, Y. (2016) 'Effect of partial PEGylation on particle uptake by macrophages †', *Nanoscale*, 9. doi: 10.1039/c6nr07353k.

Sanders, M. (2011) 'Pulmonary Drug Delivery: An Historical Overview', in Smyth, H. D. C. and Hickey, A. J. (eds) *Controlled Pulmonary Drug Delivery*. New York, NY: Springer New York, pp. 51–73. doi: 10.1007/978-1-4419-9745-6_3.

Sanna, V. *et al.* (2015) 'Effect of chitosan concentration on PLGA microcapsules for controlled release and stability of resveratrol', *International Journal of Biological Macromolecules*. Elsevier, 72, pp. 531–536. doi: 10.1016/j.ijbiomac.2014.08.053.

Sansone, F. *et al.* (2018) 'Particle technology applied to a lactose/NaCMC blend: Production and characterization of a novel and stable spray-dried ingredient', *Powder Technology*. Elsevier B.V., 329(May), pp. 304–312. doi: 10.1016/j.powtec.2018.01.043.

Santos, A. C. *et al.* (2019) 'Targeting Cancer Via Resveratrol-Loaded Nanoparticles Administration: Focusing on In Vivo Evidence', *The AAPS Journal*. Springer International Publishing, 21(4), p. 57. doi: 10.1208/s12248-019-0325-y.

Santos, D. *et al.* (2017) 'Spray Drying: An Overview', in Pignatello, R. (ed.) *Biomaterials - Physics and Chemistry - New Edition*. InTech. doi: 10.5772/intechopen.72247.

Sarker, S. D. and Nahar, L. (2019) *Chemistry for Pharmacy Students: General, Organic, and Natural Product Chemistry*, *Chemistry for Pharmacy Students: General, Organic, and Natural Product Chemistry*. Hoboken, NJ: Wiley. doi: 10.1002/9781118687529.

Sayes, C. M. (2020) 'Nanotoxicology: Developing a Responsible Technology', in *Women in Nanotechnology*. Springer, pp. 43–55. doi: 10.1007/978-3-030-19951-7.

Sayes, C. M., Reed, K. L. and Warheit, D. B. (2007) 'Assessing Toxicity of Fine and Nanoparticles: Comparing In Vitro Measurements to In Vivo Pulmonary Toxicity Profiles', *Toxicological Sciences*. Narnia, 97(1), pp. 163–180. doi: 10.1093/toxsci/kfm018.

Schulze, C. *et al.* (2008) 'Not ready to use overcoming pitfalls when dispersing nanoparticles in physiological media', *Nanotoxicology*. Taylor & Francis, 2(June), pp. 51–61. doi: 10.1080/17435390802018378.

Schuster, B. S. *et al.* (2013) 'Nanoparticle diffusion in respiratory mucus from humans without lung disease', *Biomaterials*. NIH Public Access, 34(13), p. 3439. doi: 10.1016/J.BIOMATERIALS.2013.01.064.

Semenova, E. A., Nagel, R. and Berns, A. (2015) 'Origins, genetic landscape, and emerging therapies of small cell lung cancer', *Genes & development*, 29(14), pp. 1447–1462. doi: 10.1101/gad.263145.

Shagholani, H., Ghoreishi, S. M. and Mousazadeh, M. (2015) 'Improvement of interaction between PVA and chitosan via magnetite nanoparticles for drug delivery application', *International Journal of Biological Macromolecules*. Elsevier, 78, pp. 130–136. doi: 10.1016/j.ijbiomac.2015.02.042.

- Sham, J. O. H. *et al.* (2004) 'Formulation and characterization of spray-dried powders containing nanoparticles for aerosol delivery to the lung', *International Journal of Pharmaceutics*. Elsevier, 269(2), pp. 457–467. doi: 10.1016/j.ijpharm.2003.09.041.
- Shao, C. *et al.* (2011) 'Acid-base jointly promoted copper(I)-catalyzed azide-alkyne cycloaddition', *Journal of Organic Chemistry*, 76(16), pp. 6832–6836. doi: 10.1021/jo200869a.
- Sharma, S. *et al.* (2016) 'PLGA-based nanoparticles: A new paradigm in biomedical applications', *TrAC - Trends in Analytical Chemistry*. Elsevier B.V., 80, pp. 30–40. doi: 10.1016/j.trac.2015.06.014.
- Shen, J. *et al.* (2018) 'Resveratrol delivery by ultrasound-mediated nanobubbles targeting nucleus pulposus cells', *Nanomedicine*, 13(12), pp. 1433–1446. doi: 10.2217/nnm-2018-0019.
- Shen, S. *et al.* (2017a) 'High drug-loading nanomedicines: progress, current status, and prospects.', *International journal of nanomedicine*. Dove Press, 12, pp. 4085–4109. doi: 10.2147/IJN.S132780.
- Shen, S. *et al.* (2017b) 'High drug-loading nanomedicines: Progress, current status, and prospects', *International Journal of Nanomedicine*. Dove Medical Press Ltd., pp. 4085–4109. doi: 10.2147/IJN.S132780.
- Shlomovitz, I., Speir, M. and Gerlic, M. (2019) 'Flipping the dogma – phosphatidylserine in non-apoptotic cell death', *Cell Communication and Signaling*. Cell Communication and Signaling, 17(1), pp. 1–12.
- Shukla, S. *et al.* (2005) 'Porous gold nanospheres by controlled

transmetalation reaction: A novel material for application in cell imaging', *Chemistry of Materials*, 17(20), pp. 5000–5005. doi: 10.1021/cm051165f.

Shwetha, H. R. *et al.* (2019) 'Ex vivo culture of oral keratinocytes using direct explant cell culture technique.', *Journal of oral and maxillofacial pathology : JOMFP*. Wolters Kluwer -- Medknow Publications, 23(2), pp. 243–247. doi: 10.4103/jomfp.JOMFP_105_19.

Siddiqui, I. A. *et al.* (2009) 'Introducing Nanochemoprevention as a Novel Approach for Cancer Control: Proof of Principle with Green Tea Polyphenol Epigallocatechin-3-Gallate'. doi: 10.1158/0008-5472.CAN-08-3978.

Singh, C. K., Ndiaye, M. A. and Ahmad, N. (2015) 'Resveratrol and cancer: Challenges for clinical translation', *Biochimica et Biophysica Acta (BBA) - Molecular Basis of Disease*. Elsevier, 1852(6), pp. 1178–1185. doi: 10.1016/J.BBADIS.2014.11.004.

Singh, G. and Pai, R. S. (2014) 'Optimized PLGA nanoparticle platform for orally dosed *trans*-resveratrol with enhanced bioavailability potential', *Expert Opinion on Drug Delivery*. Taylor & Francis, 11(5), pp. 647–659. doi: 10.1517/17425247.2014.890588.

Singh, S. K. *et al.* (2017) 'Preparation and in-vitro/in-vivo characterization of *trans*-resveratrol nanocrystals for oral administration', *Drug Delivery and Translational Research*. Springer US, 7(3), pp. 395–407. doi: 10.1007/s13346-017-0362-y.

Singh, S. K., Lillard, J. W. and Singh, R. (2018) 'Reversal of drug resistance by planetary ball milled (PBM) nanoparticle loaded with resveratrol and docetaxel in prostate cancer', *Cancer Letters*. Elsevier, 427, pp. 49–62. doi:

10.1016/J.CANLET.2018.04.017.

Siu, F. Y. *et al.* (2018) 'Galactosylated PLGA nanoparticles for the oral delivery of resveratrol: enhanced bioavailability and in vitro anti-inflammatory activity.', *International journal of nanomedicine*. Dove Press, 13, pp. 4133–4144. doi: 10.2147/IJN.S164235.

Sivalingam, G. and Madras, G. (2004) 'Modeling of Lipase Catalyzed Ring-Opening Polymerization of ϵ -Caprolactone', *Biomacromolecules*, 5(2), pp. 603–609. doi: 10.1021/bm0344405.

Smith, B. D. *et al.* (2009) 'Future of Cancer Incidence in the United States: Burdens Upon an Aging, Changing Nation', *Journal of Clinical Oncology*, 27(17), pp. 2758–2765. doi: 10.1200/JCO.2008.20.8983.

Soares, P. I. P. *et al.* (2016) 'Chitosan-based nanoparticles as drug delivery systems for doxorubicin: Optimization and modelling', *Carbohydrate Polymers*. Elsevier Ltd., 147, pp. 304–312. doi: 10.1016/j.carbpol.2016.03.028.

Soleas, G. J., Yan, J. and Goldberg, D. M. (2001a) 'Measurement of trans-resveratrol,(+)-catechin, and quercetin in rat and human blood and urine by gas chromatography with mass selective detection', in *Methods in enzymology*. Elsevier, pp. 130–145.

Soleas, G. J., Yan, J. and Goldberg, D. M. (2001b) 'Ultrasensitive assay for three polyphenols (catechin, quercetin and resveratrol) and their conjugates in biological fluids utilizing gas chromatography with mass selective detection', *Journal of Chromatography B: Biomedical Sciences and Applications*. Elsevier, 757(1), pp. 161–172. doi: 10.1016/S0378-4347(01)00142-6.

Song, Z. *et al.* (2018) 'Endothelial growth factor receptor-targeted and reactive oxygen species-responsive lung cancer therapy by docetaxel and resveratrol encapsulated lipid-polymer hybrid nanoparticles', *Biomedicine and Pharmacotherapy*. Elsevier, 105(28), pp. 18–26. doi: 10.1016/j.biopha.2018.05.095.

Soppimath, K. S. *et al.* (2001) 'Biodegradable polymeric nanoparticles as drug delivery devices', *Journal of Controlled Release*, 70(1–2), pp. 1–20. doi: 10.1016/S0168-3659(00)00339-4.

Sosnik, A. and Seremeta, K. P. (2015) 'Advantages and challenges of the spray-drying technology for the production of pure drug particles and drug-loaded polymeric carriers', *Advances in Colloid and Interface Science*. Elsevier B.V., 223, pp. 40–54. doi: 10.1016/j.cis.2015.05.003.

Souza, S. D., Dorati, R. and Deluca, P. P. (2014) 'Effect of hydration on physico-chemical properties of end-capped plga', *Advances in Biomaterials*, pp. 1–23.

Spiro, S. G. and Silvestri, G. A. (2005) 'One Hundred Years of Lung Cancer', *American Journal of Respiratory and Critical Care Medicine*. American Thoracic Society, 172(5), pp. 523–529. doi: 10.1164/rccm.200504-531OE.

Steckel, H. and Eskandar, F. (2003) 'Factors affecting aerosol performance during nebulization with jet and ultrasonic nebulizers', *European Journal of Pharmaceutical Sciences*, 19(5), pp. 443–455. doi: 10.1016/S0928-0987(03)00148-9.

Stocke, N. A. *et al.* (2015) 'Formulation and characterization of inhalable magnetic nanocomposite microparticles (MnMs) for targeted pulmonary

delivery via spray drying.’, *International journal of pharmaceutics*. NIH Public Access, 479(2), pp. 320–8. doi: 10.1016/j.ijpharm.2014.12.050.

Storme, G. *et al.* (2016) ‘The cost of cancer care is not related to its outcomes.’, *Ecancermedicalscience*. ecancer Global Foundation, 10, p. 687. doi: 10.3332/ecancer.2016.687.

Suarez, S. and Hickey, A. J. (2000) ‘Drug properties affecting aerosol behavior’, in *Respiratory Care*, pp. 652–666.

Suchonwanit, P. and McMichael, A. J. (2018) ‘Alopecia in Association with Malignancy: A Review’, *American Journal of Clinical Dermatology*. Springer International Publishing, 19(6), pp. 853–865. doi: 10.1007/s40257-018-0378-1.

Sukhanova, A. *et al.* (2018) ‘Dependence of Nanoparticle Toxicity on Their Physical and Chemical Properties’, *Nanoscale Research Letters*. Nanoscale Research Letters, 13. doi: 10.1186/s11671-018-2457-x.

Suktham, K. *et al.* (2018) ‘Efficiency of resveratrol-loaded sericin nanoparticles: Promising bionanocarriers for drug delivery’, *International Journal of Pharmaceutics*. Elsevier, 537(1–2), pp. 48–56. doi: 10.1016/j.ijpharm.2017.12.015.

Sullivan, R. *et al.* (2011) ‘Delivering affordable cancer care in high-income countries’, *The Lancet Oncology*, 12(10), pp. 933–980. doi: 10.1016/S1470-2045(11)70141-3.

Summerlin, N. *et al.* (2015) ‘Resveratrol nanoformulations: Challenges and opportunities’, *International Journal of Pharmaceutics*. Elsevier, 479(2), pp.

282–290. doi: 10.1016/J.IJPHARM.2015.01.003.

Sun, L. *et al.* (2013) 'A SUMOylation-Dependent Pathway Regulates SIRT1 Transcription and Lung Cancer Metastasis', *JNCI: Journal of the National Cancer Institute*. Narnia, 105(12), pp. 887–898. doi: 10.1093/jnci/djt118.

Sun, L. *et al.* (2017) 'Resveratrol inhibits lung cancer growth by suppressing M2-like polarization of tumor associated macrophages', *Cellular Immunology*. Elsevier Inc., 311, pp. 86–93. doi: 10.1016/j.cellimm.2016.11.002.

Sung, J. C., Pulliam, B. L. and Edwards, D. A. (2007) 'Nanoparticles for drug delivery to the lungs', *Trends in Biotechnology*. Elsevier Current Trends, 25(12), pp. 563–570. doi: 10.1016/J.TIBTECH.2007.09.005.

Suska, F. *et al.* (2005) 'Monocyte viability on titanium and copper coated titanium', *Biomaterials*, 26(30), pp. 5942–5950. doi: 10.1016/j.biomaterials.2005.03.017.

Tahara, K. *et al.* (2009) 'Improved cellular uptake of chitosan-modified PLGA nanospheres by A549 cells', *International Journal of Pharmaceutics*, 382(1–2), pp. 198–204. doi: 10.1016/j.ijpharm.2009.07.023.

Takeuchi, I. *et al.* (2018) 'Effects of l-leucine on PLGA microparticles for pulmonary administration prepared using spray drying: Fine particle fraction and phagocytotic ratio of alveolar macrophages', *Colloids and Surfaces A: Physicochemical and Engineering Aspects*. Elsevier, 537, pp. 411–417. doi: 10.1016/J.COLSURFA.2017.10.047.

Tawfeek, H. *et al.* (2011) 'Poly(Glycerol Adipate-co- ω -Pentadecalactone) Spray-Dried Microparticles as Sustained Release Carriers for Pulmonary

Delivery', *Pharmaceutical Research*. Springer US, 28(9), pp. 2086–2097. doi: 10.1007/s11095-011-0433-6.

Tawfeek, H. M. *et al.* (2013) 'Dry powder inhalation of macromolecules using novel PEG-co-polyester microparticle carriers', *International Journal of Pharmaceutics*. Elsevier, 441(1–2), pp. 611–619. doi: 10.1016/j.ijpharm.2012.10.036.

Tawfeek, H. M. (2013) 'Evaluation of PEG and mPEG-co-(PGA-co-PDL) microparticles loaded with sodium diclofenac', *Saudi Pharmaceutical Journal*. Elsevier, 21(4), pp. 387–397. doi: 10.1016/J.JSPS.2012.11.006.

Tawfeek, H. M. *et al.* (2017) 'Colonic delivery of indometacin loaded PGA-co-PDL microparticles coated with Eudragit L100-55 from fast disintegrating tablets', *International Journal of Pharmaceutics*, 531(1), pp. 80–89. doi: 10.1016/j.ijpharm.2017.08.069.

Tayade, P. T. and Kale, R. D. (2004) 'Encapsulation of water-insoluble drug by a cross-linking technique: Effect of process and formulation variables on encapsulation efficiency, particle size, and in vitro dissolution rate', *AAPS Journal*, 6(1), pp. 1–8.

Taylor, L. (2012) 'Cancer "costing UK £15.8 billion a year"', *PharmaTimes online*, 8 November. Available at: http://www.pharmatimes.com/news/cancer_costing_uk_15.8_billion_a_year_976281 (Accessed: 13 May 2019).

Thein-Han, W. W. *et al.* (2004) 'Transdermal delivery controlled by a chitosan membrane', *Drug Development and Industrial Pharmacy*. Taylor & Francis, 30(4), pp. 397–404. doi: 10.1081/DDC-120030934.

Thompson, C. J. *et al.* (2006) 'Enzymatic synthesis and evaluation of new novel ω -pentadecalactone polymers for the production of biodegradable microspheres', *Journal of Microencapsulation*, 23(2), pp. 213–226. doi: 10.1080/02652040500444123.

Thompson, C. J. *et al.* (2007) 'Evaluation of ibuprofen-loaded microspheres prepared from novel copolyesters', *International Journal of Pharmaceutics*, 329(1–2), pp. 53–61. doi: 10.1016/j.ijpharm.2006.08.019.

Thompson, C. J. *et al.* (2008) 'Synthesis and Evaluation of Novel Polyester-Ibuprofen Conjugates for Modified Drug Release', *Drug Development and Industrial Pharmacy*, 34(8), pp. 877–884. doi: 10.1080/03639040801929075.

Thompson, C. J. *et al.* (2009) 'Preparation and evaluation of microspheres prepared from novel polyester-ibuprofen conjugates blended with non-conjugated ibuprofen', *Journal of Microencapsulation*, 26(8), pp. 676–683. doi: 10.3109/02652040802656333.

Thorley, A. J. and Tetley, T. D. (2013) 'New perspectives in nanomedicine', *Pharmacology & Therapeutics*. Pergamon, 140(2), pp. 176–185. doi: 10.1016/J.PHARMTHERA.2013.06.008.

Tobimatsu, Y. *et al.* (2014) 'A click chemistry strategy for visualization of plant cell wall lignification', *Chemical Communications*. Royal Society of Chemistry, 50(82), pp. 12262–12265. doi: 10.1039/x0xx00000x.

Toh, C.-K. *et al.* (2018) 'A Decade of Never-smokers Among Lung Cancer Patients—Increasing Trend and Improved Survival', *Clinical Lung Cancer*. Elsevier, 19(5), pp. e539–e550. doi: 10.1016/J.CLLC.2018.03.013.

Tomé-Carneiro, J. *et al.* (2013) 'Resveratrol and Clinical Trials: The Crossroad from In Vitro Studies to Human Evidence', *Current Pharmaceutical Design*, 19, pp. 6064–6093. Available at: <https://www.ingentaconnect.com/content/ben/cpd/2013/00000019/00000034/art00003?crawler=true&mimetype=application/pdf> (Accessed: 26 June 2019).

Tomoda, K. *et al.* (2008) 'Preparation and properties of inhalable nanocomposite particles: Effects of the size, weight ratio of the primary nanoparticles in nanocomposite particles and temperature at a spray-dryer inlet upon properties of nanocomposite particles', *Colloids and Surfaces B: Biointerfaces*, 64(1), pp. 70–76. doi: 10.1016/j.colsurfb.2008.01.016.

Tomoda, K. *et al.* (2009) 'Preparation and properties of inhalable nanocomposite particles for treatment of lung cancer', *Colloids and Surfaces B: Biointerfaces*, 71(2), pp. 177–182. doi: 10.1016/j.colsurfb.2009.02.001.

Torre, L. A. *et al.* (2016) 'Global Cancer Incidence and Mortality Rates and Trends-An Update'. doi: 10.1158/1055-9965.EPI-15-0578.

Tralongo, P. *et al.* (2011) 'Cancer patient-centered home care: a new model for health care in oncology.', *Therapeutics and clinical risk management*. Dove Press, 7, pp. 387–92. doi: 10.2147/TCRM.S22119.

Travis, W. D., Brambilla, E. and Riely, G. J. (2013) 'New pathologic classification of lung cancer: Relevance for clinical practice and clinical trials', *Journal of Clinical Oncology*, 31(8), pp. 992–1001. doi: 10.1200/JCO.2012.46.9270.

Trotta, V. *et al.* (2015) 'In vitro biological activity of resveratrol using a novel inhalable resveratrol spray-dried formulation', *International Journal of*

Pharmaceutics. Elsevier B.V., 491(1–2), pp. 190–197. doi: 10.1016/j.ijpharm.2015.06.033.

Trüeb, R. M. (2009) 'Chemotherapy-induced alopecia', *Seminars in cutaneous medicine and surgery*. Elsevier Inc., 28(1), pp. 11–14. doi: 10.1097/SPC.0b013e3283409280.

Trujillo, M. *et al.* (2019) 'Green methodologies for copper(I)-catalyzed azide-alkyne cycloadditions: A comparative study', *Molecules*, 24(5), pp. 1–12. doi: 10.3390/molecules24050973.

Turecek, P. L. *et al.* (2016) 'PEGylation of Biopharmaceuticals: A Review of Chemistry and Nonclinical Safety Information of Approved Drugs', *Journal of Pharmaceutical Sciences*. Elsevier Ltd, 105(2), pp. 460–475. doi: 10.1016/j.xphs.2015.11.015.

Ulasli, S. S. *et al.* (2013) 'Anticancer effects of thymoquinone, caffeic acid phenethyl ester and resveratrol on A549 non-small cell lung cancer cells exposed to benzo(a)pyrene', *Asian Pacific Journal of Cancer Prevention*, 14(10), pp. 6159–6164. doi: 10.7314/APJCP.2013.14.10.6159.

Ungaro, F. *et al.* (2012) 'Dry powders based on PLGA nanoparticles for pulmonary delivery of antibiotics: Modulation of encapsulation efficiency, release rate and lung deposition pattern by hydrophilic polymers', *Journal of Controlled Release*. Elsevier, 157(1), pp. 149–159. doi: 10.1016/J.JCONREL.2011.08.010.

University of Oxford (2012) *Cancer costs the UK economy £15.8bn a year*. Available at: <http://www.ox.ac.uk/news/2012-11-07-cancer-costs-uk-economy-£158bn-year> (Accessed: 7 April 2019).

Varma, M. V. S. *et al.* (2004) 'Factors affecting mechanism and kinetics of drug release from matrix-based oral controlled drug delivery systems', *American Journal of Drug Delivery*, 2(1), pp. 43–57. doi: 10.2165/00137696-200402010-00003.

Vega-Avila, E. and Pugsley, M. K. (2011) 'An overview of colorimetric assay methods used to assess survival or proliferation of mammalian cells', *Proceedings of the Western Pharmacology Society*, 54(March 2014), pp. 10–14.

Vijayakumar, M. R. *et al.* (2016) 'Resveratrol loaded PLGA: d - α -tocopheryl polyethylene glycol 1000 succinate blend nanoparticles for brain cancer therapy', *RSC Advances*. The Royal Society of Chemistry, 6(78), pp. 74254–74268. doi: 10.1039/c6ra15408e.

Vittorio, O. *et al.* (2017) 'Polyphenols delivery by polymeric materials: challenges in cancer treatment', *Drug Delivery*. Taylor & Francis, 24(1), pp. 162–180. doi: 10.1080/10717544.2016.1236846.

Voigt, M. *et al.* (2019) 'Surface modification of nanoparticles and nanovesicles via click-chemistry', in Weissig, V. and Elbayoumi, T. (eds) *Pharmaceutical Nanotechnology: Methods in Molecular Biology*. Humana, New York, NY, pp. 235–245. doi: 10.1007/978-1-4939-9516-5_16.

Vrbková, S., Dračinský, M. and Holý, A. (2007) 'Bifunctional acyclic nucleoside phosphonates: 2. Symmetrical 2-[[bis(phosphono)methoxy]methyl]ethyl derivatives of purines and pyrimidines', *Collection of Czechoslovak Chemical Communications*, 72(7), pp. 965–983. doi: 10.1135/cccc20070965.

Wagland, R. *et al.* (2016) 'Prevalence of cancer chemotherapy-related

problems, their relation to health-related quality of life and associated supportive care: a cross-sectional survey', *Supportive Care in Cancer*. Springer Berlin Heidelberg, 24(12), pp. 4901–4911. doi: 10.1007/s00520-016-3346-4.

Walle, T. *et al.* (2004) 'High absorption but very low bioavailability of oral resveratrol in humans', *Drug Metabolism and Disposition*, 32(12), pp. 1377–1382. doi: 10.1124/dmd.104.000885.

Wan, S. *et al.* (2018) 'Resveratrol-loaded PLGA nanoparticles: Enhanced stability, solubility and bioactivity of resveratrol for non-alcoholic fatty liver disease therapy', *Royal Society Open Science*, 5(11). doi: 10.1098/rsos.181457.

Wang, C., Ho, P. C. and Lim, L. Y. (2010) 'Wheat germ agglutinin-conjugated PLGA nanoparticles for enhanced intracellular delivery of paclitaxel to colon cancer cells', *International Journal of Pharmaceutics*. Elsevier B.V., 400(1–2), pp. 201–210. doi: 10.1016/j.ijpharm.2010.08.023.

Wang, H. *et al.* (2013) 'Resveratrol inhibits TGF- β 1-induced epithelial-to-mesenchymal transition and suppresses lung cancer invasion and metastasis', *Toxicology*. Elsevier, 303, pp. 139–146. doi: 10.1016/J.TOX.2012.09.017.

Wang, J. *et al.* (2017) 'Formulation of water-in-oil-in-water (W/O/W) emulsions containing trans-resveratrol', *RSC Advances*. Royal Society of Chemistry, 7(57), pp. 35917–35927. doi: 10.1039/c7ra05945k.

Wang, K., Hawley, M. C. and DeAthos, S. J. (2003) 'Conversion of glycerol to 1,3-propanediol via selective dehydroxylation', *Industrial and Engineering*

Chemistry Research, 42(13), pp. 2913–2923. doi: 10.1021/ie020754h.

Wang, P. and Sang, S. (2018) 'Metabolism and pharmacokinetics of resveratrol and pterostilbene', *BioFactors*, 44(1), pp. 16–25. doi: 10.1002/biof.1410.

Wang, Q. *et al.* (2003) 'Bioconjugation by Copper (I) -Catalyzed Azide-Alkyne [3 + 2] Cycloaddition', (I), pp. 3192–3193. doi: 10.1021/ja021381e.

Wani, T. U., Raza, S. N. and Khan, N. A. (2019) 'Nanoparticle opsonization: forces involved and protection by long chain polymers', *Polymer Bulletin*. Springer Berlin Heidelberg, (0123456789). doi: 10.1007/s00289-019-02924-7.

Warheit, D. B., Sayes, C. M. and Reed, K. L. (2009) 'Nanoscale and fine zinc oxide particles: Can in vitro assays accurately forecast lung hazards following inhalation exposures?', *Environmental Science and Technology*, 43(20), pp. 7939–7945. doi: 10.1021/es901453p.

Wei, Y. *et al.* (2018) 'Factors relating to the biodistribution & clearance of nanoparticles & their effects on in vivo application', *Nanomedicine*, 13(12), pp. 1495–1512. doi: 10.2217/nnm-2018-0040.

Weinberger, S. E., Cockrill, B. A. and Mandel, J. (2019) 'Pulmonary Anatomy and Physiology: The Basics', in Weinberger, S. E., Cockrill, B. A., and Mandel, J. (eds) *Principles of Pulmonary Medicine*. Seventh Ed. Elsevier, pp. 1–18. doi: 10.1016/B978-0-323-52371-4.00004-0.

Weng, C. J. *et al.* (2009) 'Mechanisms of apoptotic effects induced by resveratrol, dibenzoylmethane, and their analogues on human lung carcinoma cells', *Journal of Agricultural and Food Chemistry*, 57(12), pp. 5235–5243. doi:

10.1021/jf900531m.

Weyermann, J., Lochmann, D. and Zimmer, A. (2005) 'A practical note on the use of cytotoxicity assays', *International Journal of Pharmaceutics*, 288(2), pp. 369–376. doi: 10.1016/j.ijpharm.2004.09.018.

Wilhelm, S. *et al.* (2016) 'Analysis of nanoparticle delivery to tumours', *Nature Reviews Materials*, 1, p. 16014. doi: 10.1038/natrevmats.2016.14.

Witschi, H. (2001) 'A Short History of Lung Cancer', *Toxicological Sciences*. Oxford University Press, 64(1), pp. 4–6. doi: 10.1093/toxsci/64.1.4.

Wörle-Knirsch, J. M., Pulskamp, K. and Krug, H. F. (2006) 'Oops they did it again! Carbon nanotubes hoax scientists in viability assays.', *Nano letters*, 6(6), pp. 1261–8. doi: 10.1021/nl060177c.

Wright Muelas, M. *et al.* (2018) 'Rational cell culture optimization enhances experimental reproducibility in cancer cells', *Scientific Reports*. Springer US, 8(1), pp. 1–16. doi: 10.1038/s41598-018-21050-4.

Wu, C. *et al.* (2010) 'Ultrabright and Bioorthogonal Labeling of Cellular Targets Using Semiconducting Polymer Dots and Click Chemistry', *Angewandte Chemie International Edition*. John Wiley & Sons, Ltd, 49(49), pp. 9436–9440. doi: 10.1002/anie.201004260.

Wu, J. *et al.* (2017) 'Preparation and biological activity studies of resveratrol loaded ionically cross-linked chitosan-TPP nanoparticles', *Carbohydrate Polymers*. Elsevier Ltd., 175, pp. 170–177. doi: 10.1016/j.carbpol.2017.07.058.

Wu, M. *et al.* (2017) 'Resveratrol-loaded glycyrrhizic acid-conjugated human

serum albumin nanoparticles wrapping resveratrol nanoparticles: Preparation, characterization, and targeting effect on liver tumors', *Journal of Biomaterials Applications*, 32(2), pp. 191–205. doi: 10.1177/0885328217713357.

Yamamoto, H. *et al.* (2005) 'Surface-modified PLGA nanosphere with chitosan improved pulmonary delivery of calcitonin by mucoadhesion and opening of the intercellular tight junctions', *Journal of Controlled Release*. Elsevier, 102(2), pp. 373–381. doi: 10.1016/J.JCONREL.2004.10.010.

Yang, L. *et al.* (2018) 'Response of plant secondary metabolites to environmental factors', *Molecules*, 23(4), pp. 1–26. doi: 10.3390/molecules23040762.

Yang, Q. *et al.* (2015) 'A novel long noncoding RNA AK001796 acts as an oncogene and is involved in cell growth inhibition by resveratrol in lung cancer', *Toxicology and Applied Pharmacology*. Academic Press, 285(2), pp. 79–88. doi: 10.1016/J.TAAP.2015.04.003.

Yang, W. *et al.* (2014) 'Projected Supply of and Demand for Oncologists and Radiation Oncologists Through 2025: An Aging, Better-Insured Population Will Result in Shortage', *Journal of Oncology Practice*. American Society of Clinical Oncology Alexandria, VA, 10(1), pp. 39–45. doi: 10.1200/JOP.2013.001319.

Yildiz-Peköz, A. *et al.* (2018) 'Preparation and characterization of doripenem-loaded microparticles for pulmonary delivery', *Journal of Aerosol Medicine and Pulmonary Drug Delivery*, 31(6), pp. 347–357. doi: 10.1089/jamp.2017.1378.

Yin, H.-T. *et al.* (2013) 'In vitro and in vivo Evaluation of the Antitumor Efficiency of Resveratrol Against Lung Cancer', *Asian Pacific Journal of*

Cancer Prevention. Asian Pacific Organization for Cancer Prevention, 14(3), pp. 1703–1706. doi: 10.7314/APJCP.2013.14.3.1703.

You, Z. *et al.* (2010) 'A functionalizable polyester with free hydroxyl groups and tunable physiochemical and biological properties', *Biomaterials*, 31(12), pp. 3129–3138. doi: 10.1016/j.biomaterials.2010.01.023.

Young, P. M. *et al.* (2008) 'Composite carriers improve the aerosolisation efficiency of drugs for respiratory delivery', 39, pp. 82–93. doi: 10.1016/j.jaerosci.2007.10.003.

Youngren-Ortiz, S. R. *et al.* (2017) 'Development of Optimized, Inhalable, Gemcitabine-Loaded Gelatin Nanocarriers for Lung Cancer.', *Journal of aerosol medicine and pulmonary drug delivery*. Mary Ann Liebert, Inc., 30(5), pp. 299–321. doi: 10.1089/jamp.2015.1286.

Yousuf Zafar, S. (2016) 'Financial Toxicity of Cancer Care: It's Time to Intervene', *Journal of the National Cancer Institute*. Narnia, 108(5), p. djv370. doi: 10.1093/jnci/djv370.

Yu, X.-D. *et al.* (2016) 'Resveratrol inhibits oral squamous cell carcinoma through induction of apoptosis and G2/M phase cell cycle arrest', *Tumor Biology*. Springer Netherlands, 37(3), pp. 2871–2877. doi: 10.1007/s13277-015-3793-4.

Yu, Y.-H. *et al.* (2013) 'MiR-520h-mediated FOXC2 regulation is critical for inhibition of lung cancer progression by resveratrol', *Oncogene*. Nature Publishing Group, 32(4), pp. 431–443. doi: 10.1038/onc.2012.74.

Yuan, L. *et al.* (2015) 'Resveratrol induces cell cycle arrest via a p53-

independent pathway in A549 cells', *Molecular Medicine Reports*. Spandidos Publications, 11(4), pp. 2459–2464. doi: 10.3892/mmr.2014.3100.

Zafar, S. Y. *et al.* (2013) 'The financial toxicity of cancer treatment: a pilot study assessing out-of-pocket expenses and the insured cancer patient's experience.', *The oncologist*. AlphaMed Press, 18(4), pp. 381–90. doi: 10.1634/theoncologist.2012-0279.

Zambaux, M. F. *et al.* (1999) 'Preparation and characterization of protein C-loaded PLA nanoparticles', *Journal of Controlled Release*, 60(2–3), pp. 179–188. doi: 10.1016/S0168-3659(99)00073-5.

Zhang, H. and Grinstaff, M. W. (2014) 'Recent advances in glycerol polymers: Chemistry and biomedical applications', *Macromolecular Rapid Communications*. Wiley-VCH Verlag, 35(22), pp. 1906–1924. doi: 10.1016/j.physbeh.2017.03.040.

Zhang, J. *et al.* (2015) 'P62 regulates resveratrol-mediated Fas/Cav-1 complex formation and transition from autophagy to apoptosis.', *Oncotarget*. Impact Journals, LLC, 6(2), pp. 789–801. doi: 10.18632/oncotarget.2733.

Zhang, T. *et al.* (2018) 'Inhalation treatment of primary lung cancer using liposomal curcumin dry powder inhalers', *Acta Pharmaceutica Sinica B*. Elsevier, 8(3), pp. 440–448. doi: 10.1016/J.APSB.2018.03.004.

Zhao, J. and Stenzel, M. H. (2018) 'Entry of nanoparticles into cells: The importance of nanoparticle properties', *Polymer Chemistry*, 9(3), pp. 259–272. doi: 10.1039/c7py01603d.

Zhao, W. *et al.* (2010) 'Resveratrol down-regulates survivin and induces

apoptosis in human multidrug-resistant SPC-A-1/CDDP cells', *Oncology reports*. Spandidos Publications, 23(1), pp. 279–286. doi: 10.3892/or.

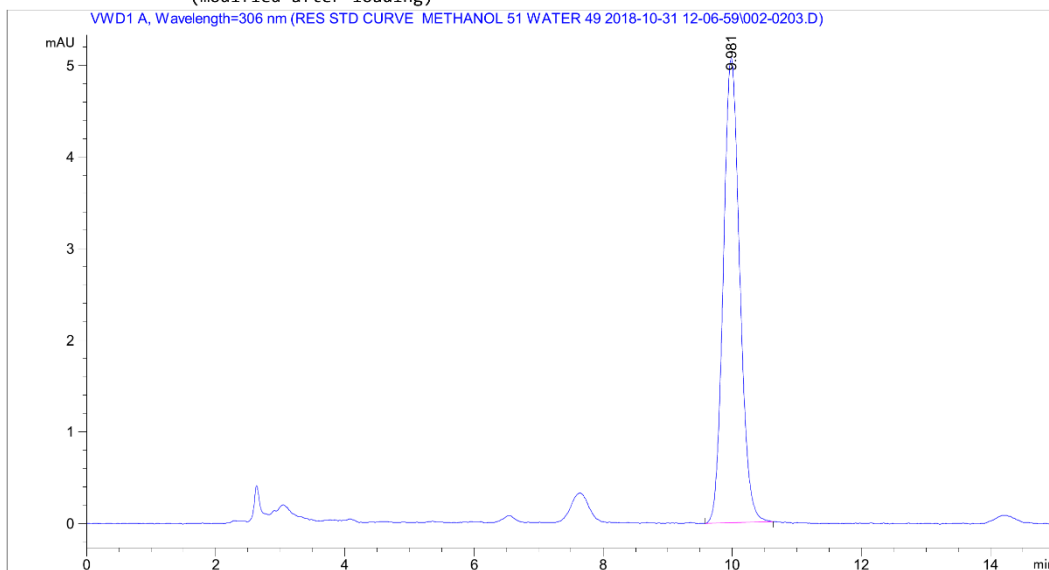
Zu, Y. *et al.* (2016) 'Preparation and in vitro / in vivo evaluation of resveratrol-loaded carboxymethyl chitosan nanoparticles', *Drug Delivery*, 23(3), pp. 981–991. doi: 10.3109/10717544.2014.924167.

Zwicker, V. E. *et al.* (2019) 'A Fluorogenic Probe for Cell Surface Phosphatidylserine Using an Intramolecular Indicator Displacement Sensing Mechanism', *Angewandte Chemie - International Edition*, 58(10), pp. 3087–3091. doi: 10.1002/anie.201812489.

7 Appendix

Data File C:\CHEM32\...\RES STD CURVE METHANOL 51 WATER 49 2018-10-31 12-06-59\002-0203.D
Sample Name: 1 mcg/ml

```
=====
Acq. Operator   : SYSTEM                      Seq. Line :    2
Acq. Instrument : LC 1                        Location  : Vial 2
Injection Date  : 31-Oct-18 1:38:05 PM        Inj       :    3
                                           Inj Volume: 20.000 µl
Acq. Method     : C:\CHEM32\1\DATA\RES STD CURVE METHANOL 51 WATER 49 2018-10-31 12-06-59
                  \ASH RES MEOH.H2051.49.M
Last changed    : 31-Oct-18 1:04:32 PM by SYSTEM
Analysis Method : C:\CHEM32\1\DATA\RES STD CURVE METHANOL 51 WATER 49 2018-10-31 12-06-59
                  \ASH RES MEOH.H2051.49.M (Sequence Method)
Last changed    : 01-Nov-18 12:40:41 PM by SYSTEM
                  (modified after loading)
=====
```



```
=====
Area Percent Report
=====
```

```
Sorted By      :      Signal
Multiplier     :      1.0000
Dilution       :      1.0000
Do not use Multiplier & Dilution Factor with ISTDs
```

Signal 1: VWD1 A, Wavelength=306 nm

Peak #	RetTime [min]	Type	Width [min]	Area [mAU*s]	Height [mAU]	Area %
1	9.981	BB	0.2730	89.60395	5.07341	100.0000

```
Totals :                      89.60395  5.07341
```